THE UNIVERSITY OF MICHIGAN

INDUSTRY PROGRAM OF THE COLLEGE OF ENGINEERING

A STUDY OF RADIAL GAS-TURBINES

Professor Nagao Mizumachi
University of Tokyo

Translated by

Chao-te Lin
Graduate Student in
Comparative Literature

November, 1960

IP-476

PREFACE

The literature on design of radial inflow turbines is rather limited. This treatise gives the results of a detailed study of the theory of radial inflow turbine design made in Japan by Professor Mizumachi of the University of Tokyo. The results are supported by experimental data on several radial inflow turbines. The study makes a substantial contribution to this field of engineering and the translation into English makes the design procedure and data available to a larger segment of the engineering profession.

Frank L. Schwartz
Professor of Mechanical Engineering

TABLE OF CONTENTS

		Page
PREFACE		ii
LIST OF FIGURES		iv
NOMENCLATURE		x
CHAPTER		
1.0	INTRODUCTION	1
2.0	CHARACTERISTICS OF RADIAL GAS TURBINES	5
	2.1 Outline	5
	2.2 Characteristic of Straight Radial-Vaned Turbines	6
	2.3 Comparison Between Radial-Straight Vanes and Curved Vanes	40
	2.4 Partial-Load Characteristics	56
3.0	THE NOZZLE	71
	3.1 Outline	71
	3.2 Test Equipment	71
	3.3 Results of the Experiment	78
	3.4 Analysis of Losses	81
	3.5 Nozzle Designing Procedure	91
	3.6 Summary	97
4.0	A STUDY OF THE FLOW IN AN EXDUCER	101
	4.1 Outline	101
	4.2 Theoretical Analysis	101
	4.3 Experimental Verification of the Analysis	112
	4.4 Summary	116
5.0	EXPERIMENTAL STUDY OF RADIAL TURBINES	119
	5.1 Outline	119
	5.2 Test Turbines	119
	5.3 Test Equipment and Procedures	120
	5.4 Results of the Test	131
	5.5 Performance of the Test Turbines	158
	5.6 Summary	167
6.0	CONCLUSION	169
BIBLIOGRAPHY		171

LIST OF FIGURES

Figure		Page
1.1	Types of Radial Turbine.....	2
2.1		7
2.2	T-S Diagram.....	7
2.3	Velocity Diagram.....	7
2.4		7
2.5	Internal Efficiency.....	22
2.6	Internal Efficiency.....	22
2.7	Outlet Velocity Distribution.....	23
2.8	Internal Efficiency and Net Efficiency.....	23
2.9		27
2.10	Maximum Net Efficiency.....	27
2.11	Blade Inlet Breadth.....	29
2.12	Nozzle Angle.....	29
2.13	Peripheral Velocity.....	30
2.14	Reaction.....	30
2.15		31
2.16		31
2.17		32
2.18		32
2.19		32
2.20	The Value of q Giving the Maximum Efficiency.....	34
2.21	The Maximum Net Efficiency.....	34
2.22	The Most Suitable Outlet Outside Diameter.....	35
2.23	The Most Suitable Blade Inlet Breadth.....	35
2.24	The Most Suitable Reaction.....	36

LIST OF FIGURES (CONT'D)

Figure		Page
2.25	The Most Suitable Peripheral Velocity.....	36
2.26	The Most Suitable Blade Diameter.....	37
2.27	The Most Suitable Number of Revolution.....	37
2.28	The Most Suitable Blade Diameter.....	37
2.29	The Most Suitable Number of Revolution.....	38
2.30	The Most Suitable Peripheral Velocity.....	38
2.31		41
2.32	Curved Vane.....	42
2.33	Velocity Diagram.....	42
2.34	i-s Diagram.....	42
2.35	Internal Efficiency.....	50
2.36	Circumferential Velocity.....	50
2.37	Circumferential Velocity.....	50
2.38	Circumferential Velocity.....	51
2.39	Number of Revolutions.....	51
2.40	Reaction.....	53
2.41	Reaction.....	53
2.42	Reaction.....	54
2.43	Outside Radius of Turbine Outlet.....	54
2.44	Blade Inlet Breadth.....	55
2.45	Velcoity Diagram.....	61
2.46	The Value of $K(\zeta_s = 0.8)$.....	61
2.47	The Value of $K(\zeta_s = 1.0)$.....	61
2.48	Reaction.....	62
2.49	Gas Flow.....	62

LIST OF FIGURES (CONT'D)

Figure		Page
2.50		66
2.51	Torque.....	66
2.52	Output Power.....	68
2.53	Internal Efficiency.....	68
3.1	Circumferential Nozzles.....	72
3.2	Nozzle Test Equipment.....	73
3.3	Photography of Nozzle Test Equipment.....	74
3.4	Test Nozzles.....	76
3.5	Straight Nozzle Wings.....	77
3.6	Isometrical Drawings of the Test Nozzles.....	77
3.7		79
3.8	Measuring Points of Nozzle Outlet Pressure.....	79
3.9	Outlet Pressure Distribution of Nozzle.....	80
3.10	Velocity Coefficient of Nozzle.....	82
3.11	Loss Coefficient of Nozzle.....	82
3.12	Mean Efflux Angle.....	83
3.13		83
3.14		87
3.15	Friction Resistance Coefficient.....	87
3.16	Velocity Diagram.....	96
3.17	Secondary Loss Characteristic Number.....	96
3.18		92
3.19		92
3.20	Total Loss Coefficient.....	95
3.21	The Most Suitable Pitch of Nozzles.....	96

LIST OF FIGURES (CONT'D)

Figure		Page
3.22	The Greatest Velocity Coefficient.....	96
3.23		98
3.24		98
4.1		102
4.2		102
4.3	Velocity and Pressure Distribution of Exducer Inlet and Outlet.....	107
4.4	Distribution of K.....	107
4.5		107
4.6	Stream Lines in the Exducer.....	110
4.7		110
4.8	Stream Lines in the Exducer.....	110
4.9		111
4.10	Stream Lines in the Exducer.....	111
4.11	A-Type Exducer.....	113
4.12	B-Type Exducer.....	114
4.13	Outlet Velocity Distribution of A-Type Exducer.....	115
4.14	Outlet Velocity Distribution of B-Type Exducer.....	115
5.1	Test Turbine No. 1.....	121
5.2	Test Turbine No. 1.....	122
5.3	Test Turbine No. 2.....	123
5.4	Test Turbine No. 2.....	124
5.5	Test Turbine No. 1 Equipment.....	126
5.6	Yaw Meter.....	127
5.7	Structure of Yaw Meter.....	127
5.8	Test Turbine No. 2 Equipment.....	129

Figure		Page
5.9	Test Turbine No. 2 Equipment.....	130
5.10	Velocity Diagram.....	132
5.11	Distribution of Outlet Static and Dynamic Pressures (Test Turbine No. 1).....	134
5.12	Absolute Efflux Angle (Test Turbine No. 1).....	134
5.13	Axial Flow Velocity (Test Turbine No. 1).....	135
5.14	Flow Distribution (Test Turbine No. 1).....	135
5.15	Comparison of Gas Flow.....	135
5.16	Relative Efflux Angle (Test Turbine No. 1).....	136
5.17	Relative Efflux Angle (Test Turbine No. 2).....	136
5.18	Slip Angle (Test Turbine No. 1).....	137
5.19	Slip Angle (Test Turbine No. 1).....	137
5.20	Slip Angle (Test Turbine No. 2).....	138
5.21	i-s Diagram.....	138
5.22		140
5.23	Loss in Nozzle (Test Turbine No. 1).....	140
5.24	Internal Efficiency (Test Turbine No. 1).....	142
5.25	Leaving Loss (Test Turbine No. 1).....	142
5.26	Shock Loss (Test Turbine No. 1).....	142
5.27	Temperature Efficiency (Test Turbine No. 1).....	146
5.28	Heat Loss (Test Turbine No. 1).....	146
5.29	Loss in Blade (Test Turbine No. 1).....	146
5.30	Distribution of Losses (Test Turbine No. 1).....	147
5.31	Ratio of Mean Loss (Test Turbine No. 1).....	148
5.32	Blade Velocity Coefficient (Test Turbine No. 1).....	150
5.33	Blade Velocity Coefficient (Test Turbine No. 2).....	150

Figure		Page
5.34	Average Blade Velocity Coefficient.....	151
5.35	Slip Diagram.....	151
5.36	Turbine Exit Radii mm.....	152
5.37	Turbine Exit Radii mm.....	152
5.38	Spiral Flows.....	153
5.39	Spiral Flow Caused by Blade Rotation.....	153
5.40	Turbine Exit Radii mm.....	156
5.41	Spiral Flow Caused by Exducer Curvature.....	156
5.42	Spiral Flow Caused by Blade Curvature.....	157
5.43	Method to Determine Blade Efflux Angle.....	157
5.44	Average Temperature Efficiency (Test Turbine No. 1)..	159
5.45	Average Temperature Efficiency (Test Turbine No. 1)..	159
5.46	Average Internal Efficiency (Test Turbine No. 1).....	160
5.47	Average Internal Efficiency (Test Turbine No. 1).....	160
5.48	Gas Flow (Test Turbine No. 1).....	161
5.49	Gas Flow (Test Turbine No. 1).....	161
5.50	Net Output Power (Test Turbine No. 2).....	163
5.51	Gas Flow (Test Turbine No. 2).....	163
5.52	Mean Efflux Angle of Nozzle (Test Turbine No. 2).....	164
5.53	Reaction (Test Turbine No. 2).....	164
5.54	Angle of Blade Inlet Elevation (Test Turbine No. 2)..	165
5.55	Absolute Efflux Angle.....	165
5.56	Absolute Efflux Velocity.....	166
5.57	Net Adiabotic Efficiency (Test Turbine No. 2).....	166

NOMENCLATURE

Geometrical Measures:

R_1 = Blade inlet radius

R_{20} = Blade outlet outside radius

R_{2i} = Blade outlet inside radius

B_1 = Blade inlet breadth

R_{1N} = Nozzle outlet attaching radius

s = Pitch of nozzle circle

ℓ = Chord of nozzle wall

t = Pitch of straight nozzle

c = Chord (Hypotenuse) of straight nozzle

o = Breadth of the shortest passage in the straight nozzle outlet

α = Mean efflux angle of nozzle

β_2 = Relative efflux angle of blade

β_{e1}, β_{e2} = Geometrical efflux angles of blade

δ = Absolute efflux angle

i = Angle of relative elevation at blade inlet

Pressures:

p_0 = Total turbine inlet pressure

p_1 = Static pressure at blade inlet

p_2 = Static pressure at turbine outlet

p_z = Atmospheric pressure

Velocity:

c_1 = Blade inlet absolute velocity

w_1 = Blade inlet relative velocity

U_1 = Blade inlet circumferential velocity

c_2 = Blade outlet absolute velocity

w_2 = Blade outlet relative velocity

u_2 = Blade outlet circumferential velocity

c_1' = Velocity at the time of the equal entropy expansion from the turbine inlet conditions to the blade inlet pressure

w_2' = Relative velocity at the lossless blade outlet

c''_{02} = Theoretical jet velocity at the time of the equal entropy expansion from the turbine inlet conditions to the outlet pressure

$c_0 = \sqrt{2gJc_pT_0}$

a_0 = Velocity of sound in gas at the turbine inlet

Temperatures:

T = Absolute Centigrade temperature

t = Centigrade temperature

T_0, t_0 = Total temperature at turbine inlet

T_1, t_1 = Temperature at blade inlet

T_2, t_2 = Temperature at blade outlet

T''_2, t''_2 = Temperature at the time of the equal entropy expansion from the turbine inlet conditions to the outlet pressure

T'_2, t'_2 = Temperature at the time of the equal entropy expansion from the blade inlet conditions to the outlet pressure

T'_1, t'_1 = Temperature at the time of the equal entropy expansion from the turbine inlet conditions to the blade inlet pressure

Enthalpy:

i''_{02} = Enthalpy at the time of the equal entropy expansion from the turbine inlet conditions to the outlet pressure

i_{02} = Enthalpy from the turbine inlet conditions to the outlet pressure

i'_{01} = Enthalpy at the time of the equal entropy expansion from the turbine inlet conditions to the blade inlet pressure

i_{01} = Enthalpy from the turbine inlet conditions to the blade inlet

i'_{12} = Enthalpy at the time of the equal entropy expansion from the blade inlet conditions to the outlet pressure

i_{12} = Enthalpy from the blade inlet conditions to the outlet pressure

Coefficients:

q = Characteristic quantity of radial turbine gas flow

φ = Nozzle velocity coefficient

ψ_1 = Blade velocity coefficient caused by blade inlet loss

ψ_2 = Blade velocity coefficient

ψ_{2m} = Average blade velocity coefficient

ζ = Coefficient of losses in nozzle, coefficient of losses in exducer

ζ_w = Coefficient of side wall friction loss in blade

ζ_p = Coefficient of profile friction loss in blade

ζ_s = Coefficient of secondary loss in blade

c_f = Coefficient of friction resistance in nozzle

C_L = Coefficient of lift in nozzle

C_{Ds} = Coefficient of secondary loss resistance in nozzle

λ = Characteristic number of secondary loss in nozzle

Densities:

γ_0 = Turbine inlet gas density

γ_1 = Blade inlet gas density

γ_2 = Blade outlet gas density

Efficiencies:

η_i = Internal efficiency

η_θ = Temperature efficiency

η_e = Net adiabatic efficiency

Output powers:

L_i = Internal output power

L_{is} = Theoretical output power at the time of the equal entropy expansion from the turbine inlet conditions to the outlet pressure

N_f = Disk friction loss horsepower

Others:

G = Turbine Gas Flow

r = Reaction

k = Gas adiabatic exponent

R* = Gas constant

g = Gravitational acceleration

$s = (p_1/p_0)^{(k-1/k)}$

$s_0 = (p_2/p_0)^{(k-1/k)}$

CHAPTER 1

INTRODUCTION

The radial turbine is used, in combination with the compressor and the combuster, as the gas turbine prime mover, and also as the exhaust turbo-charger of the internal combustion engine. It is also combined with the compressor and the cooler in the expansion engine to produce refrigeration cycles. The purpose of the present paper is to describe the investigation on the radial inward flow turbine which uses gas as a working fluid.

Though most of the gas turbines that have been used are the large gas turbine prime mover of aircrafts, electric generation, vessels and other heavy vehicles, recent studies and investigations have found the small gas turbines (less than several hundred horse powers) also in use for automobiles, fire-engines, jet-engines, small-sized vessels, as well as for electric generation. It is necessary for such small gas turbines to obtain the maximum efficiency in a relatively small number of revolutions. Such radial turbines are replacing the axial turbines as the small gas turbine prime mover, not only because of the high efficiency they obtain within a small number of revolutions, but because of their relatively simple structure, and because of the ease and the low cost with which they are constructed.

The radial turbine can be divided into the pure radial-flow turbine and the mixed-flow turbine according to the types of the flow of the working fluid (Figure 1.1). The pure radial-flow turbine is the turbine in which the flow in the turbine blade moves in the direction of the radii, whereas the mixed-flow turbine is one in which the flow moves towards the radii at the inlet of the blade, but continues in the direction of the axis through the exducer at the outlet of the blade.

Publications of studies concerning the radial turbine are relatively few. In the field of the pure radial-flow turbine, theoretical studies are made by Sugawara and Nakamura[1] especially in cases where the proportion of the outside diameter in the blade approximates 1, and O.E. Balje[2] proposes a simple hypothesis concerning the losses of the flow in the blade as well as in the nozzle, and makes calculation of certain special cases. Mori[3] also publishes a general theoretical analysis of the pure radial-flow turbine. It is to be noted, however, that, in comparison with the mixed-flow turbine, the pure radial-flow turbine is low in efficiency, small in gas flow, and cannot be used when the expansion ratio is very low. Accordingly most of the radial turbines that are being tested nowadays are the mixed-flow turbines.[4],[5],[6],[7],[8],[9]

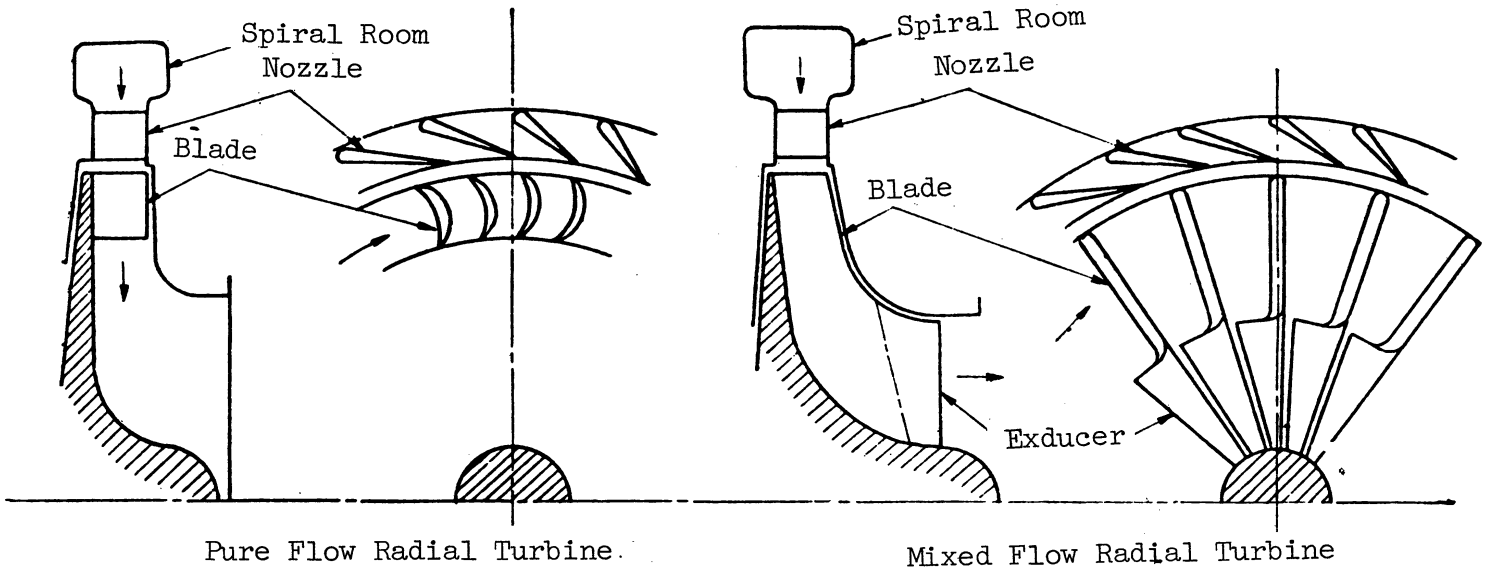

Figure 1.1. Types of Radial Turbine.

Almost no basic study of the mixed-flow turbine has been published, except Mori's[10] theoretical investigation which appeared after the publication of the author's theoretical study that follows.

The present study of mixed radial-flow turbines has been carried on according to the following plan. In order to make clear the characteristics of radial turbines at design point, a theoretical investigation is made of the flow in radial turbines from a new standpoint, which results in finding the conditions giving the maximum turbine efficiency. The mixed radial-flow turbines are divided into those possessing straight radial vanes (Figure 1.1) and those possessing curved vanes (Figure 2.32). It has been discovered that the maximum efficiency of the radial turbine possessing straight radial vanes can be obtained under the condition that the axial absolute velocity at the turbine outlet should be distributed in such manner as the velocity at outside radius is zero and increases towards the outlet inside radii.

The study thus makes clear the determinants of the principal conditions under which the turbine is to produce the maximum efficiency. Then the design procedure giving the maximum efficiency can be generalized by using the non-dimensional quantity, q, representing the relation between gas flow, condition of gas at turbine inlet and the impeller diameter, in which cases, efficiency, revolution of impeller, mean efflux angle from the nozzle and geometrical dimension of impeller can all be represented by the quantity q. Differences of the characteristics between the straight-vaned radial-turbine and the curved-vaned radial-turbine are investigated theoretically, by which merits and demerits are demonstrated in each case respectively. Using the results obtained by the theoretical investigation, the most suitable working range for a radial gas turbine can be made clear. In the investigation of the partial-load characteristics of a radial turbine with straight vanes, with reference to the results of the experimental turbine, it is clarified how quantity of flow, output torque, power and efficiency vary in accordance with the variation of revolution, expansion ratio, and temperature of inlet gas. In this case, theoretical equations are presented in the form of non-dimensional quantities, which agree fairly well with the results of experiment by the test turbine.

The above theory is calculated on the basis of the velocity diagram at the inlet and outlet of the blade. In order to give the velocity diagram, it is necessary to find out what kind of geometrical form should be given to the nozzle and the blade. Very little study has been published concerning the flow inside the radial-turbine nozzle and the blade.

Theoretical and experimental investigation was therefore made on the nozzle in order to measure the losses which occur in radial turbine nozzles. Using the experimental formula for each loss, nozzle design procedures are presented, by which the total loss in a nozzle can be minimized, producing an excellent nozzle with the velocity coefficient as high as $0.975 \sim 0.985$.

The study of the turbine blade is concerned with three principal problems: namely, the investigation of the hydrodynamic losses occurring in the blade, the study of slip factor in a turbine blade, and the study of the flow in an exducer. It is very difficult to analyze the losses in a turbine blade, as its complex geometrical form and high speed of revolution often induce losses resulting from surface friction and relative rotation. In the test turbines, the losses are therefore measured and represented in the form of the blade-loss coefficient. Concerning the slip caused by highly intense relative rotation of the flow in the blade, the character of slip and the cause of its occurrence are found, being useful for design of the vanes and blade outlet.

The function of the exducer is to distribute the axial velocity at the turbine outlet. In order to prevent the flow from moving radially, it is necessary to keep the movement around the axial line inside the cylinder. This is done by balancing the centrifugal force acting on the flow in the exducer with the radial pressure gradient of the flow. As the result of the theoretical analysis of the flow in the exducer the existence of the exducer can be shown, not only satisfying the condition for obtaining the highest turbine efficiency, but also making the centrifugal force acting on the flow balance with the radial pressure gradient of the flow. In addition, the analytical results are verified experimentally by the test turbines, with which it was possible to measure the losses that are hard to calculate theoretically. Namely, the losses in nozzles and moving blades, the shock loss at blade inlet, the leaving loss and the heat loss are made clear quantitatively.

In the performance tests of No. 2 gas turbine, whose design was based upon the above-mentioned results, its effective maximum adiabatic efficiency reached 90%--a performance much superior to the performance demonstrated by this type of gas turbine heretofore in use, whose efficiency is about 78 $\sim$ 86%.

CHAPTER 2

CHARACTERISTICS OF RADIAL GAS TURBINES

2.1. Outline

The characteristics of radial turbines may be considered under two aspects. The first to be considered is the performance of the turbine when it is used alone. The point at which the turbine is used alone is called the design point. The conditions governing the design point include the entire expansion ratio, the quantity of gas flow, gas pressure and temperature at the turbine inlet, and the number of revolutions. In order to design a turbine that would give the maximum efficiency, that is, that would satisfy those conditions, it is necessary to clarify the changes in the turbine efficiency by means of measuring the efflux angle of nozzle and exducer, the outside impeller diameter, the breadth of the blade inlet, the outside diameter and radius of the blade outlet. The first aspect then, puts emphasis upon the characteristics of the radial turbine at the design point. The second aspects are the characteristics of the turbine that are observed when the turbine is used at points other than the design point, for these extra points must be taken into account when load characteristics are attributed to the turbine. The clarification of those points is also required when the turbine is used as the prime mover in combination with the compressor in order to determine the nature of accelerated motion, the matching of the turbine partial-load characteristics with the partial-load characteristics in general, and the possible danger of gas flowing into the diffuser area of the compressor. The second, then, is concerned with the partial-load characteristics of the turbine.

In order to clarify the turbine characteristics at the design point, analysis is made of a turbine with straight-radial vanes, and of a turbine with curved vanes respectively. Because of the complex operations and the problems involving the strength of vanes to meet the rapid revolutions of the radial turbine, the manufacturers have hitherto confined themselves to the turbines with straight-radial vanes. A theoretical comparison was made between the straight-radial vanes and the curved vanes in order to find out if a higher efficiency could be developed and the number of revolutions be reduced by using the curved vanes. The most suitable working range was made clear on the basis of such theoretical observations as stated above.

A study of the turbine characteristics at the design point indicates that the curved vanes have little value of use except in very special cases. It was therefore necessary to study the partial-load characteristics with reference to the results of the experimental turbine that had straight radial vanes. It was then theoretically made clear

how quantity of flow, output torque, power, and efficiency vary in accordance with the variation of revolution, expansion ratio and temperature of inlet gas. In this case, theoretical equations are presented in the form of non-dimensional quantities, which agree fairly well with the results of experiment by the test turbine.

2.2. Characteristics of Straight Radial-Vaned Turbines[11]

2.2.1. Analysis of the Characteristics

Consideration is given here to the gas condition in the straight radial-vaned turbine, as shown in Figure 2.1. The gas passes from the turbine inlet to the spiral chamber, expands in the nozzle that has been set upon the circle, flows into the blade, and is discharged from the exducer. The passage is shown in the T-S diagram of Figure 2.2. The point 0 represents the condition of the turbine inlet with the total pressure p_0, and the total temperature T_0. The expansion from the point 0 to the blade inlet pressure p_1 is represented by 1, whereas the equal entropy expansion from 0 to the pressure p_1 is represented by 1'. In the blade, the expansion recurs from 1 to the blade outlet pressure p_2; 2 represents the actual condition at the blade outlet, whereas 2' represents the expansion entropy from 1 to p_2. The total temperature at point 2 is represented by 3.

Figure 2.3 is a velocity diagram when the shock loss is prevented at the blade inlet of the straight radial vanes. The absolute velocity of the jet from the nozzle, and the average efflux angle of the nozzle are represented by c_1 and d respectively. U_1 is the circumferential velocity at the blade inlet, w_1 the relative flow velocity. In order to prevent the gas from rotating at the turbine outlet, the absolute flow velocity at the blade outlet must be measured only when the flow is moving in the direction of the axis. The velocity diagram under this condition is given in Figure 2.3. c_2 represents the absolute flow velocity, u_2 the circumferential velocity at any point of the outlet, w_2 the relative flow velocity, and β_2 the relative efflux angle. The gas flow, G, passing through the nozzle, is expressed as follows:

$$G = 2\pi R_1 B_1 \epsilon_1 c_1 \sin d \cdot \frac{1}{v_1} \tag{2.1}$$

R_1 represents the radius of the blade inlet, B_1, the breadth of the blade inlet, ϵ_1 the modified coefficient of the thickness of the blade vanes, v_1 the specific volume of gas at the same point.

If φ is the coefficient of velocity at the time of expansion from the turbine inlet pressure, p_0, to the blade inlet pressure, p_1,

$$c_1 = \varphi c_1' \tag{2.2}$$

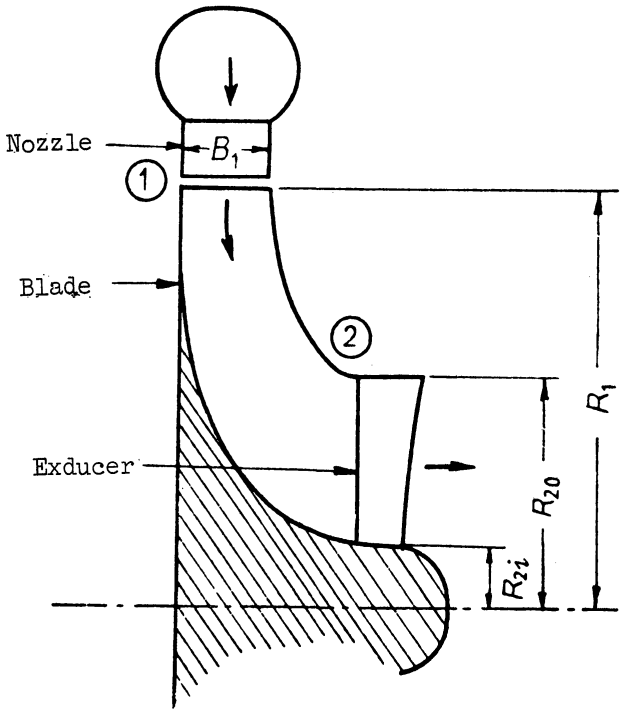

Figure 2.1.

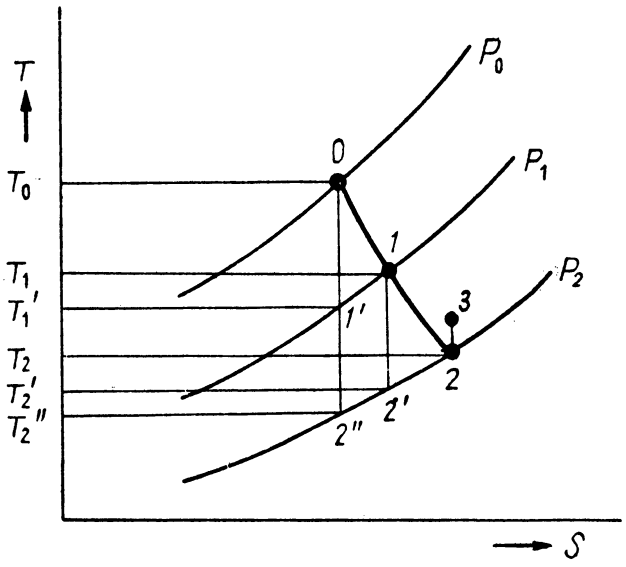

Figure 2.2. T-S Diagram.

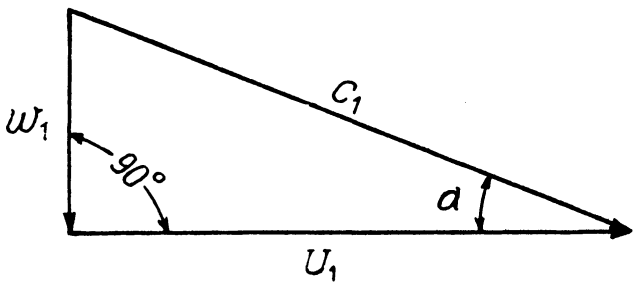

Blade Inlet

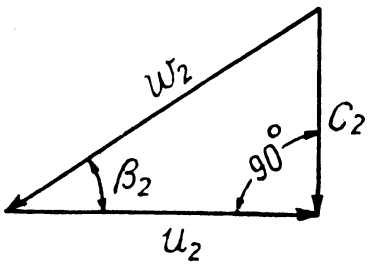

Blade Outlet.

Figure 2.3. Velocity Diagram.

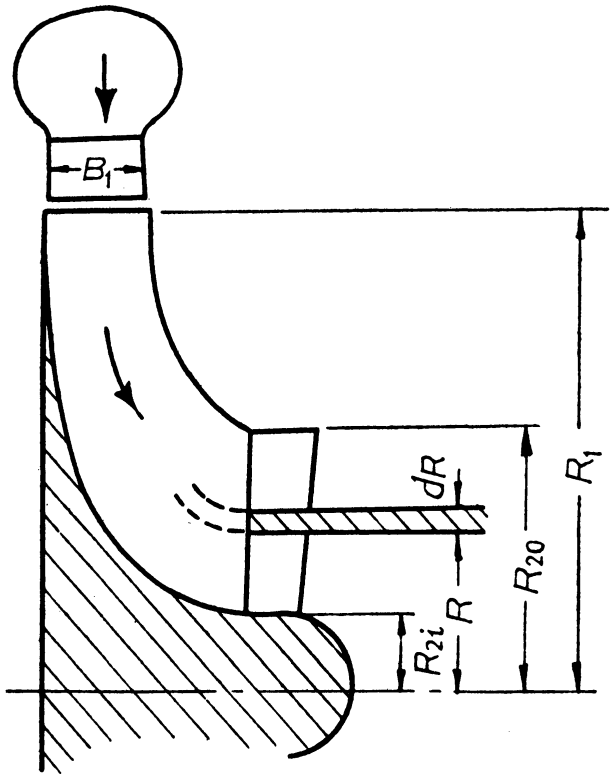

Figure 2.4.

φ is the coefficient of velocity with reference to the total loss of gas in the spiral chamber and the nozzle, c_1', the velocity at the time of the equal entropy expansion, can be obtained as follows:

$$c_1' = \sqrt{2gJc_p(T_0-T_1')} = \sqrt{2gJc_p}\sqrt{T_0(1-s)} \quad . \tag{2.3}$$

If g is the acceleration of gravity, J is the mechanical equivalent of heat, c_p is the specific heat of gas at constant pressure, T_1' is the temperature at the 1' point, s can be obtained as follows:

$$s = \left(\frac{p_1}{p_0}\right)^{(k-1/k)} = \frac{T_1'}{T_0} \quad . \tag{2.4}$$

In the above formula, $k = c_p/c_v$.

If T_1 is the actual temperature at the blade inlet, the absolute velocity of the blade influx is:

$$c_1 = \sqrt{2gJc_p(T_0-T_1)} \quad . \tag{2.5}$$

From the formulas (2.2), (2.3), and (2.5),

$$\frac{T_1}{T_0} = 1 - \varphi^2 (1-s) \quad . \tag{2.6}$$

If the gas constant is R*, the specific volume at the blade outlet v_1 is:

$$v_1 = \frac{R^*T_1}{p_1} = \frac{R^*}{p_1} T_0 \left\{1-\varphi^2(1-s)\right\} \tag{2.7}$$

From the formulas (2.2) and (2.3),

$$c_1 = \varphi \sqrt{2gJc_pT_0 \left(1 - \frac{T_1'}{T_0}\right)}$$
$$= \varphi \sqrt{2gJc_pT_0\ (1-s)} \quad . \tag{2.8}$$

By substituting the v_1 and c_1 in the formula (2.1),

$$G = 2\pi R_1 B_1 \epsilon_1 \sin\alpha \cdot \varphi \sqrt{2gJc_pT_0(1-s)}$$
$$\times \frac{p_1}{R^*T_0} \frac{1}{\sqrt{1 - \varphi^2\ (1-s)}} \quad . \tag{2.9}$$

And the sound velocity in the gas at the turbine inlet, a_0, is:

$$a_0 = \sqrt{gkR^*T_0} \quad . \tag{2.10}$$

If the thermodynamic formula,

$$c_p = \frac{R^*}{J} \frac{k}{k-1}$$

and a_0 and c_p are substituted in the formula (2.9), the following formula can be obtained:

$$G = 2\pi R_1^2\ a_0\gamma_0\epsilon_1 \frac{B_1}{R_1} \sin d \cdot \varphi\sqrt{\frac{2}{k-1}} \cdot \frac{(p_1/p_0)\sqrt{1-s}}{1-\varphi^2(1-s)} \quad . \tag{2.11}$$

In the above formula, γ_0 is the density of gas at the turbine inlet.

In order to express the gas flow, G, in non-dimensional quantity, q will be defined as in the following formulas:

$$q \equiv \frac{G}{2\pi R_1^2 a_0 \gamma_0}$$

$$= \frac{V_0}{2\pi R_1^2 a_0} \qquad (2.12)$$

$$= \frac{1}{2\pi R_1^2}\sqrt{\frac{R^*}{gk}}\, G \frac{\sqrt{T_0}}{p_0} \quad .$$

V_0 represents the cubic flow of gas at the turbine inlet, while q is called the characteristic quantity of gas flow.

From (2.11) and (2.12), q is obtained as follows:

$$q = \varphi\sqrt{\frac{2}{k-1}}\,\epsilon_1 \frac{B_1}{R_1} \sin\alpha \frac{(p_1/p_0)\sqrt{1-s}}{1-\varphi^2(1-s)} \quad . \qquad (2.13)$$

We shall consider next the flow in the blade. While we may regard the flow at the blade inlet as being equal and uniform, the blade loss and the working against the blade will vary in accordance with the gas flow passing through each radius of the blade outlet. Consideration is therefore given to the gas which passes through the diminutive radius d_R at any blade outlet radius R. Figure 2.4 shows the velocity diagram of this outgoing gas.

If, at the blade outlet, the flow moves in the direction of the axis, the pressure becomes the atmospheric pressure p_2, and the enthalpy at the time of the equal entropy expansion from 1 under the pressure p_1 to the pressure p_2 is represented by i_{12}, the following formula can be obtained, with ΔE representing the total loss in the blade:

$$\frac{w_1^2}{2g} + Ji_{12'} = \frac{w_2^2}{2g} + \frac{1}{2g}(U_1^2 - u_2^2) + \Delta E \quad . \qquad (2.14)$$

From the above formula,

$$\frac{\frac{w_1^2}{2g}}{\frac{U_1^2}{2g}} + \frac{Ji_{12'}}{\frac{U_1^2}{2g}} = \frac{\frac{w_2^2}{2g}}{\frac{U_1^2}{2g}} + \left\{1 - \left(\frac{R}{R_1}\right)^2\right\} + \frac{\Delta E}{\frac{U_1^2}{2g}} \qquad (2.14.1)$$

If the velocity coefficient ψ_1 represents the loss at the blade inlet, and ψ_2 the velocity coefficient of the blade, formula (2.14) becomes:

$$\psi_1^2 \frac{w_1^2}{2g} + Ji_{12'} = \frac{1}{\psi_2^2} \cdot \frac{w_2^2}{2g} + \frac{1}{2g}(U_1^2 - u_2^2) \qquad (2.14.2)$$

From the velocity diagram at the blade inlet,

$$w_1^2 = c_1^2 - U_1^2 \qquad (2.15)$$

Therefore,

$$\frac{w_1^2}{2g} = \frac{c_1^2}{2q} - \frac{U_1^2}{2g}$$

$$= \varphi^2 Jc_p T_0 (1-s) - \frac{U_1^2}{2g}$$

$$= \varphi^2 \frac{2}{k-1} \cdot \frac{a_0^2}{2g} (1-s) - \frac{U_1^2}{2g} \qquad (2.16)$$

The enthalpy, $i_{12'}$ at the time of the equal entropy expansion in the blade is as follows:

$$i_{12'} = c_p(T_1 - T_{2'})$$

$$= c_p T_0 \{1 - \varphi^2(1-s)\} \left(1 - \frac{s_0}{s}\right) \qquad (2.17)$$

But

$$s_0 = \left(\frac{p_2}{p_0}\right)^{(k-1/k)}$$

When the formulas (2.16) and (2.17) are substituted in (2.14.2),

$$\frac{2\theta}{k-1} = \frac{1}{\psi_2^2}\left(\frac{w_2}{a_0}\right)^2 + (1+\psi_1^2)\left(\frac{U_1}{a_0}\right)^2 - \left(\frac{u_2}{a_0}\right)^2 \tag{2.18}$$

But θ will be:

$$\theta = 1 - \varphi^2 (1-\psi_1^2)(1-s) - s_0\left(\frac{1-\varphi^2}{s} + \varphi^2\right) \tag{2.19}$$

When the total turbine expansion ratio, p_0/p_2 is given, θ corresponds to the function of s only (the function of p_1/p_0 only).

The angle of relative flow β_2 at the blade outlet is

$$\cos\beta_2 = \frac{u_2}{w_2} \tag{2.20}$$

From the formulas (2.18) and (2.20),

$$\tan\beta_2 = \psi_2\sqrt{\left(\frac{R_1}{R}\right)^2\left\{\frac{2\theta}{k-1}\left(\frac{a_0}{U_1}\right)^2 - (1+\psi_1^2)\right\} - \left(\frac{1}{\psi_2^2} - 1\right)} \tag{2.21}$$

The absolute velocity of the flow, c_2, is:

$$c_2 = u_2 \tan\beta_2 \tag{2.22}$$

From the formulas (2.21) and (2.22),

$$c_2 = \psi_2 U_1 \times \sqrt{\left\{\frac{2\theta}{k-1}\left(\frac{a_0}{U_1}\right)^2 - (1+\psi_1^2)\right\} - \left(\frac{1}{\psi_2^2} - 1\right)\left(\frac{R}{R_1}\right)^2} \tag{2.23}$$

The gas, dG, that flows through the diminutive radius dR at the radius R is:

$$dG = 2\pi R dR \epsilon_2 c_2 \gamma_2 \tag{2.24}$$

In the above formula, the coefficient, ϵ_2, represents the decrease of the flowing area by the thickness of the exducer vanes; and γ_2 for the density of gas at the outlet.

$$\gamma_2 = \frac{p_2}{R^* T_2} \tag{2.25}$$

The following formula is obtained by substituting (2.23) and (2.25) with (2.24).

$$dG = 2\pi\omega\epsilon_2 \sqrt{1-\psi_2^2} \cdot \frac{p_2}{R^* T_2} R \sqrt{a^2-R^2}\, dR \tag{2.26}$$

a represents the velocity at the angle of rotation.

$$a^2 = R_1^2 \frac{\frac{2\theta}{k-1}\left(\frac{a_0}{U_1}\right)^2 - (1+\psi_1^2)}{\frac{1}{\psi_2^2} - 1} \tag{2.27}$$

Therefore, the total gas flow, G, at the turbine outlet is $\int_{R_{2i}}^{R_{20}} dG$.

R_{2i} and R_{20} represent the inside radius and outside radius of the exducer. For this integration, tne expression within the square root in formula (2.26) must be positive, which means that expression within the square root in the formula (2.23) must also be positive. It is clear from formula (2.23) that, as R increases, the expression within ν becomes negative, that is, counter current takes place.

We shall next consider the outlet temperature, T_2. As the actual enthalpy in the blade is $Jc_p (T_1-T_2)$, the following formula of energy is obtained:

$$\frac{w_1^2}{2g} + Jc_p (T_1 - T_2) = \frac{w_2^2}{2g} + \frac{1}{2g}(U_1^2 - u_2^2) \tag{2.28}$$

From (2.14.2) and (2.28),

$$Jc_p (T_2 - T_2') = (1 - \psi_1^2)\frac{w_1^2}{2g} + \left(\frac{1}{\psi_2^2} - 1\right)\frac{w_2^2}{2g} \tag{2.29}$$

As the pressure at the blade outlet is considered uniform over the whole radius, T_2' is invariable, regardless of the outlet radius. Formula (2.18) shows that the relative outlet velocity, w_2, varies in accordance with the

outlet radius R. Therefore, the outlet temperature, T_2, corresponds to the function of the outlet radius R, and decreases as R decreases (that is, towards the center of the outlet), and becomes higher where R is greater (that is, towards the outside wall). Since T_2 is a complicated function of R, it is difficult to integrate formula (2.26) in the direction of radius. However, since the variation of T_2 becomes the variation of density, the variation of density is comparatively little, even if T_2 changes $40 \sim 50^{\circ}C$ in the direction of radius when the outlet gas temperature ranges from $400 \sim 600^{\circ}C$. The average temperature at the outlet, T_{2m}, can thus be considered uniform, regardless of R so long as the integration is concerned. From the integration of (2.26), the total flow G will be:

$$G = \int_{R_{2i}}^{R_{20}} dG$$

$$= 2\pi\omega\epsilon_2 \frac{\sqrt{1-\psi_2^2}}{3} \cdot \frac{p_2}{R^* T_{2m}} R_{20}^3 \left[\left\{ \left(\frac{a}{R_{20}} \right)^2 - \left(\frac{R_{2i}}{R_{20}} \right)^2 \right\}^{3/2} \right.$$

$$\left. - \left\{ \left(\frac{a}{R_{20}} \right)^2 - 1 \right\}^{3/2} \right] \qquad (2.30)$$

The gas flow at the blade outlet (2.30) must be equal to the gas flow at the blade inlet (2.11). From (2.30) and (2.11), the following formula will be obtained:

$$\frac{B_1}{R_1} = \frac{\epsilon_2}{\epsilon_1} \frac{\sqrt{1-\psi_2^2}}{3} \left(\frac{R_{20}}{R_1} \right)^3 \frac{p_2}{p_0} \cdot \frac{T_0}{T_{2m}} \cdot \frac{1}{\tan\alpha} \times$$

$$\left\{ 1 - \varphi^2 (1-s) \right\} \frac{p_0}{p_1} \left[\left\{ \left(\frac{a}{R_{20}} \right)^2 - \left(\frac{R_{2i}}{R_{20}} \right)^2 \right\}^{3/2} \right.$$

$$\left. - \left\{ \left(\frac{a}{R_{20}} \right)^2 - 1 \right\}^{3/2} \right] \qquad (2.31)$$

And

$$\left(\frac{a}{R_{20}}\right)^2 = \frac{\frac{2\theta}{k-1}\left(\frac{a_0}{U_1}\right)^2 - (1+\psi_1^2)}{\left(\frac{1}{\psi_2^2}-1\right)\left(\frac{R_{20}}{R_1}\right)^2} \tag{2.32}$$

The solution of the outlet average temperature, T_{2m}, will be explained later.

We shall consider the problems of efficiency, and output power. The angular momentum per specific weight at the blade inlet is:

$$\frac{1}{g} c_1 \cos\alpha \cdot R_1 = \frac{U_1 R_1}{g}$$

The angular momentum at the blade outlet equals zero since the gas flows uniformly in the direction of axis. Thus the variation of the angular momentum per second is U_1R_1/g. If the angular velocity is ω, the internal output L_i per specific weight will be:

$$L_i = \frac{U_1 R_1}{g}\omega = \frac{U_1^2}{g} \tag{2.33}$$

And the work of the equal entropy expansion L_{is} from the turbine inlet to the turbine outlet pressure will be:

$$L_{is} = Jc_pT_0(1-s_0) \tag{2.34}$$

Therefore, the internal efficiency η_i will be:

$$\eta_i = \frac{L_i}{L_{is}} = \frac{(k-1)\left(\frac{U_1}{a_0}\right)^2}{1-s_0} \tag{2.35}$$

The actual net output of the shaft must be measured by subtracting the friction loss of the blade disk from the internal output. The friction loss of the disk is generally expressed by the following formula.[13][16]

$$N_f = fD^2u^3\gamma \times 10^{-6} \text{ HP} \tag{2.36}$$

In the above formula, D represents the outside radius, u the circumferential velocity, γ the gas density, and all are expressed in metric units, and f stands for the constant. Accordingly the loss of horse power, L_f, per specific weight is:

$$L_f = \frac{75\ N_f}{G}$$

$$= 4.68 \times 10^{-4} f \frac{1}{q} \cdot \frac{\gamma_1}{\gamma_0} \cdot \frac{U_1}{a_0} \cdot \frac{U_1^2}{g} \tag{2.37}$$

The actual net output, L_e, is:

$$L_e = L_i - L_f$$

$$= \frac{U_1^2}{g}\left(1 - 4.68 \times 10^{-4} f \frac{1}{q} \cdot \frac{\gamma_1}{\gamma_0} \cdot \frac{U_1}{a_0}\right) \tag{2.38}$$

And the net efficiency η_e is:

$$\eta_\epsilon = \frac{L_e}{L_{is}}$$

$$= \eta_i\left(1 - 4.68 \times 10^{-4} f \frac{1}{q} \cdot \frac{\gamma_1}{\gamma_0} \cdot \frac{U_1}{a_0}\right) \tag{2.39}$$

The values of U_1/a_0 and γ_1/γ_0 in the formulas (2.35) and (2.39) are given respectively as follows:

$$\frac{U_1}{a_0} = \frac{c_1 \cos d}{a_0} = \varphi\sqrt{\frac{2}{k-1}} \cos \alpha \cdot \sqrt{1-s} \tag{2.40}$$

$$\frac{\gamma_1}{\gamma_0} = \frac{p_1}{p_0} \cdot \frac{T_0}{T_1} = \frac{p_1}{p_0} \cdot \frac{1}{1-\varphi^2(1-s)} \tag{2.41}$$

If $i_{02}"$ represents the enthalpy at the time of the equal entropy expansion from the turbine inlet conditions to the turbine outlet pressure (see Figure 2.2), and $i_{1'2}"$ the enthalpy at the time of the equal entropy expansion from the point 1' above the blade inlet pressure, p_i, to the turbine outlet pressure, p_2, the reaction r will be:

$$r = \frac{i_{1'2}"}{i_{02}"} \quad \frac{T_{1'} - T_{2}"}{T_0 - T_{2}"} = 1 - \frac{1 - s}{1 - s_0} \tag{2.42}$$

The value of s in (2.31) can be determined by giving the five non-dimensional quantities, viz. $p_0/p_{2'}$ for the total turbine expansion ratio, α, for the average flow angle of the nozzle, and B_1/R_1, R_{20}/R_1, R_{2i}/R_1 for the geometric dimensional ratio. This will determine the expansion ratio p_0/p_1 of the nozzle. The efficiency in this case can be obtained from the formulas (2.35) and (2.39). As (2.12) indicates, the non-dimensional characteristic quantity of the gas flow q is a function of B_1/R_1, α, and s only. It is clear from the definition of the characteristic quantity q in (2.12) that, with the uniform q the turbines maintain similar geometric forms, and give the uniform efficiency and the uniform reaction, even if G, R and the turbine inlet conditions are different.

When the total turbine expansion ratio, p_0/p_2, is given by the above procedures, the efficiency and reaction of turbines with uniform α, B_1/R_1, R_{20}/R_1, R_{2i}/R_1, and their gas-flow characteristic quantity q, can be determined by the use of the velocity coefficient of the nozzle φ, and the velocity coefficient of the blade, ψ_1, ψ_2. At the same time, the relative flow angle β_2 of the turbine outlet can be given by using formula (2.21).

In actual calculation, s in (2.31) cannot be obtained by giving p_0/p_2, α, B_1/R_1, R_{20}/R_1, R_{2i}/R_1, as it is a negative function; instead, B_1/R_1 should be determined by giving s, p_0/p_2, α_1, R_{20}/R_i, R_{2i}/R_i.

2.2.2. Loss Coefficient

The above calculations use the velocity coefficient of the nozzle φ, and the velocity coefficient of the disk f. These values are functions of forms and the Reynolds number, and do not render themselves in simple formulas. It is therefore quite a complex operation to deal with these loss coefficients as functions of forms and Reynolds number. Instead, the average loss coefficient is presumed within the possible ranges of forms and Reynolds numbers in order to seek the maximum efficie cy conditions which will be modified, in actual designing, in accordance with the variations of the loss coefficient.

(a) The velocity coefficient of the nozzle, φ

Much study has been done concerning the velocity coefficient of the nozzle used in axial turbines. According to Flügel,[12] Stodola,[13]

the φ of the axial turbine nozzle ranges between $0.95 \sim 0.97$. No study has been published with regard to the circumferential nozzle used in radial turbines. In general, the φ of the radial turbine nozzle ranges between $0.95 \sim 0.98$, which will be further described in Chapter 3.

It is difficult to generalize the varieties of form that are taken by the loss of the spiral chamber from the turbine inlet to the nozzle inlet. O.E. Balje(2) gives the loss in the following formula:

$$\text{Loss} = q_{sc} \frac{U_1^2}{g}$$

The value ranging between $0.02 \sim 0.06$ is given to q_{sc} by Balje. If φ_1 is the velocity coefficient incurred by the loss of the nozzle only, the total loss from the turbine inlet to the nozzle outlet will be as follows:

$$\frac{c_1'^2}{2g} - \frac{c_1^2}{2g} = (1 - \varphi_1^2) \frac{c_1'^2}{2g} + q_{sc} \frac{U_1^2}{g}$$

$$\fallingdotseq (1 - \varphi_1^2 + q_{sc}) \frac{c_1'^2}{2g}$$

$$(\because c_1' \fallingdotseq U_1)$$

If φ is the velocity coefficient incurred by the total loss, including the loss of the spiral chamber and the nozzle,

$$\frac{c_1'^2}{2g} - \frac{c_1^2}{2g} = (1 - \varphi^2) \frac{c_1'^2}{2g}$$

Therefore,

$$\varphi^2 = \varphi_1^2 - q_{sc} \tag{2.43}$$

Since $\varphi_1 = 0.95 \sim 0.98$, and $q_{sc} = 0.02 \sim 0.06$, the value of φ will be $0.97 \sim 0.92$. The following calculation is made with reference to the cases in which $\varphi = 0.95$, and $\varphi = 0.93$.

(b) The velocity coefficient of the blade

No study has been published with regard to the velocity coefficient of the blade used in radial turbines, except the results of the author's experiments with test radial turbines, which will be treated in detail in Chapter 5. The following describes the results of the study of vanes used in conventional axial turbines.

Emmert[14] gives the loss of vanes used in recent gas turbines in the following formula:

$$\frac{w_2^2}{2g} = \Phi_E^2 \left(i_{12}' + c_1 \Phi_v^2 \frac{w_1^2}{2g} \right) \tag{2.44}$$

In the above formula,

Φ_E^2 = expansion energy coefficient

c_1 = incidence coefficient

Φ_v^2 = kinetic energy coefficient.

Since $\Phi_E^2 = \Phi_v^2$, ψ_1 and ψ_2 in (2.14.2) can be obtained:

$$\left.\begin{aligned} \psi_1^2 &= c_1 \Phi_v^2 \\ \psi_2^2 &= \Phi_E^2 \end{aligned}\right\} \tag{2.45}$$

The value of Φ_E^2 varies according to the angle of the curvature. When the angle is 90°, $\Phi_E^2 = 0.90 \sim 0.93$. The incidence coefficient $c_1 = 1$, when there is no collision in the passage to the blade. Accordingly, if $\Phi_E^2 = 0.90$, $\psi_1 = \psi_2 = 0.95$, and if $\Phi_E^2 = 0.93$, $\psi_1 = \psi_2 = 0.96$.

Ainley[15] expresses below the loss of axial vanes in gas turbines after experimenting with straight vanes in wind-tunnel tests.

$$\text{Total Loss} = \zeta \frac{w_2^2}{2g} \tag{2.46}$$

When the angle of curvature is 90°, $\zeta = 0.07 \sim 0.12$. If $\zeta = 0.12$, $\psi_1 = 0.97$, and $\psi_2 = 0.97$.

Stodola[13] gives ζ the value of 0.36, when the angle is 90°. In this case, $\psi_1 = 0.91$, and $\psi_2 = 0.92$.

A study of the blade used in radial turbines shows that the flow moves first in the direction of the radii; when given the curvature of 90° in the blade, it moves towards the axial line; and finally it is curved by the exducer to form an almost rectangular movement against the axial line. In other words, there are two large curvatures. The loss will be greater when compared with the vanes used in the axial turbine that has only one near-rectangular curvature. However, the loss coefficient of the blade inlet is almost equal to that used in the axial turbine, and ψ_2 will be worse than the latter. The result obtained from the author's experimental radial turbines shows that

$$\psi_1 = 1.0, \qquad \psi_2 = 0.78 \sim 0.79.$$

Calculation will therefore be made with reference to the cases in which $\psi_1 = 1.0$, $\psi_2 = 0.92$ for small losses, and $\psi_1 = 0.95$, $\psi_2 = 0.85$ for great losses.

(c) Friction loss of disk

As for the friction loss of disk, Stodola[13] and Pfleiderer[16] give the formula (2.36). The value of f in the formula varies according to the gap between the disk and the outside wall, the form of the disk and the Reynolds number. Stodola gives $f = 1.1 \sim 1.2$, whereas Pfleiderer gives $f = 1.0$, when the disk adjoins the outside wall. Accordingly the following calculation is done with the presumption that $f = 1.0$.

2.2.3. Conditions for the Maximum Efficiency

Both the internal efficiency and the net efficiency of the radial turbine is given in (2.35) and (2.39) respectively. In (2.39) the effect of the disk friction loss, expressed in the second row of the equation, ranges between $0.02 \sim 0.03$. When the total expansion ratio p_0/p_2 of the turbine is fixed, the internal efficiency, η_i, remains as a function of U_1/a_0 only, and it increases in proportion to the value of U_1/a_0, which when the average flow angle of the nozzle is fixed, increases as s becomes smaller. In other words, the smaller the value of p_1/p_2, and the smaller the value of the reaction r, the greater the value of U_1/a_0. Accordingly, the internal efficiency η_i increases as r decreases when p_0/p_2 and α are fixed.

The next step is to change the reaction r, by changing B_1/R_1 while the values of p_0/p_2, α, R_{20}/R_1, and R_{2i}/R_1 remain fixed. The change of the internal efficiency under such circumstances is shown in

Figures 2.5 and 2.6. As indicated on top of the figures, both are under conditions $p_0/p_2 = 1.2$, $R_{20}/R_1 = 0.6$, $R_{2i}/R = 0.3$, with Figure 2.5 showing a smaller loss when $\varphi = 0.95, \psi_1 = 1.0, \psi_2 = 0.92$, and Figure 2.6 showing a greater loss when $\varphi = 0.93, \psi_1 = 0.95, \psi_2 = 0.85$.

When α is fixed, r decreases and η_i increases gradually as B_1/R_1 becomes smaller. When r reaches below a certain value, the expressions within the square root in (2.21), (2.23) and (2.26) become negative. The reaction cannot be reduced below the reaction that occurs at the moment when the expression within the square root changes from the positive to the negative. At such a moment, η_i reaches its maximum value. Figure 2.7 shows the velocity distribution at the blade outlet towards the radius, when $\alpha = 20^\circ$, and B_1/R_1 and r are reduced gradually.

It will be observed that the velocity distribution takes the form of curve 1 when both B_1/R_1 and reaction have a greater value, while it takes the form of curve 3 with c_2 and β_2 approaching 0 if we reduce the value of B_1/R_1 and reaction to 0.047 and 0.426 respectively. A further reduction of B_1/R_1 and r will result in counter current because of the negative expression within the square root of (2.21), (2.23), and (2.26). Accordingly, the curve 3 shows the possible maximum efficiency when $\alpha = 20^\circ$, as this is the case in which the blade loss and leaving loss of the turbine stand at the minimum.

Figure 2.8 shows the difference between internal efficiency and net efficiency. As the values of B_1/R_1 and reaction become greater, the disk friction will have less influence upon efficiency, and vice versa. At a maximum, however, the values of B_1/R_1 and r remains the same for both η_i and η_e. Accordingly both internal and net efficiencies reach the maximum under the same condition.

Since the maximum efficiency will be obtained when $\beta_2 = 0$ in the outside radius of the blade outlet, that is, when the expression with the square root form in (2.21) equals 0, the following formula will follow when $R = R_{20}$, and $\beta_2 = 0$ in (2.21):

$$\left(\frac{R_1}{R_{20}}\right)^2 \left\{ \frac{2\theta}{k-1} \left(\frac{a_0}{U_1}\right)^2 - (1 + \psi_1^2) \right\} - \left(\frac{1}{\psi_2^2} - 1\right) = 0 \qquad (2.47)$$

This may be re-expressed as:

$$\left(\frac{U_1}{a_0}\right)^2 = \frac{\frac{2\theta}{k-1}}{(1+\psi_1^2) + \left(\frac{1}{\psi_2^2} - 1\right)\left(\frac{R_{20}}{R_1}\right)^2} \qquad (2.47.1)$$

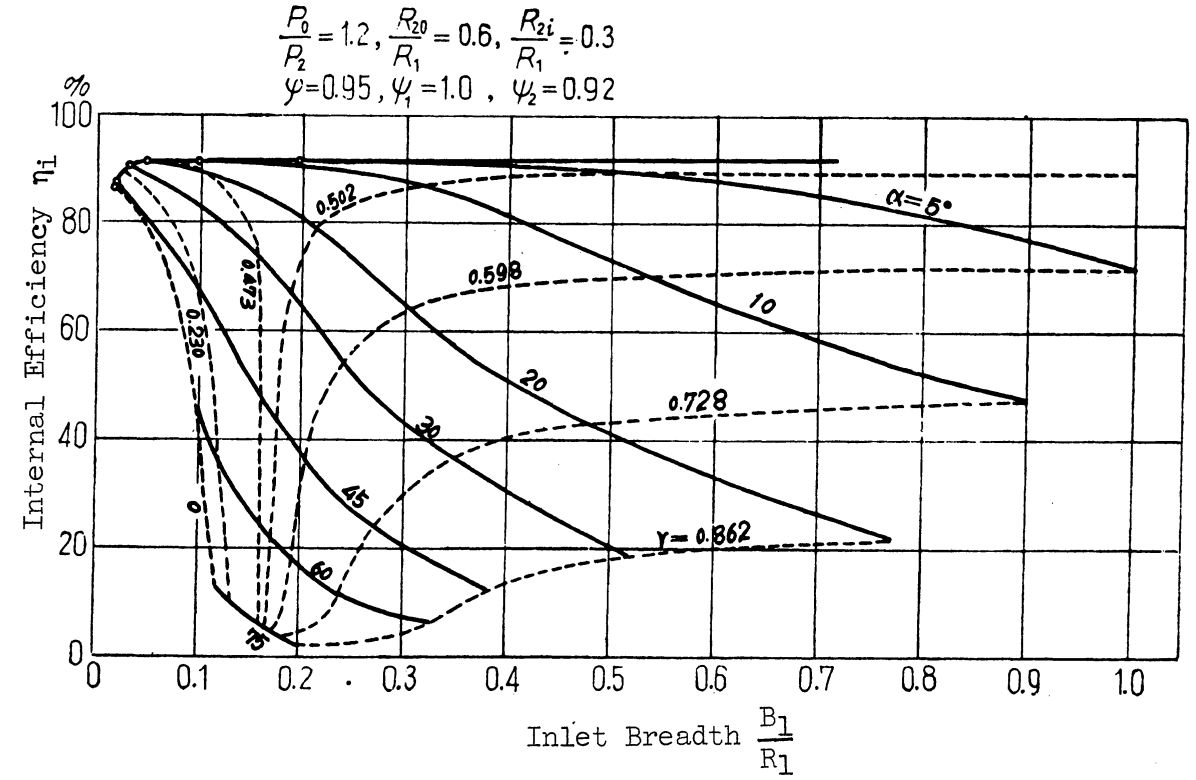

Figure 2.5. Internal Efficiency.

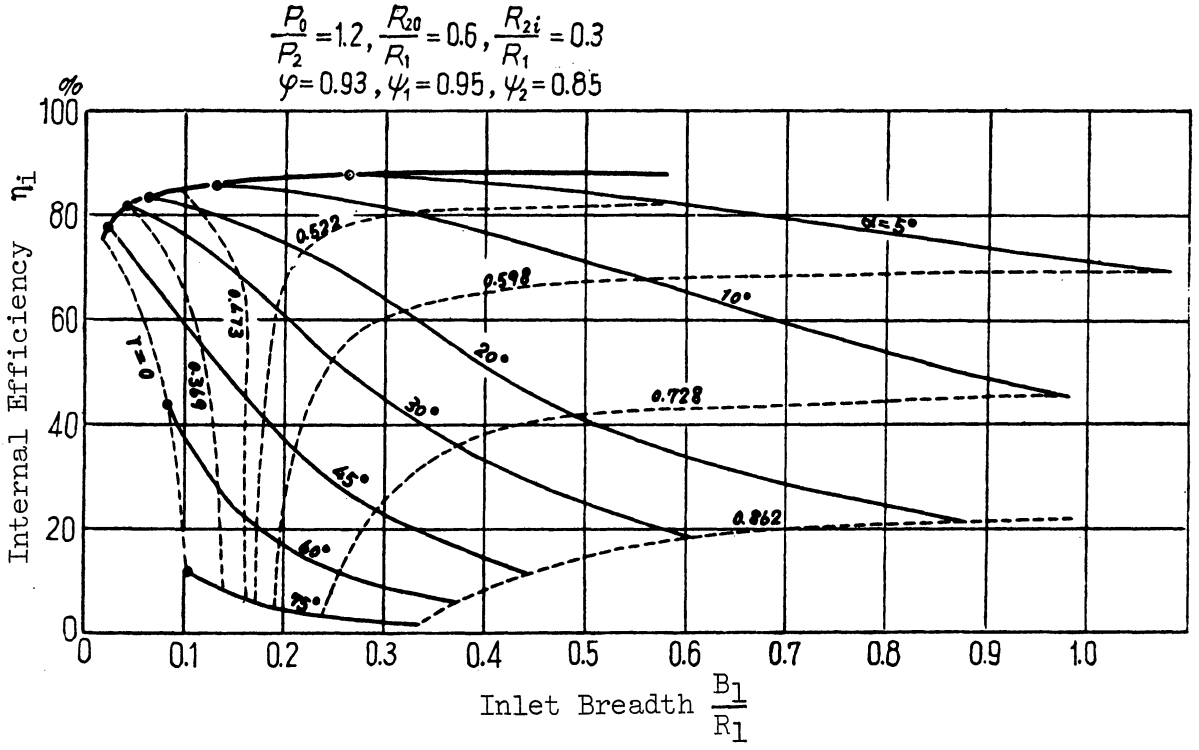

Figure 2.6. Internal Efficiency.

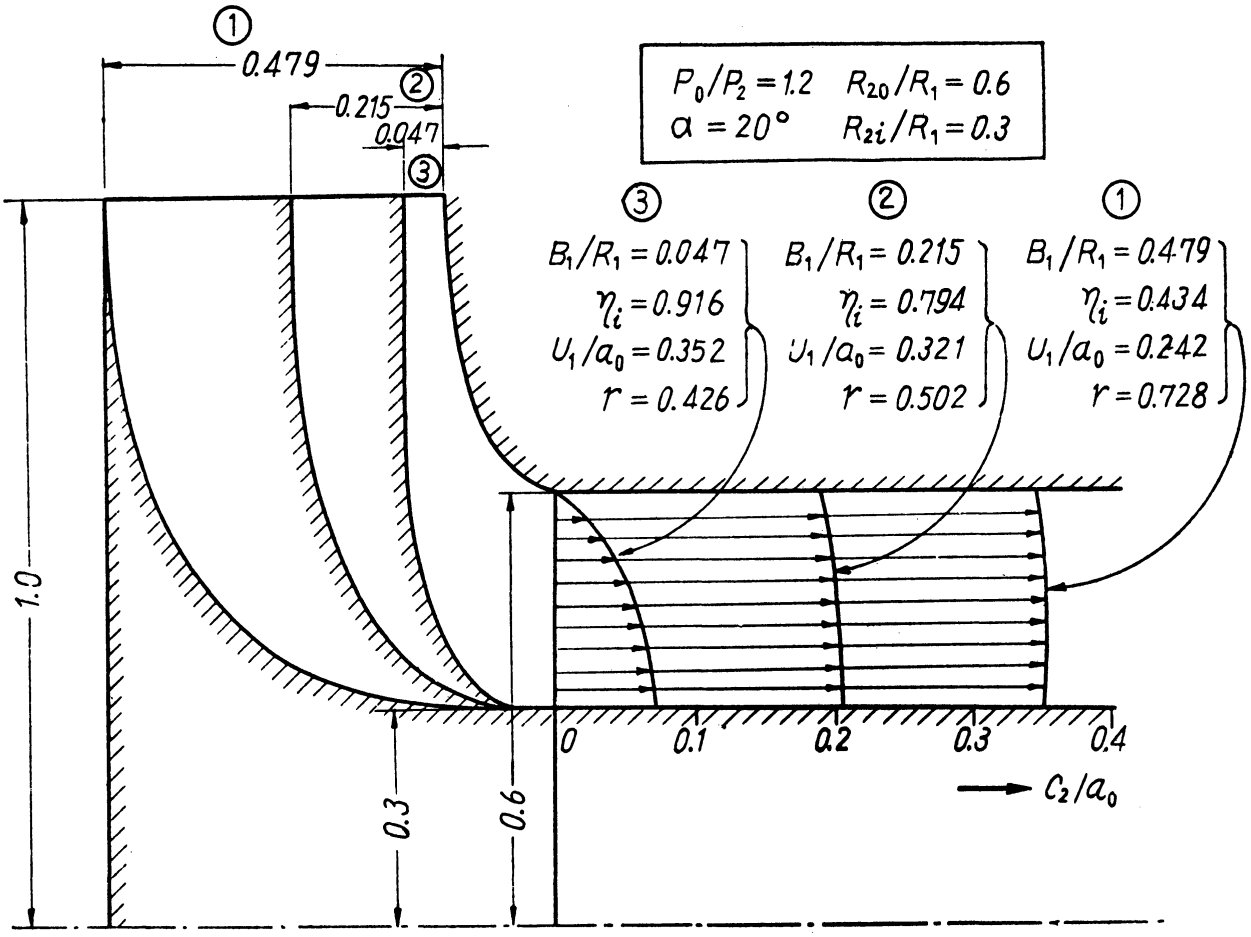

Figure 2.7. Outlet Velocity Distribution.

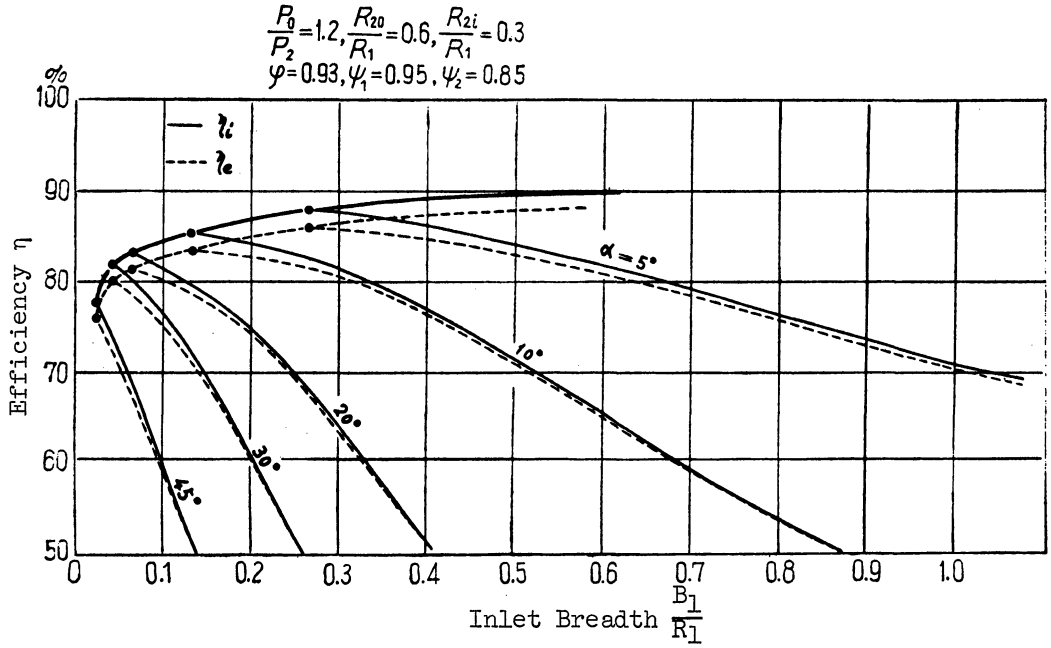

Figure 2.8. Internal Efficiency and Net Efficiency.

Accordingly, from (2.47) and (2.23), it will be clear that,

$$\left(\frac{a}{R_{20}}\right)^2 - 1 = 0 \tag{2.48}$$

under which condition the efficiency reaches its maximum. Substituting the expressions of (2.48) with that of (2.31),

$$\frac{B_1}{R_1} = \frac{\epsilon_2}{\epsilon_1}\frac{\sqrt{1-\psi_2^2}}{3} \cdot \frac{p_2}{p_0} \cdot \frac{T_0}{T_{2m}} \cdot \frac{1}{\tan\alpha} \quad x$$

$$\left\{1-\varphi^2(1-s)\right\} \frac{p_0}{p_1}\left\{\left(\frac{R_{20}}{R_1}\right)^2 - \left(\frac{R_{2i}}{R_1}\right)^2\right\}^{3/2} \tag{2.49}$$

Substituting again the expression of (2.19) and (2.40) with that of (2.47),

$$\cos^2\alpha = \frac{1}{\varphi^2\left\{\left(\frac{1}{\psi_2^2}-1\right)\left(\frac{R_{20}}{R_1}\right)^2 + (1+\psi_1^2)\right\}} \quad x$$

$$\left[\frac{1}{1-s} - \varphi^2(1-\psi_1^2) - s_0\left\{\frac{1}{s(1-s)} - \frac{\varphi^2}{s}\right\}\right] \tag{2.50}$$

By eliminating s from (2.49) and (2.50), the relation among R_{20}/R_1, R_{2i}/R_1, B_1/R_1, and α will be made clear when the maximum efficiency is obtained. Conversely, the value of s will be determined by clarifying R_{20}/R_1, B_1/R_1, R_{2i}/R_1, and α. With the value of s made clear, it is possible to determine the value of U_1/a_0 from (2.40), that of q from (2.13), that of η_i from (2.35), that of η_e from (2.39) and that of r from (2.42). The curve indicating η_i and η_e thus obtained will be the line connecting the maximum efficiency points in the Figures 2.5, 2.6, and 2.8.

From (2.21) and (2.47), the relative flow angle β_2 at the blade outlet will be:

$$\tan \beta_2 = \sqrt{1 - \psi_2^2} \Big/ \sqrt{\left(\frac{R_{20}}{R}\right)^2 - 1} \tag{2.51}$$

In order to compute from (2.49), the average outlet temperature T_{2m} must be first obtained as described below. Even though a greater efficiency is obtained with a smaller inside radius, R_{2i}/R_1, of the outlet, the geometrical dimensions of the exducer and its fittings make it impossible to reduce the inside radius beyond a certain limit. In general, $R_{2i}/R_1 = 0.1$, which means that the circumferential velocity at the inside radius of the outlet is considerably smaller than that of the inlet. By eliminating U_2 from (2.18),

$$\frac{2\theta}{k - 1} = \frac{1}{\psi_2^2}\left(\frac{w_{2i}}{a_0}\right)^2 + (1 + \psi_1^2)\left(\frac{U_1}{a_0}\right)^2 \tag{2.18.1}$$

The relative velocity w_{2i} at the inside radius of the outlet will be thus obtained from (2.18.1) and (2.47):

$$w_{2i} = \sqrt{1 - \psi_2^2} \cdot \frac{R_{20}}{R_1} U_1 \tag{2.52}$$

The relative velocity w_{20} at the outside diameter of the outlet will also be obtained from (2.18):

$$w_{20} = \frac{R_{20}}{R_1} U_1 \tag{2.53}$$

From (2.29), the gas temperature, T_{2i}, at the inside radius of the outlet, and the gas temperature, T_{20}, at the outside radius of the outlet will be obtained respectively from (2.29),

$$\left.\begin{aligned} Jc_p\,(T_{2i} - T_2') &= (1 - \psi_1^2)\,\frac{w_1^2}{2g} + \left(\frac{1}{\psi_2^2} - 1\right)\frac{w_{2i}^2}{2g} \\ Jc_p\,(T_{20} - T_2') &= (1 - \psi_1^2)\,\frac{w_1^2}{2g} + \left(\frac{1}{\psi_2^2} - 1\right)\frac{w_{20}^2}{2g} \end{aligned}\right\} \tag{2.54}$$

By substituting the above formula with (2.52) and (2.53), the average outlet temperature, T_{2m} will be obtained:

$$T_{2m} = \frac{T_{20} + T_{2i}}{2}$$

$$\left.\begin{aligned} \frac{T_{2m}}{T_0} = \frac{T_2'}{T_0} + \frac{k-1}{2}\Bigg[(1-\psi_1^2)\tan^2\alpha \\ + \frac{(1-\psi_2^2)(2-\psi_2^2)}{2\psi_2^2}\left(\frac{R_{20}}{R_1}\right)^2\Bigg]\left(\frac{U_1}{a_0}\right)^2 \end{aligned}\right\} \qquad (2.55)$$

T_{2m}/T_0 will equal T_2'/T_0 when no loss occurs in the blade, that is, when $\psi_1 = 1$, $\psi_2 = 1$, in the above formula.

$$\frac{T_2'}{T_0} = \frac{T_1}{T_0} \cdot \frac{T_2'}{T_1} = \frac{1-\varphi^2(1-s)}{s} s_0 \qquad (2.56)$$

Accordingly, when the values of α, p_0/p_1, R_{20}/R_1, are given in both (2.55) and (2.56), T_{2m}/T_0 can be obtained.

Figure 2.9 shows the net efficiency, η_e, with R_{2i}/R_1 as parameter, and when $p_0/p_2 = 1.2$, $R_{20}/R_1 = 0.7$ ($\varphi = 0.93$, $\psi_1 = 0.95$, $\psi_2 = 0.85$). The dotted line in Figure 2.9 indicates the envelope of the group of curved lines with R_{2i}/R_1 as parameter, that is, the maximum efficiency to be obtained when $R_{20}/R_1 = 0.7$. R_{2i}/R_1, q, α, r, and U_1/a_0 can thus be calculated from the above-expressed formulas with reference to each point contained in the envelope. η_e, R_{2i}/R, q, α, r, and U_1/a_0 for the maximum efficiency can be obtained likewise with different values of R_{20}/R_1. The group of curved lines giving the obtainable maximum efficiency with reference to every different value of R_{20}/R_1, is shown in Figure 2.10, using the axis of abscissa for the gas flow characteristic quantity q.

The real lines in Figure 2.10 use R_{20}/R_1 while the dotted lines use R_{2i}/R_1 as parameters respectively. It will be known from the figure that the smaller the value of R_{2i}/R_1, that is, the smaller the axial radius of the blade outlet, the greater will be the efficiency. For, as shown in (2.14.2), the relative velocity of the flow, w_2, is greater in the outside radius than in the inside radius, and since the blade loss is directly proportional to w_2^2, the loss is far smaller in the inside radius than in the outside radius. This means that the gas flow in the inside radius produces greater work and higher efficiency than that in the outside radius. Accordingly, the enlargement of the inside radius of the outlet results in the disuse of the most efficient part of the radial turbine that obtains its maximum efficiency by concentrating the gas flow into

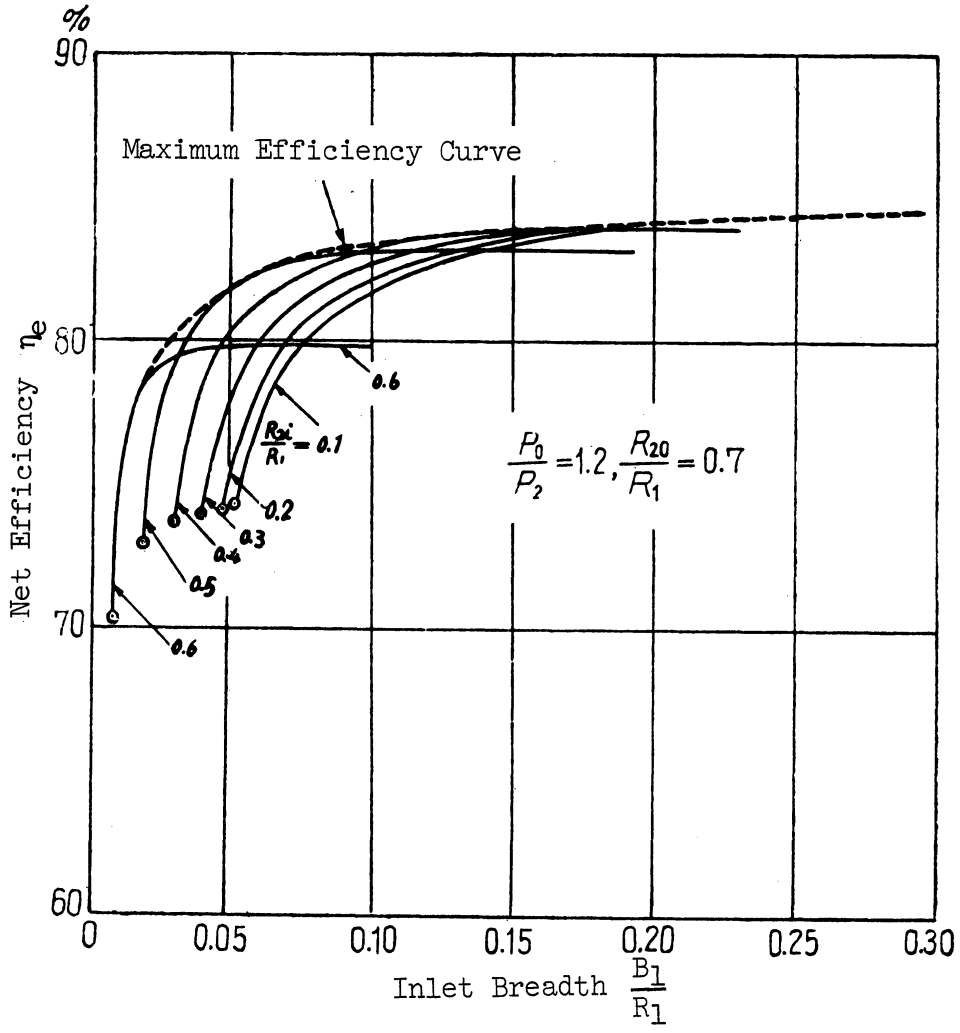

Figure 2.9.

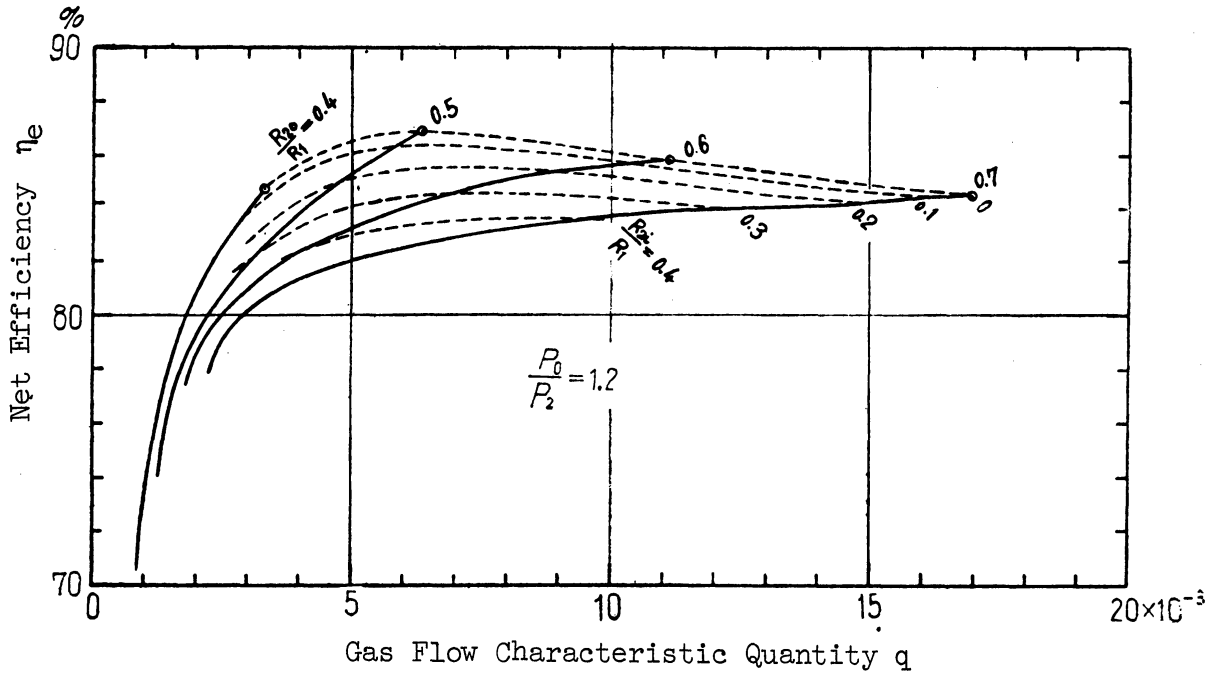

Figure 2.10. Maximum Net Efficiency.

the inside radius, and by preventing as much as possible the gas from flowing into the outside radius. The axial flow velocity distribution of the turbine outlet will therefore take the form as indicated by the curved line (3) in Figure 2.7.

Figure 2.10 indicates that the maximum efficiency will be obtained, and the net efficiency, η_e, equals (ranges between) 85 87%, when $R_{2i}/R_1 = 0.1$ and $q = (4 \sim 10) \times 10^{-3}$. This confirms the existence of the most suitable gas flow characteristic quantity, q, to indicate the maximum efficiency, when the total expansion ratio of the turbine is given, and the minimum R_{2i}/R_1 is used.

It will be clear from (2.12) that the gas flow characteristic quantity, q, diminishes as the blade outside radius, R_1, becomes larger, when the gas flow, G, the temperature and the pressure of the gas are given. Though it is characteristic of q to increase, it is better from the point of view of efficiency to reduce q while enlarging R_1. The q will also increase as the gas flow increases, and thereby reduce the efficiency. Consequently the radial turbine will have a better and greater efficiency with a small gas flow than with a large gas flow. In other words, the smaller the specific speed, the greater the efficiency.

The values of B_1/R_1, α, U_1/a_0, and r, corresponding to each curved line of Figure 2.10, are shown in Figures 2.11, 2.12, 2.13, and 2.14. By using these diagrams (2.11 - 2.14), the values of q, R_{20}/R_1, R_{2i}/R_1, B_1/R_1, α, U_1/a_0, γ, will be obtained when the gas flow, inlet gas temperature, inlet and outlet gas pressures are given. From (2.12), it will be understood that the clarification of q leads to determine G, T_0, p_0, which in turn will determine the principal dimensions of the turbine, viz. R_{20}, R_{2i}, and B_1, and the number of revolutions.

Applying the same procedure to the case when $P_0/P_2 = 2.5$, the result will take the forms as illustrated in Figures 2.15 - 2.19. As shown in Figure 2.15, when q is less than 3×10^{-3}, the expansion ratio of the nozzle becomes greater than the limited expansion ratio, in which case a special consideration will be required.

2.2.4. The Size of the Turbine Giving the Maximum Efficiency and the Number of Its Revolutions

Figures 2.10 and 2.15 show that, when the total expansion ratio p_0/p_2 of the turbine is given, a greater efficiency can be obtained by diminishing the outlet axial radius, R_{2i}/R_1, of the turbine blade. Since an exducer must be attached to the axial radius, its minimum dimensions will be determined by the geometrical form of the exducer and by the problems of its operation. In general, 0.1 is the limit of R_{2i}/R_1, and it is very difficult to reduce it further. The existence of the gas-flow characteristic quantity, q, giving the maximum efficiency will thus be confirmed by giving the total expansion ratio of the turbine and its R_{2i}/R_1.

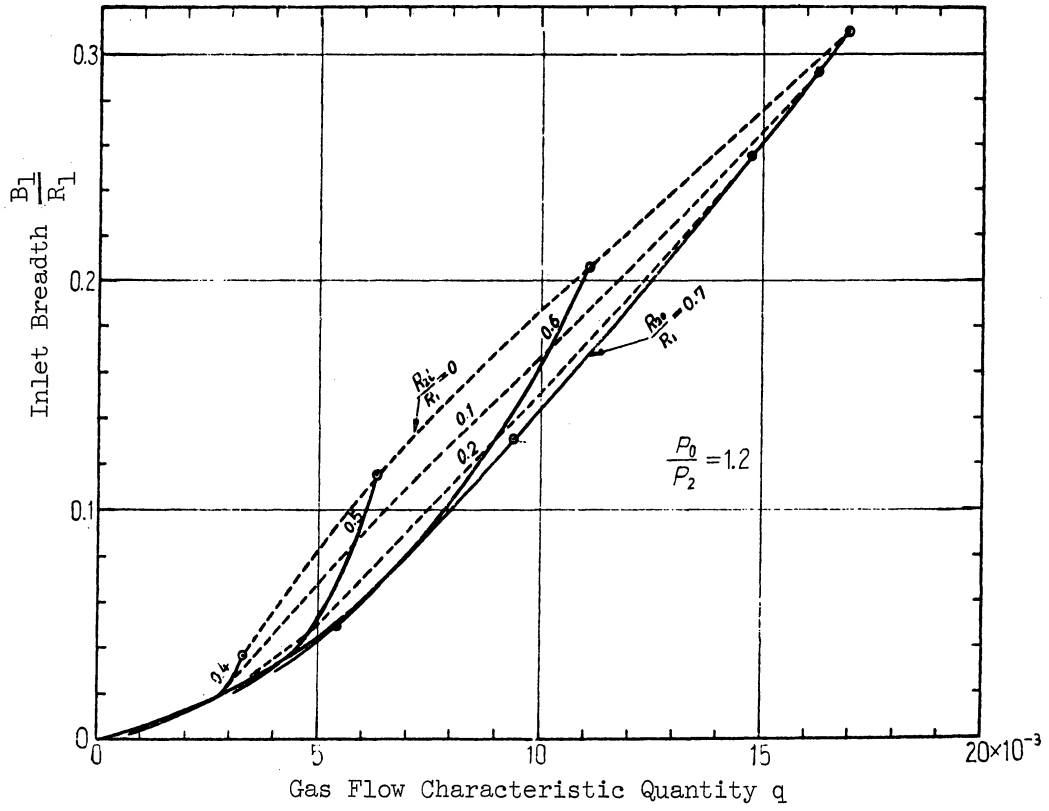

Figure 2.11. Blade Inlet Breadth.

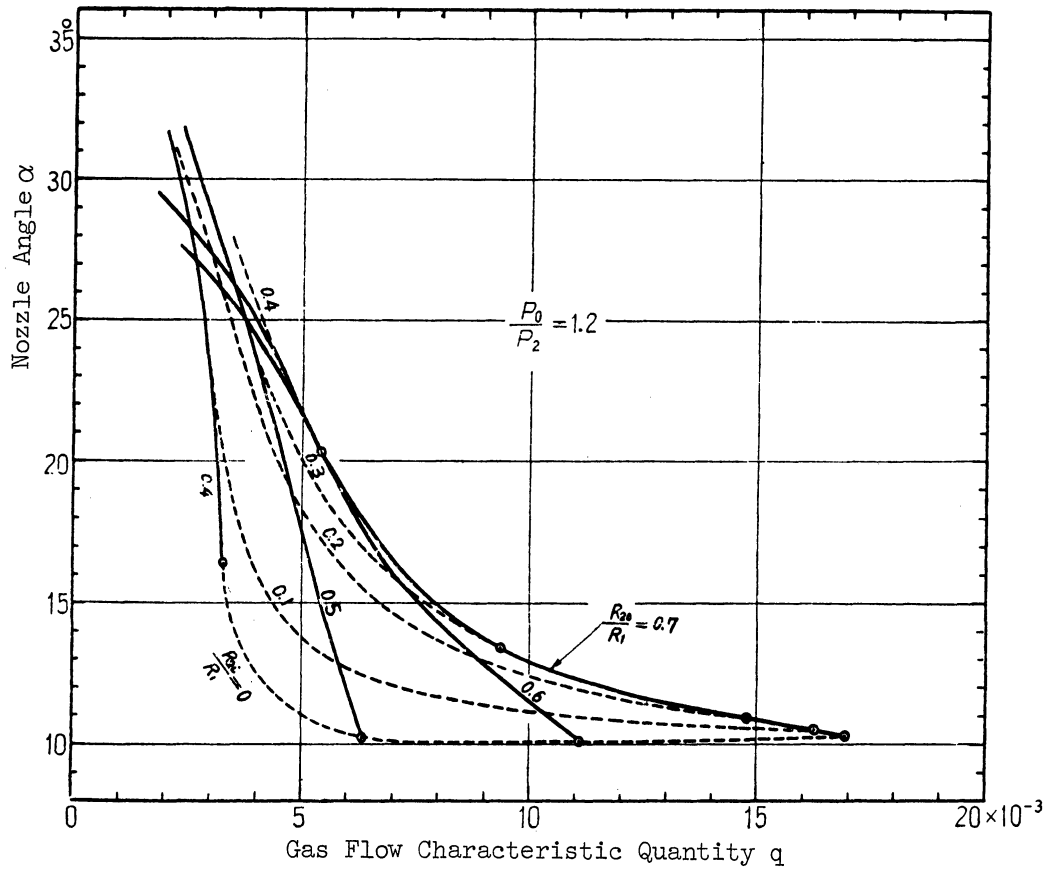

Figure 2.12. Nozzle Angle.

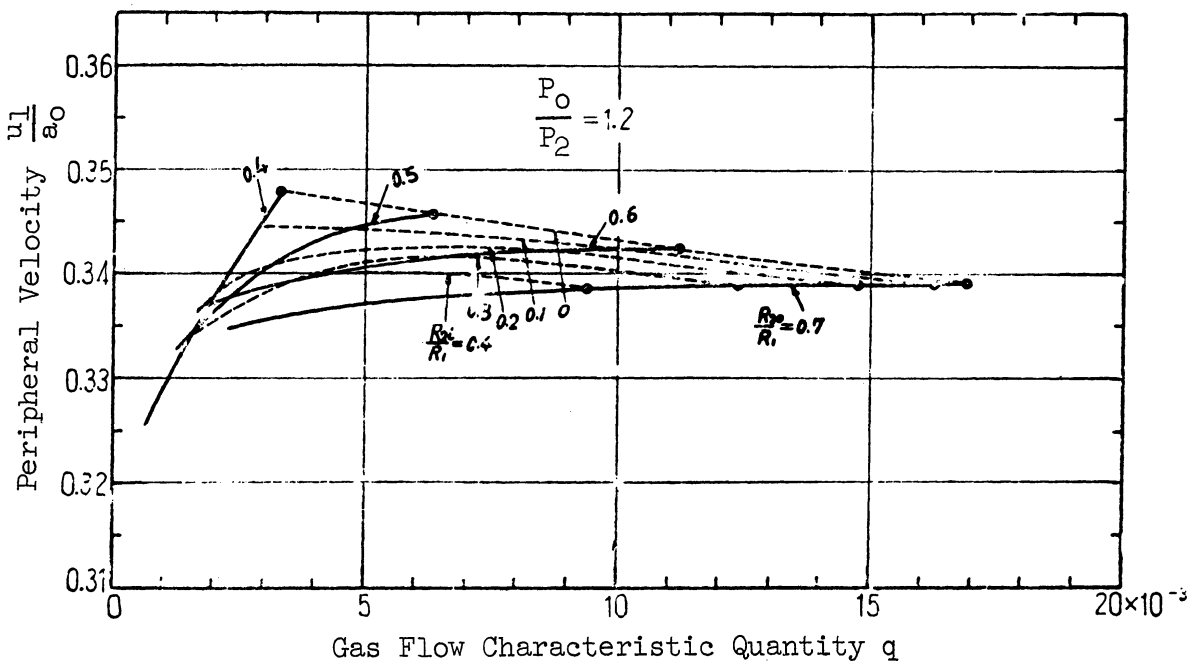

Figure 2.13. Peripheral Velocity.

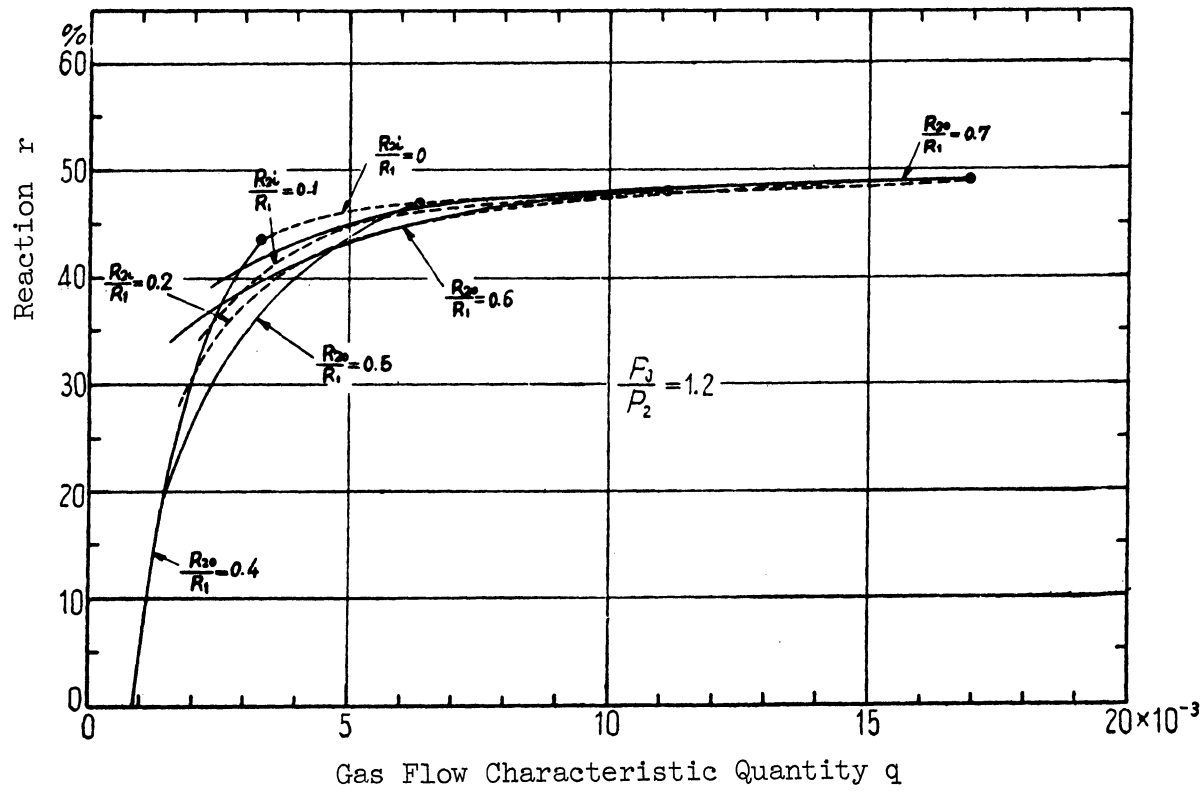

Figure 2.14. Reaction.

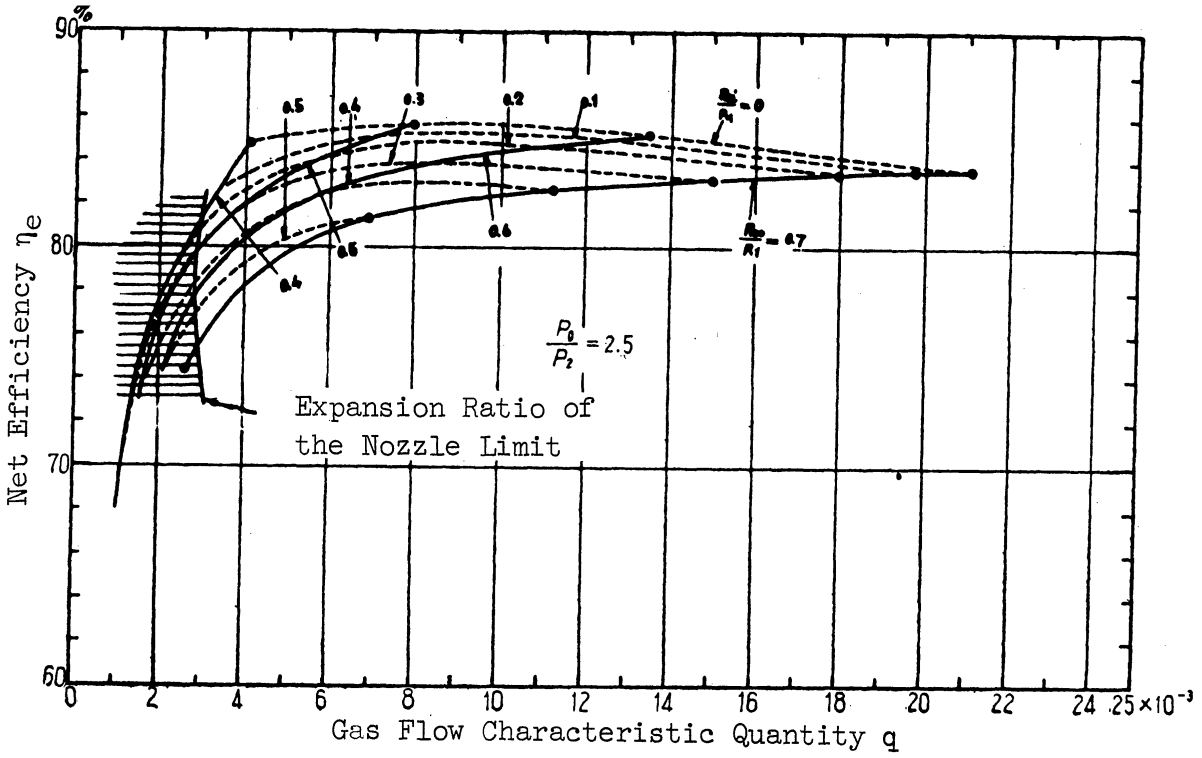

Figure 2.15.

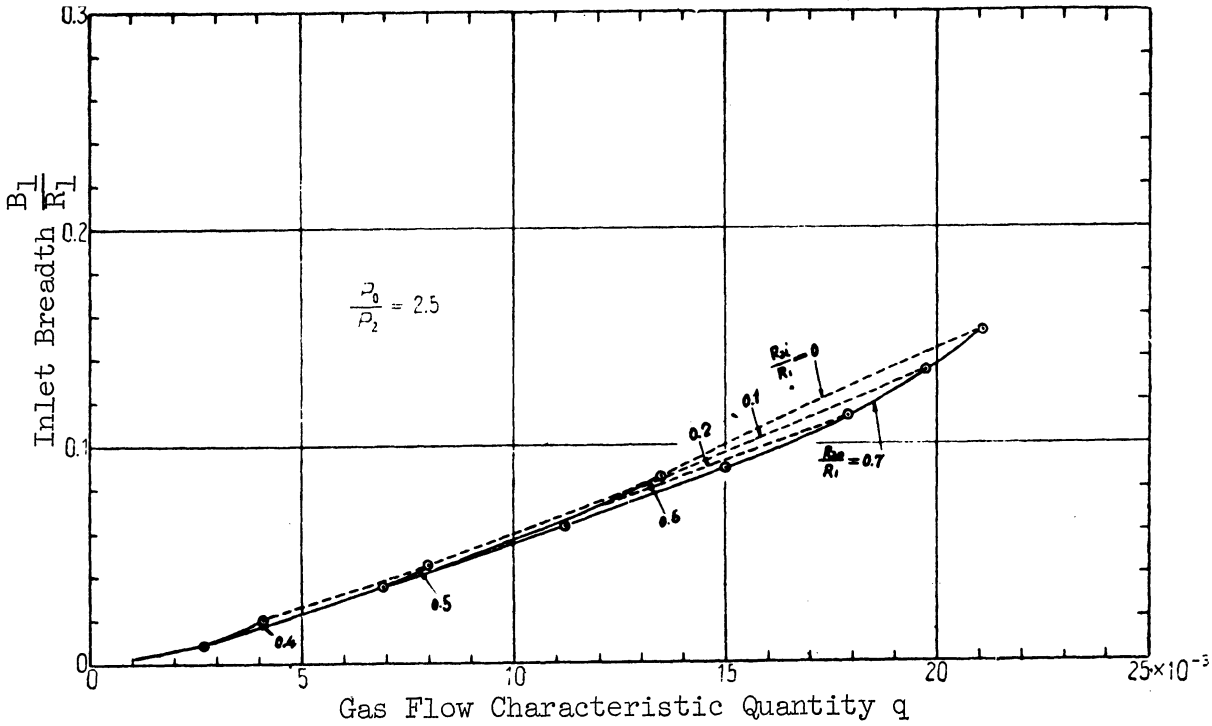

Figure 2.16.

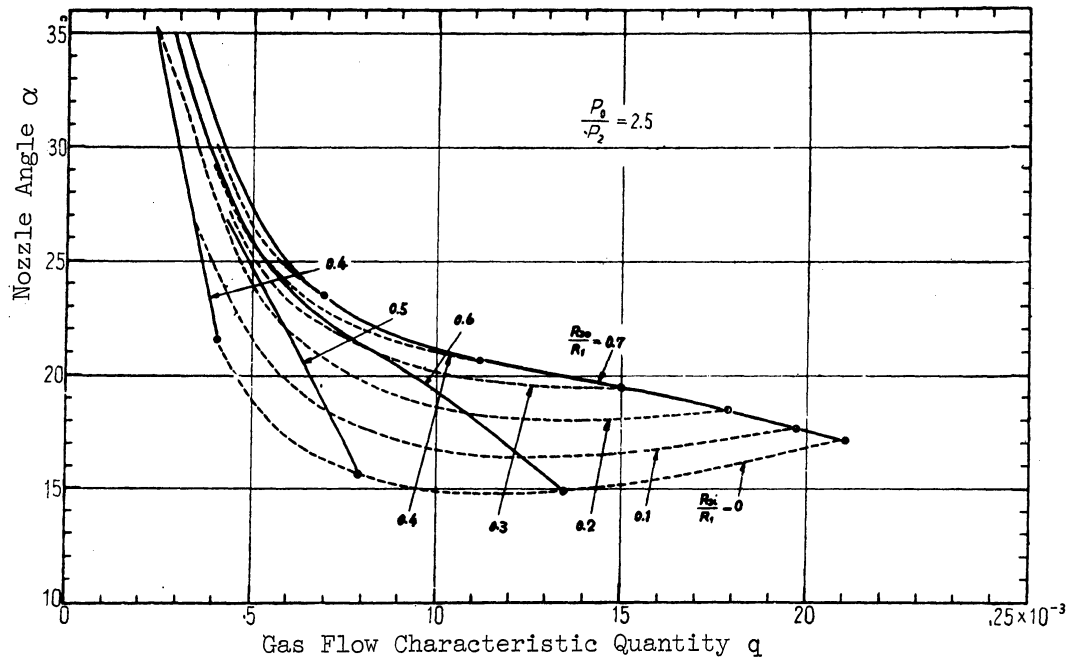

Figure 2.17.

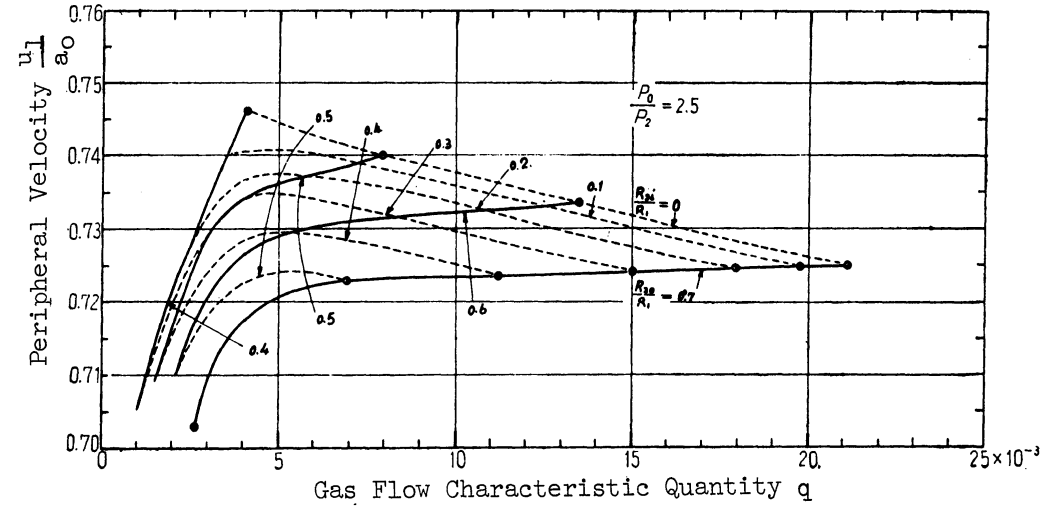

Figure 2.18.

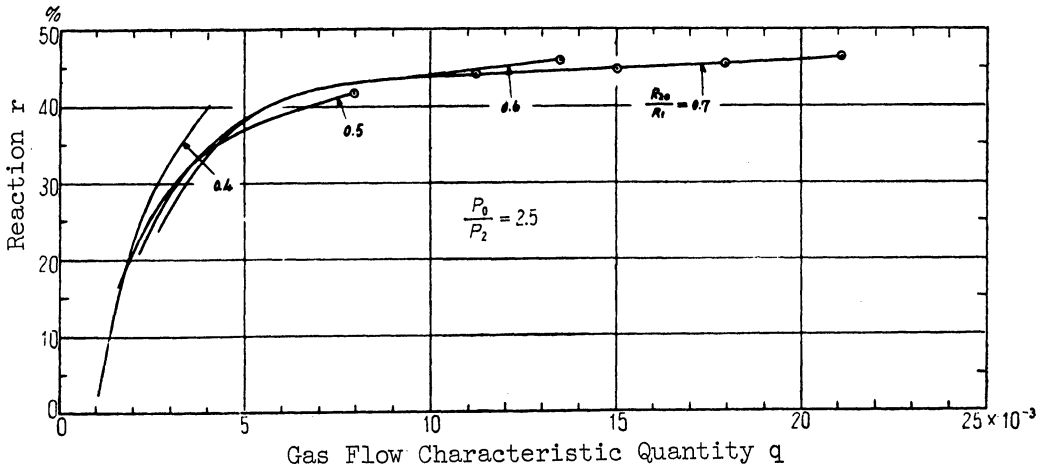

Figure 2.19.

By thus determining the value of the most suitable q, the blade outside radius, R_1, will be clarified from (2.12) when the gas flow and the conditions of the gas at the turbine inlet are given. Figure 2.20 shows the correlation between the turbine expansion ratio and the gas-flow characteristic quantity, q, giving the maximum efficiency. The value of q increases slightly as the total expansion ratio increases. Accordingly it will be clear from (2.12) that the blade radius becomes smaller as the expansion ratio becomes greater. It is difficult to design a turbine with a great blade radius because of the intensity that is due to the general tendency of the radial turbine towards a great number of revolutions and the great quantity of gas flow. It is desirable, therefore, to design a turbine in such a way that its expansion ratio increases and at the same time its gas flow diminishes. This confirms the theory that the radial turbine is most efficient when it has high expansion ratio, small gas flow, and small specific speed.

The efficiency under such conditions is shown in Figure 2.21, with Figures 2.22 - 2.25 illustrating R_{20}/R_1, B_1/R_1, γ, U_1/a_0. The blade inlet breadth, B_1/R_1, becomes narrower with the increase of the turbine expansion ratio, whereas the blade-outlet outside-radius, R_{20}/R_1, increases slightly with the expansion ratio, and falls within the range of 0.50 0.55. The most suitable reaction, r, approximates to $0.43 \sim 0.48$ with any expansion ratio. The circumferential velocity, U_1/a_0, increases with the expansion ratio. The increase of the expansion ratio will thus result in the diminution of the blade outside radius, and the subsequent increase of the circumferential velocity will produce an extremely great number of revolutions. A high gas temperature at the turbine inlet also results in the increase of the sound velocity, a_0. This means that the value of U_1 increases while U_1/a_0 remains the same. Consequently, the circumferential velocity and the number of revolutions will increase with the rise of the gas temperature.

The conditions under which the maximum efficiency is to be obtained are thus determined by procedures as described above. Figures 2.26, 2.27, 2.28, and 2.29 show the blade radius and the number of revolutions to be required with the gas temperature set at 650°C and 800°C respectively, and the parameter being the net output of the turbine.

From Figures 2.26 - 2.29, it will be clear that with the large output gas turbine, the number of revolutions is low, and the blade radius large, whereas with the small gas turbine, the number of revolutions high, and the blade radius small. Figure 2.30 shows the circumferential velocity at the temperatures of 650°C and 800°C respectively.

2.2.5. Examples of Numerical Solutions

We will now apply the above-described procedures for designing a radial turbine with straight vanes to an exhaust turbine with the following principal dimensions:

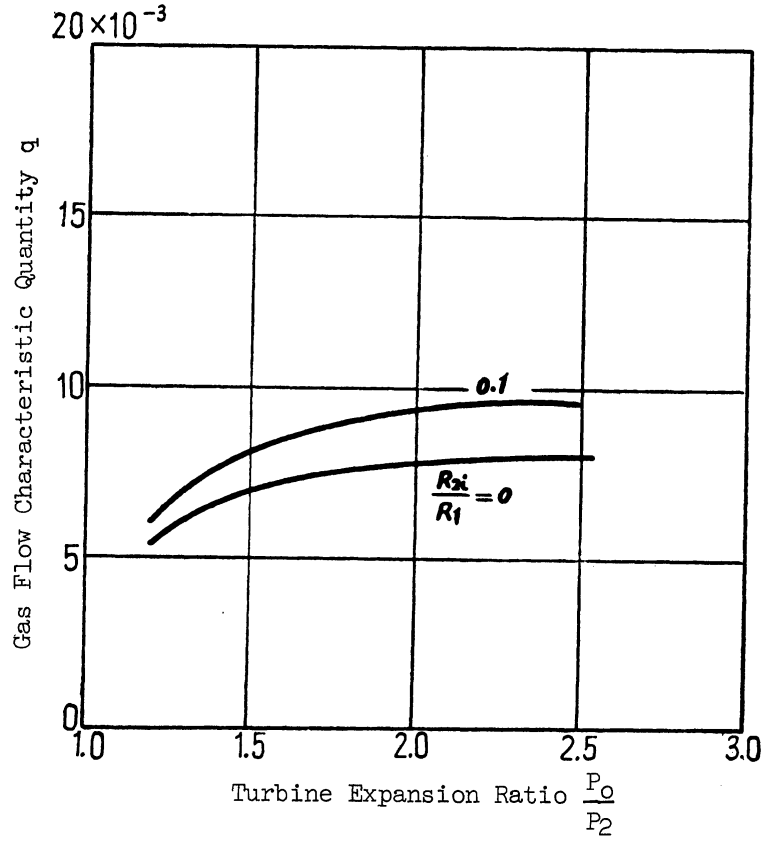

Figure 2.20. The Value of q Giving the Maximum Efficiency.

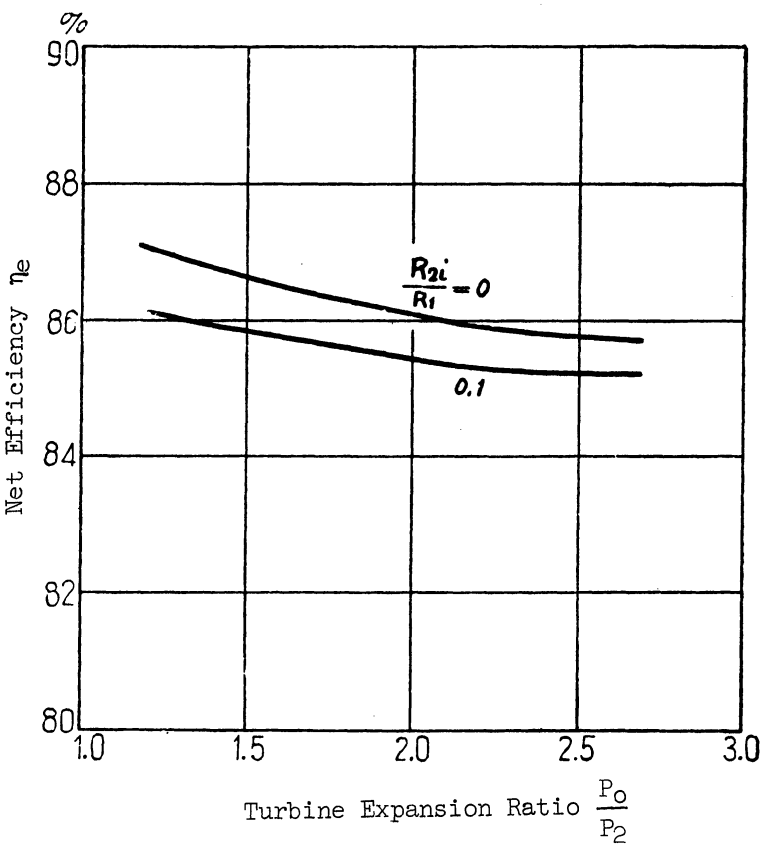

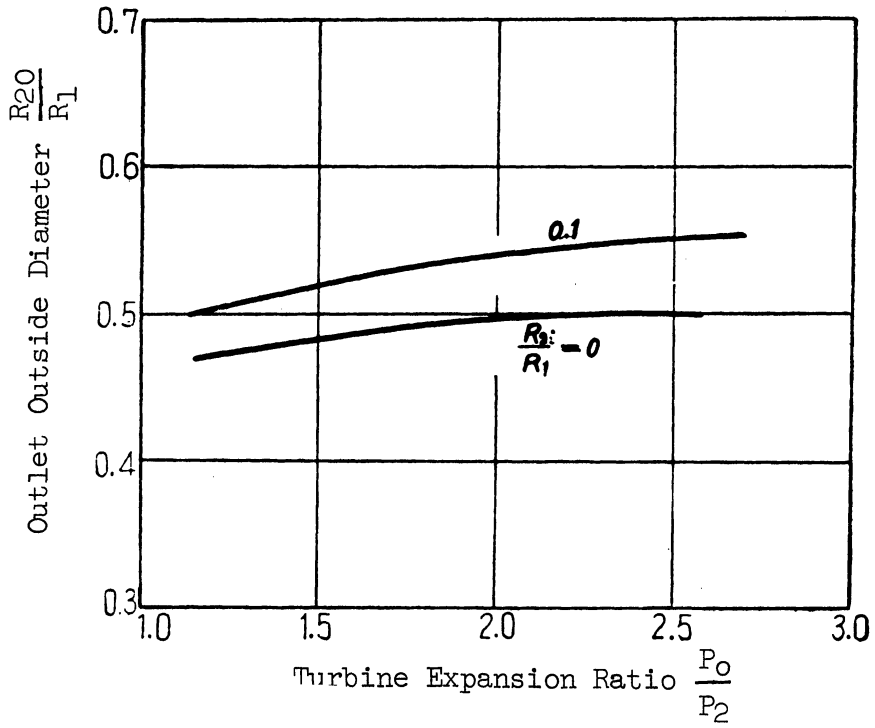

Figure 2.22. The Most Suitable Outlet Outside Diameter.

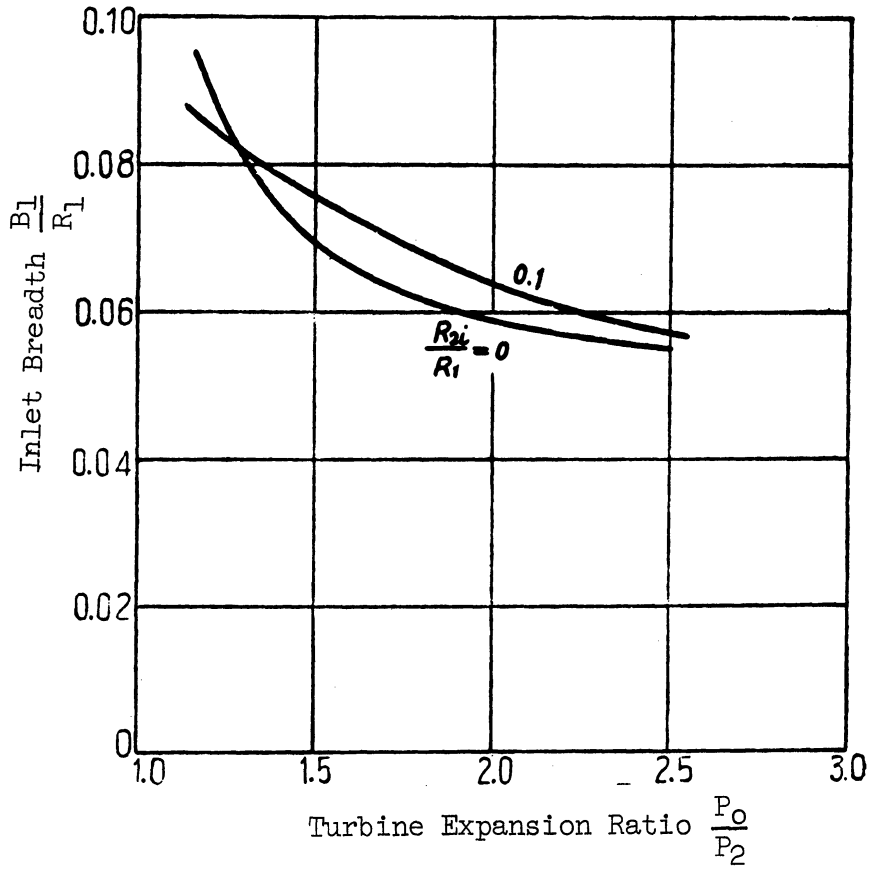

Figure 2.23. The Most Suitable Blade Inlet Breadth.

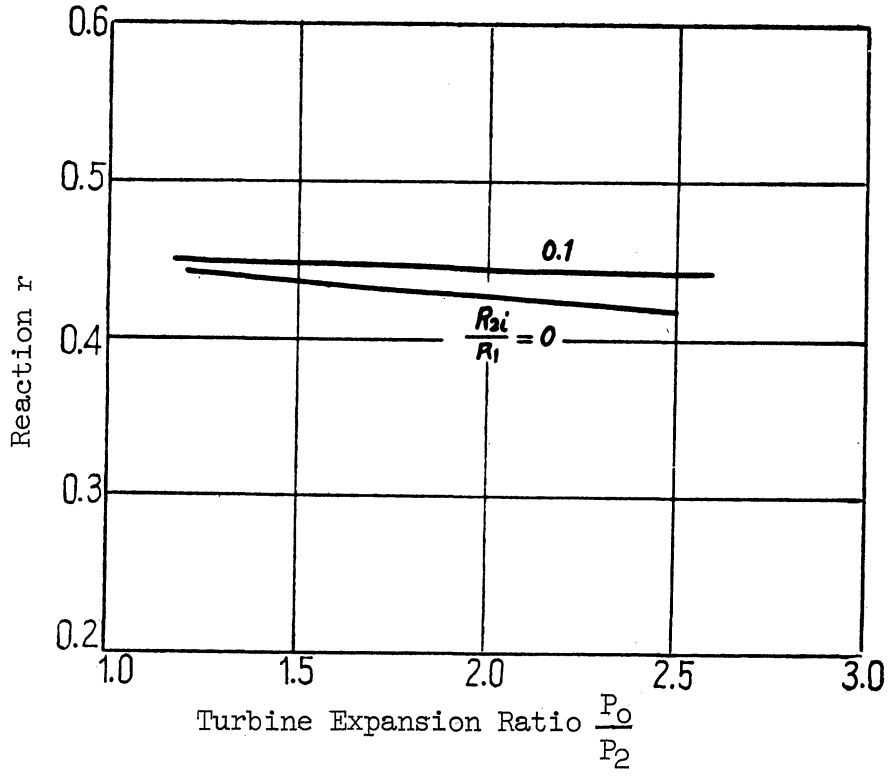

Figure 2.24. The Most Suitable Reaction

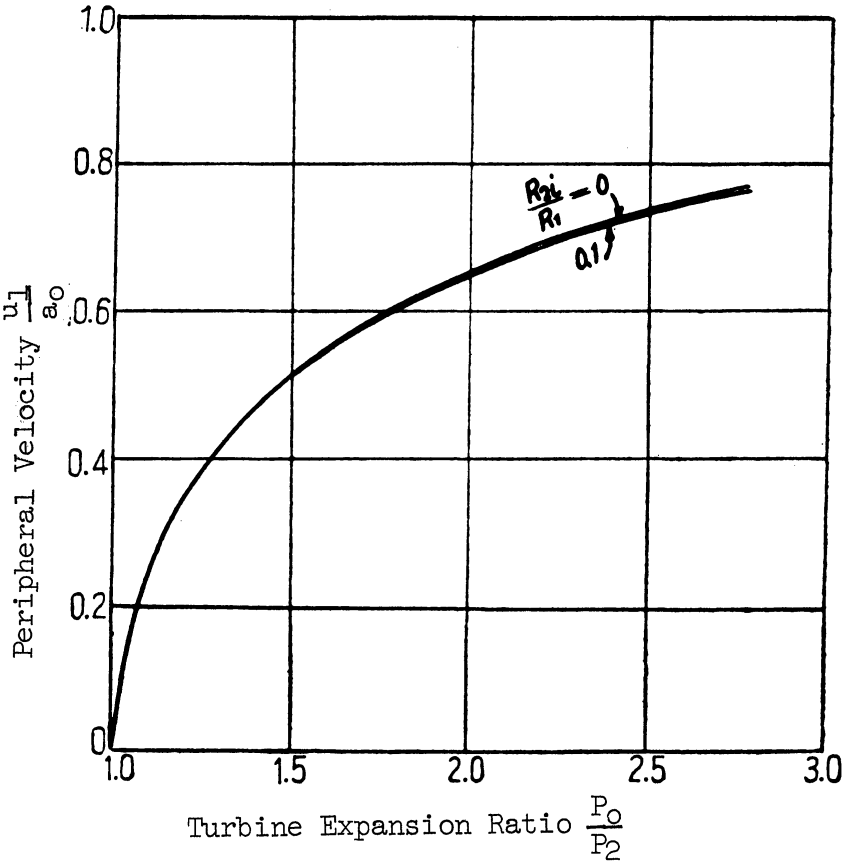

Figure 2.25. The Most Suitable Peripheral Velocity

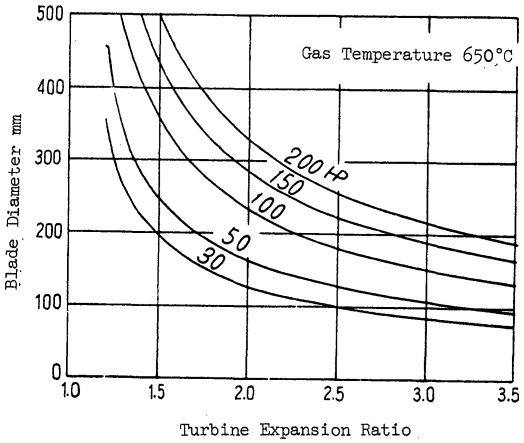

Figure 2.26. The Most Suitable Blade Diameter.

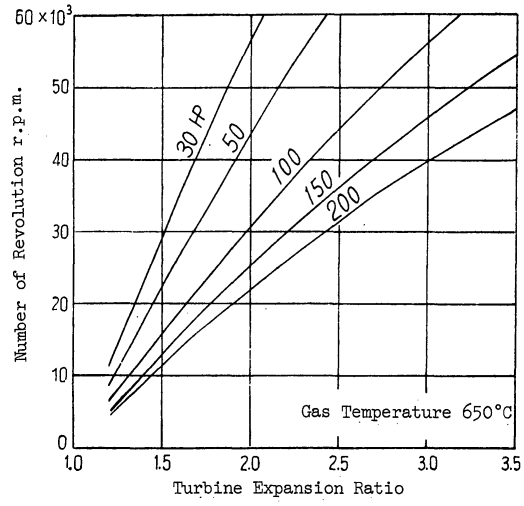

Figure 2.27. The Most Suitable Number of Revolution.

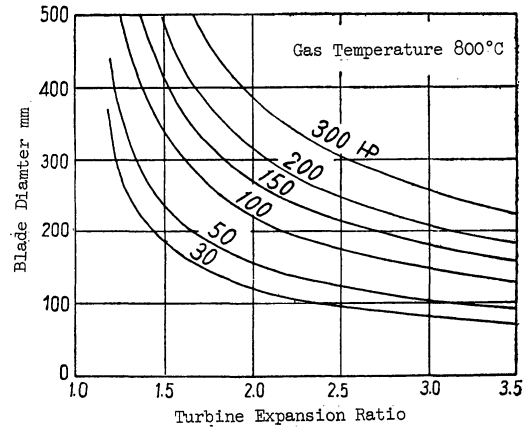

Figure 2.28. The Most Suitable Blade Diameter.

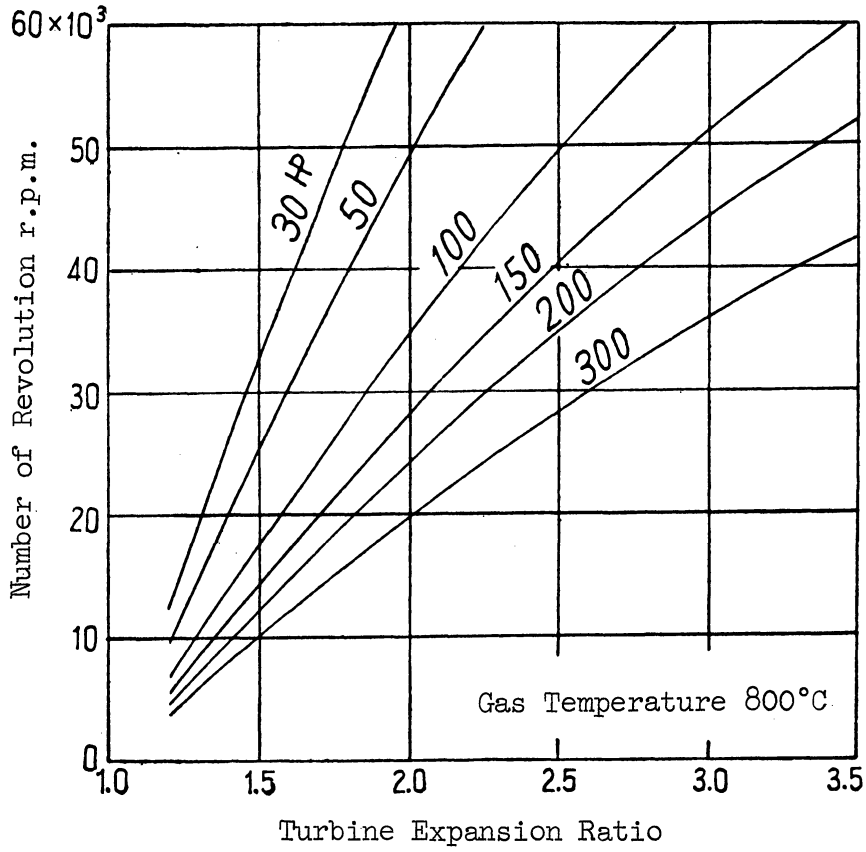

Figure 2.29. The Most Suitable Number of Revolution.

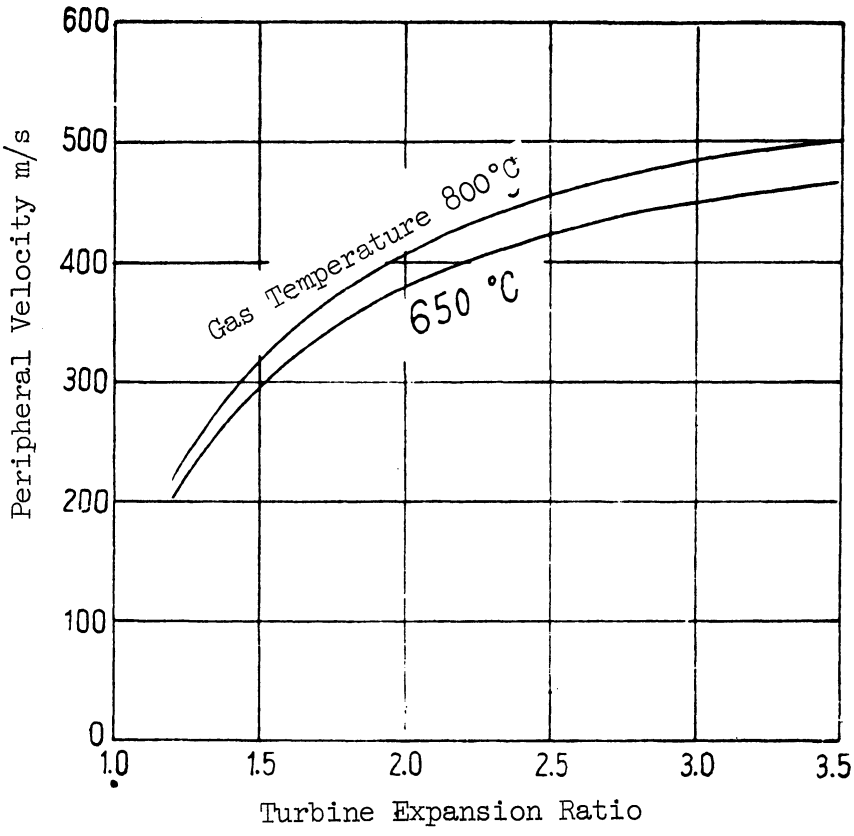

Figure 2.30. The Most Suitable Peripheral Velocity.

Turbine total expansion ratio	1.2
Gas flow N_m^3/mn	25
Gas temperature at turbine inlet °C	500

Gas flow passing through the turbine:
G = 0.545 kg/sec

Gas density at the turbine inlet:
γ_0 = 0.526 kg/m (R* = 29.54)

Sound velocity at the gas temperature 500°C:
a_0 = 544 m/sec (k = 1.323, using standard official ratio of mixture)

R_{2i}/R_1 = 0.1 will be adopted for the axial radius of the blade outlet.

From Figure 2.20, η_e reaches its maximum when p_0/p_2 = 1.2, and q = 5.9 x 10^{-3}. Because of the large quantity of the gas flow, however, the blade outside radius, R_1, will increase as a result of q equaling 5.9 x 10^{-3}. Accordingly, the designing will be made with the value of q being 5.88 x 10^{-3}, 10.29 x 10^{-3}, 16.25 x 10^{-3}. The following table will be obtained for those three cases from Figures 2.10 - 2.14.

	A	B	C
q	16.25 x 10^{-3}	10.29 x 10-3	5.88 x 10^{-3}
R_{20}/R_1	0.7	0.6	0.5
R_{2i}/R_1	0.1	0.1	0.1
η_e	0.845	0.857	0.864
r	0.490	0.477	0.461
α	10° 31'	11°15'	12°44'
U_1/a_0	0.3391	0.3424	0.3457
R_1 mm	137	172	227
B_1 mm	40.0	29.4	19.4
R_{20} mm	96.0	103.2	113.5
R_{2i} mm	13.7	17.2	22.7
U_1 m/s	184.9	186.6	188.4
n rpm	12,880	10,360	7,930
β_{20}	0	0	0
β_{2i}	74°41'	72°13'	68°49'

The relative efflux angle β_2 will be obtained from (2.51).

Figure 2.31 graphically expresses the results as shown in the above table. With $q = 5.88 \times 10^{-3}$, the result will be a large radius of the vanes, and a low number of revolutions, even though its efficiency is the highest of all the three cases. The number of revolutions must be determined with reference to the characteristics of the compressor to be used in combination. The case in which $q = 10.29 \times 10^{-3}$, and the number of revolutions is 10.360 rpm will be found most suitable.

2.3. Comparison between Radial-Straight Vanes and Curved Vanes

Because the use of curved vanes presents certain difficulties in strength as well as in operation, the radial-straight vanes have been favored by the manufacturers of mixed-flow radial turbines. The use of straight vanes is, however, not without its own problems. In spite of its high efficiency and strength, the extremely rapid revolutions of straight vanes make it difficult to design a shaft bearing suitable for its velocity. In addition, the number of its revolutions is often controlled by the limit in the number of revolutions of the shaft bearing.

For a moment we shall put aside the questions of strength and operational difficulties of the curved vanes, and consider the theoretical possibility of developing, by using curved vanes, an efficiency as high as that of straight vanes, and of reducing its number of revolutions. As in the case of straight vanes, an exducer will be attached to the vane outlet in order to prevent the rotatory motion around the axis of the gas flow. Based upon the results obtained from the study of radial-straight vanes, a comparison will be made between the characteristics of curved vanes and those of straight vanes.

2.3.1. Methods of Calculation

Figure 2.32 shows the curved-vane radial-turbine forming a curved angle, δ, at the blade inlet. $\delta > 0$ when the angle is curved backward against the direction of the revolution.

Figure 2.33 shows the velocity diagrams of the blade inlet and outlet.

Caution must be taken at a designing point so as to prevent a collision (shock) of gas flowing in the direction of δ at the blade inlet. At the blade outlet the absolute velocity of the flow must be parallel to the axial line so that a rotatory motion may be eliminated. Figure 2.34 shows in the i-s diagram the condition of the gas inside the turbine.

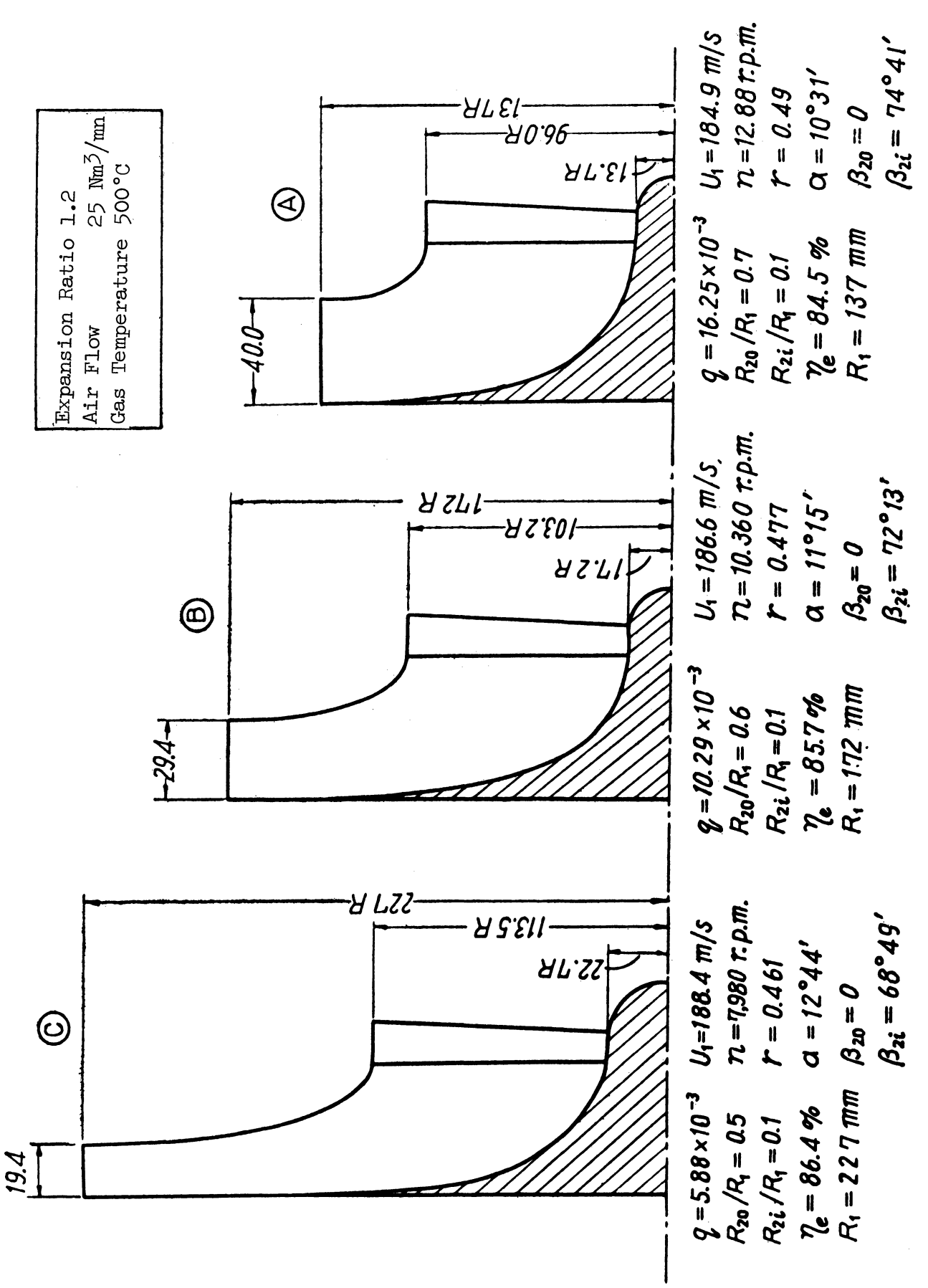
Expansion Ratio 1.2
Air Flow 25 Nm³/mn
Gas Temperature 500°C
A
B
C
19.4
29.4
40.0
227R
113.5R
22.7R
172R
103.2R
17.2R
137R
96.0R
13.7R
q = 5.88×10⁻³
R20/R1 = 0.5
R2i/R1 = 0.1
ηe = 86.4 %
R1 = 227 mm
U1 = 188.4 m/s
n = 7,980 r.p.m.
r = 0.461
α = 12°44'
β20 = 0
β2i = 68°49'
q = 10.29×10⁻³
R20/R1 = 0.6
R2i/R1 = 0.1
ηe = 85.7 %
R1 = 172 mm
U1 = 186.6 m/s
n = 10.360 r.p.m.
r = 0.477
α = 11°15'
β20 = 0
β2i = 72°13'
q = 16.25×10⁻³
R20/R1 = 0.7
R2i/R1 = 0.1
ηe = 84.5 %
R1 = 137 mm
U1 = 184.9 m/s
n = 12.88 r.p.m.
r = 0.49
α = 10°31'
β20 = 0
β2i = 74°41'

Figure 2.31.

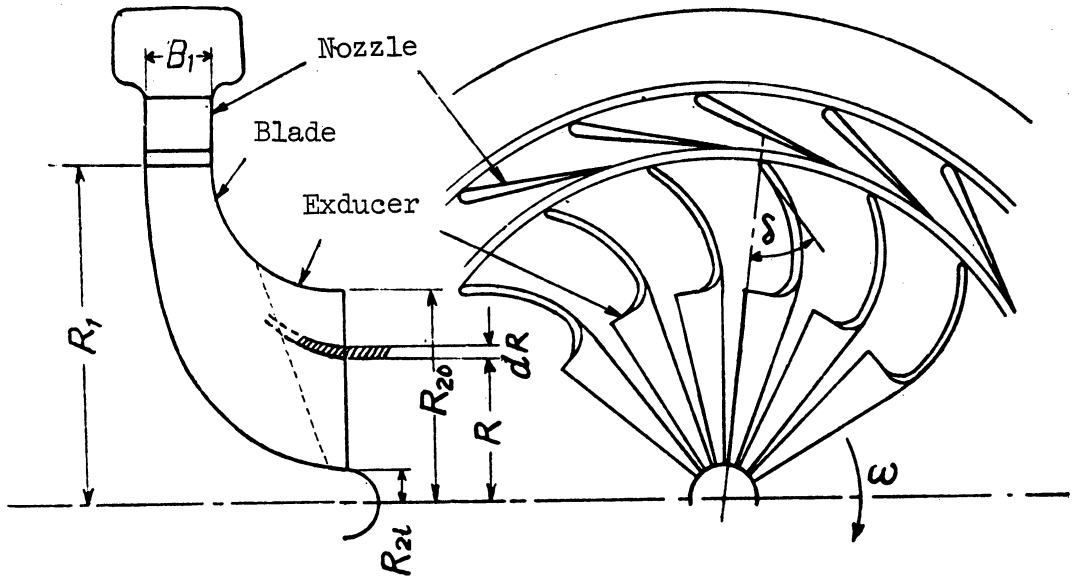

Figure 2.32 Curved Vane

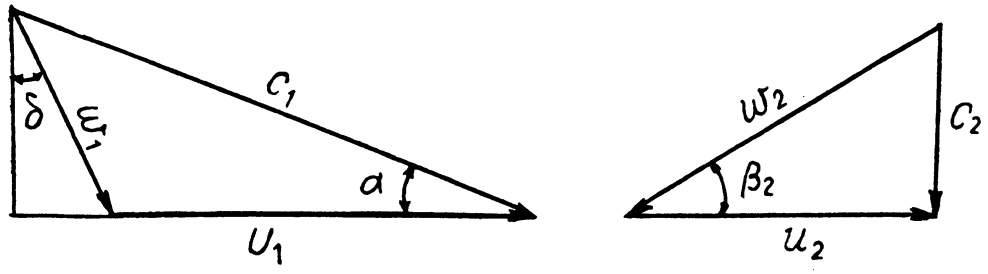

Blade Inlet Blade Outlet

Figure 2.33. Velocity Diagram

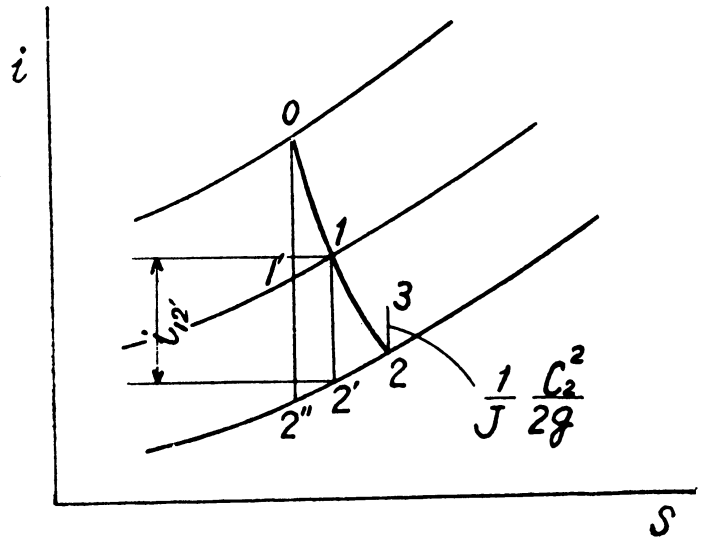

Figure 2.34. i-s Diagram.

With regard to the gas passing the diminutive radius dR at any radial point of the turbine, the following formula will be obtained expressing the energy of the gas flowing inside the blade.

$$\frac{w_1^2}{2g} + Ji_{12'} = \frac{1}{\psi_2^2} \cdot \frac{w_2^2}{2g} + \frac{1}{2g}(U_1^2 - u_2^2) \qquad (2.57)$$

ψ_2 stands for the velocity coefficient of the blade and $i_{12'}$ for the fall of heat at the time of the equal entropy expansion from the blade-inlet condition (p_1, T_1) up to the turbine-outlet pressure, and can be expressed as follows:

$$i_{12'} = c_p (T_1 - T_2')$$

$$= c_p T_0 \{1 - \varphi^2(1-s)\}\left(1 - \frac{s_0}{s}\right) \qquad (2.58)$$

where:

T_0 = turbine inlet temperature

T_1 = blade inlet temperature

T_2' = temperature at the time of the equal entropy expansion from the blade inlet conditions up to the turbine outlet pressure

φ = velocity coefficient of the nozzle

s and s_0 can be obtained as follows:

$$s = \left(\frac{p_1}{p_0}\right)^{(k-1/k)} \quad , \quad s_0 = \left(\frac{p_2}{p_0}\right)^{(k-1/k)}$$

(k: adiabatic exponent)

Also from the velocity diagram (Figure 2.33),

$$w_1 = \frac{c_1 \cos \alpha - U_1}{\sin \delta} = \frac{c_1 \sin \alpha}{\cos \delta} \qquad (2.59)$$

$$a^2 \equiv \frac{1}{\frac{1}{\varphi_2^2} - 1} \cdot \frac{1}{\omega^2} \left(w_1^2 + 2gJi_{12'} - U_1^2 \right) \qquad (2.60)$$

(ω = the velocity at the angle of revolution)

The dimensional quantity of length is expressed by a, which is unrelated to the position of the turbine-outlet radius, and can be determined only by the blade-inlet conditions. The value of a will be calculated as follows from (2.57), (2.58), and (2.59).

$$\left(\frac{a}{R_{20}}\right)^2 = \frac{1}{\frac{1}{\psi_2^2} - 1} \left(\frac{c_0}{U_1}\right)^2 \left(\frac{R_1}{R_{20}}\right)^2 \left[\varphi^2 (1-s) \frac{\sin^2 \alpha}{\cos^2 \delta} \right.$$

$$\left. + \left\{ 1 - \varphi^2 (1-s) \right\} \left(1 - \frac{s_0}{s} \right) - \left(\frac{U_1}{c_0} \right)^2 \right] \qquad (2.61)$$

Here R_{20} stands for the outside radius of the blade outlet and c_0 will be obtained as follows:

$$c_0 = \sqrt{2gJc_pT_0}$$

When the total turbine expansion ratio, p_0/p_2, the gas flow, G, and the blade radius, R_1, are given in a radial turbine, the condition under which the maximum efficiency is to be obtained, require that $\tan\beta_2 = 0$ in the blade-outlet outside-radius, R_{20}. This condition can be satisfied regardless of the form of the vanes, and can be re-expressed as follows:

$$\tan\beta_2 = \frac{c_2}{u_2} \qquad (2.62)$$

Since

$$c_2^2 = w_2^2 - u_2^2 \qquad (2.63)$$

and substituting w_2 from (2.57) with the above formula,

$$c_2 = \omega\sqrt{1 - \psi_2^2}\ \sqrt{a^2 - R^2} \qquad (2.64)$$

$$\tan \beta_2 = \sqrt{1 - \psi_2^2}\sqrt{\left(\frac{a}{R}\right)^2 - 1} \tag{2.62.1}$$

If $R = R_{20}$, $\tan \beta_2 = 0$, then,

$$\left(\frac{a}{R_{20}}\right)^2 - 1 = 0 \tag{2.65}$$

From (2.61) and (2.65)

$$\left[\varphi^2 (1 - s) \frac{\sin^2\alpha}{\cos^2\delta} + \{1 - \varphi^2 (1 - s)\}\left(1 - \frac{s_0}{s}\right)\right] x$$

$$\left(\frac{c_0}{U_1}\right)^2 - 1 = \left(\frac{1}{\psi_2^2} - 1\right)\left(\frac{R_{20}}{R_1}\right)^2 \tag{2.66}$$

From (2.59)

$$c_1 \cos \alpha - U_1 = \tan \delta \cdot c_1 \sin \alpha \tag{2.59.1}$$

From (2.8)

$$c_1 = \varphi \sqrt{1 - sc_0} \tag{2.8.1}$$

By substituting (2.8.1) with (2.59.1),

$$\left(\frac{U_1}{c_0}\right)^2 = \varphi^2 (1 - s)(\cos \alpha - \sin \alpha \cdot \tan \delta)^2 \tag{2.67}$$

The following formula with regard to U_1/c_0 will be obtained by eliminating s from both (2.66) and (2.67):

$$a\left(\frac{U_1}{c_0}\right)^4 - b\left(\frac{U_1}{c_0}\right)^2 + c = 0 \tag{2.68}$$

In the above formula,

$$\left.\begin{aligned} a &= \frac{A^2}{\varphi^2}\ (A^2 + B) \\ b &= (A^2 + B) + \frac{A^2}{\varphi^2} - A^2 s_0 \\ c &= 1 - s_0 \\ A^2 &= \frac{1}{(\cos\alpha - \sin\alpha \cdot \tan\delta)^2} \\ B &= 1 + \left(\frac{1}{\varphi_2^2} - 1\right)\left(\frac{R_{20}}{R_1}\right)^2 - A^2 \frac{\sin^2\alpha}{\cos^2\delta} \end{aligned}\right\} \qquad (2.69)$$

It will be clear from (2.68) that U_1/c_0 is the function of α, δ, R_{20}/R_1, and p_0/p_2 only, and, when producing the maximum efficiency, will be determined as identical to the radix of the formula (2.68).

The reaction then will be:

$$r = \frac{i_{1'2''}}{i_{02''}} = 1 - \frac{1}{1 - s_0} \frac{A^2}{\varphi^2} \left(\frac{U_1}{c_0}\right)^2 \qquad (2.70)$$

The internal efficiency, η_i, will be:

$$\eta_i = \frac{L_i}{L_{is}}$$

whereas L_i and L_{is} will be obtained respectively as follows:

$$L_i = \frac{1}{g} c_1 \cos\alpha \cdot U_1$$

$$L_{is} = J c_p T_0 (1 - s_0) = \frac{c_0^2}{2g} (1 - s_0)$$

Therefore,

$$\eta_i = \frac{2 \cos \alpha}{1 - s_0} A \left(\frac{U_1}{c_0}\right)^2 \tag{2.71}$$

The gas flow dG passing dR at any radial point, R, of the turbine will be:

$$dG = 2\pi R dR c_2 \gamma_2$$

As in the case of straight-radial vanes, the total gas flow, G, can be obtained by integrating those values with regard to the total area of the turbine outlet:

$$G = 2\pi\omega \frac{\sqrt{1 - \psi_2^2}}{3} \gamma_2 R_{20}^3 \left[\left\{\left(\frac{a}{R_{20}}\right)^2 - \left(\frac{R_{2i}}{R_{20}}\right)^2\right\}^{3/2} - \left\{\left(\frac{a}{R_{20}}\right)^2 - 1\right\}^{3/2}\right] \tag{2.72}$$

By substituting the conditions expressed in (2.65) with (2.72),

$$\frac{G\sqrt{T_0}}{p_0} \cdot \frac{1}{2\pi R_1^2}\sqrt{\frac{R^*}{gk}} = \sqrt{\frac{2}{k-1}} \frac{\sqrt{1 - \psi_2^2}}{3}$$

$$x \frac{1}{s_0} \cdot \frac{p_2}{p_0} \cdot \frac{U_1}{c_0}\left\{\left(\frac{R_{20}}{R_1}\right)^2 - \left(\frac{R_{2i}}{R_1}\right)^2\right\}^{3/2} \tag{2.73}$$

The non-dimensional characteristic quantity, q, of the gas flow such as defined in (2.12) can be calculated from (2.73) as follows:

$$q = \sqrt{\frac{2}{k-1}} \cdot \frac{\sqrt{1 - \psi_2^2}}{3} \cdot \frac{1}{s_0} \cdot \frac{p_2}{p_0} \cdot \frac{U_1}{c_0} x \left\{\left(\frac{R_{20}}{R_1}\right)^2 - \left(\frac{R_{2i}}{R_1}\right)^2\right\}^{3/2} \tag{2.74}$$

The value of U_1/c_0, as a function of α, δ, R_{20}/R_1, can be determined from (2.68) while (2.70) and (2.71) lead to the determination of the reaction and the efficiency respectively. By giving the value of R_{2i}/R_1, the value of q can also be made clear from (2.74). Conversely, by giving the values of p_0/p_2, q, R_{2i}/R_1, α, and δ, those of U_1/c_0, R_{20}/R_1, r, and η_t can be obtained. When q is made clear, R_1 can be determined from (2.12) and the number of revolutions can also be determined from the value of U_1/c_0.

The breadth of the nozzle, B_1, is determined as follows:

$$G = 2\pi R_1 B_1 c_1 \gamma_1 \sin \alpha$$

By substituting the above formula with (2.8.1), (2.12) and (2.7),

$$\frac{B_1}{R_1} = \sqrt{\frac{k-1}{2}} \cdot \frac{q}{\varphi \sin \alpha} \cdot \frac{p_0}{p_1} \cdot \frac{1 - \varphi^2 (r - s)}{\sqrt{1 - s}} \qquad (2.75)$$

2.3.2. Characteristics Compared

By thus clarifying the total turbine expansion ratio, p_0/p_2, the gas-flow characteristic quantity, q, the inside-radius ratio of the turbine outlet, R_{2i}/R_1, the average efflux angle, α, and the blade inlet angle, δ, all the conditions under which the maximum efficiency is reached can be determined.

Among the above variables, the total turbine expansion ratio is given at the beginning of designing. The gas-flow characteristic quantity, q, is defined in (2.12). Since the gas flow, G, and the gas temperature of the turbine inlet are given at the time of designing, q can take a variety of values according to the size of the blade inlet radius, R_1. That is, q increases as the radius decreases, when the gas flow and the gas temperature are given, and it also increases in proportion to the rise of the gas temperature when the gas flow is fixed. However, since the most suitable characteristic quantity proves to be a rather small value when the total turbine expansion ratio is given, it is necessary to adopt a rather great blade-inlet radius.

Though the efficiency can also be improved by reducing as much as possible the inside-radius ratio of the turbine outlet, R_{2i}/R_1, the possibility is limited by the attachment of an exducer. The calculations below are therefore made under the following conditions:

The inside-radius ratio of the turbine outlet: $R_{2i}/R_1 = 0.1$

The velocity coefficient of the nozzle: $\varphi = 0.97$

The velocity coefficient of the blade: $\psi_1 = 1.0$, $\psi_2 = 0.78$

The adiabatic exponent of the gas: $k = 1.323$

The total turbine expansion ratio: $p_0/p_2 = 2.5$

(a) Efficiency

The results of the efficiency computation are shown in Figure 2.35. Consideration is given to the effects of the total turbine expansion ratio, the gas flow, and the gas temperature at the turbine inlet upon the curved angle of the blade inlet, δ. With reference to the fixed curved line of q, it will be observed that a greater efficiency is obtainable with a greater value of δ. The use of rear curved vanes will therefore result in a slightly better efficiency than the use of straight vanes, though the difference is not very conspicuous. Front curved vanes should not be used.

The efficiency varies greatly according to the gas-flow characteristic quantity. A better efficiency can be obtained by enlarging the blade inlet radius, R_1, and by reducing q when the gas flow and the gas temperature are given. The value of q as small as q = (5 10) x 10^{-3} cannot be adopted for actual use, because the curved angle in such a case cannot be expected to have any influence upon the efficiency.

(b) Circumferential velocity and number of revolutions

The non-dimensional circumferential velocity, U_1/c_0, is shown in Figures 2.36, 2.37, and 2.38. Assuming again that q is fixed, it will be noted that U_1/c_0 shows little change by the curved angle when the nozzle leaving angle α is small, whereas U_1/c_0 becomes smaller when α is enlarged. The value of U_1/c_0 shows little change regardless of q. It increases only slightly when q is reduced.

As might be understood from (2.12), the value of q is inversely proportional to that of R_1^2. As the circumferential velocity, U_1, is directly proportional to $R_1 \times N$, the number of revolutions, N, is also found to be directly proportional to $U_1 \sqrt{q}$. Figure 2.39 shows the change that takes place in the number of revolutions according to the variation of q and δ.

With the fixed value of q, the number of revolutions is reduced when δ is enlarged. Since the enlargement of δ necessitates the enlargement of the efflux angle of the nozzle, α, there will be a slight decrease in the efficiency. By adopting the absolute efflux angle, δ, of 30° and the average efflux angle, α, of 30°, the number of revolutions can be

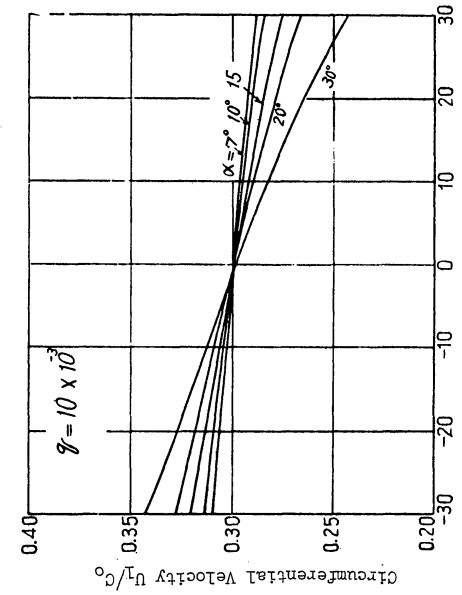

Curved Angle of Blade Inlet δ Degree
Figure 2.37. Circumferential Velocity.

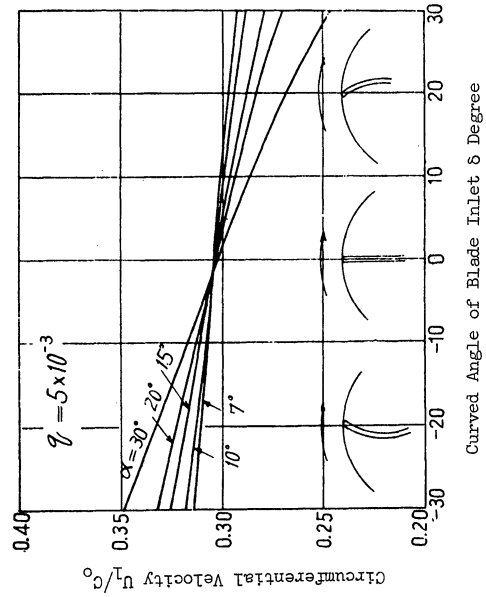

Curved Angle of Blade Inlet δ Degree
Figure 2.36. Circumferential Velocity.

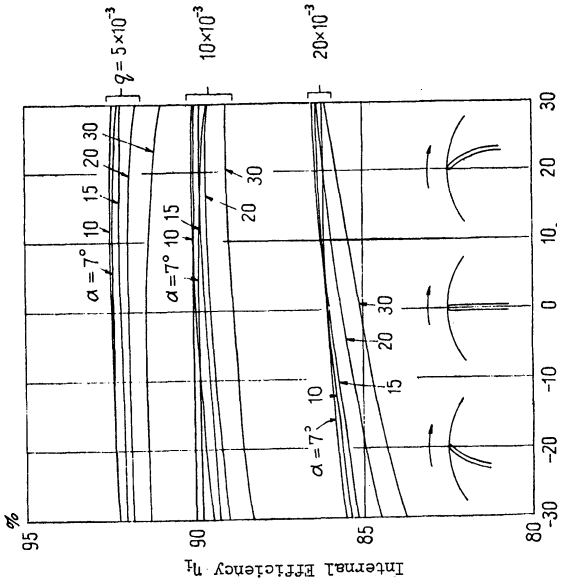

Curved Angle of Blade Inlet δ Degree
Figure 2.35. Internal Efficiency.

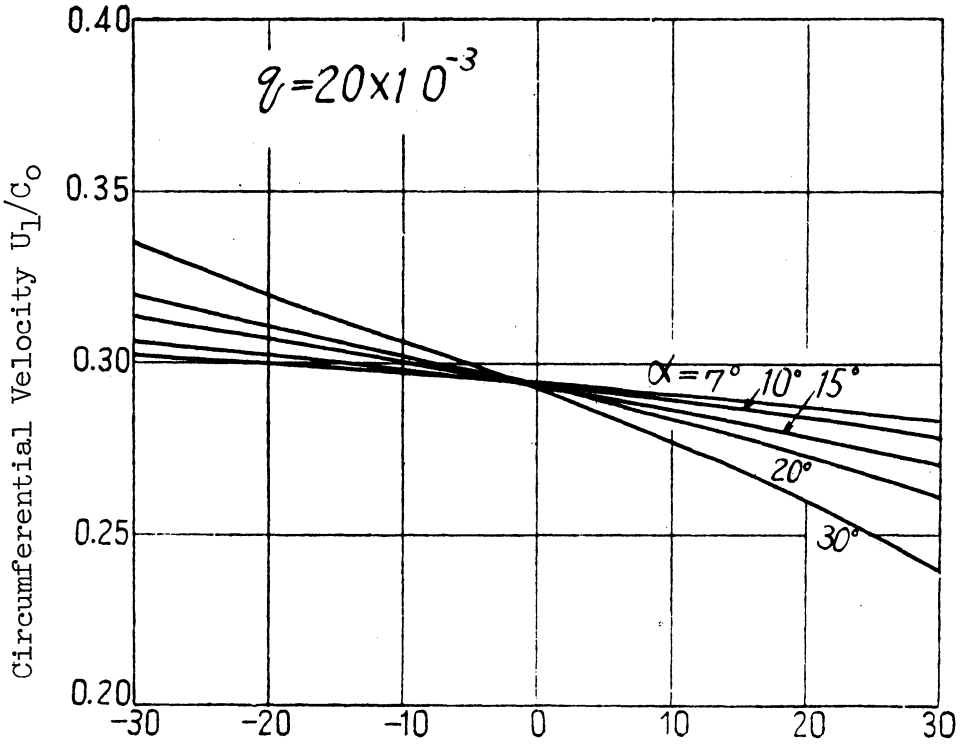

Figure 2.38. Circumferential Velocity.

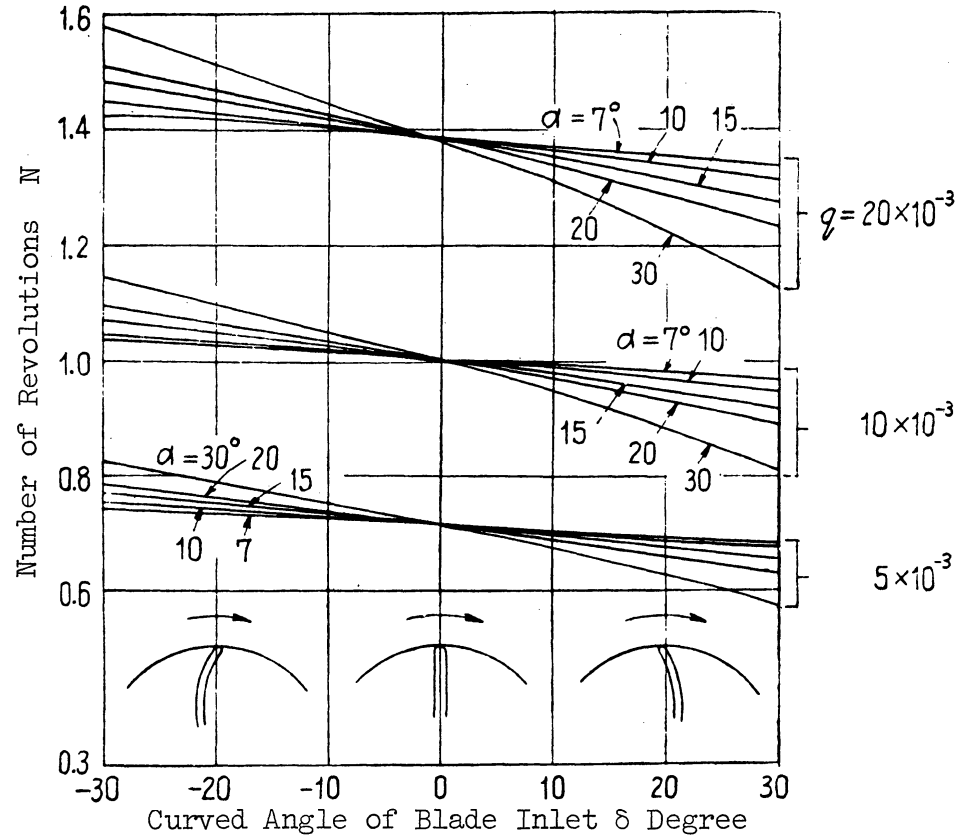

Figure 2.39 Number of Revolutions

reduced by about 20%, as compared with straight vanes, though at 0.5 1.0% sacrifice of efficiency.

It is the value of q that greatly affects the number of revolutions when the gas flow and its temperature are fixed. The number of revolutions will be reduced, and the designing of the shaft bearing is made easier by increasing R_1 and reducing q.

When the blades are geometrically similar, the centrifugal response of the vanes and rotor is directly proportional to the square of the circumferential velocity. It is therefore proportional to $(U_1/c_0)^2$ when the gas flow and its temperature are fixed. Although the number of revolutions may be reduced by enlarging R_1 and reducing q, it is clear from Figures 2.36, 2.37, and 2.38 that the reduction of q also brings about a slight increase of U_1/c_0, and of the response. However, the increase of U_1/c_0 by the reduction of q remains so negligible that, where the number of revolutions is of great concern, it is advised for the sake of better efficiency to enlarge R_1 and reduce q as much as it is structurally possible.

With the rise of gas temperature, comes the increase of q and c_0 for the same radius, R_1. The subsequent increase of U_1, of the number of revolutions as well as of the response will make designing difficult.

(c) Reaction

The reaction is shown in Figures 2.40, 2.41, and 2.42. With δ of 30° and α of 30°, the reaction will be 3 8% and approach the impulse turbine, with greater nozzle expansion ratio. With $p_0/p_2 = 2.5$, the expansion ratio of the nozzle becomes greater than the limit expansion ratio, when the reaction is reduced below 0.303. Special consideration will be required as to the form of the nozzle and its arrangement when using the reaction at such a point.

(d) Outside radius of turbine-outlet and blade-inlet breadth

The outside-radius ratio of the turbine outlet is shown in Figure 2.43. The ratio receives little effect from the curved angle of the blade inlet. Rather it is the value of q that affects the ratio, which will decrease when R_1 is enlarged and q reduced.

The ratio of the blade-inlet breadth, B_1/R_1, is shown in Figure 2.44. When both q and α are fixed, B_1 receives little influence from the curved angle of the blade inlet. As in the case of the radius ratio, it is the value of q which, by reducing itself, also reduces B_1/R_1. For instance, if:

$$q = 5 \times 10^{-3}$$

$$\alpha = 15 \sim 30^{\circ}$$

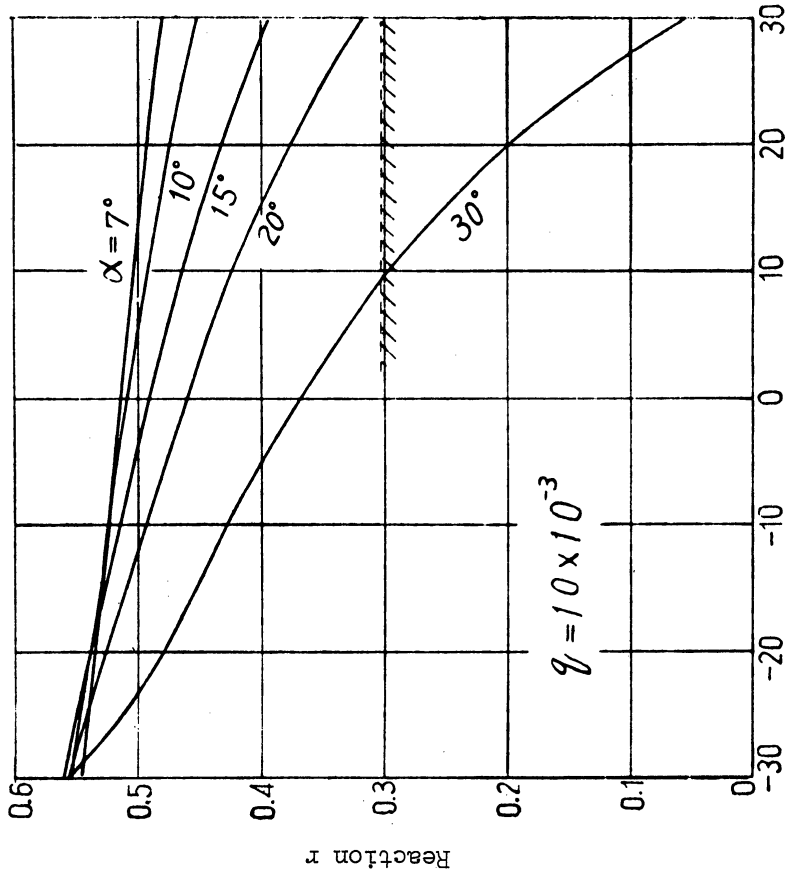

Curved Angle of Blade Inlet δ Degree

Figure 2.41 Reaction

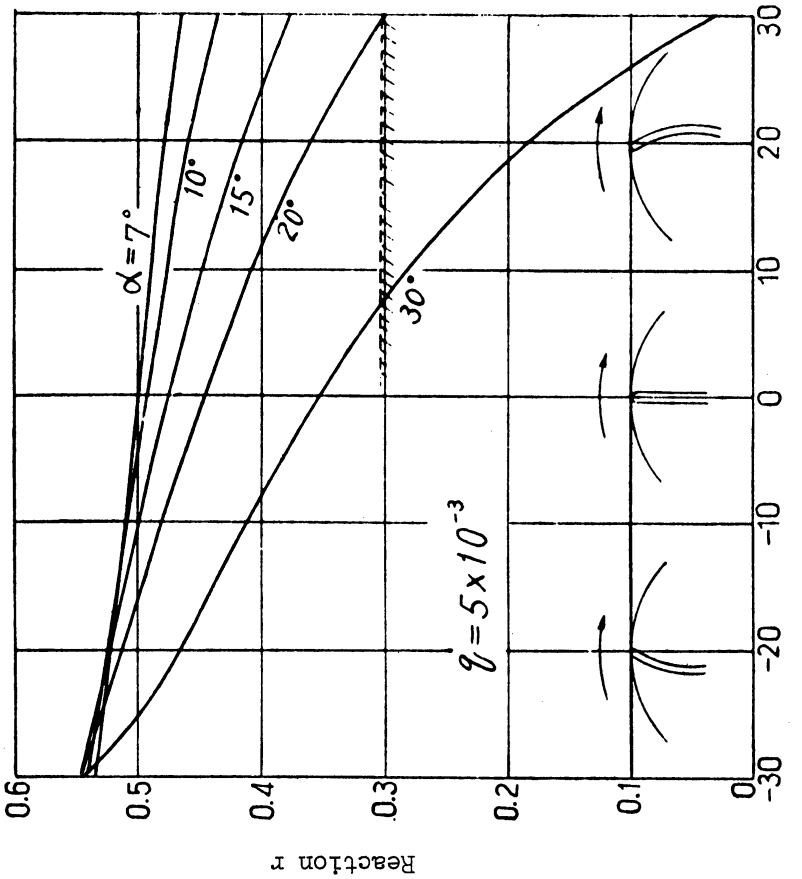

Curved Angle of Blade Inlet δ Degree

Figure 2.40 Reaction

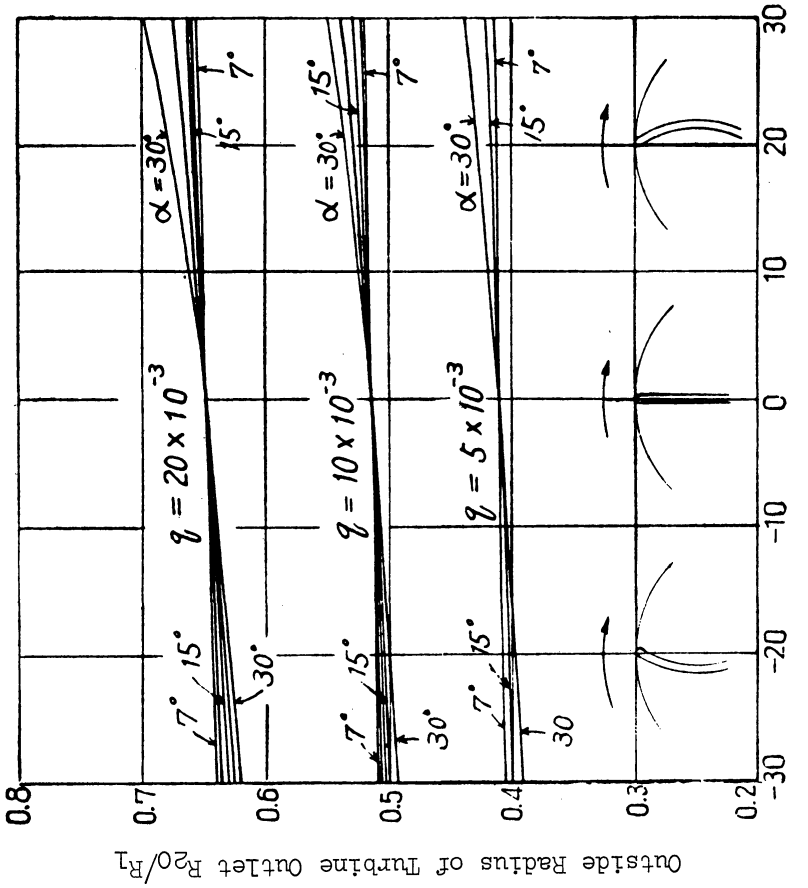

Curved Angle of Blade Inlet δ Degree

Figure 2.43 Outside Radius of Turbine Outlet.

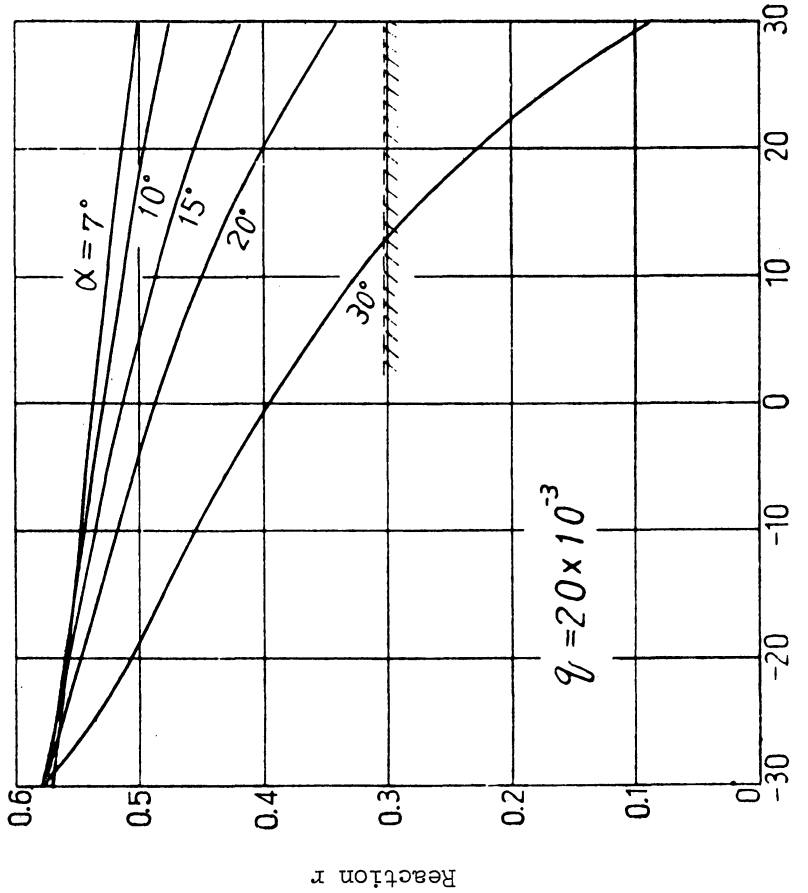

Curved Angle of Blade Inlet δ Degree

Figure 2.42 Reaction

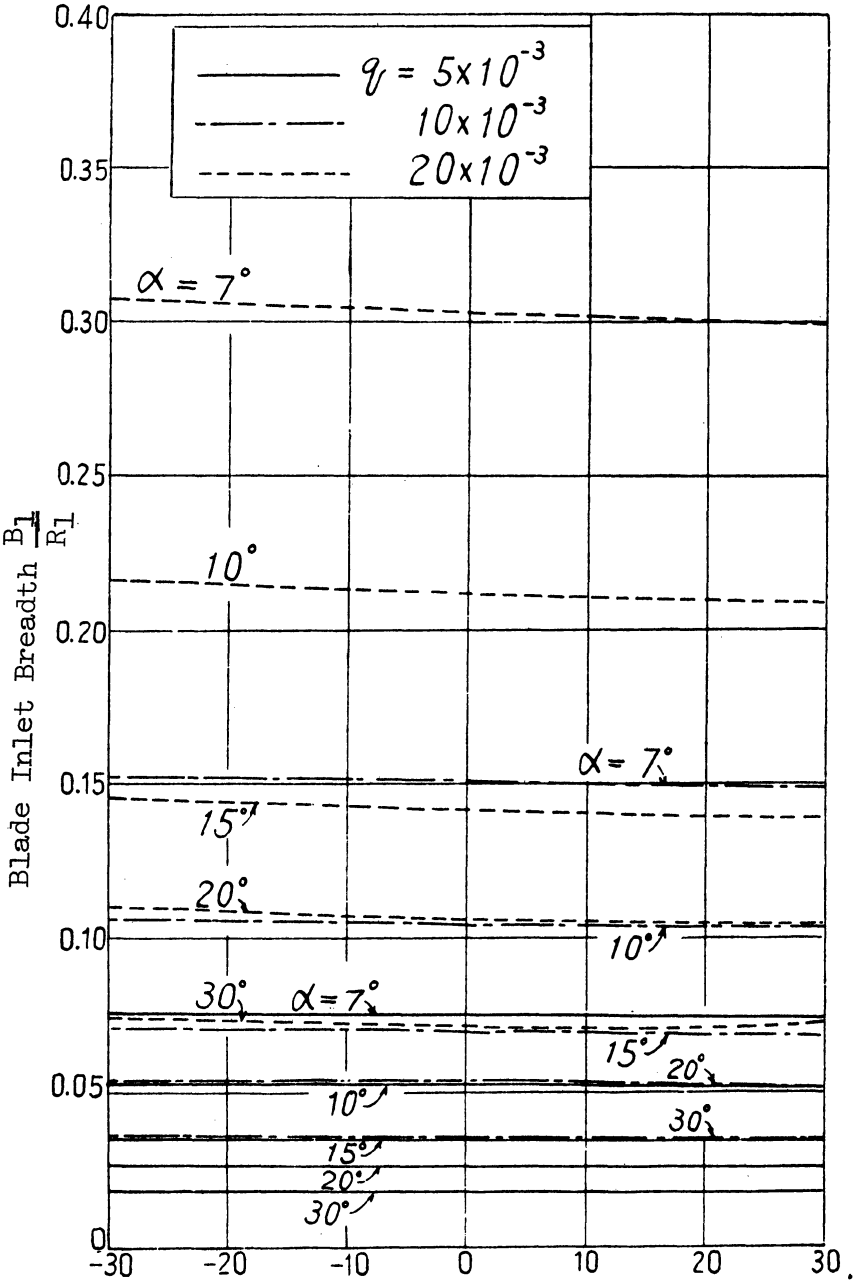

Figure 2.44 Blade Inlet Breadth.

Then $B_1/R_1 = 0.02 \sim 0.04$. When the blade radius, R, equals 100 mm, B_1 will be as small as $2 \sim 4$ mm. There must be a gap of at least $0.5 \sim 0.8$ mm between the vane and its casing in order to prevent the loss of gap from increasing which will reduce the efficiency. Accordingly too small a value of B_1/R_1 cannot be adopted. The problem of the blade-inlet breadth must be taken into account when using a small value of q.

2.3.3. Summary

(1) We can hardly expect a higher efficiency from the use of rear-curved vanes than from that of straight vanes.

(2) The number of revolutions may be reduced by the use of rear-curved vanes.

With δ of 30° and α of 30°, about 20% reduction of the number of revolutions may be attained as compared with straight vanes. This, however, involves a subsequent curtailment of reaction, as well as an increase in the expansion ratio of the nozzle, requiring a special consideration of the expansion ratio that tends to exceed the limit expansion ratio of the turbine.

(3) Heightened efficiency and reduced number of revolutions may be achieved by enlarging the blade-inlet radius, R_1, and reducing q. Even though there is little change in the centrifugal response, this will result in an extreme diminution of B_1/R_1, as well as the increase of the loss of gap at the end of the vanes. Special consideration must therefore be given when adopting a small value of q.

(4) The use of front-curved vanes only reduces the efficiency and increases the revolution numbers, and should not be adopted.

2.4. Partial-Load Characteristics

The gas-turbine prime mover is often used at points other than the designing point. In order to know the partial-load characteristics of the prime mover, it is necessary to know the partial-load characteristics of the turbine itself, of which no publication has so far been made available. The present section makes clear the partial-load characteristics of the radial turbine with straight vanes, for, as has been pointed out before, the curved vanes have little value of practical use except in very special cases. In the investigation of the partial-load characteristics of a radial turbine with straight vanes, with reference to the results of the experimental turbine, it is clarified how quantity of flow, output torque, power and efficiency vary in accordance with the variation of revolution, expansion ratio and temperature of inlet gas. In this case, theoretical equations are presented in the form of non-dimensional quantities, which are proved to agree fairly well with the results of experiment by the test turbines.

2.4.1. Methods of Calculation

Figure 2.45 shows the velocity diagram of a straight-vaned radial-turbine operating at points other than the designing point. The gas flows into the blade at the absolute velocity of c_1 at the average efflux angle of α from the nozzle. If the circumferential velocity at the blade inlet is expressed by U_1, the gas flows into the blade at the relative velocity of w_1. w_{1u} stands for the circumferential component of w_1, and c_{1r} for the radius directional component of c_1.

At the blade outlet any radius R is taken as a point of departure, with c_2 standing for the absolute velocity of the flow, U_2 for the circumferential velocity, w_2 for the relative velocity of the flow, β_2 for the relative efflux angle, w_{2u} for the circumferential component of w_2, c_{2u} and c_{2a} for the circumferential component and axial component of c_2 respectively.

(a) Gas flow and reaction

The gas flow, dG, passing the diminutive radius, dR, of the blade-outlet radius, R, is expressed as follows:

$$dG = 2\pi R w_2 \sin\beta_2 \cdot \gamma_2 dR \qquad (2.76)$$

(γ_2: density of outlet gas)

At the blade inlet, the gas flows at the relative velocity of w_1. Since the straight vanes are used in the blade, the loss of shock is expressed as $\zeta_s w_{1u}^2/2g$, ζ_s being the shock loss coefficient. Accordingly the following formula expressing the energy of the flow in the blade will be obtained:

$$\frac{c_{1r}^2}{2g} + (1 - \zeta_s)\frac{w_{1u}^2}{2g} + Ji_{12}'$$

$$= \frac{1}{\varphi_2^2} \cdot \frac{w_2^2}{2g} + \frac{1}{2g}(U_1^2 - u_2^2) \qquad (2.77)$$

In the above formula, i_{12}' represents the loss of heat at the time of the equal entropy expansion from the blade inlet to the outlet pressure, p_2, and φ_2, the velocity coefficient of the blade. Using the geometrical relation expressed in the velocity diagram, the relative velocity at the outlet w_2 can be obtained from (2.77).

$$w_2 = \psi_2 \cdot \omega \sqrt{X^2 + R^2} \tag{2.78}$$

But

$$X^2 = \frac{1}{\omega^2}\left[c_1^2 \sin^2\alpha + (1 - \zeta_s)(c_1 \cos\alpha - U_1)^2\right.$$

$$\left. + 2gJc_pT_0\{1 - \varphi^2(1 - s)\}(1 - s_0) - U_1^2\right] \tag{2.79}$$

The speed of the blade rotation is expressed by ω, the temperature of inlet gas by T_0, the turbine-inlet pressure, the blade-inlet pressure, and the turbine-outlet pressure by p_0, p_1, and p_2. s equals $(p_1/p_0)^{(k-1/k)}$. X^2 is a value unrelated to the radius point of the turbine outlet.

By substituting (2.78) with (2.76),

$$dG = 2\pi\omega\psi_2\gamma_2 \sin\beta_2 \cdot R\sqrt{X^2 + R^2}\, dR \tag{2.80}$$

The total gas flow, G, can be obtained by integrating the above formula from R_{2i} to R_{20}. ψ_2 and γ_2 can be considered to be fixed regardless of the blade radius, R. The directional distribution of the relative efflux angle, β_2, which is quite different from the geometrical attaching angle of the exducer, as will be described later in Chapter 5, varies in accordance with the number of revolutions. Strictly speaking, therefore, β_2 becomes a function of the complicated forms of R and ω, and makes the integration of (2.80) very difficult. We will then assume an approximate efflux angle from R_{2i} to R_{20}, and consider it as the average efflux angle of the blade, $\bar{\beta}_2$, whose working variations will be examined. By integrating (2.80) with this hypothetical efflux angle, $\bar{\beta}_2$, G will be obtained as follows:

$$G = \frac{2}{3}\pi\omega\psi_2\gamma_2 \sin\bar{\beta}_2\{(X^2 + R_{20}^2)^{3/2}$$

$$- (X^2 + R_{2i}^2)^{3/2}\} \tag{2.81}$$

Since the gas flow, G, at the blade inlet is expressed as in (2.11), it can be re-expressed as:

$$G = 2\pi R_1 B_1 \sin\alpha \cdot \varphi c_0 \gamma_0 \frac{(p_1/p_0)\sqrt{1 - s}}{1 - \varphi^2(1-s)} \tag{2.11.1}$$

From both (2.81) and (2.11.1),

$$\frac{3}{\psi_2} \cdot \frac{B_1}{R_1} \cdot \frac{\sin\alpha}{\sin\bar{\beta}_2} = \frac{1}{\varphi} \cdot \frac{U_1}{c_0} \left(\frac{p_2}{p_0}\right)^{1/k} \frac{p_0}{p_1} \cdot \frac{1 - \varphi^2 (1 - s)}{\sqrt{1 - s}}$$

$$\left[\left\{\left(\frac{X}{R_1}\right)^2 + \left(\frac{R_{20}}{R_1}\right)^2\right\}^{3/2} - \left\{\left(\frac{X^2}{R_1}\right) + \left(\frac{R_{2i}}{R_1}\right)^2\right\}^{3/2}\right] \qquad (2.82)$$

$(X/R_1)^2$ in the above formula is expressed as follows:

$$\left(\frac{X}{R_1}\right)^2 = \left\{\varphi\left(\frac{c_0}{U_1}\right)\sqrt{1 - s}\right\}^2 \sin^2\alpha + (1 - \zeta_s)\, x$$

$$\left[\left\{\varphi\left(\frac{c_0}{U_1}\right)\sqrt{1 - s}\right\}\cos\alpha - 1\right]^2$$

$$+ \left(\frac{c_0}{U_1}\right)^2 \left\{1 - \varphi^2 (1 - s)\right\}(1 - s_0) - 1 \qquad (2.83)$$

As will be explained in Chapter 3, the average efflux flow of the nozzle, α, remains fixed regardless of the expansion ratio. Hence in (2.82) it can be regarded as being fixed and unrelated to the operating conditions. If we suppose that the average leaving flow, $\bar{\beta}_2$, remains fixed regardless of the working conditions, we must conclude that both the first and the second halves of the equation (2.82) are also fixed and unrelated to the working conditions. The second half is represented by K.

$$K = \frac{1}{\varphi} \cdot \frac{U_1}{c_0} \left(\frac{p_2}{p_0}\right)^{1/k} \frac{p_0}{p_1} \quad \frac{1 - \varphi^2 (1 - s)}{\sqrt{1 - s}}$$

$$x \left[\left\{\left(\frac{X}{R_1}\right)^2 + \left(\frac{R_{20}}{R_1}\right)^2\right\}^{3/2} - \left\{\left(\frac{X}{R_1}\right)^2 + \left(\frac{R_{2i}}{R_1}\right)^2\right\}^{3/2}\right] \qquad (2.84)$$

K is a function of U_1/c_0, p_1/p_0, and p_2/p_0 only. With reference to the results of the experimental turbines that will be described in Chapter 5, the value of K will be expressed as in Figures 2.46 and 2.47, the former estimating the value of the collision loss coefficient, ζ_s, to be 0.8, and the latter with $\zeta_s = 1.0$. Very little difference will be noted between the two cases, whether $\zeta_s = 0.8$ or $\zeta_s = 1.0$. From those figures, it may be safely concluded that the value of K is fixed and unrelated to the general working conditions, which also tells us that the hypothetical average efflux angle of the blade, $\bar{\beta}_2$, can be adopted with safety in our calculations. Accordingly, if we can determine from (2.84) the value of K any given point (for instance at the designing point), this value can be regarded as properly pertinent to the turbine, unchanged by the working conditions. In this case, the equation (2.84) will be:

$$f\ (U_1/c_0,\ p_1/p_0,\ p_2/p_0) = 0 \tag{2.85}$$

The value of p_1/p_0 will thus be determined by U_1/c_0 (or by $U_1\sqrt{T_0}$) when the total expansion ratio, p_0/p_2, is given. This also enables us to determine the reaction, r.

$$r = 1 - \frac{1 - s}{1 - s_0} \tag{2.86}$$

Figure 2.48 shows the reactions in linear forms obtained by means of calculating the value of p_1/p_0 with reference to each U_1/c_0 when $K = 0.514$ and $p_0/p_2 = 1.20$, 1.15, and 1.09, respectively. On the other hand, the asterisks and crosses show the reactions obtained by means of measuring the static pressures of the blade inlet. The calculated values are thus proved to agree fairly well with the values derived from the experiments.

If we express the gas flow, G, in non-dimensional form,

$$\chi = \frac{G}{c_{0\gamma 0}} \cdot \frac{1}{2\pi R_1 B_1 \sin\alpha} \tag{2.87}$$

Calculating from (2.11.1)

$$\chi = \varphi \frac{p_1}{p_0} \cdot \frac{\sqrt{1 - s}}{1 - \varphi^2 (1 - s)} \tag{2.88}$$

with reference to the values of each p_0/p_2 and U_1/c_0, the equation $s = (p_1/p_0)^{(k-1/k)}$ can be determined from (2.84) and the value of χ from (2.88). Figure 2.49 shows the almost uniform concurrence of the values of χ thus calculated from (2.87) and the results of experiment by the test turbine.

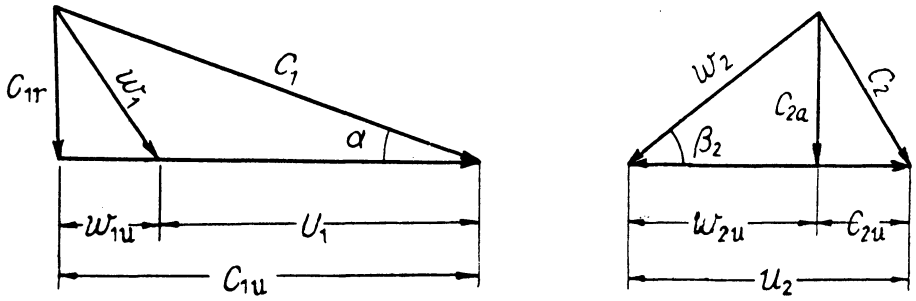

Velocity Diagram of Blade Inlet

Velocity Diagram of Blade Outlet (Radius R)

Figure 2.45 Velocity Diagram.

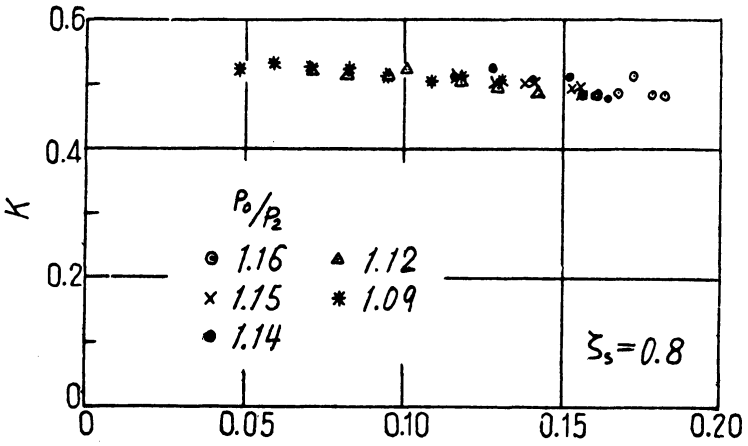

Circumferential Velocity U_1/C_o

Figure 2.46 The Value of K(ζ_s = 0.8).

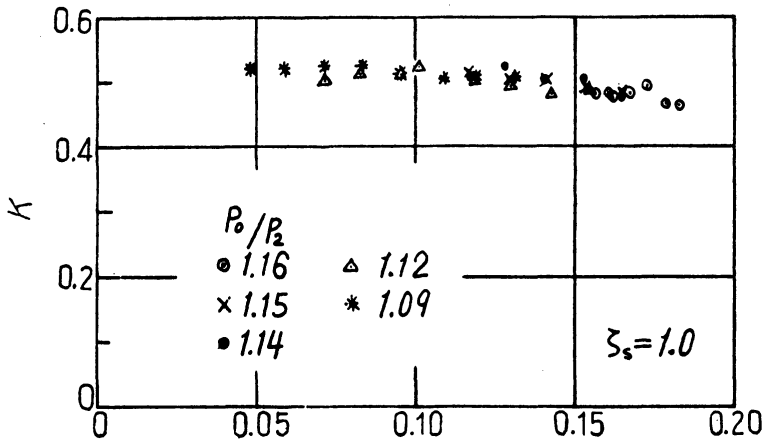

Cu Circumferential Velocity U_1/C_o

Figure 2.47 The Value of K(ζ_s = 1.0)

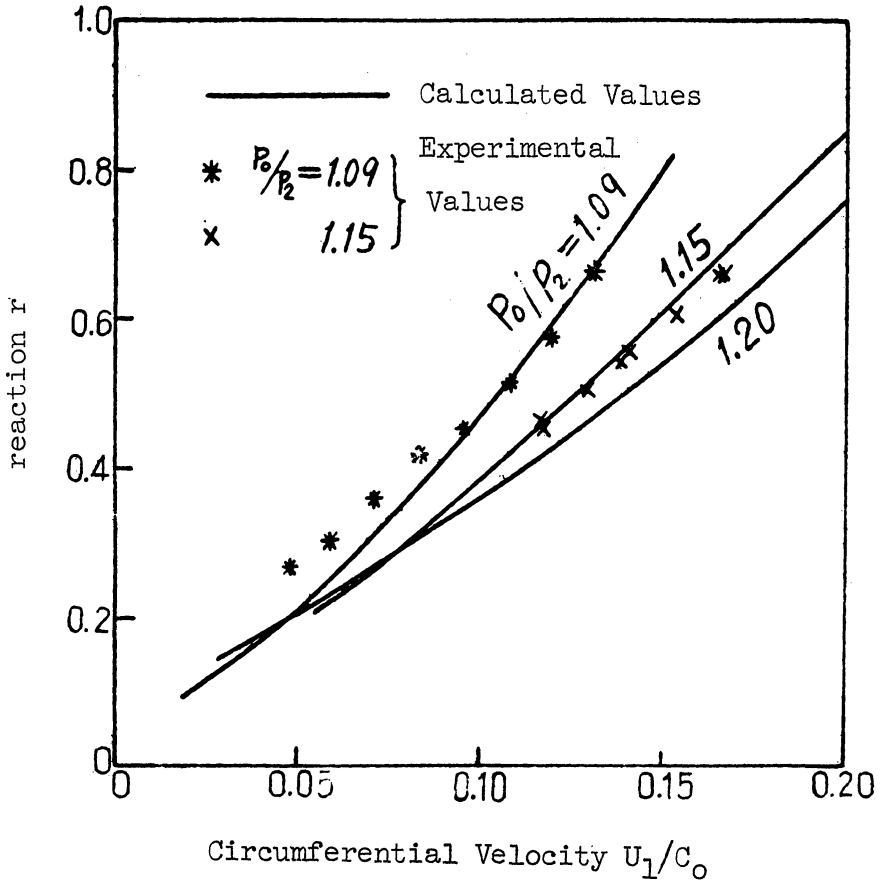

Figure 2.48 Reaction.

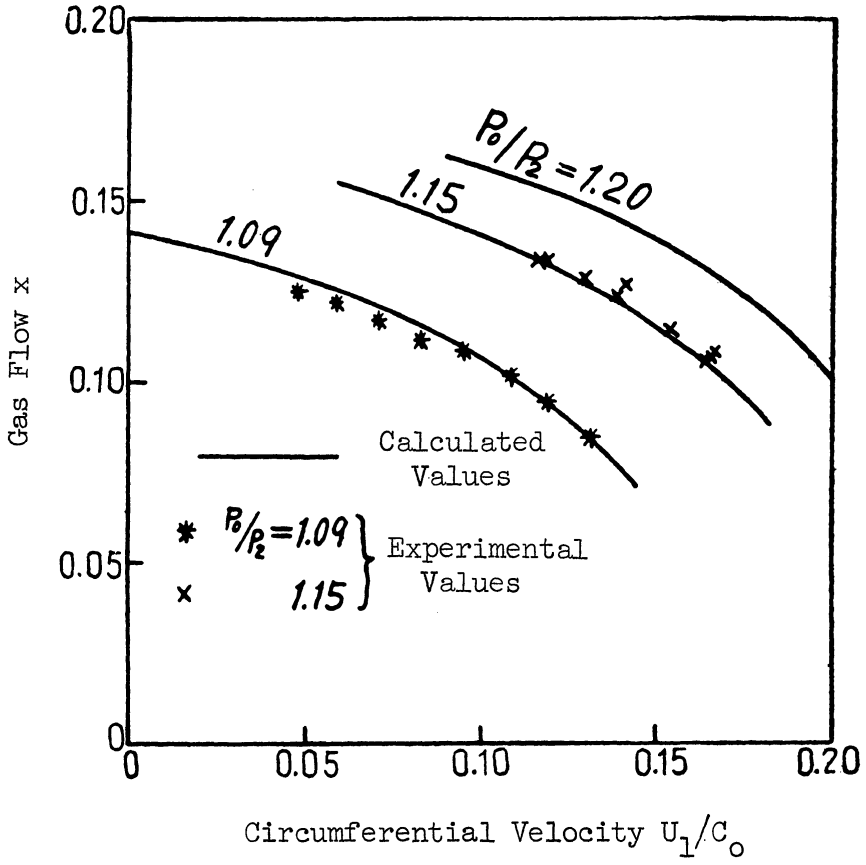

Figure 2.49 Gas Flow.

In summing up, the value of the hypothetical average efflux angle, $\bar{\beta}_2$, should be so determined that the blade-outlet gas flow obtained by integrating the whole outlet radius may be equal to the total gas flow. By thus defining $\bar{\beta}_2$ as being fixed regardless of the working conditions, we can also define the value of K as characteristic of the turbine itself. Then p_0/p_1 will be determined from (2.84) with reference to each of p_0/p_2 and $\bar{U}_1/c_0$, and the reaction and the non-dimensional gas flow, χ, can be calculated from (2.88).

(b) Output torque

The output torque working upon the blade is given in the following formula:

$$T_i = \frac{G}{g} c_1 \cos \alpha \cdot R_1 - \int_{R_{2i}}^{R_{20}} \frac{dG}{g} c_{2u} R \tag{2.89}$$

The second term of the second half of the above equation is the angular momentum of the outlet gas which, together with dG and c_{2u}, varies in such a complex manner in accordance with the outlet radius, R, that its integration becomes very difficult to be carried out. We must then make the following approximation.

It is assumed that the total outlet gas, G, passes the average radius, $\bar{R}_2$, of the blade outlet at the relative average efflux angle of $\bar{\beta}_T$. The method of deciding the values of $\bar{R}_2$ and $\bar{\beta}_T$ will be described later. The output torque, T_i, will be:

$$T_i = \frac{G}{g} \{c_1 \cos \alpha \cdot R_1 - (u_2 - w_2 \cos \bar{\beta}_T)\bar{R}_2\} \tag{2.90}$$

The outlet relative velocity, w_2, at this point can be calculated from (2.78) as follows:

$$w_2 = \psi_2 \omega \sqrt{X^2 + \bar{R}_2^2} \tag{2.91}$$

Substituting this with (2.90), T_i will be:

$$T_i = \frac{G}{g} R_1 U_1 \left\{ \varphi \frac{c_0}{U_1} \sqrt{1 - s} \cos \alpha - \left(\frac{\bar{R}_2}{R_1}\right)^2 \right.$$

$$\left. + \psi_2 \left(\frac{\bar{R}_2}{R_1}\right) \cos \bar{\beta}_T \sqrt{\left(\frac{X}{R_1}\right)^2 + \left(\frac{\bar{R}_2}{R_1}\right)^2} \right\} \tag{2.92}$$

The average efflux angle, $\bar{\beta}_T$, will therefore be:

$$\cos \bar{\beta}_T = \frac{\frac{\bar{R}_2}{R_1} - \left(\varphi \sqrt{1 - s} \cos \alpha - \frac{T_i}{G/g \cdot R_1 c_0} \right) \frac{c_0}{U_1} \cdot \frac{R_1}{\bar{R}_2}}{\psi_2 \sqrt{\left(\frac{X}{R_1}\right)^2 + \left(\frac{\bar{R}_2}{R_1}\right)^2}} \qquad (2.93)$$

Since the average radius, $\bar{R}_2$, of the blade outlet is a hypothetical point whereto all the gas flow is supposed to converge, it should be sought after at a place where most gas actually flows at the turbine outlet. According to the results obtained from the test turbine (see Figure 5.14, Chapter 5), the position of the radius wherein most gas flow will converge at the turbine outlet will be expressed as follows, regardless of any change in the working conditions:

$$\bar{R}_2 = R_{2i} + \frac{3}{4} (R_{20} - R_{2i}) \qquad (2.94)$$

Needless to say, the value of $\bar{R}_2$ varies with each particular turbine. However, the designing procedure, such as has been described in this chapter, bring about generally similar distributions of the outlet radius directions of the axial velocity, c_2, as well as the relative efflux angle, β_2, of the turbine outlet. The point, therefore, serves as a basis upon which the above formula (2.94) is established.

Figure 2.50 shows the values of $\cos \bar{\beta}_T$ obtained from (2.93) with reference to (2.94) and the actual torque, T_i, scattered around the point at which $\psi_2 \cos \bar{\beta}_T = 0.22$. However, the value of $(u_2 - w_2 \cos \bar{\beta}_T)\bar{R}_2$ in (2.90) being below about 1/10 of the value of $c_1 \cos \alpha \cdot R_1$ by which the torque, T_i, is mainly affected, there will not be any considerable change in T_i even if $\bar{\beta}_T$ is fixed. The torque, T_i, is presented in the following non-dimensional quantities:

$$\tau = \frac{T_i}{\gamma_0 T_0} \cdot \frac{1}{4\pi J c_p} \cdot \frac{1}{R_1^2 B_1 \sin \alpha} \qquad (2.95)$$

From (2.92) and (2.87),

$$\tau = \chi\left[\varphi \sqrt{1 - s} \cos \alpha - \frac{U_1}{c_0} \cdot \frac{\bar{R}_2}{R_1} \left\{ \frac{\bar{R}_2}{R_1} \right.\right.$$

$$\left.\left. - \psi_2 \cos \bar{\beta} \sqrt{\left(\frac{X}{R_1}\right)^2 + \left(\frac{\bar{R}_2}{R_1}\right)^2} \right\} \right] \qquad (2.96)$$

Figure 2.51 shows the τ calculated from (2.96) with $\psi_2 \cos \bar{\beta}_\tau = 0.22$. The calculated values are expressed in linear forms which agree fairly well with the experimental values in crosses and asterisks obtained from (2.95).

In summing up, the output torque, converging in the average radius, $\bar{R}_2$, of the blade outlet, makes it possible to consider the value of its average efflux angle, $\bar{\beta}_\tau$, as a constant, unaffected by a change in the working conditions. Accordingly, if the working condition at any given point (for instance, at the designing point) is clear, the value of $\bar{\beta}_\tau$ can be obtained from (2.93). This will then enable us to determine, from (2.96), the output torque when a change occurs in the working conditions.

(c) Output power

The output power, L_i, is expressed as follows:

$$L_i = T_i \cdot \omega \qquad (2.97)$$

When expressed in non-dimensional quantities,

$$\xi = \frac{L_i}{\gamma_0/g \cdot c_0^3 \cdot 2\pi R_1 B_1 \sin \alpha} \qquad (2.98)$$

From (2.97) and (2.95),

$$\xi = \tau \frac{U_1}{c_0} \qquad (2.99)$$

Since the value of τ with reference to each p_0/p_2 and U_1/c_0 can be calculated the value of ξ, obtained from the above formula, will be expressed in linear forms as in Figure 2.52. The figure shows an almost uniform agreement between the calculated values of the output power and the experimental values measured according to (2.98).

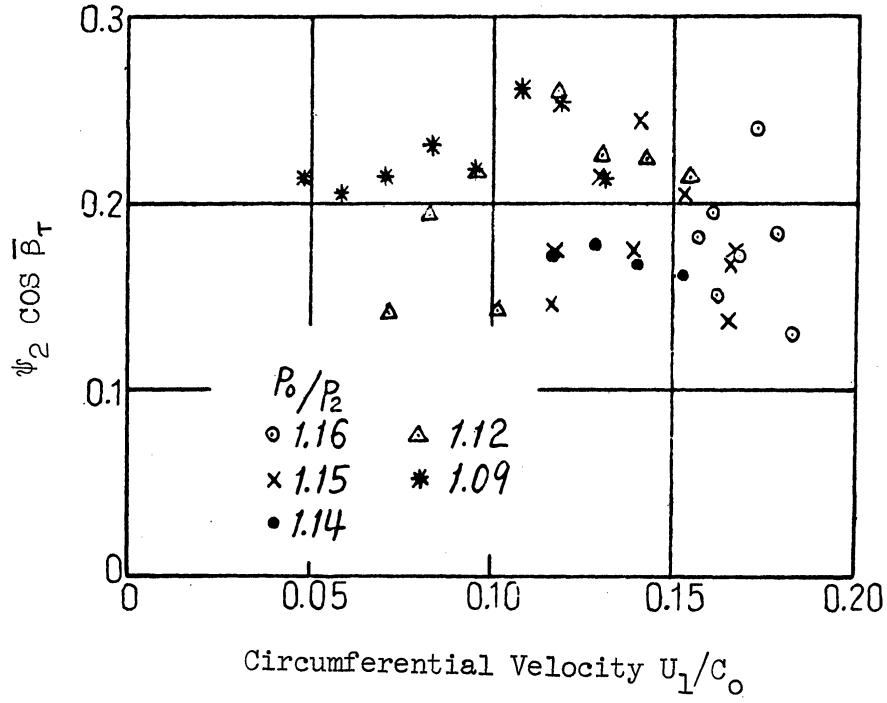

Figure 2.50

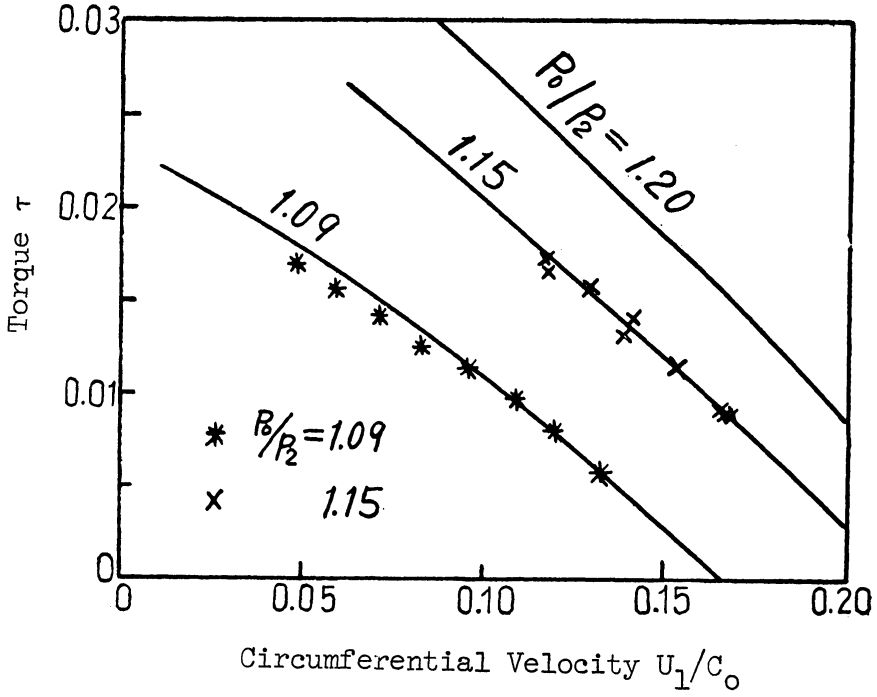

Figure 2.51 Torque.

(d) Internal efficiency

The internal efficiency, η_i, is presented as follows:

$$\eta_i = \frac{L_i}{L_{is}}$$

$$= 2\frac{U_1}{c_0} \cdot \frac{1}{1 - s_0}\left[\varphi\sqrt{1 - s}\cos\alpha - \frac{U_1}{c_0} \cdot \frac{\bar{R}_2}{R_1} \times \right.$$

$$\left. \left\{ \frac{\bar{R}_2}{R_1} - \varphi_2 \cos\bar{\beta}_T \sqrt{\left(\frac{X}{R_1}\right)^2 + \left(\frac{\bar{R}_2}{R_1}\right)^2} \right\} \right] \qquad (2.100)$$

In Figure 2.53, the linear forms indicate the values of η_i calculated from (2.100) with reference to each p_0/p_2 and U_1/c_0, whereas the asterisks and crosses show the values of η_i measured in the experiment. The dots represent the internal efficiency, η_i, obtained by subtracting the loss of turbine heat from the loss of temperature that has fallen from the turbine inlet to the turbine outlet ($p_0/p_2 = 1.09$, see Chapter 5), and the ⊙ signs represent internal efficiency obtained by measuring the outlet wind velocity distribution at each radial point of the turbine outlet and the output torque working upon the blade ($p_0/p_2 = 1.15$, see Chapter 5). Here again, a general agreement is recognized between the calculated and experimental values, even though the former tend to be somehow higher than the latter when the number of revolutions is small.

2.4.2. Summary

(1) An hypothetical average efflux angle, $\bar{\beta}_2$, of the blade outlet may be assumed when calculating the quantity of the gas flow and the reaction when the turbine is being operated at points other than the designing point. By using this hypothetical $\bar{\beta}_2$, the value of K can be defined as characteristic of the turbine proper, unrelated to its working conditions. When any given point (for instance, the designing point) of the working conditions is made clear, the value of K can be obtained, which will in turn make it possible to determine the non-dimensional quantity of the flow, X, and the reaction at the time when there is a change in the total turbine-expansion ratio, in the turbine-inlet temperature, as well as in the number of revolutions.

(2) In calculating the output torque the average radius and the average efflux angle of the blade outlet, $\bar{\beta}_T$, will be assumed. The value of $\bar{\beta}_T$ show little change in spite of the working conditions. Accordingly, if the working conditions at any given point are made clear, it is possible to determine the non-dimensional quantity of the output torque, τ, where there is a change in the working conditions.

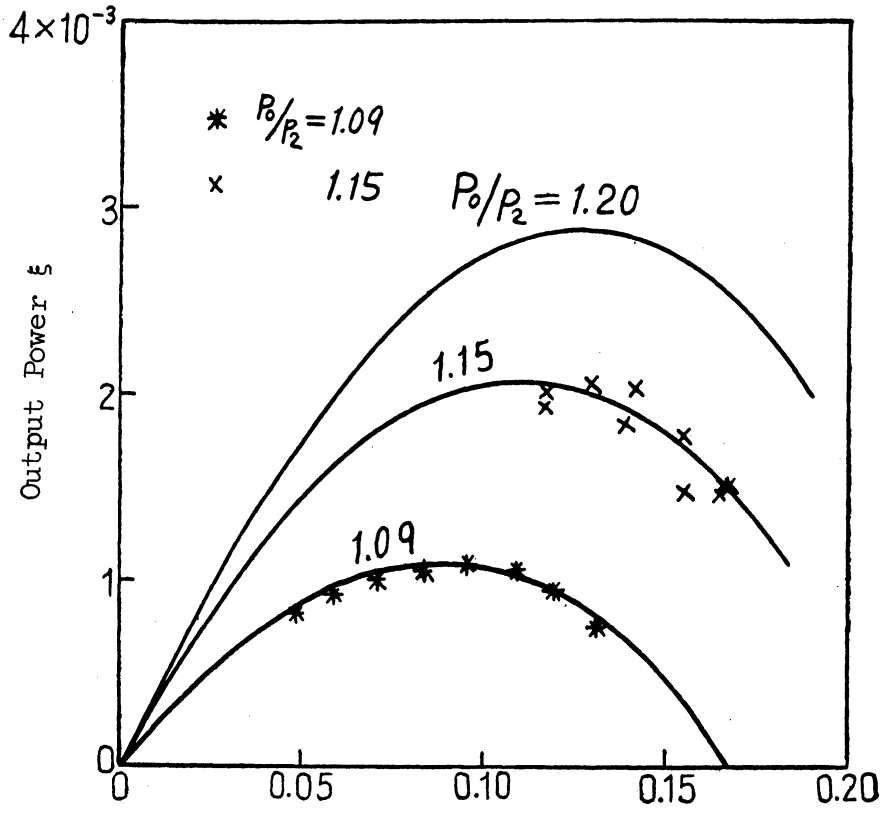

Figure 2.52 Output Power

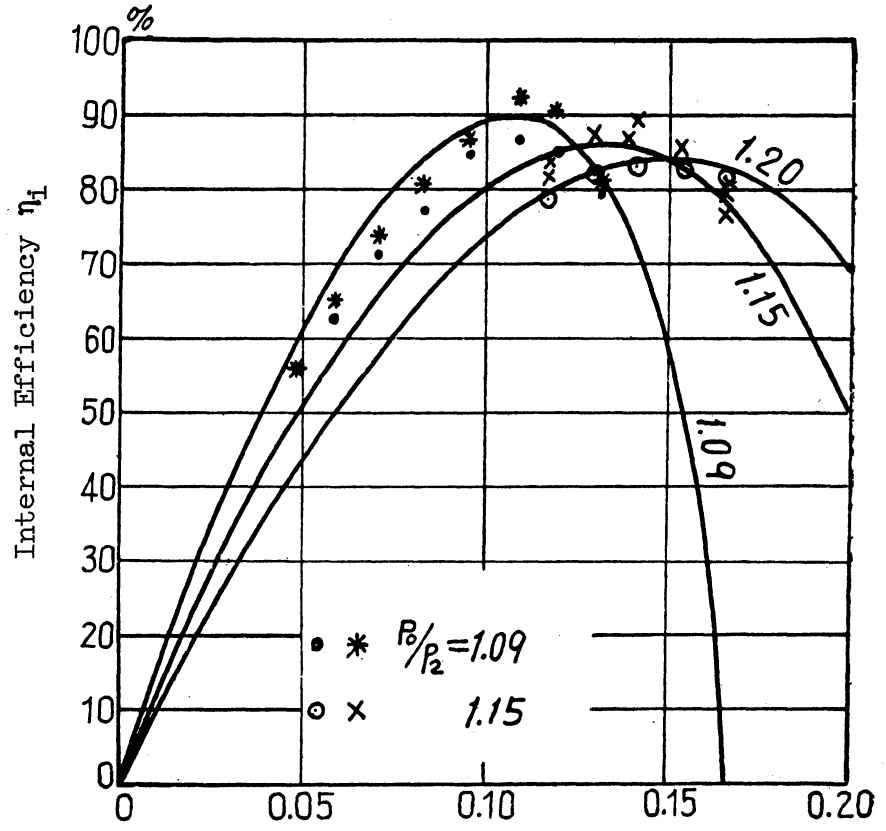

Figure 2.53 Internal Efficiency

(3) Based upon the above considerations, the calculations can be made in advance as to the output power as well as the internal efficiency in case of change in the working conditions.

CHAPTER 3

THE NOZZLE(18)

3.1. Outline

As shown in Figure 3.1, the radial turbine makes use of the nozzles which are arranged on the circle. So far, no study of this type of circular nozzles used in a radial turbine has been made available in comparison with the voluminous publications on the nozzles used in an axial turbine. Though we may avail ourselves to a certain degree of those studies of axial-turbine nozzles in our investigation of the central flow of gas which receives little influence from the lateral walls of the nozzles, we must take into account considerable differences existing between the axial-turbine nozzles and the radial-turbine nozzles in their surface friction as well as in their effects upon the gas pressure.

In the present study several types of nozzles are tested by the nozzle test equipment not using the moving blades, in which experiment, the mean efflux angles of flow from nozzles and losses in the nozzles are measured. In the theoretical studies worked out on the results obtained in the experiment, considering the losses in the nozzles in three parts, namely, side-wall friction loss, profile friction loss, and secondary loss, experimental formulas are derived in each of the losses. These formulas represent the effects of nozzle attaching angle, pitch of nozzles, aspect ratio and Reynolds number. Using the results obtained, nozzle designing procedures are presented, by which the total loss in a nozzle can be minimized and we may take the value of the nozzle velocity coefficient as high as 0.975 ~ 0.985.

3.2. Test Equipment

The nozzle test equipment is drawn in Figure 3.2 and photographically shown in Figure 3.3. The air which has been compressed in the Root and centrifugal compressors passes through the spiral chamber into the test nozzles wherein it starts to expand. The air, coming out of the nozzle, flows into the vanes (I) in which it loses most of its circumferential velocity it had acquired in the nozzle, and from which it emerges into the vanes (II) at an axial velocity, to be discharged into the atmosphere. The vanes I are formed like those used in a very common blower. The vanes II have three compartments separated by cylinders between which are attached many partition planks of about 10 mm in the direction of axis. The vanes are supported by two shaft bearings

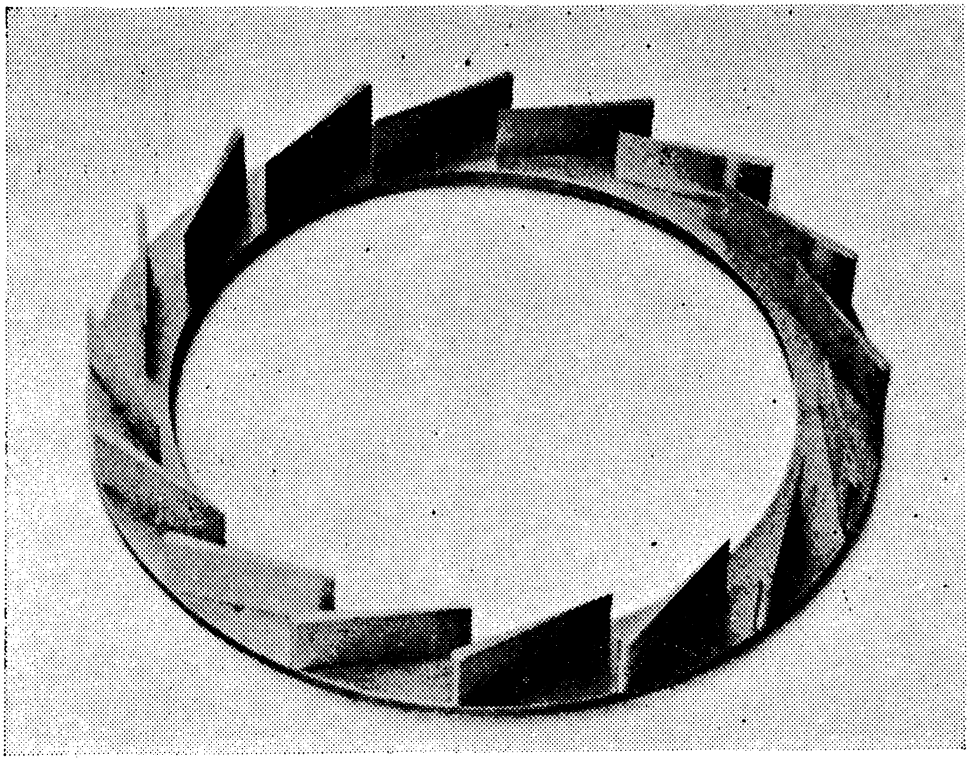

(a) ST-Type Nozzle

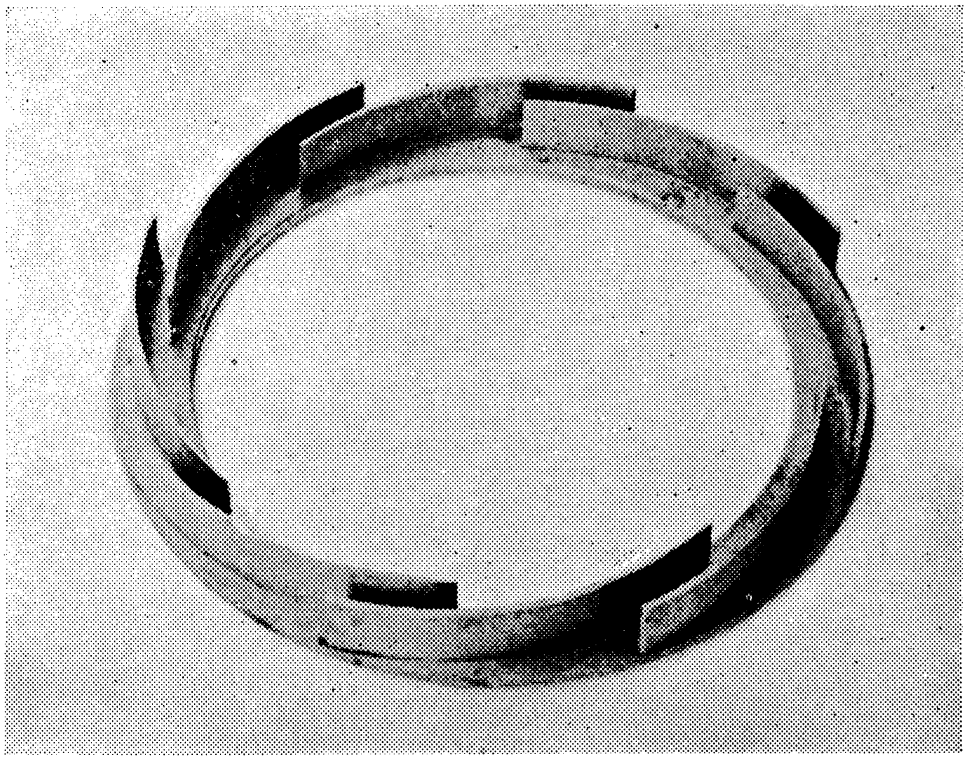

(b) SP-Type Nozzle

Figure 3.1 Circumferential Nozzles.

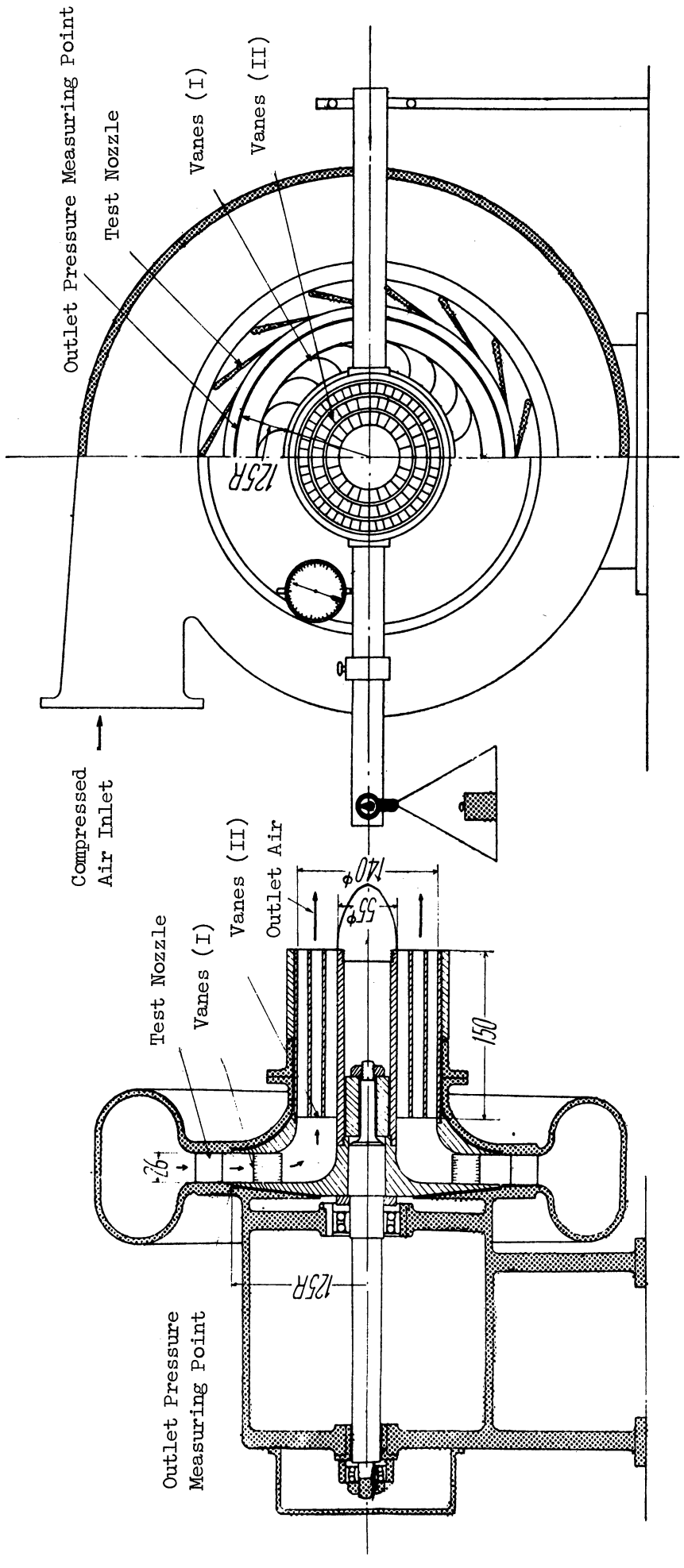

Figure 3.2 Nozzle Test Equipment.

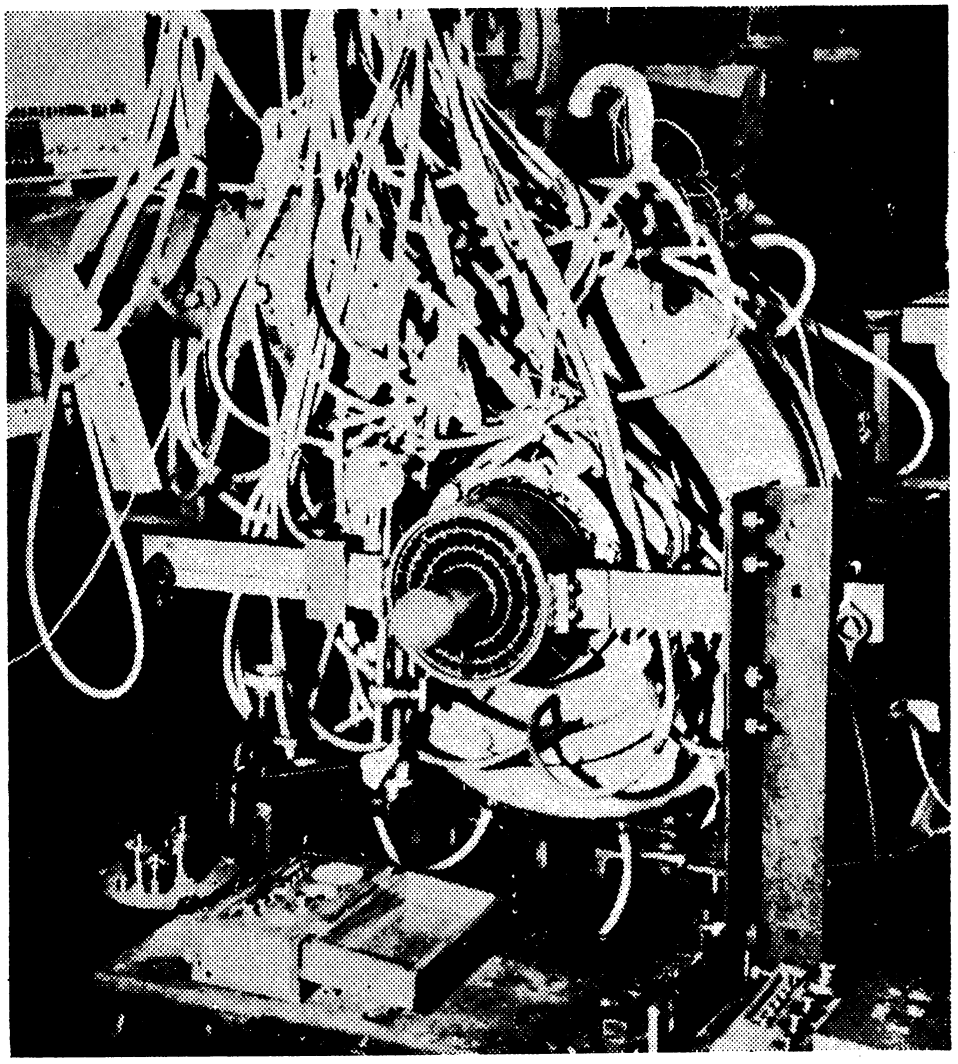

Figure 3.3 Photography of Nozzle Test Equipment.

which permit them to rotate freely with the axis. A heavy plumb-bob is used on the fixed arm of the rotatory part in order to stop the rotation. When in a state of repose, the torque of the air jetting out of the nozzle is balanced with the torque of the plumb-bob. Thus the angular momentum of the jet of air from the nozzle can be determined by measuring the torque of the plumb-bob. The flow of air is measured by using the circular nozzle aerometer at the inlet of the compressor. The total pressure of the spiral chamber inlet is obtained from both the static pressure measured by the pressure hole on the wall of the spiral chamber inlet, and the average dynamic pressure obtained by measuring the flow. The air temperature is measured by the precision mercurial thermometer of 1/10°C graduation, attached at the inlet of the spiral chamber. The pressure after the expansion in the nozzle is measured by the static pressure hole in the 125 mm radius and permits the free spiral flow of the air.

Test Nozzles

The two types of nozzles used in the test are the spiral-type (SP) nozzles and the straight-type (ST) nozzles, in both of which the equal interval is kept between each of them. The SP type is one with logarithmic spiral, while the ST type is one whose straight nozzles have round outside edges. Both types are shown in Figure 3.4. A variety of angles are adopted for both the spiral type with eight nozzles and the straight type with 16 and 20 nozzles. The breadth of the nozzles is uniformly 26 mm. The straight type uses only one kind of vane with the same measurements (see Figure 3.5), differing only in its number and its angle at which it is attached. ST-20-1 and ST-16-1, ST-20-2 and ST-16-2, share respectively the same angles of attachment, with the difference that the former of each group uses 20 vanes while the latter uses 16 vanes. The principal measurements of the test nozzles are shown below:

Types of Nozzles	SP-8	ST-16-1	ST-16-2	ST-16-3	ST-16-4	ST-20-1	ST-20-2
Number of Nozzles	8	16	16	16	16	20	20
$R_{in.}$ mm	135.0	135.0	139.0	141.8	144.2	135.0	139.0
a mm	13.28	15.09	11.30	8.43	5.80	10.51	7.30

Figure 3.6 shows these nozzles in isometrical straight system. The mathematical calculation being difficult, Figure 3.6 was based upon diagrammatic drawings.

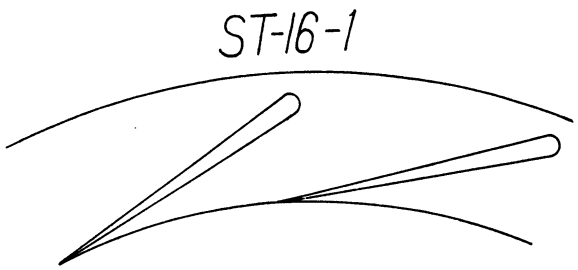

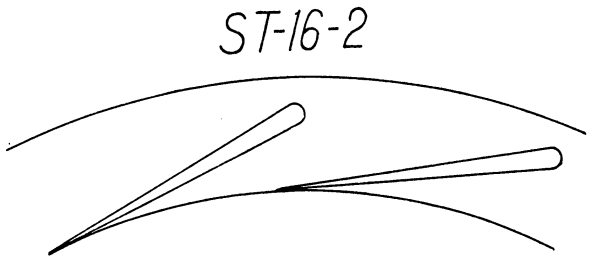

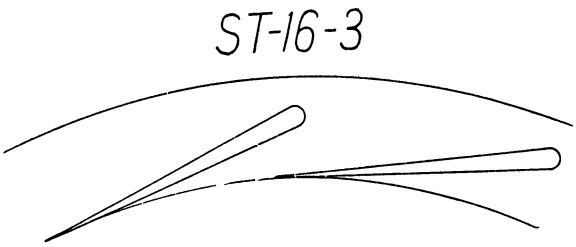

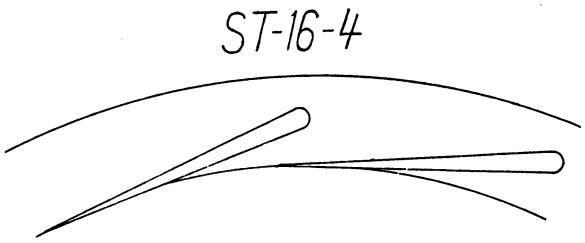

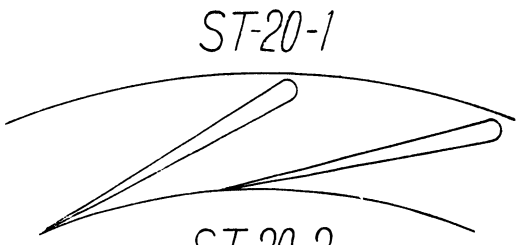

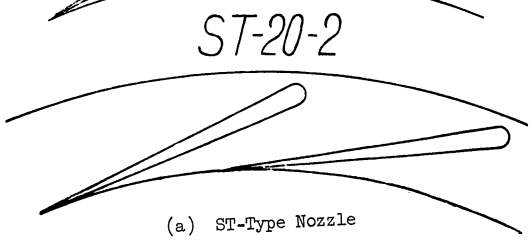

(a) ST-Type Nozzle

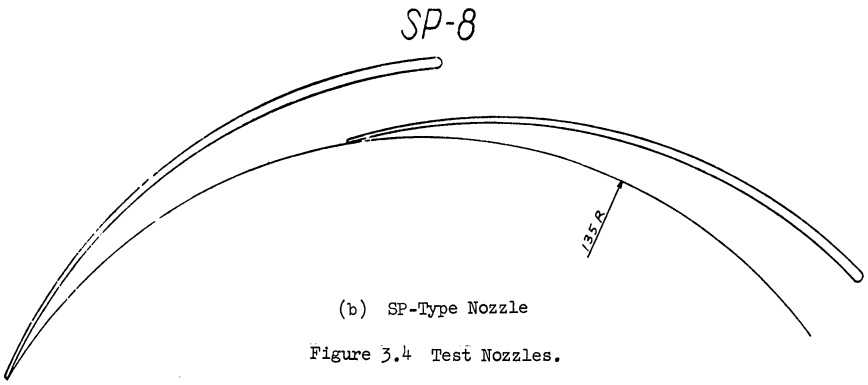

(b) SP-Type Nozzle

Figure 3.4 Test Nozzles.

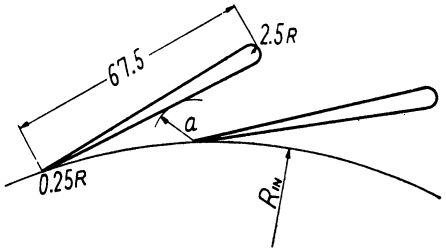

Figure 3.5 Straight Nozzle Wings

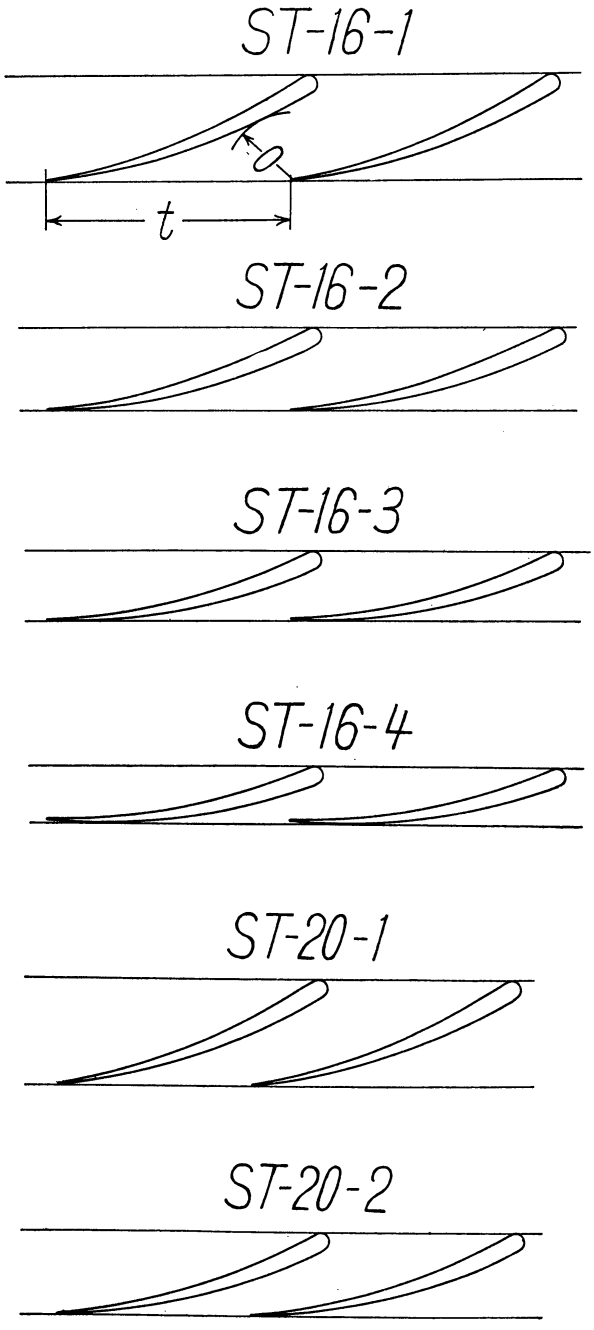

(a) ST-type Nozzle

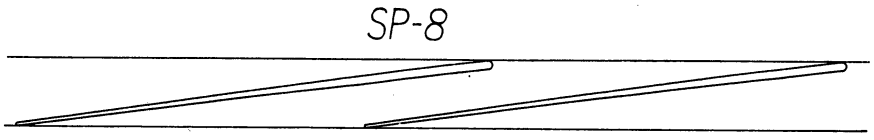

(b) SP type nozzle

Figure 3.6 Isometrical Drawings of the Test Nozzles

3.3. Results of the Experiment

Strictly speaking, the air flow after the expansion in the nozzle does not take the uniform direction. Since too much time will be needed for measuring the direction and the size of the air flow, seven pressure holes for each pitch are made on the radius, R_1, behind the nozzle so as to measure the distribution of the static pressure in the direction of the pitch (see Figures 3.7 and 3.8). The pressure distribution of the SP-type nozzles is shown in Figure 3.9(a), in which p_0 stands for the pressure of the spiral chamber inlet, p_1, for the static pressure behind the nozzle (on the radius, R_1), and p_{1m} for the average value of p_1 between each pitch. From the figure it will be noted that the change of the nozzle expansion ratio between each pitch falls within the range of $\pm 0.8\%$. In order to observe the pressure distribution on the total circumference, measurement was made of the static pressure distribution in the center of the nozzle on the radius, R_1 (see Figure 3.8). The result is also shown in Figure 3.9(b), which indicates that the change of the expansion ratio for the entire circumference also falls within the limit of 1%. We can therefore regard the mean number in the measuring points No. 26 ~ 32 which also applies to the average pressure on the entire circumference, as the pressure of the air after its expansion in the nozzle. We may put aside the change in the static pressure distribution in the direction of the nozzle wings (vanes) which is smaller than that in the direction of the pitch. The above considerations enable us to regard the flow of the air after its expansion in the nozzles as the average flow that has undergone a uniform expansion under the average pressure, p_1. The velocity of the average flow is represented by c_1, and the mean efflux angle of the flow by α. Since the flow discharged from the vanes II consist only of axial component, without any circumferential components, the angular momentum contained in the jets out of the nozzles is equal to the torque, M, measured by the plumb-bob.

$$\frac{G}{g} c_1 \cos \alpha \cdot R_1 = M \tag{3.1}$$

The total gas flow, G, is measured by the circular nozzle aerometer.

$$c_1 \sin \alpha \cdot 2\pi R_1 B_1 \gamma_1 = G \tag{3.2}$$

B_1 stands for the breadth of the nozzle and γ_1 for the post-expansion density. If c_1' represents the velocity at the time of the equal entropy expansion from the total pressure of the spiral-chamber inlet, p_0, to the post-expansion static pressure, p_1, the velocity coefficient, φ, will be:

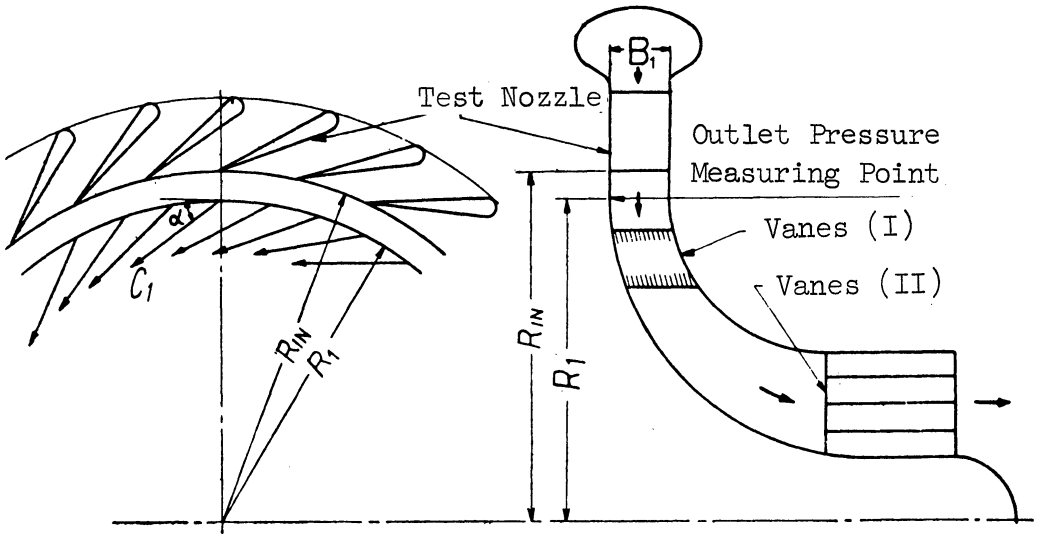

Figure 3.7

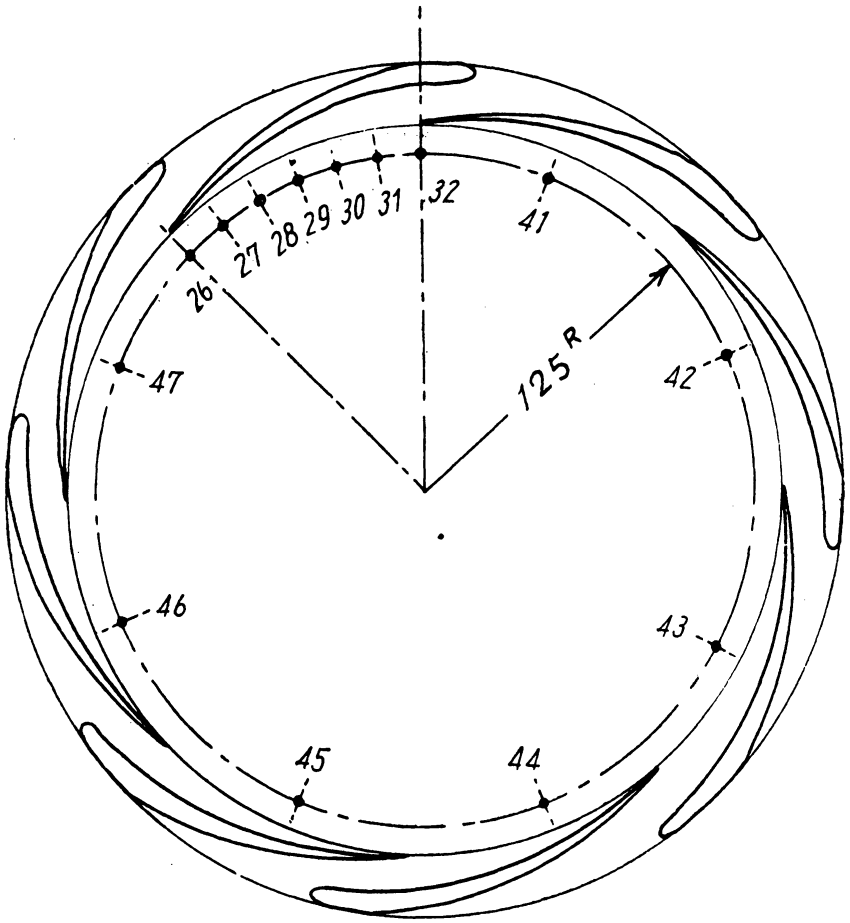

Figure 3.8 Measuring Points of Nozzle Outlet Pressure

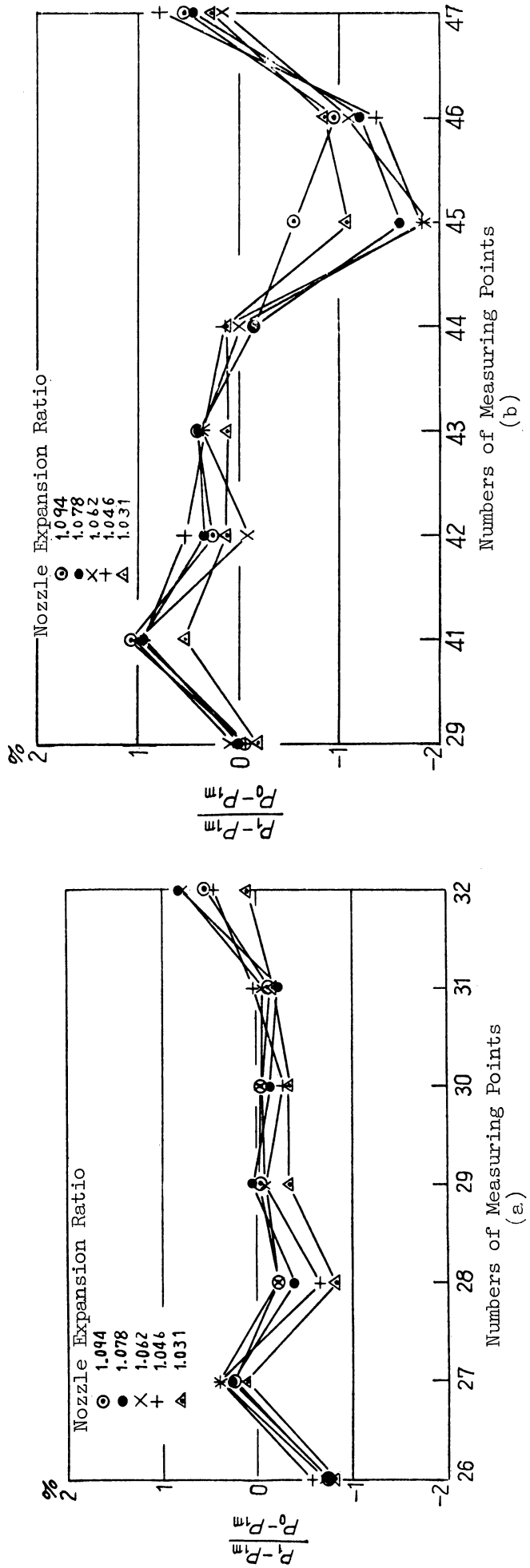

Figure 3.9 Outlet Pressure Distribution of Nozzle

$$\varphi = \frac{c_1}{c_1'} \tag{3.3}$$

c_1' can be determined by measuring the spiral chamber inlet pressure, p_0, temperature, t_0, and the post-expansion static pressure, p_1.

The post-expansion density, γ_1, can be given as follows (γ_0: inlet density):

$$\gamma_1 = \gamma_0 \frac{p_1}{p_0} \cdot \frac{1}{1 - \varphi^2 \left\{1 - \left(\frac{p_1}{p_0}\right)^{(k-1/k)}\right\}} \tag{3.4}$$

The velocity coefficient, φ, and the mean efflux angle, α, can be thus obtained by measuring p_0, p_1, G, M, t_0, in the four formulas mentioned above.

The loss coefficient, ζ, can be obtained in the formula below:

$$\zeta = \frac{\frac{\gamma_1}{2g}(c_1'^2 - c_1^2)}{\frac{\gamma_1}{2g} c_1^2} = \frac{1}{\varphi^2} - 1 \tag{3.5}$$

The correlation between the velocity coefficient, Φ, and the expansion ratio is shown in Figure 3.10, while that between the loss coefficient, ζ, and the Reynolds number, R_e (viz. the Reynolds number with reference to the chord (hypotenuse) of the nozzle and the efflux velocity, c_1) is shown in Figure 3.11. In Figure 3.12 is shown the correlation between the mean efflux angle from the nozzle and the expansion ratio. Within the experimental range, the mean efflux angle remains fixed and unrelated to the expansion ratio. Figure 3.13 shows the correlation between the mean efflux angle, α, and $\sin^{-1} 0/t$ of the straight sytem, with t standing for the pitch of the isometrical straight system and 0 for the breadth of the shortest passage in the nozzle outlet. α is the mean efflux angle with reference to the total expansion ratio of the nozzle. In the two-dimensional straight system, the efflux angle, α, almost coincides with $\sin^{-1} 0/t$ when the Mach number approximates 1, and tends to increase when the Mach number is below 1.[14][15] The mean efflux angle of the nozzle is smaller than $\sin^{-1} 0/t$ of the isometric straight system.

3.4. Analysis of Losses

Here, investigation will be made of the effects of the nozzle attaching angle, pitch of nozzles, aspect ratio and the Reynolds number upon the loss coefficient and the mean efflux angle of the nozzles.

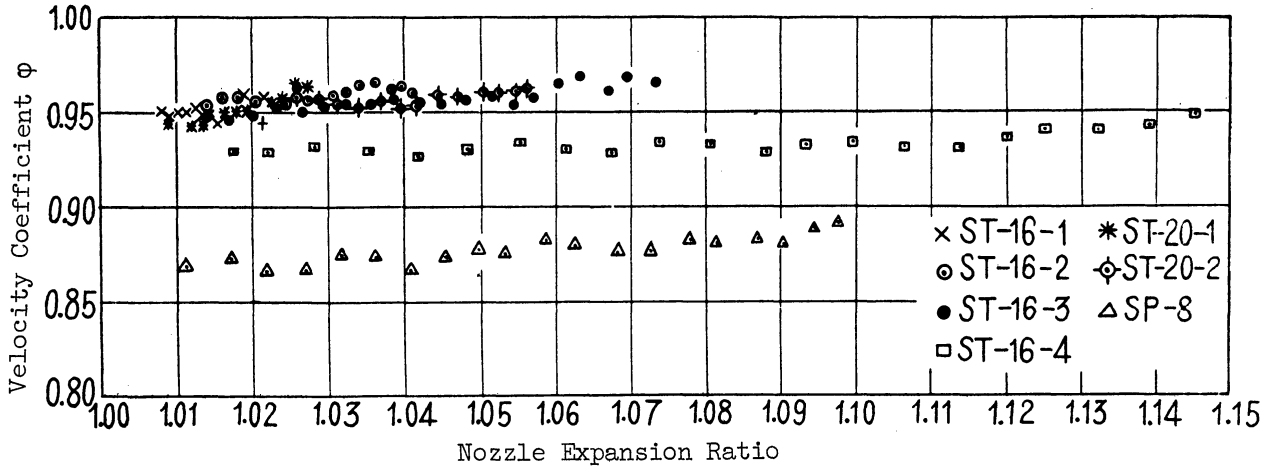

Figure 3.10 Velocity Coefficient of Nozzle

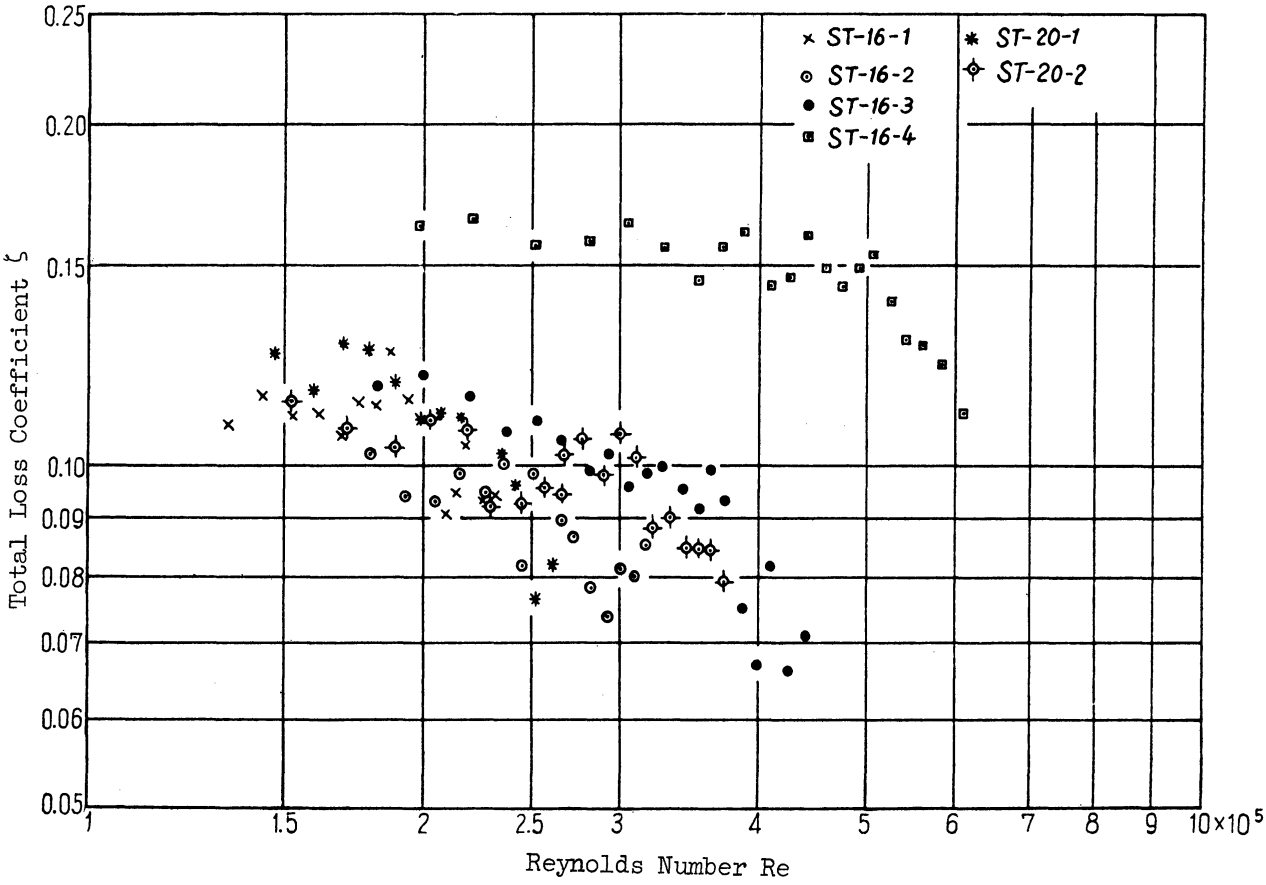

Figure 3.11 Loss Coefficient of Nozzle

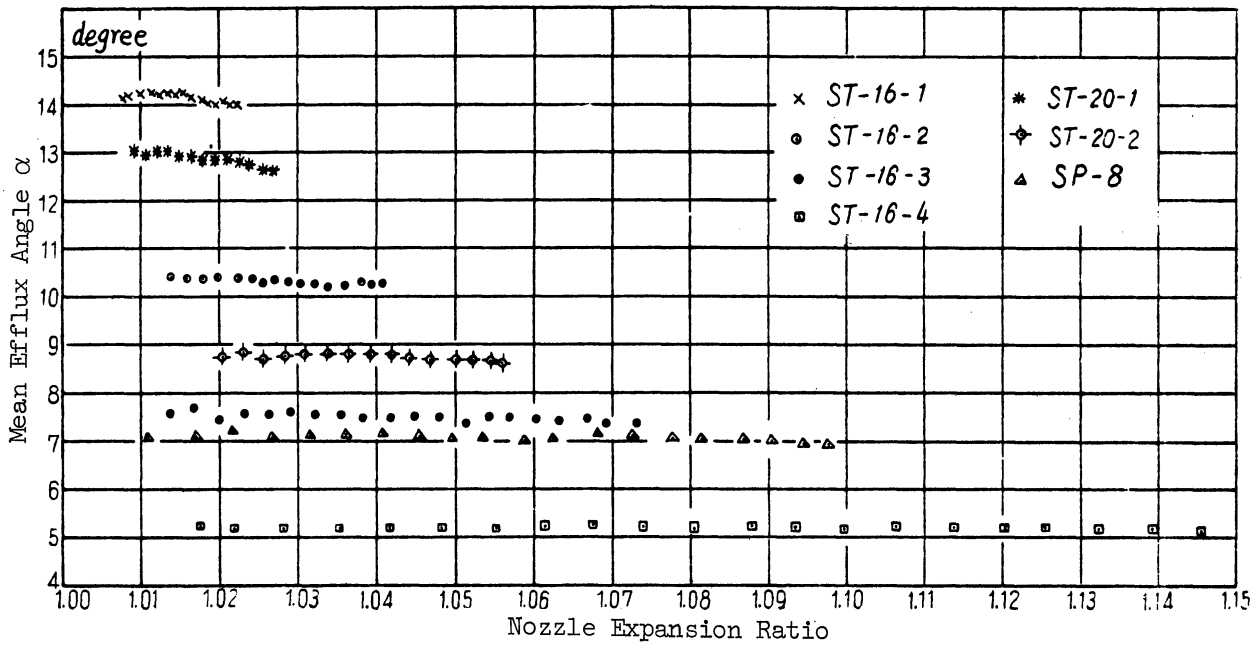

Figure 3.12 Mean Efflux Angle

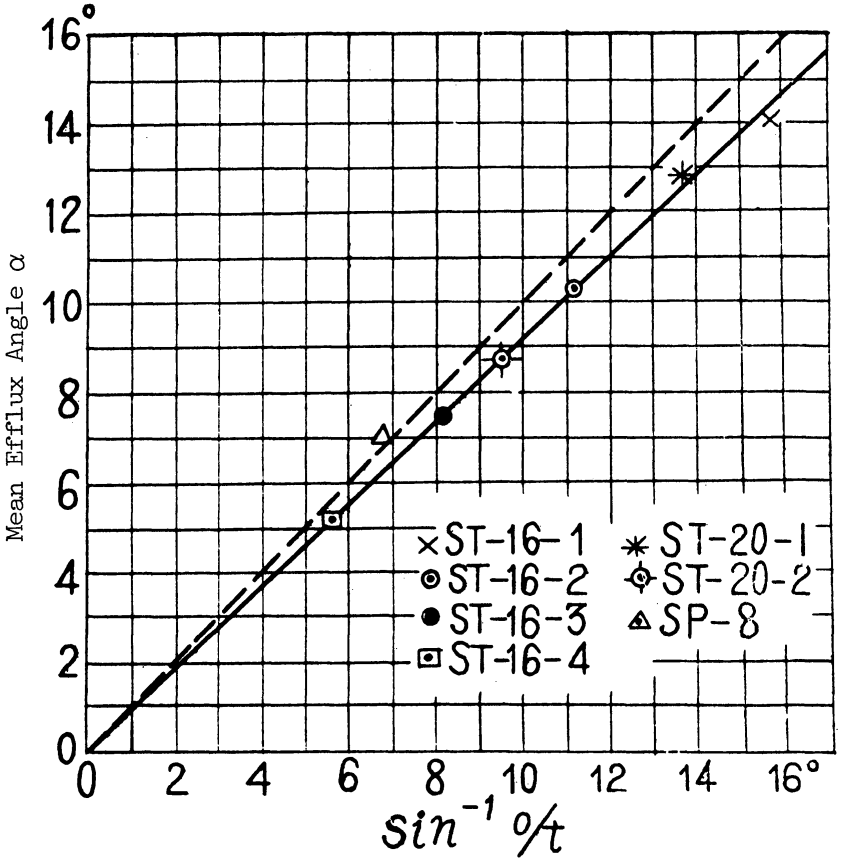

Figure 3.13

3.4.1. Mean Efflux Angle

The losses in the nozzles are considered in three parts: side-wall friction loss, profile-friction loss, and secondary loss. The side-wall friction loss is one that is caused by the friction in the side wall where the nozzles are attached; the profile friction loss is incurred by the friction in the profile, and the secondary loss is the loss caused by the spiral flow running in the nozzle with a certain radius of curvature.

Assuming a flow unaccompanied by any losses, with α^* representing the mean efflux angle (viz. the angle between the average velocity and a tangent to the circle, called lossless (loss-free) efflux angle), and c_1' representing its mean efflux velocity, the total momentum contained in the nozzle outlet will be:

$$2\pi R_{1N} B_1 \frac{\gamma_1}{g} c_1'^2 \sin^2\alpha^* \tag{3.6}$$

Here, the radius from the center to the nozzle outlet is indicated by R_{1N}, the breadth of the nozzle by B_1, and the gas density at the nozzle outlet by γ_1.

In reality, however, the momentum is affected by the side-wall friction loss and the profile-friction loss, and flows from the efflux angle at the velocity of c_1. The momentum in the radius direction at this time will be:

$$2\pi R_{1N} B_1 \frac{\gamma_1}{g} c_1^2 \sin^2 \alpha \tag{3.7}$$

Since the difference between these two momenta is due to the frictions of the side walls and profiles, it is possible to conceive of the following formula with regards to the component force of the side-wall friction, F_w, and the component force of the profile friction, F_p:

$$2\pi R_{1N} B_1 \frac{\gamma_1}{g} (c_1'^2 \sin^2\alpha^* - c_1^2 \sin^2 \alpha) = F_w + F_p \tag{3.8}$$

The velocity which is almost zero at the nozzle inlet becomes c_1 at the outlet after the expansion in the nozzle. Since the surface friction is directly proportional to the square of the velocity, we can consider that most of the side wall and profile frictions occur, not around the nozzle inlet, but rather near the nozzle outlet. Accordingly

the direction of the resultant force of all the frictions from the inlet to the outlet coincides approximately with direction of the efflux velocity. The following formulas will therefore be obtained when the friction forces work in the direction of the mean efflux angle:

$$\left.\begin{aligned} F_w &= 2A_w c_f \frac{\gamma_1}{2g} c_1^2 Z \sin \alpha \\ F_p &= 2A_p c_f \frac{\gamma_1}{2g} c_1^2 Z \sin \alpha \end{aligned}\right\} \qquad (3.9)$$

In the above formulas,

A_w = the oblique section of the wall area (see Figure 3.14)

A_p = the surface area of the nozzle vane

$= B_1 \ell$

ℓ = chord of the nozzle (hypotenuse)

Z = number of the nozzles

c_f = resistance coefficient of frictions

The circumferential pitch of the nozzle outlet, s, will be:

$$s = \frac{2\pi R_{1N}}{Z} \qquad (3.10)$$

Accordingly, from (3.8), (3.9), and (3.10),

$$\sin^2 \alpha^* = \varphi^2 \left(\frac{A_w + A_p}{sB_1} c_f \sin \alpha + \sin^2 \alpha \right) \qquad (3.11)$$

In the above formula φ is the velocity coefficient of the nozzle, and c_f is a function of the Reynolds number only. φ is naturally smaller than 1, though $\alpha^* > \alpha$, because of $\{ (A_w + A_p)/sB_1 \} c_f \sin \alpha$, which indicates that the mean efflux angle, α, of the flow is smaller than the hypothetical efflux angle of the flow from which the losses are eliminated.

By isometrically drawing the nozzle in the two-dimensional straight system, the angle of its efflux will be preserved. In the two-dimensional straight system, the flow at the nozzle outlet is for the

most part not affected by the shape of the outlet, and the mean efflux angle almost coincides with $\sin^{-1} 0/t$ (see Figure 3.6) when the outlet Mach number approximates 1. This indicates that where there is no loss by friction, the mean efflux angle will be identical to $\sin^{-1} 0/t$. The mean efflux angle of the lossless flow can thus be regarded as equal to the mean efflux angle of the two-dimensional straight system. In other words, the lossless efflux angle, α^*, equals $\sin^{-1} 0/t$. Since α and φ are clear from the results of the experiment as described in the preceding section, and since $\sin^{-1} 0/t = \alpha^*$, it is possible now to obtain the friction resistance coefficient, c_f, from (3.11). The correlation between c_f thus obtained and the Reynolds number, R_e, is shown in Figure 3.15. It may be noted from the figure that, where the Reynolds number is small, c_f of a given nozzle shows a fixed value, while it decreases as the Reynolds number becomes greater, and remains on the same curved line when the Reynolds number becomes sufficiently great. Since the Reynolds number used in an actual radial turbine falls within the range of $(5 \sim 15) \times 10^5$, the value of c_f can be expressed in the following formula, excluding the ranges of the small partial load or immediately after the start of the gas turbine.

$$c_f = 0.006 + \frac{1.55 \times 10^3}{R_e - 1.5 \times 10^5} \tag{3.12}$$

The mean efflux angle, α, of the actual nozzle can thus be obtained, first by isometrically drawing the nozzle in two-dimensional straight system from which $\sin^{-1} 0/t$ is to be determined as the lossless efflux angle, α^*, then by obtaining the value of c_f from (3.12) and finally from (3.11).

3.4.2. Loss Coefficient

By converting the side wall and profile friction losses into the pressure losses, represented respectively by δp_w and δp_p, the following formulas will be established:

$$\left.\begin{aligned} \delta p_w &= \frac{F_w}{2\pi R_{1N} B_1} \\ \delta p_p &= \frac{F_p}{2\pi R_{1N} B_1} \end{aligned}\right\} \tag{3.13}$$

Since c_f can be obtained from (3.12) and F_w, F_p from (3.9), the above formula (3.13) will determine the values of δp_w and δp_p. If the secondary loss is represented by δp_s, the total loss, δp, will be:

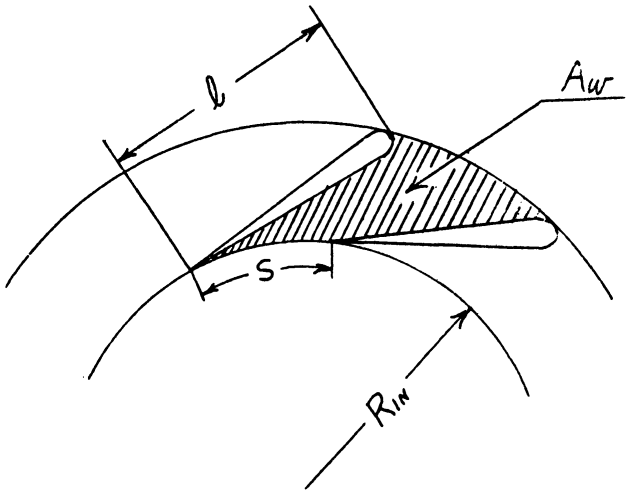

Figure 3.14

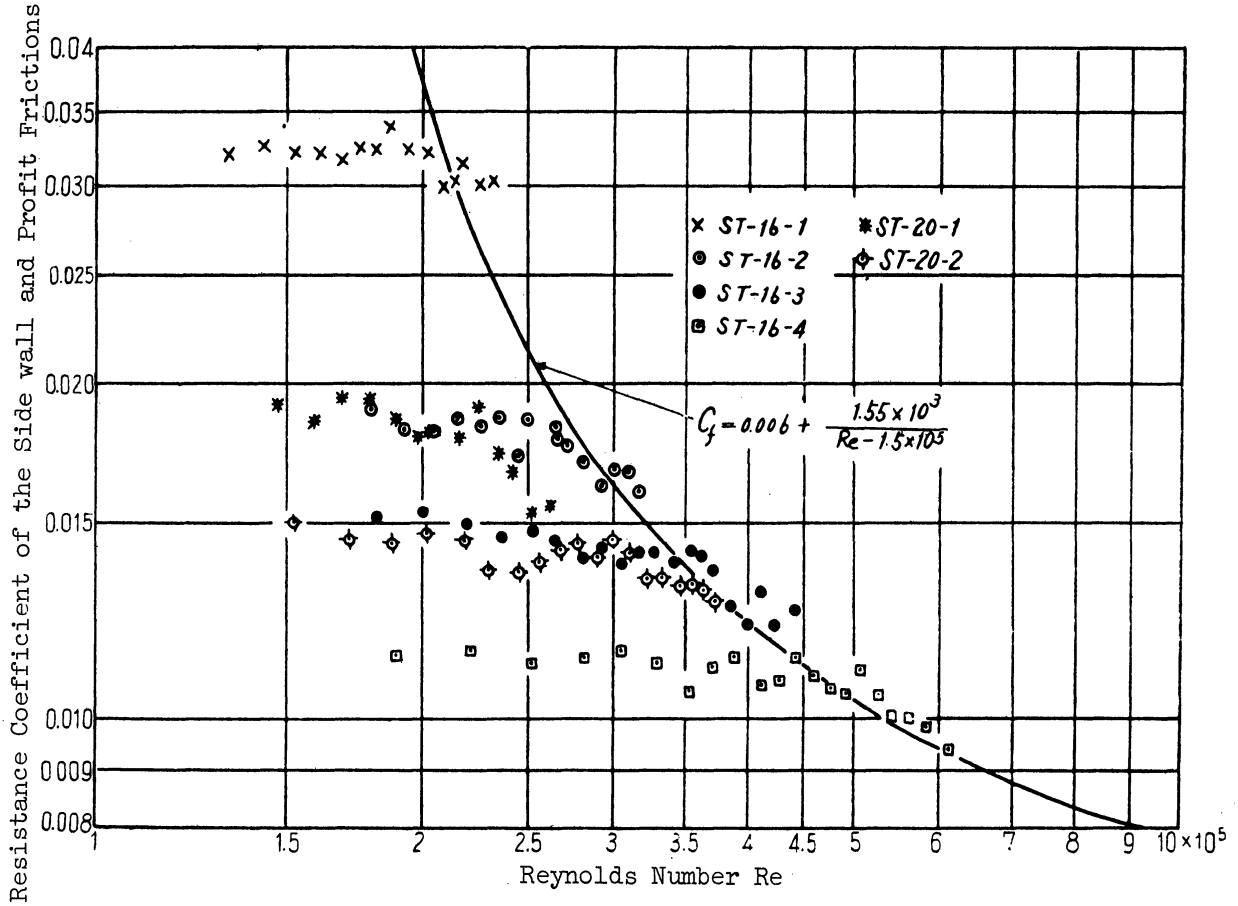

Figure 3.15 Friction Resistance Coefficient

$$\delta p = \delta p_w + \delta p_p + \delta p_s \tag{3.14}$$

If c_1 and c_1' stand for the actual efflux velocity and the lossless efflux velocity respectively,

$$\delta p_w + \delta p_p + \delta p_s = \frac{\gamma_1}{2g} (c_1'^2 - c_1^2) \tag{3.15}$$

If

ζ = total loss coefficient

ζ_w = side-wall friction-loss coefficient

ζ_p = profile friction-loss coefficient

ζ_s = secondary-loss coefficient,

then

$$\zeta = \frac{\delta p}{\frac{\gamma_1}{2g} c_1^2}, \quad \zeta_w = \frac{\delta p_w}{\frac{\gamma_1}{2g} c_1^2}, \quad \zeta_p = \frac{\delta p_p}{\frac{\gamma_1}{2g} c_1^2},$$

$$\zeta_s = \frac{\delta p_s}{\frac{\gamma_1}{2g} c_1^2} \tag{3.16}$$

From (3.14) and (3.15),

$$\zeta = \zeta_w + \zeta_p + \zeta_s = \frac{1}{\varphi^2} - 1 \tag{3.17}$$

The values of δp_w and δp_p, obtained from (3.13) in the aforementioned experiment, thus lead to determine ζ_w and ζ_p, while the total loss coefficient, ζ, obtained from the experiment, leads to determine the secondary loss coefficient, ζ_s.

In considering the secondary loss, the flow will be treated as non-compressible fluid. Though the fluid velocity is 0 in the infinite front ($R \to \infty$) of the actual nozzle inlet, we will assume the velocity, c_0, flowing in the radius direction in the infinite front in our dealing with the non-compressible isometric system. c_0 being a small number, the

assumption may be considered valid in view of the fact that the flow, after passing the nozzle, is affected mainly by the condition around the nozzle outlet, rather than by that of the nozzle inlet. The velocity diagram of the profile series is shown in Figure 3.16. If the pitch of the isometric system is represented by t, the chord (hypotenuse) by c, the coefficient of lift, C_L, will be expressed as follows:

$$C_L = 2 \frac{t}{c} \cot \alpha \cdot \sin \alpha_m \tag{3.18}$$

Here α_m is the angle formed by the tangential direction of the circumference and the average vector velocity, c_m, of the inlet velocity, c_0, and outlet velocity, c_1.

The secondary loss coefficient, ζ_s, will be expressed as follows in the form of the coefficient of profile resistance, C_{DS}:

$$C_{DS} = \zeta_s \frac{t}{c} \cdot \frac{\sin^3 \alpha_m}{\sin^2 \alpha} \tag{3.19}$$

According to the results obtained in the experiment of the straight system, the coefficient of resistance by the secondary loss, C_{DS}, is directly proportional to the square of the coefficient of lift, and hence can be expressed as follows:

$$C_{DS} = \frac{\lambda}{\frac{t}{c}} C_L^2 \tag{3.20}$$

λ, being the proportional constant and the function of the Reynolds number, is called the secondary loss characteristic number.

As the secondary loss of the nozzle can be attributed to the same cause as the secondary loss of straight system, the formula (3.20) also applies to the circular nozzle. The following formula, then, can be established from (3.18), (3.19) and (3.20):

$$\lambda = \frac{\zeta_s}{2 \cos^2 \alpha \sqrt{4 + \cot^2 \alpha}} \tag{3.21}$$

The values of ζ_s and α are obtained from the experiment. Figure 3.17 shows the correlation between λ thus obtained and the Reynolds number. It may be understood from the figure that λ is a function of the Reynolds number only and unrelated to either the attaching angle or pitch of the

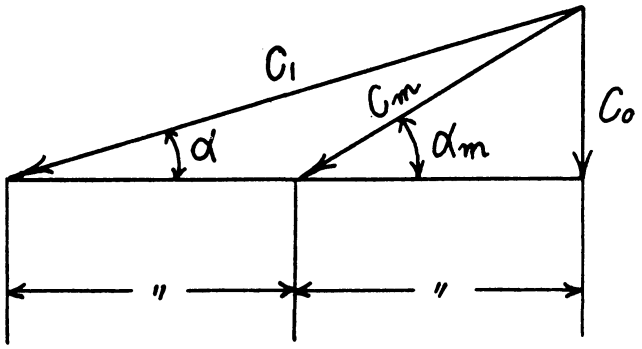

Figure 3.16 Velocity Diagram

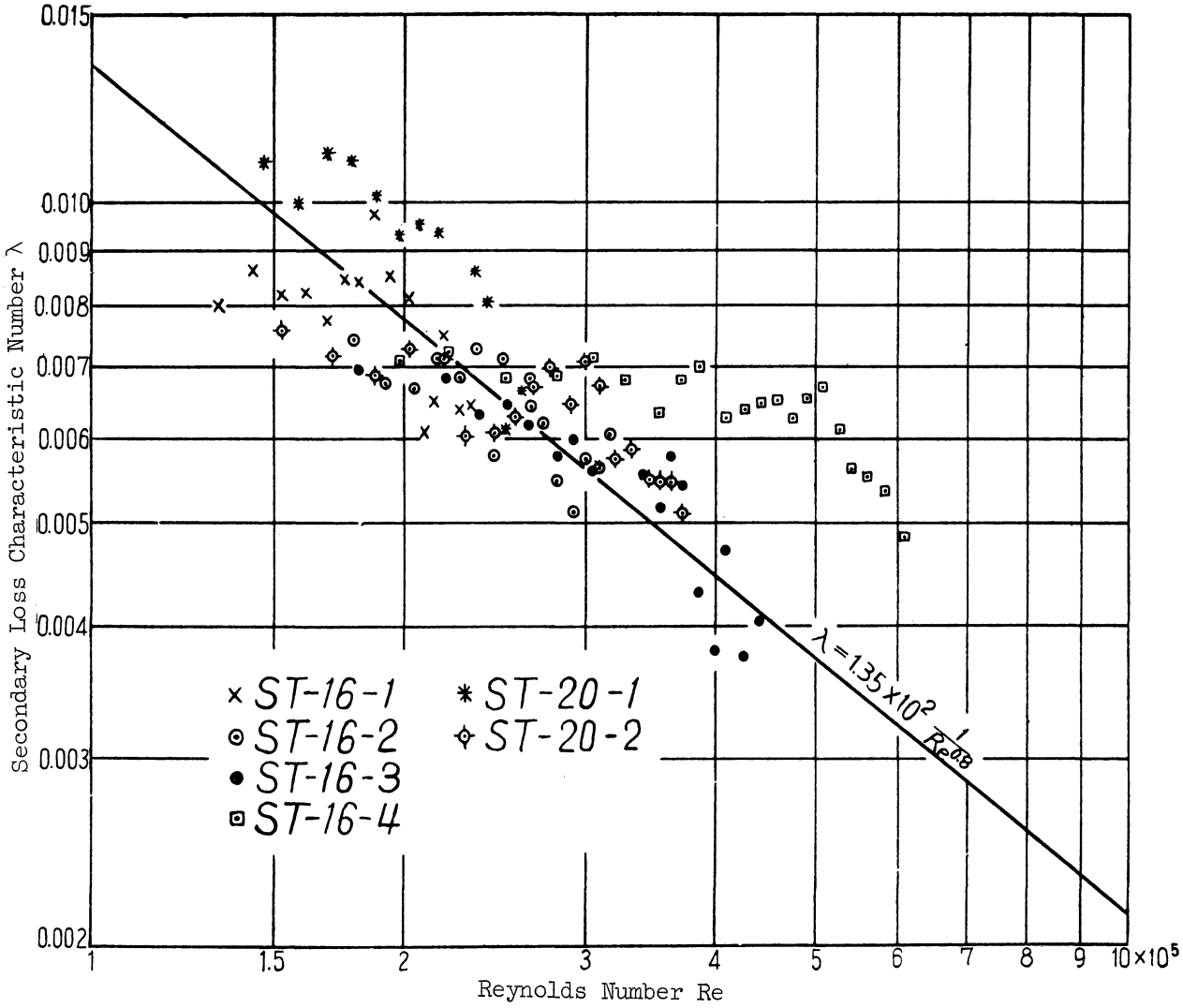

Figure 3.17 Secondary Loss Characteristic Number

nozzles. In the same figure, the signs (ST-16-4) show a special increase of loss attributable to the shape of the isometric outlet, as shown in Figure 3.18. The following formula will be obtained from the above experiment with reference to λ:

$$\lambda = 1.35 \times 10^2 \frac{1}{R_e{}^{0.8}} \tag{3.22}$$

Thus, by clarifying the geometrical forms of the nozzles and determining the Reynolds number used, it is possible to obtain the value of λ from (3.22) which in turn makes it possible to obtain the secondary loss coefficient, ζ_s, from (3.21), resulting in the clarification of ζ_w, ζ_p, and the total loss coefficient, ζ, and the velocity coefficient, φ.

3.5. Nozzle Designing Procedure

As described in Chapter 2, the following conditions must be satisfied in designing a radial turbine: the mean efflux angle, α, of the nozzle, its mean efflux velocity, c_1, its breadth, B_1, and the radius, R_{1N}, of its outlet attachment. Though various types of nozzles can be conceived according to the number of their attaching angle and pitch, we will here focus our attention on the methods of arrangement which will minimize the total loss in a nozzle. We will consider a straight-type nozzle, such as shown in Figure 3.19, arranged at regular intervals on the circle. The two nozzles surrounding any given pitch are represented by AC, BD; the chord (hypotenuse) of the straight nozzle by ℓ, the attaching radii from the center to the inlet and the outlet by R_0, R_{1N}, and the geometrical attaching angle formed by the nozzle and the tangential line by α_b.

From the formula (3.9) and (3.13),

$$\zeta_w = \frac{\delta p_w}{\frac{\gamma_1}{2g} c_1{}^2} = \frac{2A_w}{sB_1} c_f \sin\alpha \tag{3.23}$$

With reference to Figure 3.19, we can establish the following formulas:

$$\frac{A_w}{sB_1} = \frac{\pi(R_0{}^2 - R_{1N}{}^2)}{ZsB_1}$$

$$= \frac{1}{2} \cdot \frac{R_{1N}}{B_1} \left\{ \left(\frac{R_0}{R_{1N}} \right)^2 - 1 \right\} \tag{3.24}$$

$$\left(\frac{R_0}{R_{1N}} \right)^2 - 1 = \frac{\ell}{R_{1N}} \left\{ \left(\frac{\ell}{R_{1N}} \right) + 2 \sin\alpha_b \right\} \tag{3.25}$$

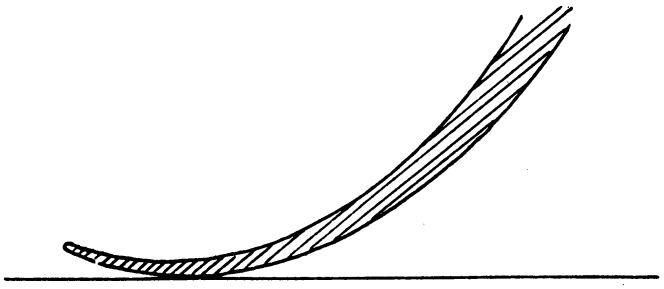

Figure 3.18

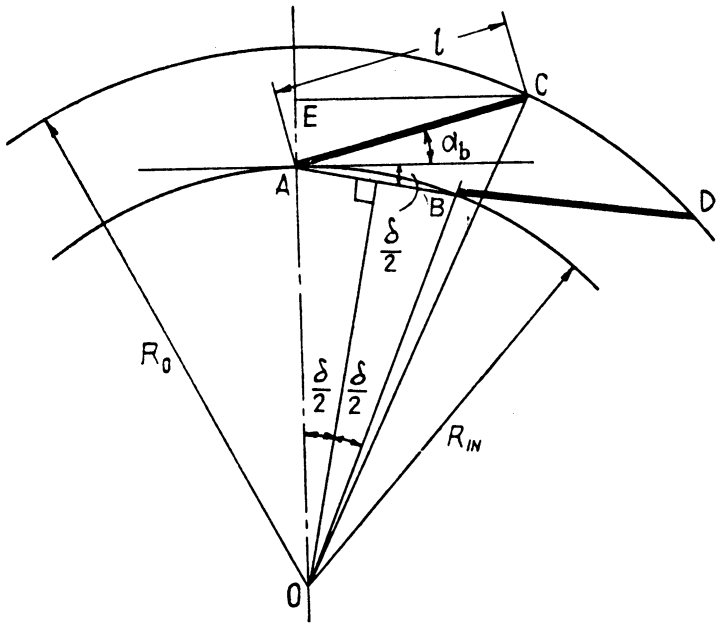

Figure 3.19

Accordingly,

$$\frac{A_w}{sB_1} = \frac{1}{2} \cdot \frac{R_{1N}}{B_1} \cdot \frac{\ell}{R_{1N}}\left(\frac{\ell}{R_{1N}} + 2 \sin \alpha_b\right) \tag{3.26}$$

Since $\angle CAB \fallingdotseq \alpha$

$$\alpha_b = \alpha - \frac{\delta}{2} \tag{3.27}$$

The chord (hypotenuse), ℓ, when excessively long, will result in an increase of loss, and when too short, will not be able to give the needed efflux angle. Since the efflux angle of the nozzle is mainly affected by the geometrical shape of the rear part of the nozzle, we can conceive of ℓ as follows:

$$\ell = \overline{AB} \cos \angle CAB \times 1.5 \fallingdotseq 1.5\ s \cos \alpha \tag{3.28}$$

By substituting (3.23) with (3.26), (3.27), and (3.28), ζ_w will be:

$$\zeta_w = \frac{3\pi}{2Z} \cdot \frac{R_{1N}}{B_1} \sin 2\alpha \left\{\frac{3\pi}{Z} \cos \alpha + 2 \sin \alpha\left(\alpha - \frac{\delta}{2}\right)\right\} c_f \tag{3.29}$$

From (3.9) and (3.13), the profile friction-loss coefficient, ζ_p, will be:

$$\zeta_p = \frac{\delta p_p}{\frac{\gamma_1}{2g} c_1^2}$$

$$= 2 \frac{\ell}{s} \sin \alpha \cdot c_f$$

$$= \frac{3}{2} \sin 2\alpha \cdot c_f \tag{3.30}$$

From (3.21), the secondary loss coefficient will be:

$$\zeta_s = 2\lambda \cos^2\alpha \sqrt{4 + \cot^2 \alpha} \qquad (3.21.1)$$

Next, the Reynolds number, R_e, which is obtained with reference to the chord (hypotenuse), ℓ, and the jet velocity, c_1, must be converted to R_{e1} obtained with reference to the outlet attaching radius, R_{1N}, and c_1.

$$R_{e1} = \frac{c_1 R_{1N}}{\nu_1}, \quad R_e = \frac{c_1 \ell}{\nu_1} \qquad (3.31)$$

From (3.31) and (3.28),

$$R_e = R_{e1} \frac{3\pi}{Z} \cos \alpha \qquad (3.32)$$

The above formula will enable us to determine R_e with reference to each given value of α, Z, and R_{e1}, while (3.12) and (3.22) will enable us to determine c_f and λ. With α, Z, R_{e1}, B_1/R_{1N}, thus clarified, we can determine the total loss, ζ, by obtaining ζ_w, ζ_p, and ζ_s from (3.29), (3.30) and (3.21.1).

As we modify the number of pitches, Z (with which, needless to say, varies the attaching angle α_b), without changing α, B_1/R_{1N}, and R_{e1}, the total loss coefficient, ζ, will appear as in Figure 3.20. With a certain most suitable number of pitches, Z, the total loss coefficient will be reduced to the minimum as R_{e1} increases and B_1/R_{1N} decreases, whereas, with the decreasing number of pitches, Z, the total loss coefficient will become smaller and smaller, as R_{e1} decreases and B_1/R_{1N} increases. In the latter case, the loss will be minimized by reducing the number of pitches as much as possible, even though this minimum number of pitches is determined geometrically by the efflux angle, α. To reduce the number of pitches while keeping the fixed value of α is to reduce the nozzle attaching angle, α_b. The minimum number of pitches will be obtained when $\alpha_b = 0$, that is, when the nozzle coincides with the tangential line of the circle.

Figure 3.21 shows the number of pitches, Z, giving the minimum loss with reference to each value of α, R_{e1}, and B_1/R_{1N}. The figure confirms the existence of the most suitable number of nozzle pitches for the minimum loss when R_{e1} and α have large values and B_1/R_{1N} a small value. It also shows that the loss will be minimized with the tangential nozzle when R_{e1} and α have small values and B_1/R_{1N} a large value.

Figure 3.22 shows in the form of velocity diagram the loss when using the most suitable number of pitches such as illustrated in Figure 3.21. It will be noted from Figure 3.22 that the Reynolds number, R_{e1},

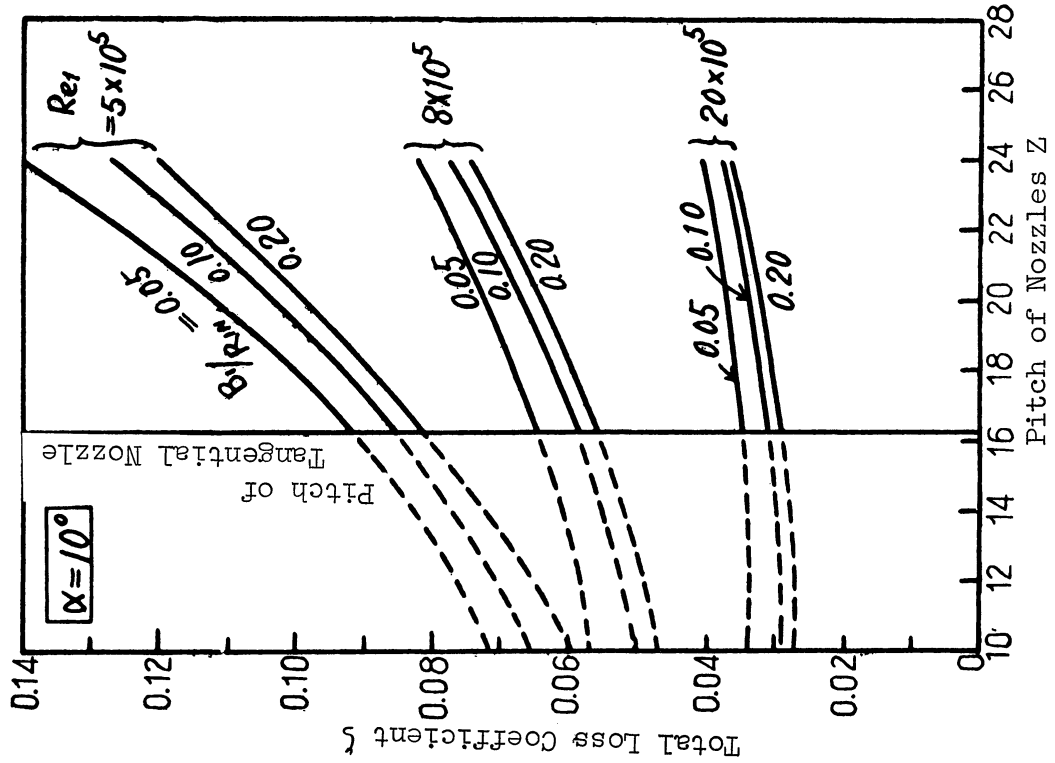

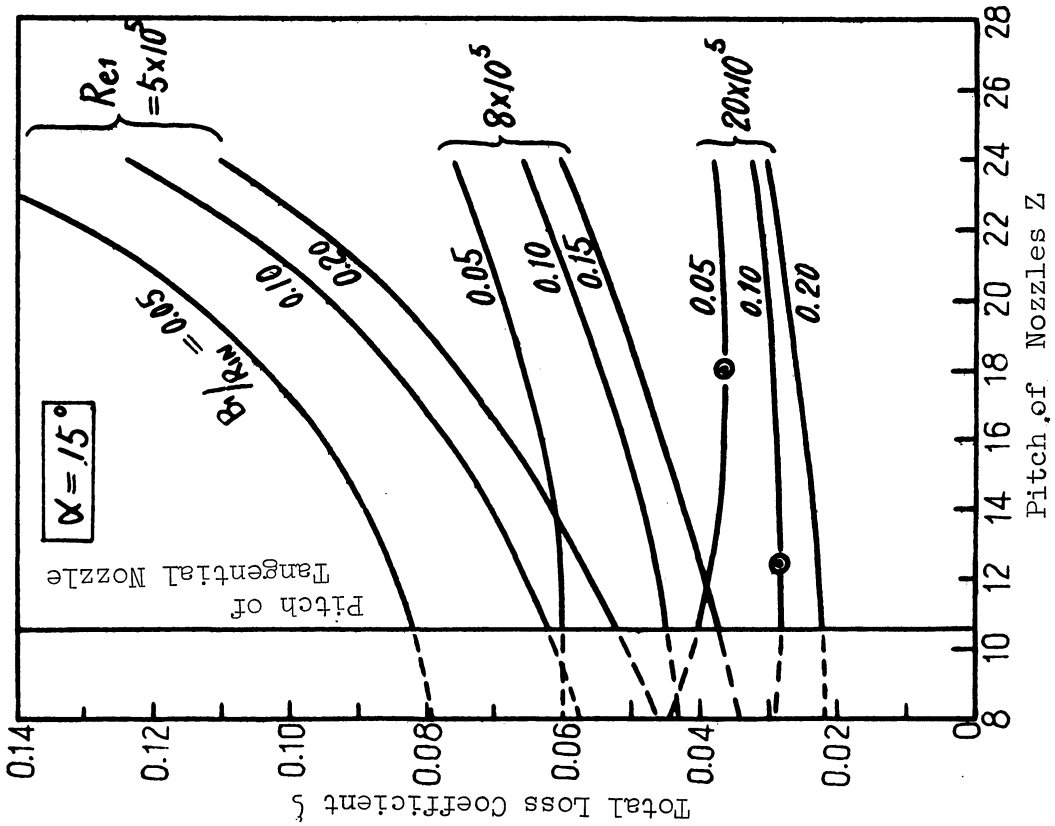

Figure 3.20 Total Loss Coefficient

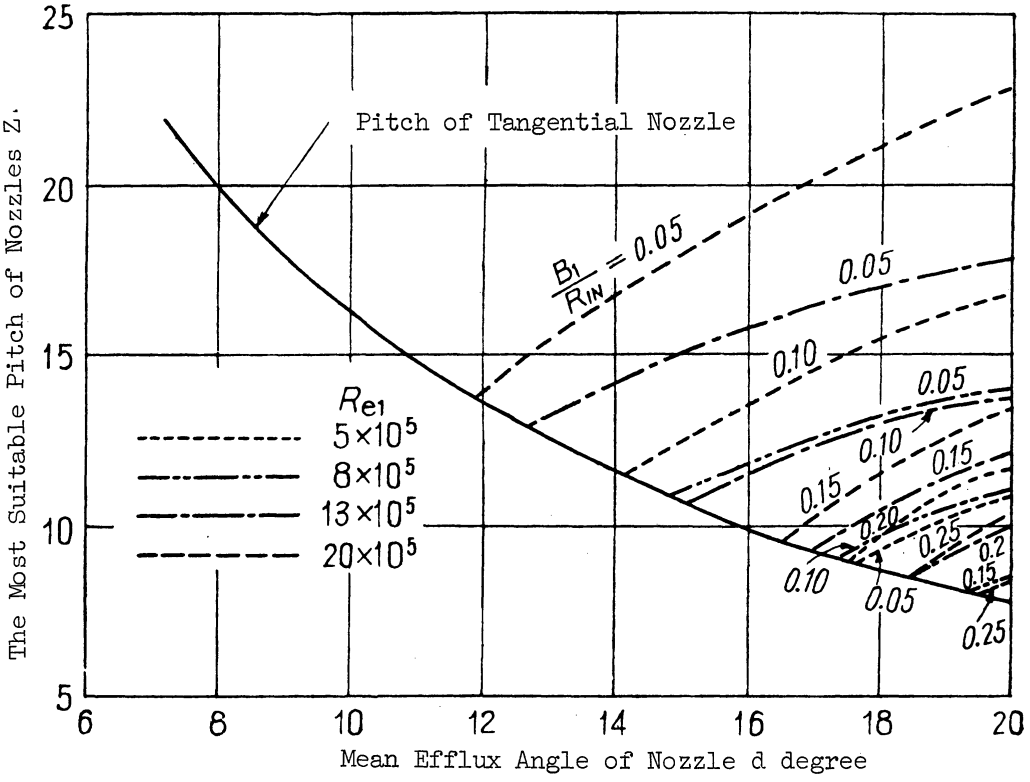

Figure 3.21 The Most Suitable Pitch of Nozzles

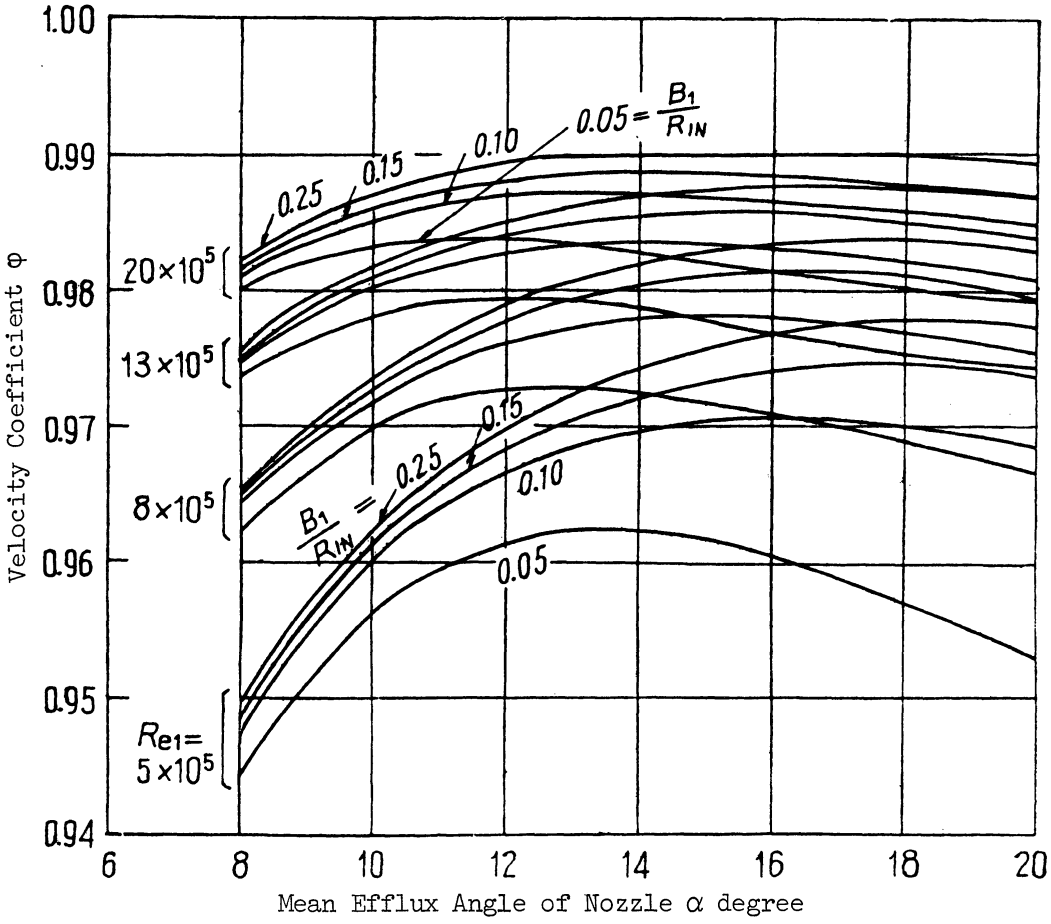

Figure 3.22 The Greatest Velocity Coefficient

shows the approximate value of (10 15) x 10^5 when adopting the total turbine expansion ratio of two and the gas temperature between 600 800°C, with the subsequent extremely high velocity coefficient of φ = 0.975 0.985. The figure also shows that the small value of B_1/R_{1N}, especially when $B_1/R_{1N} < 0.1$, results in a poor velocity coefficient, which can be ascribed to the increase of side-wall friction loss. The poor velocity coefficient, resulting from a small efflux angle of the nozzle, can be ascribed to the increase of the secondary loss. The velocity coefficient also drops sharply with small values of the Reynolds number, particularly when it is below 5 x 10^5.

As has been described so far, the number of pitches giving the minimum loss is determined by the geometrical position of the nozzle touching the circle. However, a close study of Figure 3.20 will reveal that the loss coefficient shows a tendency to be further minimized if we could reduce the value of Z. The possibility will be realized by the following steps.

It will be necessary to reduce the attaching angle, α_b, in order to reduce the value of Z while keeping the fixed value of α. As shown in Figure 3.23, however, the rear edge of the tangential nozzle (viz. when $\alpha_b = 0$) touches the tangential line of the circle in the straight system, whereas, if $\alpha_b < 0$, the straight system shows the formation of a negative angle at the nozzle outlet which, corresponding to the case of ST-16-4 of the experiment, brings about separation loss with reduction of velocity coefficient as a result. In order to avoid this, a negative camber will be given to the nozzle outlet, as shown in Figure 3.24, so as to enable the nozzle to touch the tangential line in the straight system, and at the same time to reduce the number of nozzle pitches below that of tangential nozzle pitches, thus preventing the velocity coefficient from dropping when the Reynolds number and α have small values.

3.6. Summary

(1) The losses in the nozzles are investigated under the three aspects of side-wall friction loss, profile-friction loss, and secondary loss, in each case of which experimental formulas are derived, representing the effects of the nozzle attaching angle, pitch of nozzles, aspect ratio and Reynolds number upon each of these losses.

(2) It is demonstrated that the mean efflux angle of flow from a nozzle can be obtained by means of a modification of the efflux angle, $\sin^{-1} 0/t$ (0: throat opening, t: pitch) of the two-dimensional straight system of parallel nozzles by the deviation angle due to the aforementioned losses.

(3) Nozzle designing procedures are presented using the results obtained. Thereby the total loss in a nozzle can be minimized with the resulting value of the nozzle velocity coefficient as high as 0.975 0.985

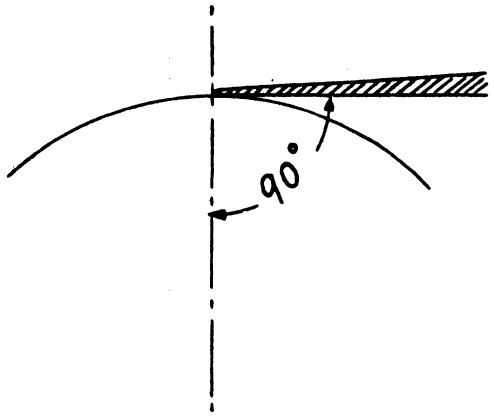

Circumferential Nozzle ($\alpha_b = 0$)

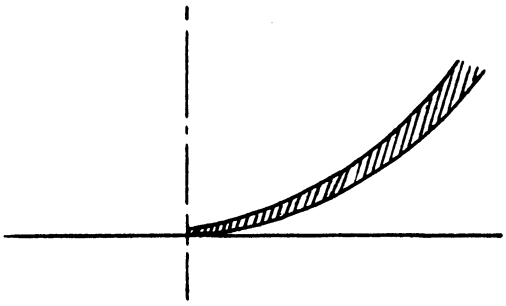

Straight System ($\alpha_b = 0$)

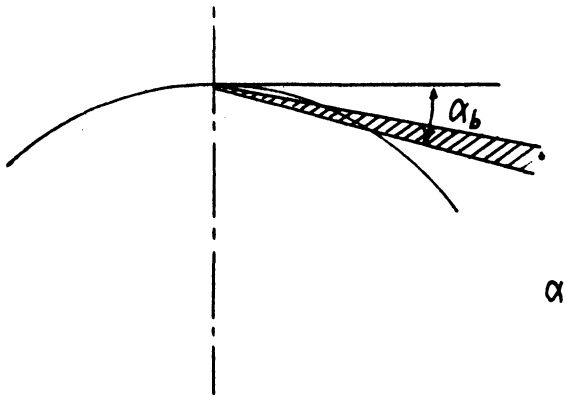

Circumferential Nozzle $\alpha_b < 0$)

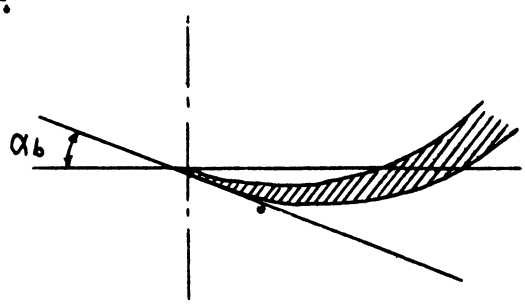

Straight System ($\alpha_b < 0$)

Figure 3.23

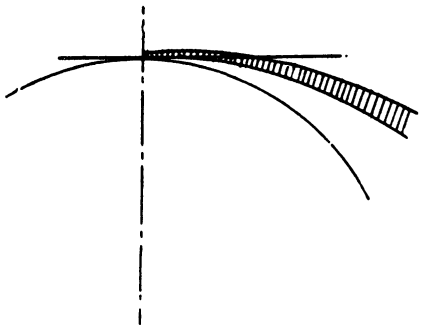

Circumferential Nozzle

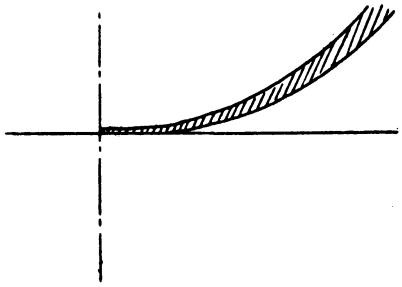

Straight System

Figure 3.24.

for a radial turbine as compared with the value of the axial-turbine nozzle velocity coefficient which falls between $0.95 \sim 0.96$. This demonstrates the capacity of radial turbines to produce a superior adiabatic efficiency. It is further demonstrated that the fall of velocity coefficient can be improved by reducing the number of nozzle pitches, as well as by giving a negative camber to the nozzle outlet when the Reynolds numbers are low.

CHAPTER 4

A STUDY OF THE FLOW IN AN EXDUCER

4.1. Outline

The axial velocity at the turbine outlet should be distributed as shown in Chapter 2 in order to take the maximum turbine efficiency. In this case, the centrifugal force acting on the flow in an exducer should balance with the radial-pressure gradient of the flow. Accordingly, a relative efflux angle such as shown in (2.51) and a velocity distribution, such as illustrated by the curved line (3) of Figure 2.7, are considered with regards to their capacity to satisfy the aforementioned conditions. Theoretical analysis is conducted to determine the shape of stream in an exducer that will prevent a radial flow, with the result that numerical solutions are obtained for three representative types of exducers. These solutions furnish the useful data in designing of an exducer. In addition, the analytical results are verified experimentally by the test turbine.

4.2. Theoretical Analysis

Consideration will be given to an exducer, such as shown in Figure 4.1, with A representing any given point on any given radius, R, in the exducer. The circumferential velocity at this point is represented by u_2, the relative velocity by w, the absolute velocity by c, the angle formed by w, the circle by β, and the pressure by p. The velocity diagram at this point is shown in Figure 4.2(a). The flow passing over the radius, R, is discharged at the point, B, whose relative velocity, absolute velocity, and the angle formed by its relative velocity and the circle, are represented respectively by w_2, c_2, and β_2. The velocity diagram at the point B is shown in Figure 4.2(b). As the absolute velocity at the exducer outlet is uniformly in the direction of the axis, the pressure upon each point of the same radius at the exducer outlet can also be considered to be uniformly represented by p_2.

The expansion that takes place in the exducer is relatively small as compared with the expansion that takes place in the blade, that is, from the blade inlet up to the exducer inlet. Accordingly the flow in the exducer can be regarded as being non-compressible. Therefore,

$$w \sin \beta = w_2 \sin \beta_2 = c_2 = u_2 \tan \beta_2 \qquad (4.1)$$

From (4.1),

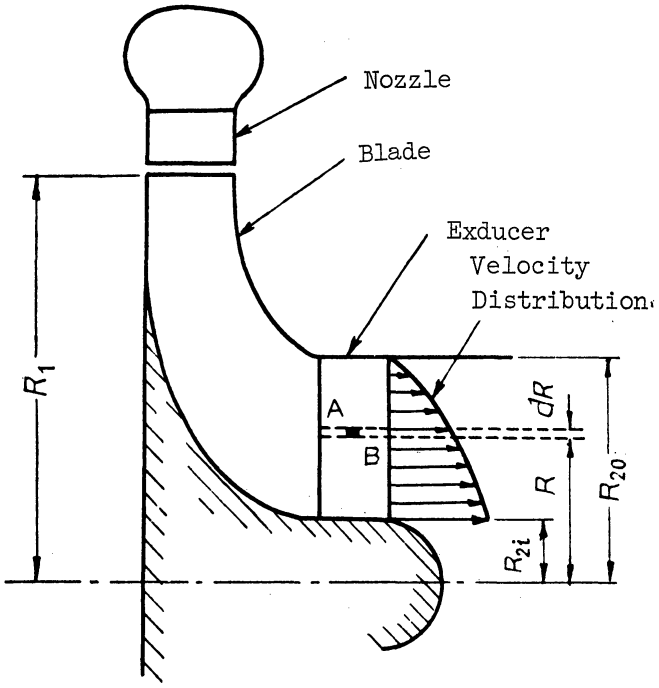

Figure 4.1

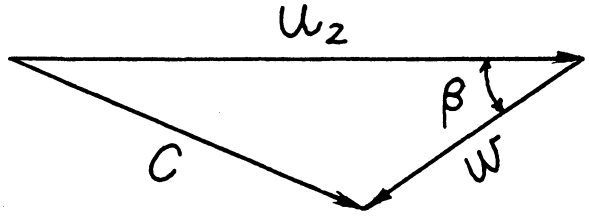

(a)

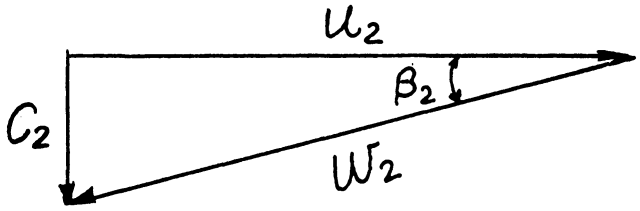

(b)

Figure 4.2 Velocity Diagram of Exducer.

$$\left.\begin{aligned} w_2 &= \frac{u_2}{\cos \beta_2} \\ w &= \frac{u_2 \tan \beta_2}{\sin \beta} \end{aligned}\right\} \qquad (4.1.1)$$

With ζ representing the coefficient of the loss in the exducer, the following formula of energy can be established:

$$p + \frac{\rho}{2} w^2 = p_2 + \frac{\rho}{2} w_2^2 + \zeta \frac{\rho}{2} \cdot \frac{w^2 + w_2^2}{2} \qquad (4.2)$$

From (4.1.1) and (4.2),

$$p = p_2 + \frac{\rho}{2}\left(1 + \frac{\zeta}{2}\right) \frac{u_2^2}{\cos^2 \beta_2}$$

$$- \frac{\rho}{2}\left(1 - \frac{\zeta}{2}\right) u_2^2 \frac{\tan^2 \beta_2}{\sin^2 \beta} \qquad (4.3)$$

From (2.51), the relative efflux angle of the exducer outlet, giving the maximum efficiency, should be:

$$\tan \beta_2 = \sqrt{1 - \psi_2^2} \sqrt{\left(\frac{R_{20}}{R}\right)^2 - 1} \qquad (4.4)$$

ψ_2 represents the coefficient of the blade velocity. From (4.3) and (4.4), therefore,

$$\mu = \mu_2 + \left(1 + \frac{\zeta}{2}\right) r^2$$

$$+ (1 - \psi_2^2) \left\{ \zeta - \left(1 - \frac{\zeta}{2}\right) \theta^2 \right\} (1 - r^2) \qquad (4.5)$$

But

$$\mu = \frac{p}{\frac{\rho}{2} u_{20}^2}, \quad \mu_2 = \frac{p_2}{\frac{\rho}{2} u_{20}^2}$$

$$r = \frac{R}{R_{20}}$$

u_{20} = the circumferential velocity of the outside radius, R_{20}, of the exducer outlet.

$$\theta = \frac{1}{\tan\beta}$$

Accordingly, the radial pressure gradient, $d\mu$, at the point A will be obtained from (4.5) as follows:

$$d\mu = 2r \left[\left(1 + \frac{\zeta}{2}\right) - (1 - \psi_2^2) \left\{ \zeta - \left(1 - \frac{\zeta}{2}\right) \theta^2 \right\} \right.$$

$$\left. - (1 - \psi_2^2) \left(1 - \frac{\zeta}{2}\right) \left(\frac{1}{r} - r\right) \theta \frac{d\theta}{dr} \right] dr \qquad (4.6)$$

On the other hand, the centrifugal force, dF, acting upon the diminutive mass, dm, at the point, A, is:

$$dF = dm \frac{c_u^2}{R} = \rho A dR \frac{(u_2 - w \cos\beta)^2}{R} \qquad (4.7)$$

A, in the above formula represents the area of the diminutive mass perpendicular to the radius. By substituting (4.7) with (4.1.1),

$$dF = \frac{\rho A}{R} u_2^2 \left(1 - \frac{\tan\beta_2}{\tan\beta}\right)^2 dR \qquad (4.8)$$

The pressure gradient, dp, to be balanced with this centrifugal force is:

$$dF = Adp \qquad (4.9)$$

From (4.8) and (4.9),

$$dp = \frac{\rho}{R} u_2^2 \left(1 - \frac{\tan \beta_2}{\tan \beta}\right)^2 dR \qquad (4.10)$$

Thus the formula for the pressure gradient to be balanced with the centrifugal force will be:

$$d\mu = 2r \left(1 - \frac{\tan \beta_2}{\tan \beta}\right)^2 dr \qquad (4.10.1)$$

In order that the $d\mu$ of (4.6) be equal to the $d\mu$ of (4.10.1), it is necessary to clarify the correlation between β (or θ) and r. The following differential equation will be obtained from (4.6) and (4.10.1):

$$\left(1 - \psi_2^2\right)\left(1 - \frac{\zeta}{2}\right)\left(\frac{1}{r} - r\right) \theta \frac{d\theta}{dr}$$

$$+ \left(1 - \psi_2^2\right)\left(\frac{1}{r^2} - 2 + \frac{\zeta}{2}\right) \theta^2$$

$$- 2\sqrt{1 - \psi_2^2}\sqrt{\frac{1}{r^2} - 1}\ \theta - \left(\psi_2^2 - \frac{1}{2}\right)\zeta = 0 \qquad (4.11)$$

which represents the shape of stream when the centrifugal force is balanced with the radial pressure gradient so as to produce the maximum efficiency.

Though (4.11) can be solved as an equation of the first degree, it develops into too complex a formula to be solved easily. For practical purposes, it would be easier to hypothetically eliminate the loss from the exducer in our analysis. Assuming therefore that $\zeta = 0$ in (4.11),

$$\theta \left\{\frac{d\theta}{dr} - \frac{r\left(2 - \frac{1}{r^2}\right)}{1 - r^2}\theta - \frac{2}{a\sqrt{1 - r^2}}\right\} = 0 \qquad (4.12)$$

But $$a = \sqrt{1 - \psi_2^2}$$

In (4.12), the expressions, $\theta = 0$, therefore, $\beta = \pi/2$, indicate the conditions of the exducer inlet where the radial flow changes into the axial flow. It will be understood, therefore, that at the exducer inlet, a balance is kept between the radial-pressure gradient and the centrifugal force. If the pressure, the absolute velocity and the relative velocity at the exducer inlet are represented respectively by p_e, c_e, w_e, the following formulas will be obtained, with $\beta = \pi/2$ from (4.1) and (4.5):

$$\left.\begin{aligned} \frac{c_e}{u_{20}} &= \sqrt{1 - \psi_2^2(1-r^2)} = \frac{w_2}{u_{20}} \\ \frac{w_e}{u_{20}} &= \sqrt{1 - \psi_2^2}\,\sqrt{1 - r^2} = \frac{c_2}{u_{20}} \\ \mu_e &= \frac{p_e}{\frac{\rho}{2} u_{20}^2} = \mu_2 + r^2 \end{aligned}\right\} \qquad (4.13)$$

which is illustrated by Figure 4.3.

As to the flow in the exducer, the following formula can be obtained from (4.12):

$$\frac{d\theta}{dr} - \frac{r\left(2 - \frac{1}{r^2}\right)}{1 - r^2}\theta - \frac{2}{a\sqrt{1 - r^2}} = 0 \qquad (4.14)$$

which can be solved as follows:

$$\theta = \frac{1}{a} \cdot \frac{r}{\sqrt{1 - r^2}} - \frac{K}{r\sqrt{1 - r^2}} \qquad (4.15)$$

K is an integral constant whose value is determined by the axial position.

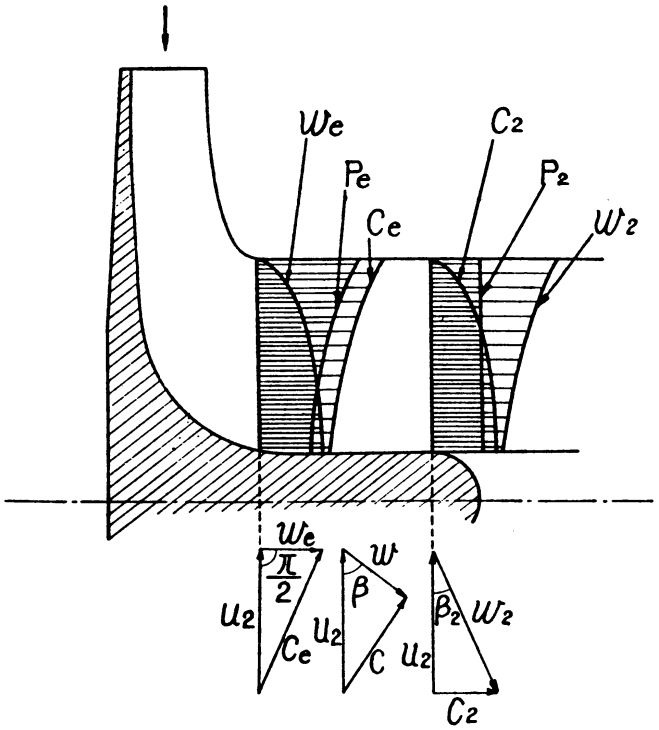

Figure 4.3 Velocity and Pressure Distribution of Exducer Inlet and Outlet

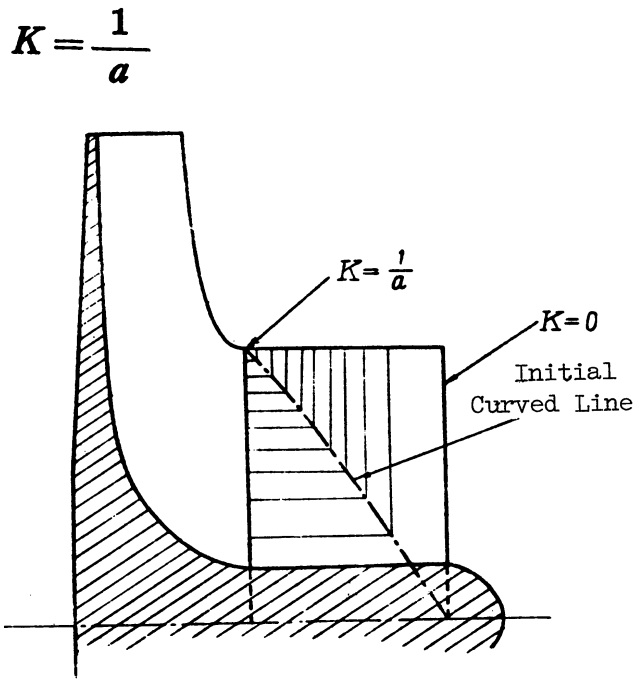

Figure 4.4 Distribution of K.

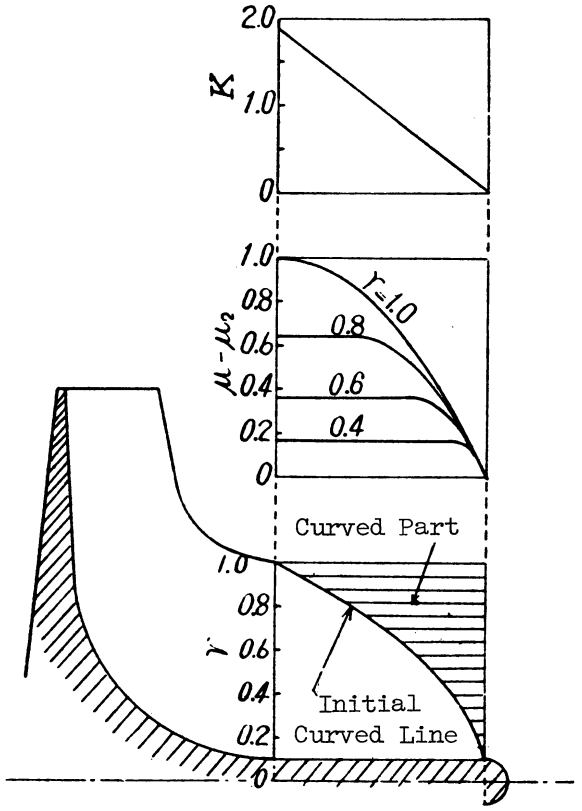

Figure 4.5

The correlation between θ and r at the exducer outlet, given already in (4.4), will be re-expressed as follows:

$$\theta = \frac{1}{a\sqrt{\frac{1}{r^2} - 1}} \tag{4.4.1}$$

The value of K at the exducer outlet may be obtained by substituting (4.15) with (4.4.1):

$$K = 0 \tag{4.16}$$

As $\beta = \pi/2$, $\theta = 0$ at the exducer inlet, the value of β will decrease as the flow approaches the exducer outlet. If $\theta = 0$ in (4.15),

$$K = \frac{r^2}{a} \tag{4.17}$$

Since $r = 1$ in the outside-radial position of the exducer inlet,

$$K = \frac{1}{a} \tag{4.18}$$

whereas $r = 0$ in the axial center of the exducer inlet,

$$K = 0 \tag{4.19}$$

Accordingly, the distribution of K in the exducer will take the form as shown in Figure 4.4.

Of the various possible types for the distributions of K, the following three will be considered to be most representative.

4.2.1.

Type 1, when K is distributed in proportion to the axial distance from the exducer inlet to its outlet.

The said proportional distribution of K is shown in Figure 4.5.

From (4.17), the position, r, in which the stream begins to curve from $\beta = \pi/2$ (which may be called the initial curved line) can be obtained with reference to each value of K. Since the value of K is determined by

each axial position, the initial curved line of each axial position can be obtained as shown in Figure 4.5. By obtaining the value of θ at each r from (4.15) with reference to the value of K, the tangents to the stream can be determined. In other words, the stream line can be determined by obtaining the curved line touching these tangents, as shown in Figure 4.6.

The pressure in the exducer is given in (4.5). When $\zeta = 0$,

$$\mu = \mu_2 + r^2 - a^2\theta^2 (1-r^2) \qquad (4.5.1)$$

From (4.5.1) and (4.15),

$$u - \mu_2 = aK\left(2 - \frac{aK}{r^2}\right) \qquad (4.20)$$

The formula (4.20) enables us to know the conditions in which occurs the fall of the pressure at each radial position, as shown also in Figure 4.5. It will be noted from the figure that, when K is distributed proportionally to the axial distance, a rather steep fall of pressure will take place near the exducer outlet.

4.2.2.

Type 2, when the pressure at r = 1 is reduced in proportion to the axial distance.

Since the type 1 results in an abrupt fall of pressure near the exducer outlet, we will consider the case where r = 1, that is, the case of directly reducing the pressure in the outside radius of the exducer outlet. The distribution of K in each axial position is determined from (4.20). By using the value of K thus obtained, we can determine the pressure and the point of initial curved line in each axial position, as shown in Figure 4.7. The stream lines in this case are shown in Figure 4.8.

4.2.3.

Type 3, when a straight line is used as the initial curved line.

When we take the straight line connecting the outside radial position of the exducer inlet with the axial center of the exducer outlet, the distributions of K and the pressure appear as shown in Figure 4.9, and its stream lines as in Figure 4.10.

The following observations will be made from a comparison of the three above-mentioned types. In type 1 (that is, Section 4.2.1), the initial curved line begins to form a curvature closest to the exducer outlet, with a steep fall of pressure at the outlet as a result. Whereas in type

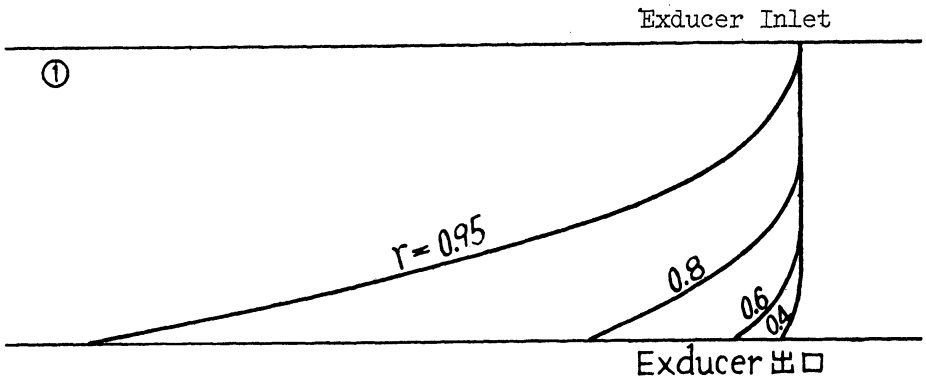

Figure 4.6 Stream Lines in the Exducer

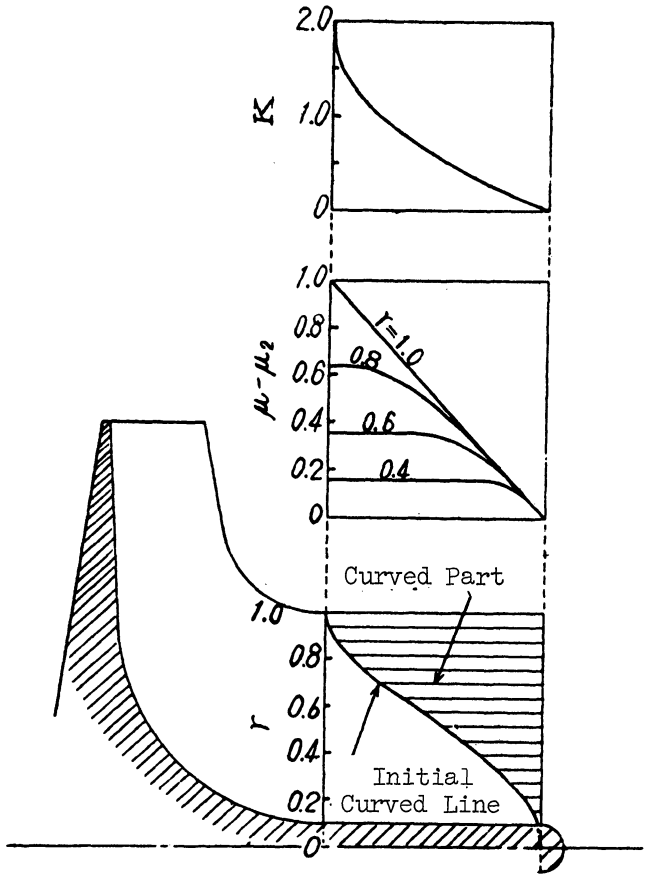

Figure 4.7

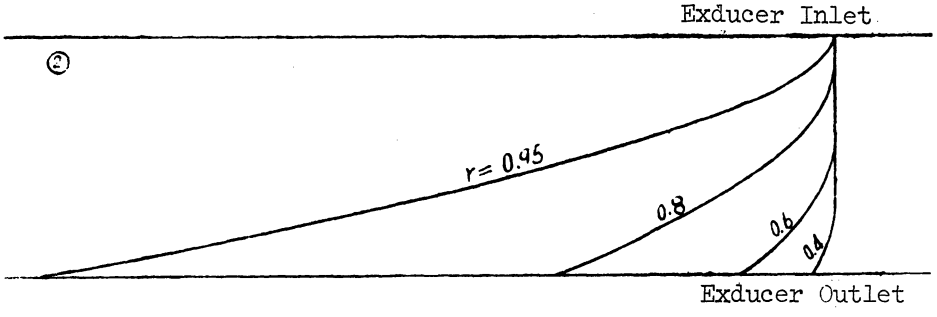

Figure 4.8 Stream Lines in the Exducer.

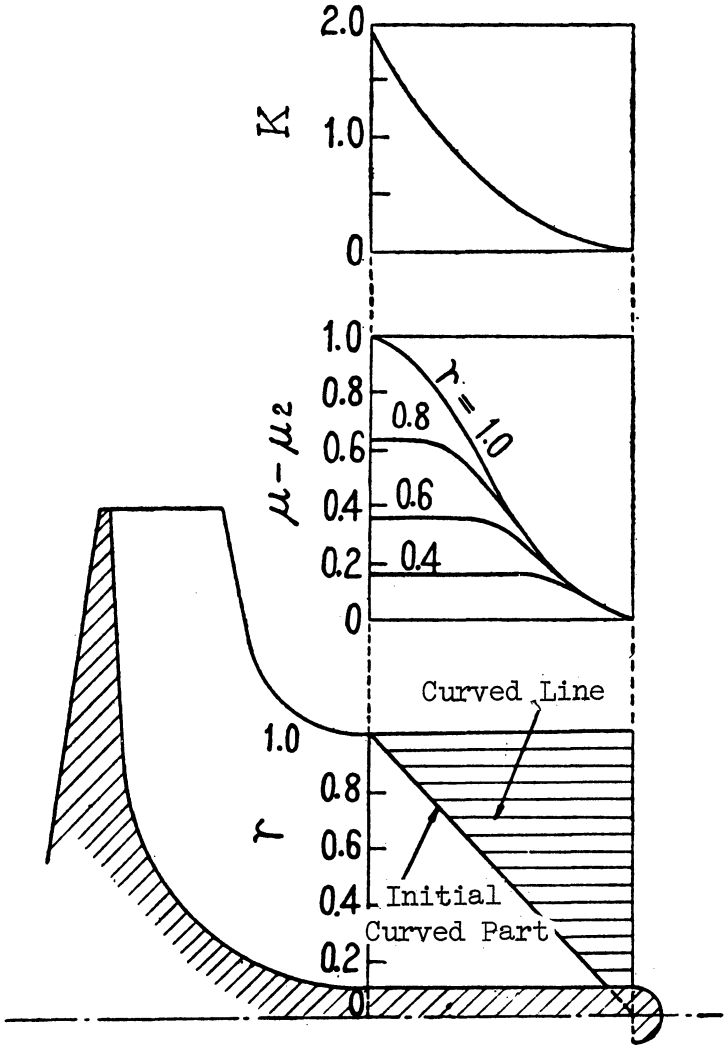

Figure 4.9

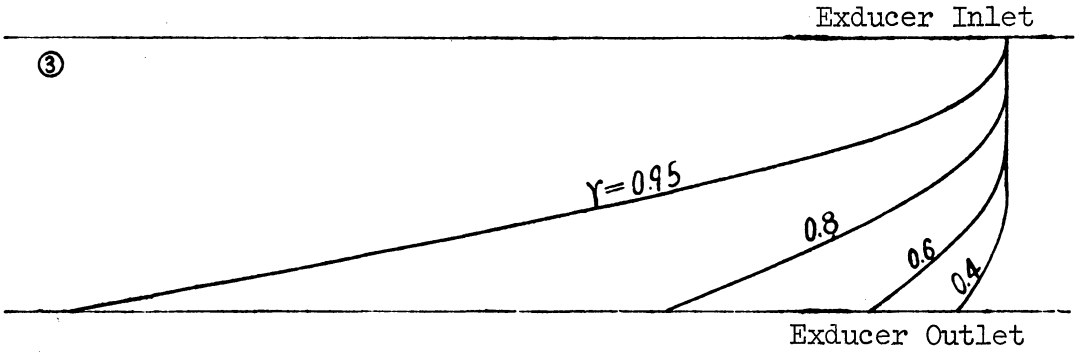

Figure 4.10 Stream Lines in the Exducer

2 (Section 4.2.2), the curvature is formed at once near the outside radius of the exducer, resulting in the mildest fall of pressure. However, in type 3 (Section 4.2.3) a steep fall of pressure takes place near the exducer inlet. However, the type 2 necessitates a rather large curvature of the stream line of the outside radius close to the exducer inlet, increasing the length of the stream line, and thus presenting some difficulties of designing and operation. Since it is desirable, from the point of view of operation, to reduce as much as possible the length of the stream line, the point of initial curvature should be put off as far as the type 1. Considering thus the problems of operation and the conditions of pressure fall, the type 1 should be adopted for the exducer outside radius and the type 3 for the central part of the exducer.

4.3. Experimental Verification of the Analysis

In either one of the three types of stream lines that we have analysed in the preceding section, it is necessary that the curvature be formed near the exducer inlet while putting off the point of initial curvature as far back as possible towards the axial center. In order to prove the above theory, comparative experiments were made with two different types of exducers. The type A shows a case completely opposite to the theory expounded above, namely, a type of exducer in which the initial curvature is slow in the exducer outside radius, while it becomes fast and abrupt in the central part of the exducer. Conversely, the type B is one in which the initial curvature is fast in the outside radius and slow in the central part, and whose initial curved line (not of the stream lines, but the geometrical initial curved line of the exducer) forms a straight line as in the case of 4.2.3 (see Figure 4.9). Both types A and B have 13 vanes, the same kinds of straight radial blades with a 250 mm radius, and the same curvature at each radial position of the vane outlet so as to form the efflux angle of outlet as illustrated in (4.4). The measurements of both types are shown in Figures 4.11 and 4.12 respectively.

These exducers were attached to the test turbine No. 1. (Details of the experiment will be described later in Chapter 5.) In the experiment, the size and the direction of the absolute efflux velocity at each radial position of the exducer outlet were measured in Yaw meter while keeping the fixed expansion ratio of the turbine and modifying the number of its revolutions. The figures 4.13 and 4.14 show the outlet velocity distribution of each of these exducers, with c_{2a} representing the axial component of the absolute efflux velocity and a_0 the sound velocity of gas at the turbine inlet.

Numerical solutions (see Chapter 2) for the radial distribution of the absolute velocity of the turbine outlet at the designing point will be expressed as follows:

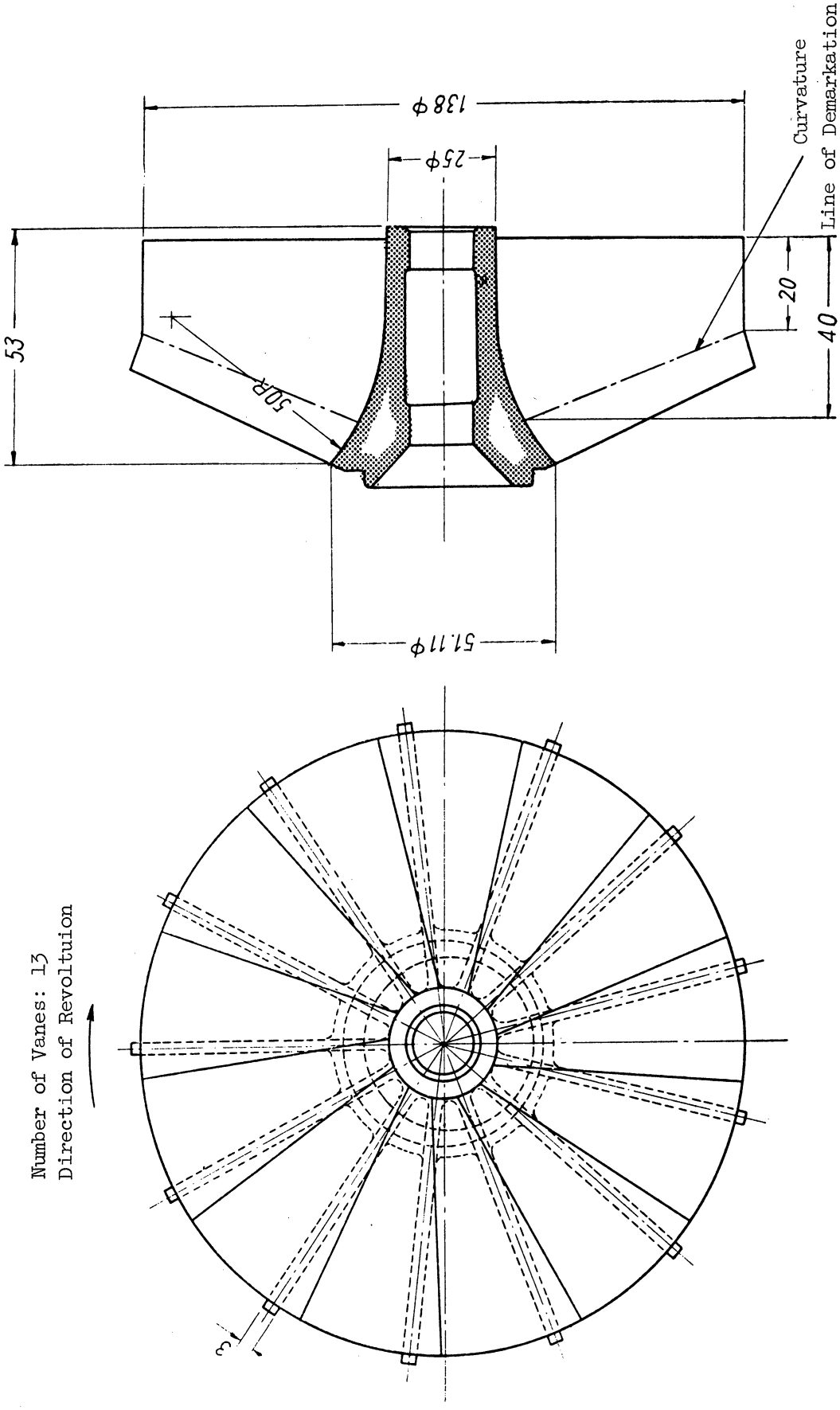

Figure 4.11 A-Type Exducer

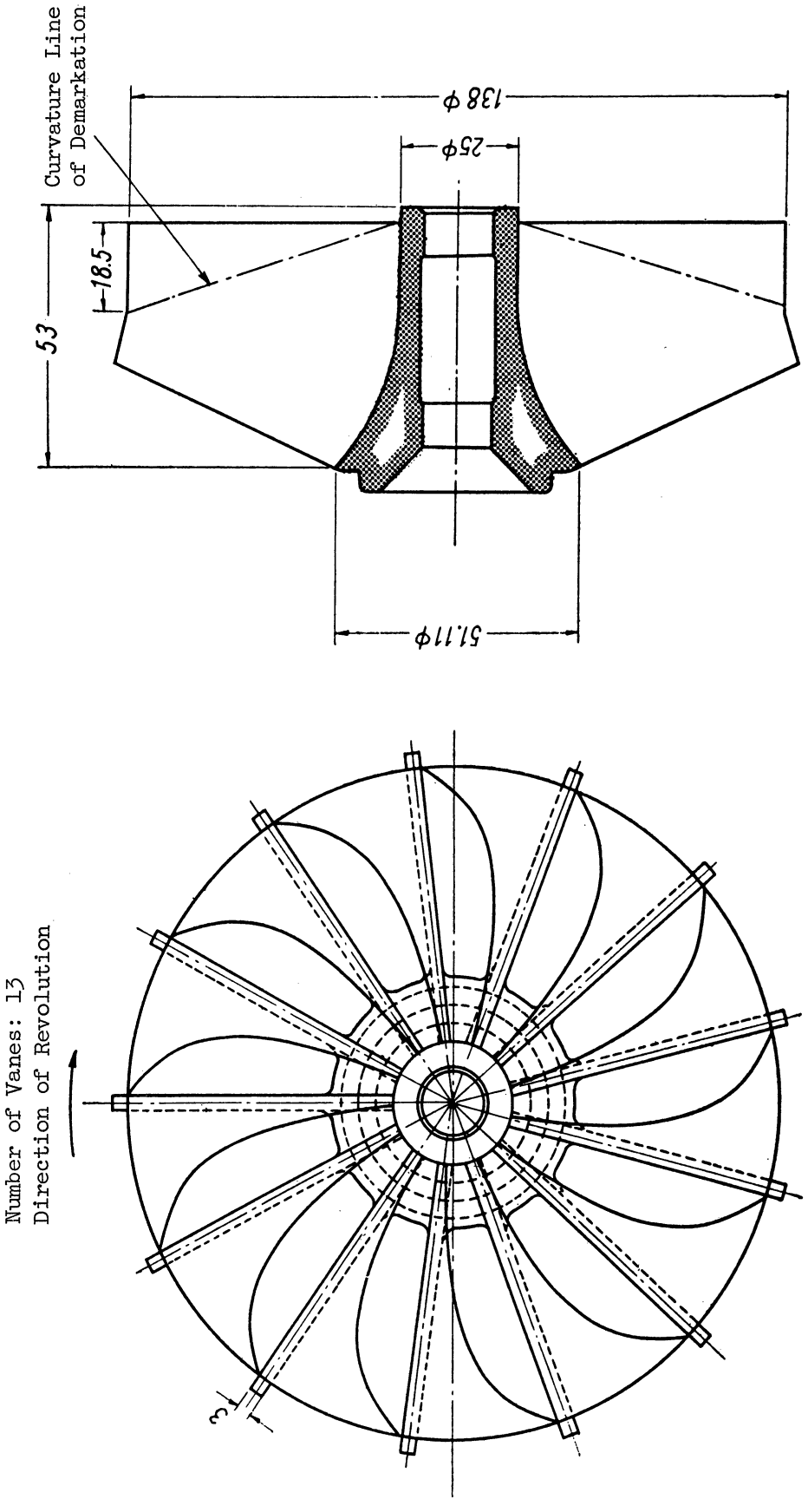

Figure 4.12 B-Type Exducer.

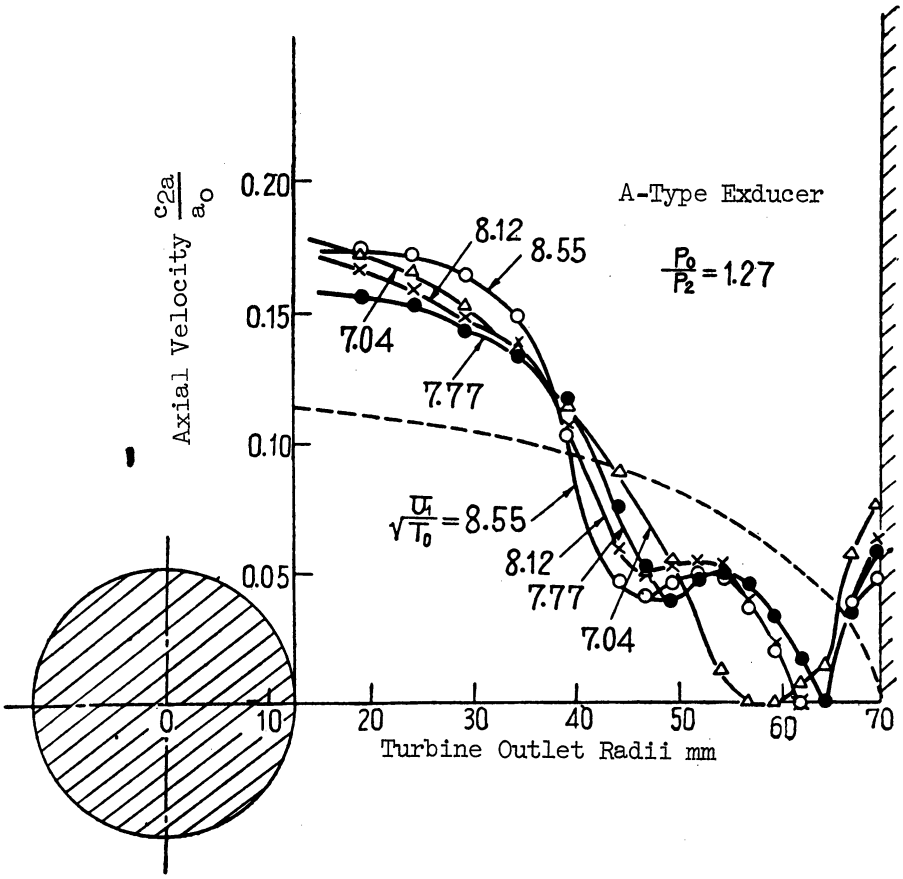

Figure 4.13 Outlet Velocity Distribution of A-Type Exducer.

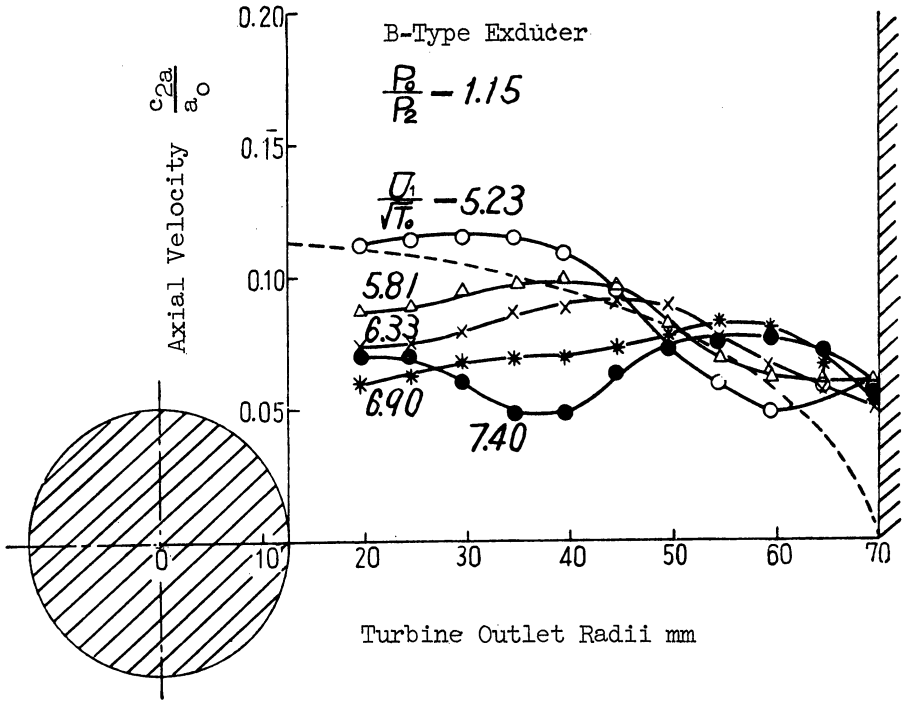

Figure 4.14 Outlet Velocity Distribution of B-Type Exducer.

$$\left(\frac{c_2}{a_0}\right)^2 = \psi_2^2 \left(\frac{U_1}{a_0}\right)^2 \left[\left\{\frac{2\theta}{k-1}\left(\frac{a_0}{U_1}\right)^2 - (1+\psi_1^2)\right\}\right.$$

$$\left. - \left(\frac{1}{\psi_2^2} - 1\right)\left(\frac{R}{R_1}\right)^2\right] \qquad (4.21)$$

In the above formula,

$$\theta = 1 - \psi^2(1 - \psi_1^2)(1 - s) - s_0\left(\frac{1-\varphi^2}{s} + \varphi^2\right)$$

$$s = (p_1/p_0)^{(k-1/k)}, \quad s_0 = (p_2/p_0)^{(k-1/k)}$$

The designing points of this turbine include the expansion ratio, 1.30, and the reaction, 48.3%, $U_1/\sqrt{T_0} = 8.05$. The velocity distributions under these conditions are shown in the dotted lines of Figures 4.13 and 4.14. Though the designing points differ slightly from the conditions of the experiment, the results of the experiment show the following points.

In the type A exducer in which the balance between the centrifugal force and the radial pressure gradient is disregarded, the velocity tends to decrease toward the outside wall, and to increase toward the center where the flow as a whole concentrates. This can be explained by the maintenance of the high pressure due to the length of $\beta = \pi/2$ on the outside wall, and, on the other hand, by the abrupt fall of pressure caused by the sudden curvature of flow in the central position. As a result of the extremely high pressure towards the outside wall, and the extremely low pressure towards the center, the flow shows a tendency to pass from the outside wall to the center. On the other hand, the type B exducer in which the curvature of the vane towards the outside wall is fast enough to warrant the fall of pressure, and slow enough, in the center, to maintain the high pressure, thus balancing the centrifugal force and the radial pressure gradient, gives a velocity distribution that corresponds fairly well to the designed plan (as illustrated in Figure 4.14).

4.4. Summary

(1) It is theoretically demonstrated that an exducer in which the centrifugal force is balanced with the radial pressure gradient can be

obtained when the axial velocity at the turbine outlet is distributed for the purpose of taking the maximum efficiency (as shown in Chapter 2).

(2) The balance can be realized by making an early curvature towards the outside radius of the exducer, and a late (slow) curvature towards the center. Considering the conditions of pressure in the exducer and the difficulties of operation, a modified form of the straight line initial curvature, such as illustrated in 4.2.1, has been found most suitable for the purpose of obtaining the maximum efficiency.

CHAPTER 5

EXPERIMENTAL STUDY OF RADIAL TURBINES(23),(24),(25)

5.1. Outline

Test turbines, prepared for experiment, are designed by the procedure mentioned above. In the experiment, problems relative to hydrodynamics are studied in order to confirm the appropriateness of the theory presented in Chapter 2. The losses which are hard to calculate theoretically are measured so as to clarify the distribution of losses in the turbine. Namely, the losses in nozzles and moving blades, the shock loss at blate inlet, the leaving loss and the heat loss are made clear quantitatively. The velocity coefficient of radial turbine blades is obtained, furnishing useful data in turbine designing. It is further demonstrated that the work done in turbine blades is by no means equally distributed at exit radii, that is, a greater work is performed near the center of exit than at outside radii of exit. It is therefore recommended that the turbine designing procedure so far in practice, which gives a uniform axial velocity distribution at turbine outlet, be discarded in favor of one that would allow the gas to flow in the center parts of turbine outlet (as shown in Chapter 2). Concerning the slip in flow in turbine blades, its type and cause are made clear. The test turbines, designed and built upon the basis of the above-mentioned results, show a capacity to reach 90% of the effective maximum adiabatic efficiency--a performance far superior to that of the gas turbine heretofore in use whose efficiency is near about 78 86%.

5.2. Test Turbines

Two test turbines are prepared for experiment: the test turbine No. 1, using compressed air for working fluid, is intended primarily for measuring various losses in the turbine, rather than for studying the type and cause of the slip in the flow in turbine blades. However, the test turbine No. 2, using combustion gas and the blade loss coefficient obtained from the test turbine No. 2, is furnished with an exducer to study the slip phenomena, and is designed mainly for the purpose of testing the turbine efficiency. Besides the high temperature gas, the test turbine No. 2 also uses heat-resisting steel. The principal measurements of both No. 1 and No. 2 test turbines are shown in the table below:

	Turbine No. 1	Turbine No. 2
Total expansion ratio	1.3	2.0
Turbine inlet pressure, kg/cm^2 abs	1.3	2.0
Turbine outlet pressure, kg/cm^2 abs	1.0	1.0
Turbine inlet gas temperature, ^oC	50	600
Gas flow, kg/sec	0.43	0.52
Number of revolutions, r.p.m.	10,970	35,000
Output power, HP	12	110
Reaction, %	48.3	52.0
Blade outside radius, mm	250	204
Turbine outlet outside radius, mm	140	108
Turbine outlet inside radius, mm	25	40
Spiral chamber inlet radius, mm	120	110
Blade inlet breadth, mm	26	12.7
Mean efflux angle of nozzle	$10^o30'$	$15^o40'$ ($9^o30'$)
Number of nozzles	16(20)	15
Number of blade vanes	13	14
B_1/R_1	0.208	0.125
R_{20}/R_1	0.56	0.53
R_{2i}/R_1	0.10	0.196
q	8.6×10^{-3}	17.5×10^{-3}
Deceleration ratio	0.327	0.0996

The photography and the structure of both test turbines are shown respectively in Figures 5.1, 5.2, 5.3, and 5.4.

5.3. Test Equipment and Procedures

(a) Test equipment and procedures of test turbine No. 1.

The test equipment of the turbine No. 1 is shown in Figure 5.5. The air, compressed in the centrifugal and Root compressors, passes through the surge tank into the test turbine. The flow of air is measured by the circular nozzle aerometer at the compressor inlet. The

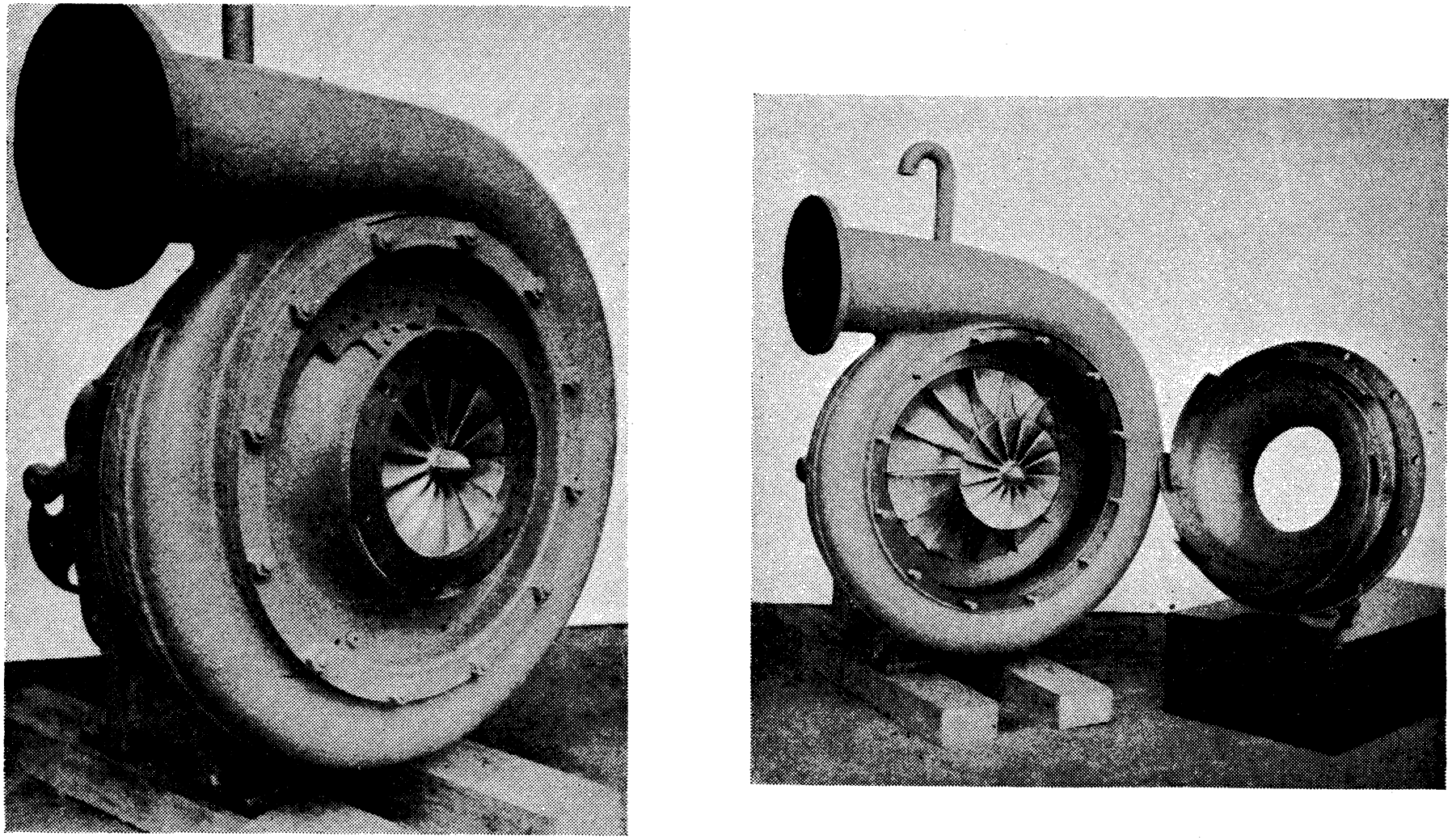

(a) (b)

Figure 5.1 Test Turbine No. 1

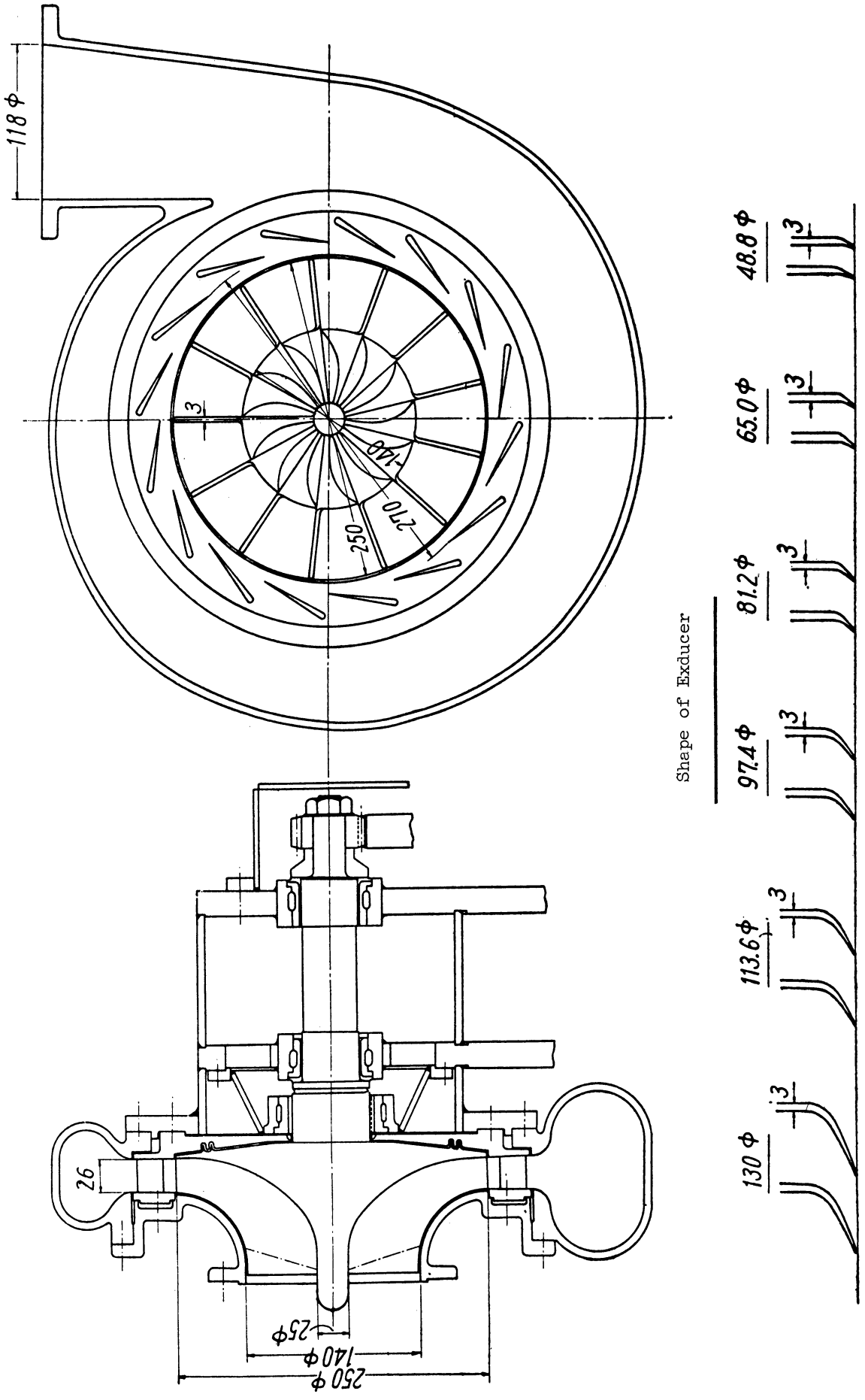

Figure 5.2 Test Turbine No. 1

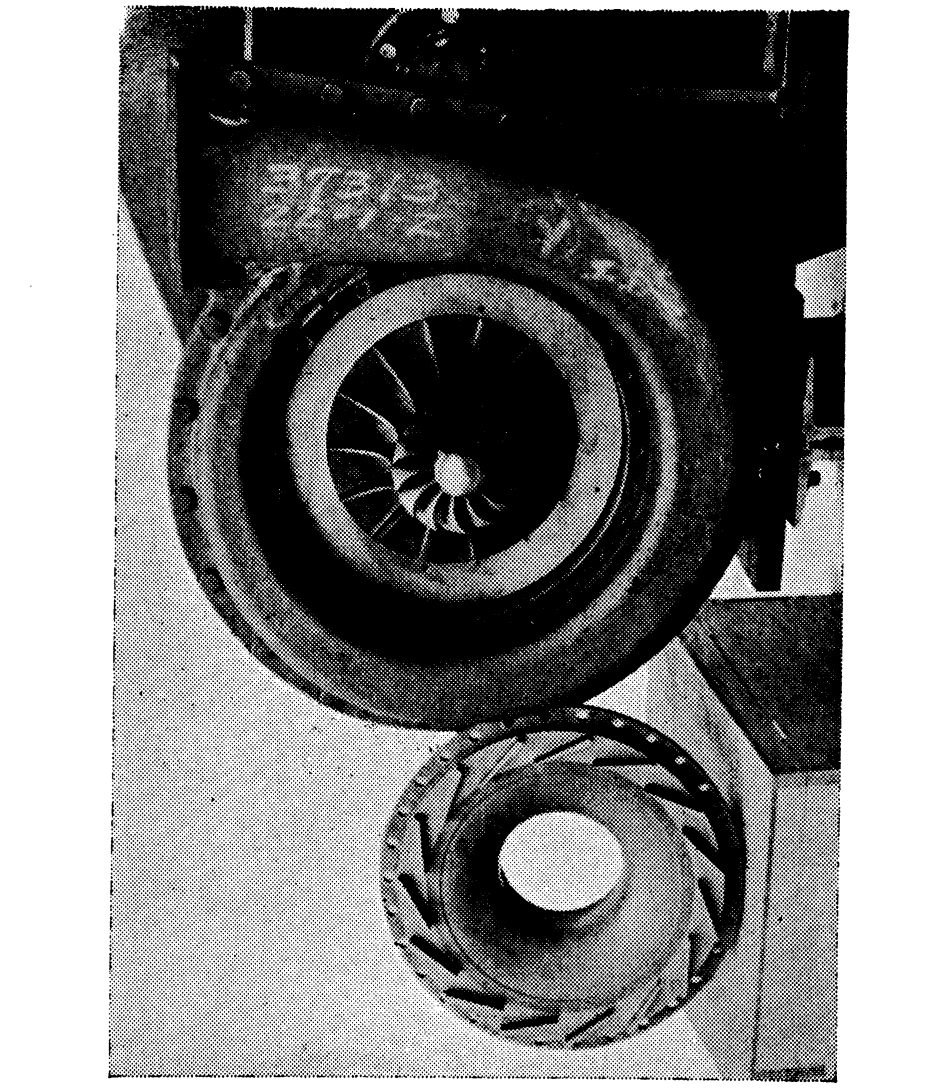

(b)

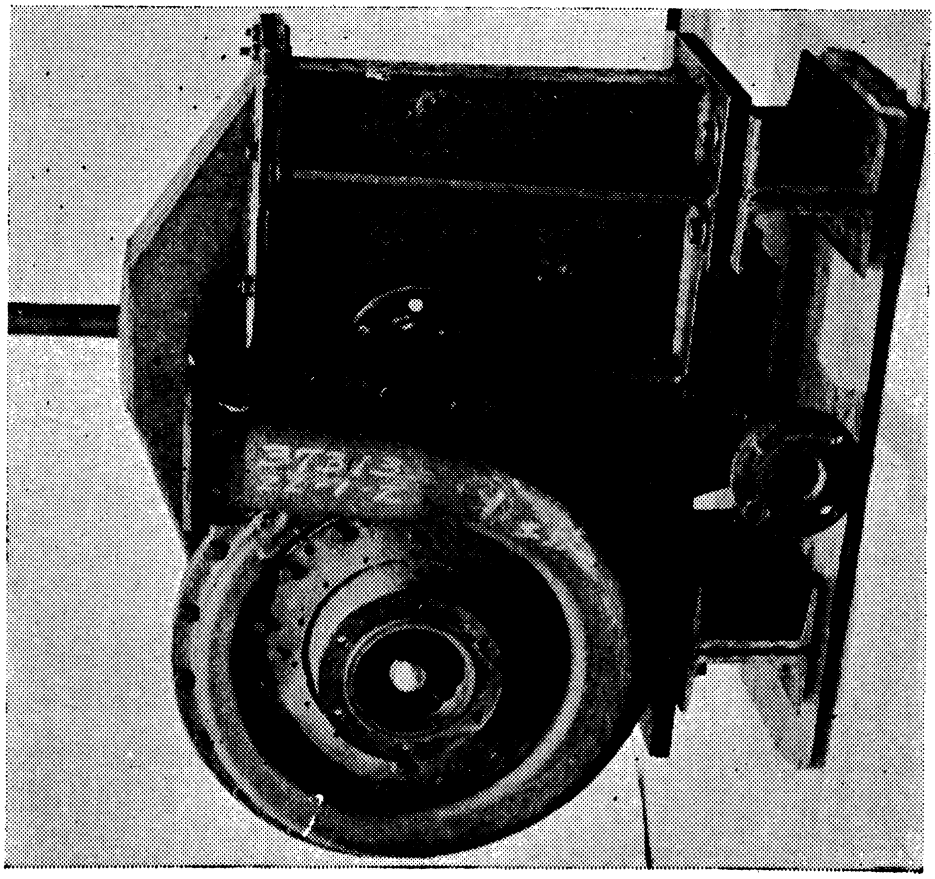

(a)

Figure 5.3 Test Turbine No. 2

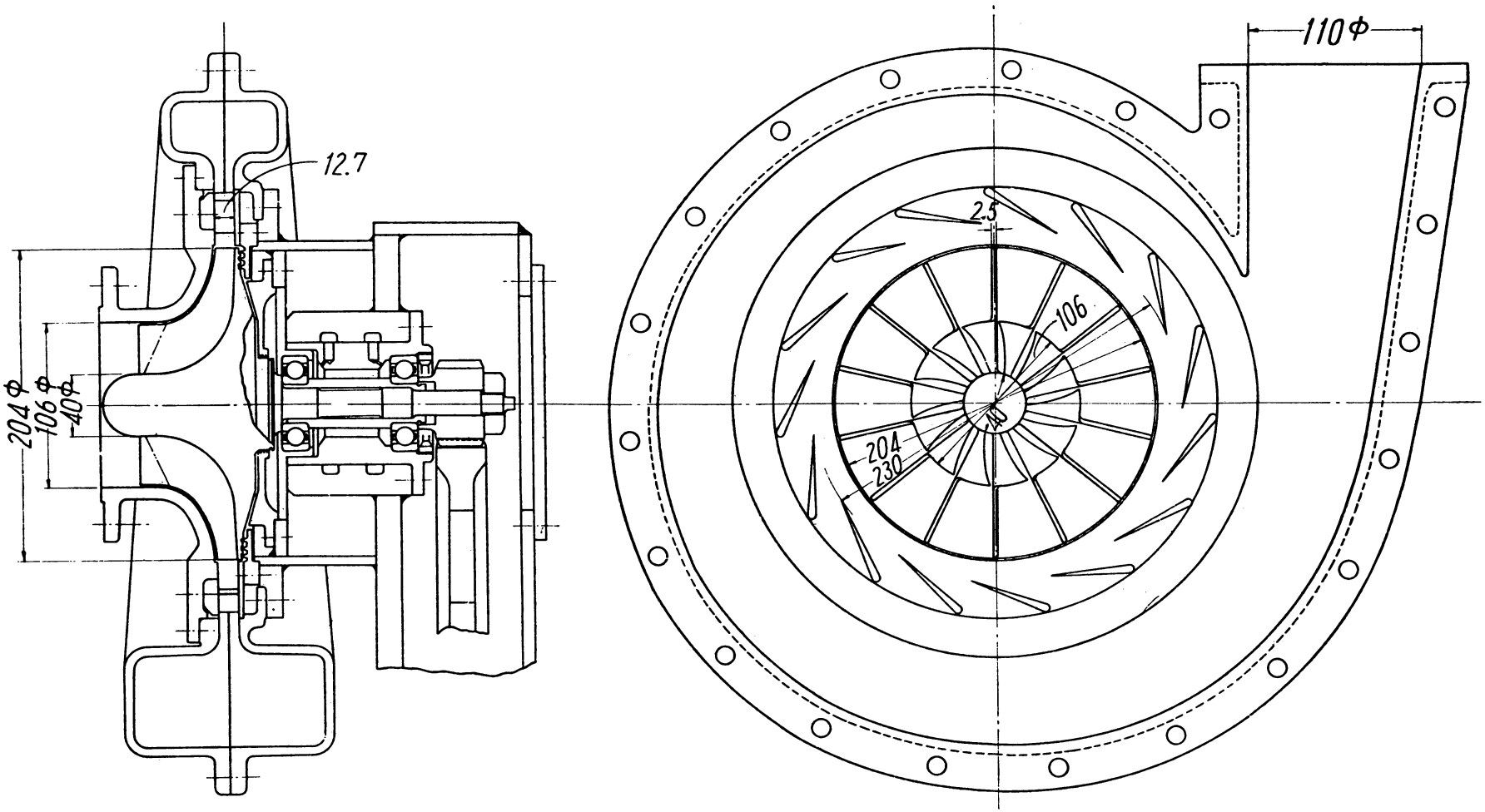

Shapes of Exducer

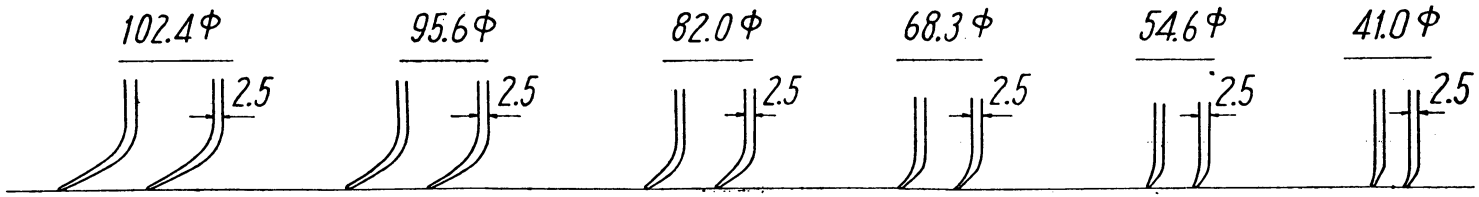

Figure 5.4 Test Turbine No. 2

air temperature at the turbine inlet is measured by a precision mercurial thermometer of 1/10°C graduation attached at the inlet of the spiral chamber. As to the turbine inlet pressure, eight pressure holes around the spiral chamber inlet are used to measure the static pressure, while the mean dynamic pressure is determined by measuring the flow. The total pressure, p_0, at the turbine inlet is determined from both the static and the dynamic pressures. The turbine output power is absorbed by the 10 kw electric dynamometer. Between the dynamometer axis and the turbine axis, a one-step toothed gearing is used to decelerate the number of turbine revolutions to 0.327. The number of revolutions of the dynamometer axis is measured by an electronically equilibrated autographic tachometer with 0.5% precision. The blade inlet pressure is measured by making pressure holes on the side wall above the blade inlet (R_1 = 125 mm). The mean number obtained from the seven pressure holes distributed over one-nozzle pitch distance of the side wall, is regarded as the blade inlet pressure, p_1. In order to study the change of pressure over the whole circle of the blade inlet, the circle is divided into the equal number to that of nozzles (viz. pitch), where the pressure holes are made. Pressure holes are made also on those points of the blade side wall where R = 115, 105, 95, 85, 75, and 70 mm, in order to study the drop of pressure in the blade. Six pressure holes are made over the circle of the turbine outlet in order to obtain the turbine outlet pressure, p_2, which is the average of those numbers measured by the holes. All pressure holes have a diameter of 1 mm. The experiments performed are of the following two kinds.

(i) Measurement of losses.

The internal efficiency of the turbine is obtained by clarifying the losses in nozzles and moving blades, the shock loss at the blade inlet, the leaving loss, the heat loss as well as the type and cause of the slip in flow in turbine blades. To do this, the temperature and pressure distributions are measured at each radius of the turbine outlet which is opened to the atmosphere.

The temperature distribution is measured by a precision mercurial thermometer of 1/10°C graduation. As to the velocity distribution, a three-hole Yaw meter as shown in Figure 5.6 is used to measure the direction and the size of the absolute efflux velocity as well as the static pressure. Figure 5.7 shows the structure of a Yaw meter, consisting of a baton of 4 mm diameter on which three pressure holes of 0.3 mm diameter are made. The pressure on those holes is made equal by rotating the Yaw meter, by means of which the direction of the flow is studied, and the total pressure obtained from h_0. The dynamic pressure is obtained by measuring h_1 which is directly proportional to the dynamic pressure. The static pressure is obtained by subtracting the dynamic pressure from the total pressure, h_0. The Yaw meter must be examined beforehand by a wind-tunnel.

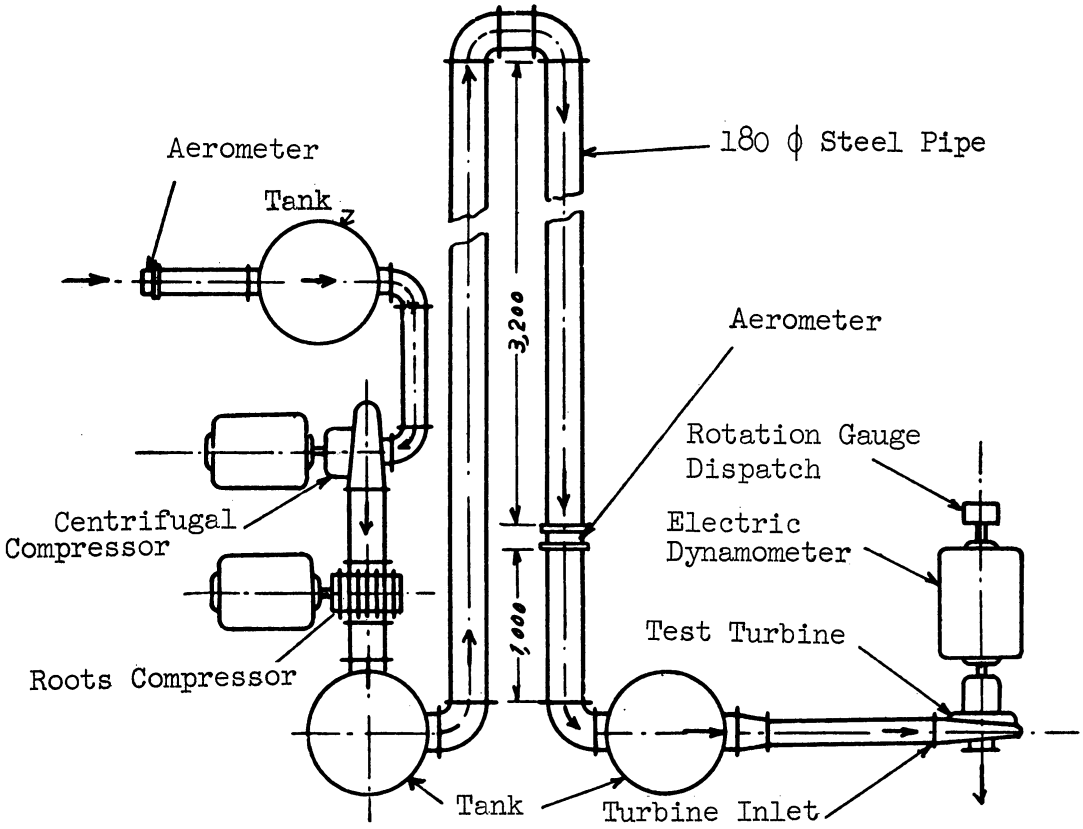

Figure 5.5 Test Turbine No. 1 Equipment

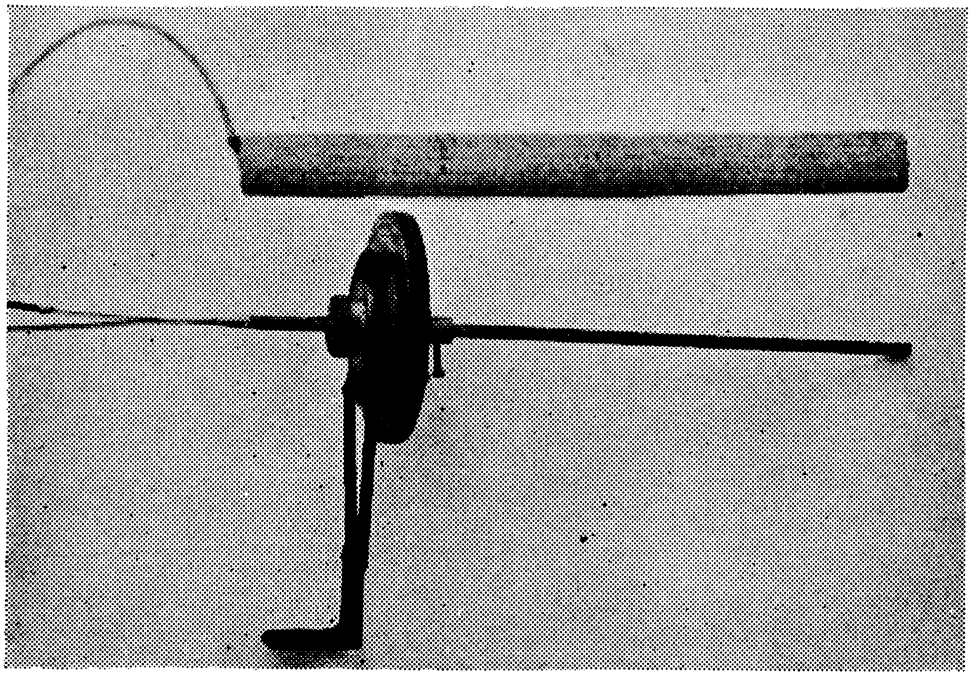

Figure 5.6 Yaw Meter

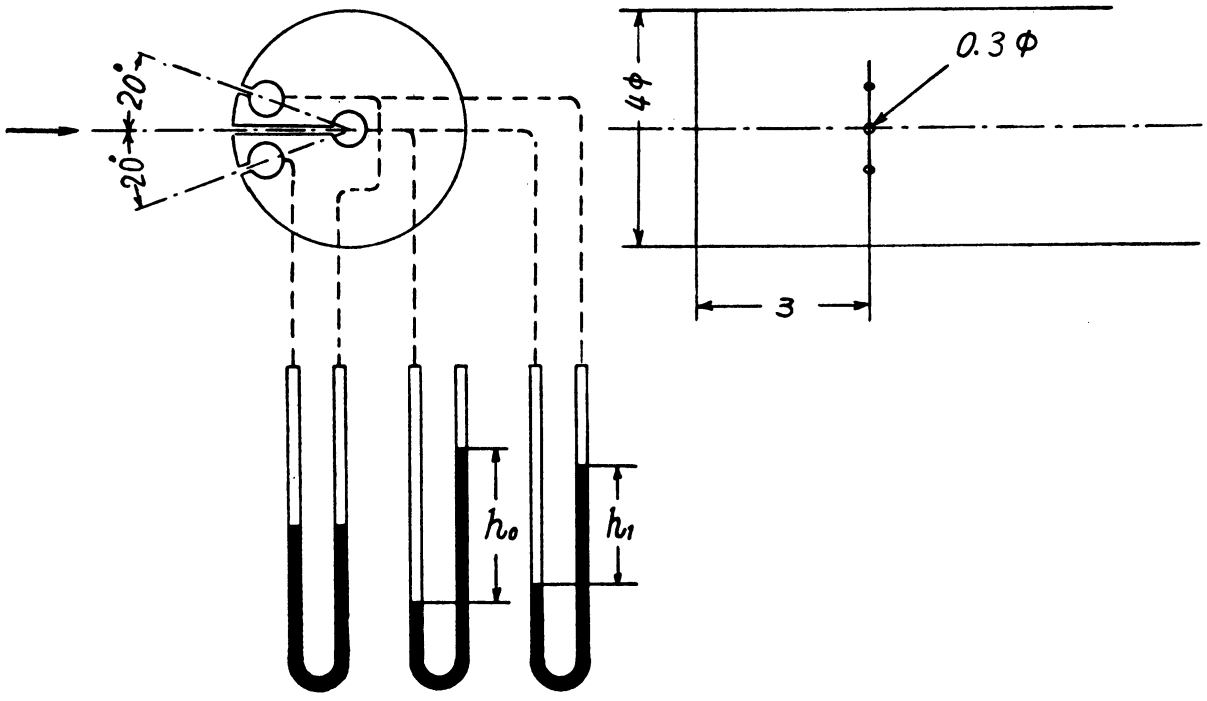

Figure 5.7 Structure of Yaw Meter

(ii) Measurement of average temperature efficiency and average internal efficiency.

Since the distribution of temperature and fluid velocity varies greatly at the turbine outlet, the following tests are taken to obtain the average temperature efficiency and the average internal efficiency of the entire gas flow.

Instead of measuring the temperature and velocity distributions, a wooden box of 45 cm x 45 cm x 45 cm is attached to the turbine outlet. The air in the turbine is led into and mixed in the box, and then discharged into the atmosphere. The air temperature in the box, measured by a mercurial thermometer, is regarded as the average temperature of the turbine outlet. The static pressure at the turbine outlet is measured at the same time, and is regarded as the turbine outlet pressure, p_2.

The above-described tests were conducted in Mizumachi Laboratory at the Institute of Industrial Science of the University of Tōkyō.

(b) Test equipment and procedures of the test turbine No. 2.

Figures 5.8 and 5.9 show the test equipment of the turbine No. 2 and its photography.

The air, compressed in the six-step turbo-compressor, is led to the combuster where it is converted into combustion gas, which, in turn, is led into the turbine. The gas, passing out of the turbine, is discharged through the conduct pipe and the aerometer into the atmosphere. The output power of the turbine, passing through the one-step helical deceleration gear (Deceleration: 0.0996), is absorbed into the 150 horse power electric dynamometer.

The flow of gas is measured by the circular aerometer (gas flow gauge) of the nozzle. The gas temperature at the turbine inlet is measured by the four thermoelectric couples attached at the spiral chamber inlet. The average of the four measured values is regarded as the average gas temperature at the turbine inlet, t_0. One of the four measured temperatures is recorded by the electronically-equilibrated thermoelectric autographic recorder. As for the gas temperature at the turbine outlet, seven thermoelectric couples are used on the radius of the turbine outlet to measure the radial temperature distribution at the turbine outlet. Four thermoelectric couples are used on the radius, the mean number of which is regarded as the gas temperature of the aerometer. The range of $\pm 1^{\circ}C$ is used for all the thermoelectric couples intended for measuring gas temperature. As for the turbine inlet pressure, four pressure holes are made on the inlet circle of the spiral chamber to measure the static pressure. The total pressure of the turbine inlet, p_0, is obtained by adding the average static pressure to the average dynamic pressure obtained from the gas flow. As for the turbine

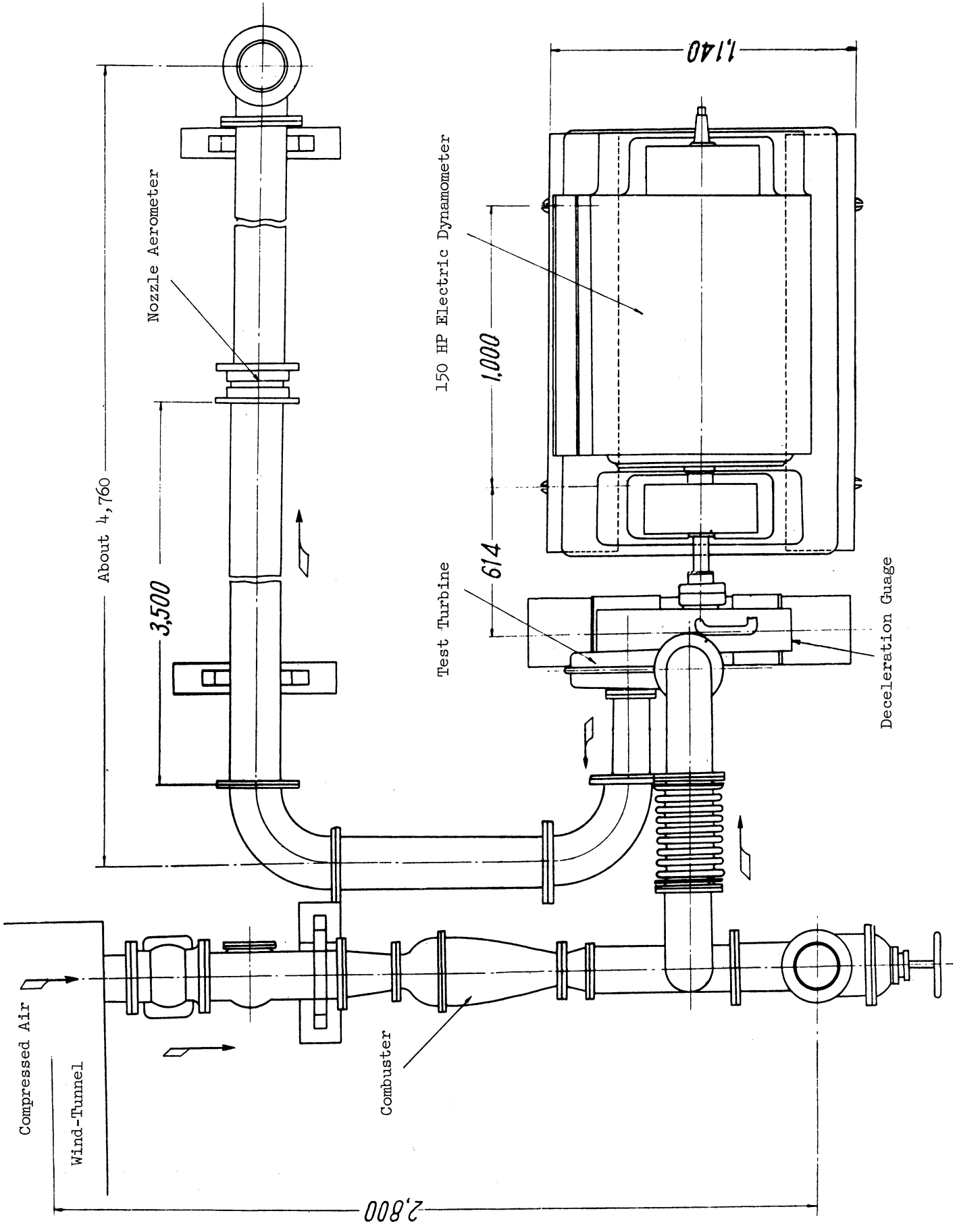

Figure 5.8 Test Turbine No. 2 Equipment

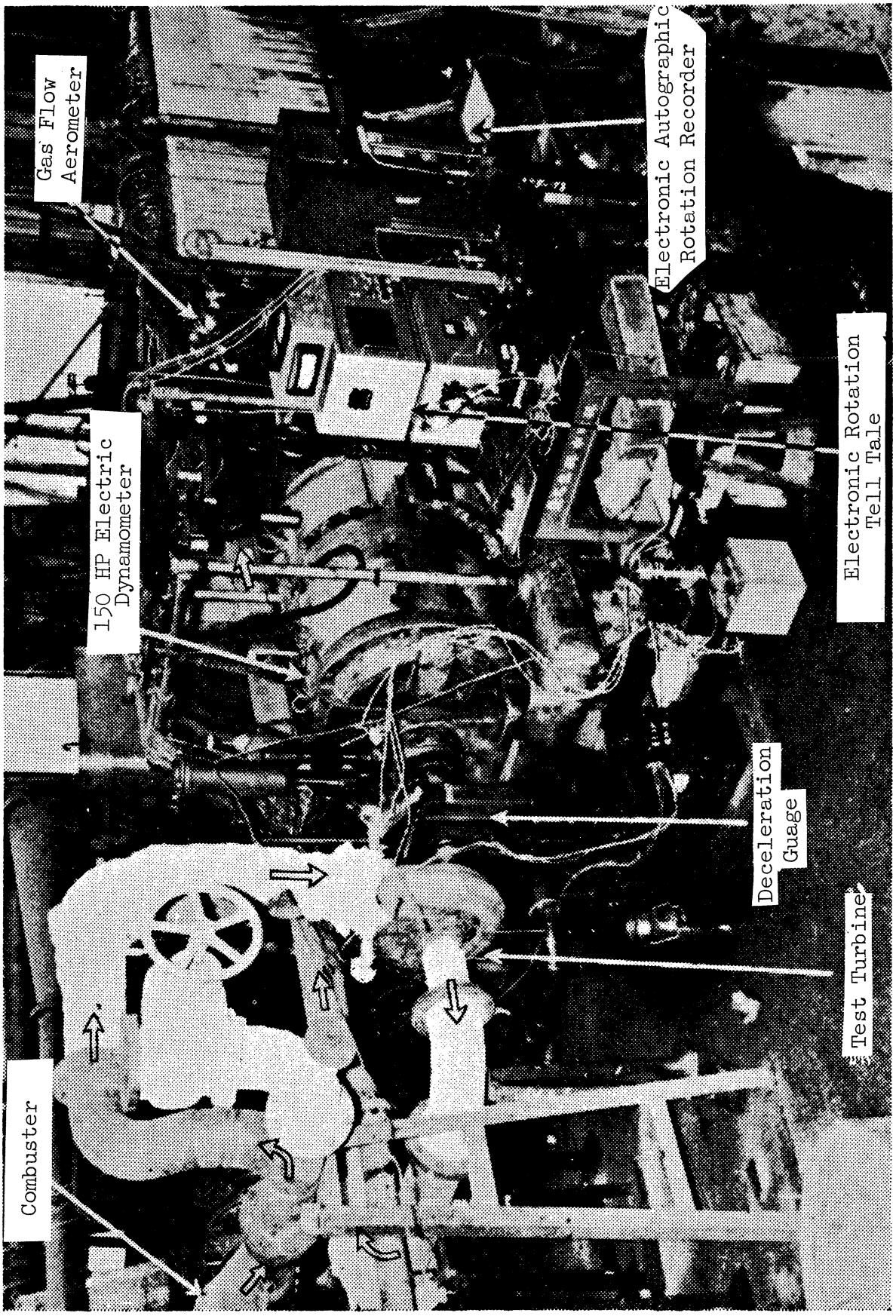

Figure 5.9 Test Turbine No. 2 Equipment

outlet pressure, six pressure holes are made on the outlet circle of the turbine to measure the static pressure, the average of which is regarded as the turbine outlet pressure, p_2. The blade inlet pressure is measured by making seven pressure holes on the blade inlet radius (R_1 = 102 mm) with each hole corresponding to each pitch of the nozzle. The average of the static pressure thus measured is regarded as the blade inlet pressure, p_1. The change of pressure at the blade inlet is studied by dividing the entire circle of the blade inlet into the same number as that of nozzles, and by making the same number of pressure holes on the division. All pressure holes have a diameter of 1 mm. The number of revolutions is obtained by recording the revolution number of the dynamometer axis on the autographic recorder, and is measured at the same time by the electronic rotation tell-tale. A range of $\pm$0.5% is used for the autographic rotation recorder, and that of $\pm$1 count (the count during the experiment: 300 ~ 1500) for the electronic rotation tell-tale. The velocity distribution on the turbine outlet radius is measured by the same Yaw meter that is used in the test turbine No. 1. The Yaw meter is attached to the turbine outlet removed from the conduct pipe. In this case, air is used instead of combustion gas. The above-described tests were conducted in the factory No. 3 of the Ishikawajima Heavy Industry K.K.

5.4. Results of the Test

Figures 5.10 shows the velocity diagram of the blade inlet and outlet (Radius R).

c_1 = average efflux velocity from nozzle

α = average efflux angle

U_1 = circumferential velocity at the blade inlet

w_1 = relative influx velocity

i = relative elevation angle against the blade (in case of radial straight vanes)

c_{1u} = circumferential component of c_1

w_{1u} = circumferential component of w_1

c_2 = absolute efflux velocity from any given radius, R, of the turbine outlet

u_2 = circumferential velocity

w_2 = relative efflux velocity

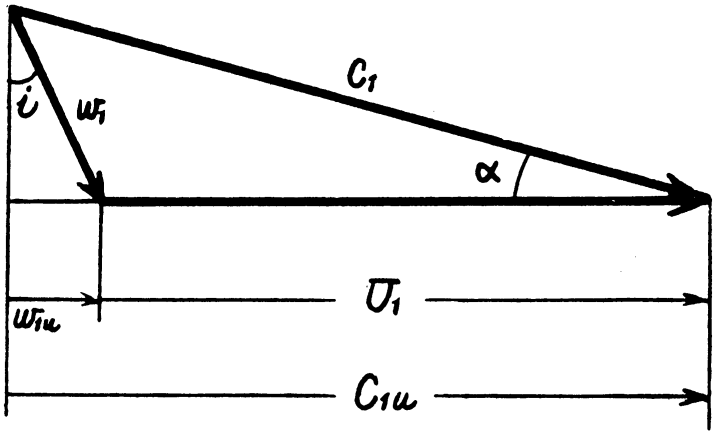

Blade Inlet

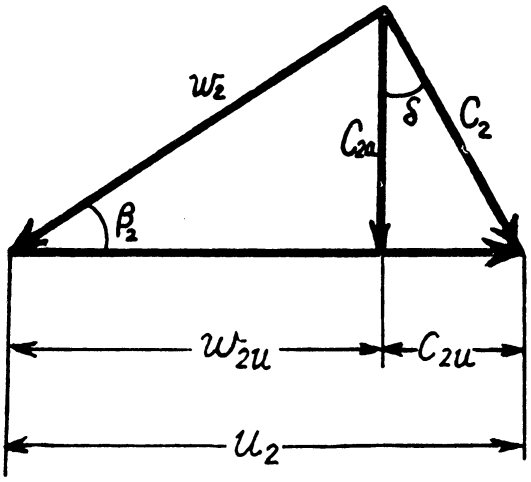

Blade Outlet

Figure 5.10 Velocity Diagram

β_2 = relative efflux angle

δ = axial angle of the absolute efflux velocity

c_{2u} = circumferential component of c_2

w_{2u} = circumferential component of w_2

c_{2a} = axial component of c_2.

Figure 5.11 shows the static pressure (h_s) and the dynamic pressure (h_d) measured at the turbine outlet radius by the Yaw meter, when the exducer is attached to the test turbine No. 1. Figure 5.12 shows the absolute efflux angles formed by the axis and the absolute efflux velocity (+: the slope in the direction of axis). In both figures, the expansion ratio p_0/p_z = 1.15 (p_z = atmospheric pressure).

The values of c_2, c_{2a}, w_2, and β_2, at each outlet radius result from the above measurements. The axial flow velocity, c_{2a}, is shown in Figure 5.13, with a_2 representing the sound velocity of gas at the turbine inlet.

The distribution of flow in each breadth of 2.5 mm of the outlet radius, obtained from the above axial velocity, is shown in Figure 5.14. The total gas flow, G, is obtained by adding up the gas-flow distributions in the whole turbine outlet radii. A comparison between the gas flow obtained from the velocity distribution and the gas flow measured by the circular nozzle aerometer at the compressor inlet is shown in Figure 5.15. This goes to prove the accuracy of the velocity-distribution measurement at the turbine outlet.

The relative efflux angles, β_2, of both test turbines No. 1 and No. 2 are shown in Figures 5.16 and 5.17. The turbine No. 1 uses the ST-16-2 nozzle and the expansion ratio of 1.15, while the turbine No. 2 uses the No. 1 nozzle and the expansion ratio of 2.0. In both cases, the flow moves at an angle sharper than the geometrical efflux angle (β_{e1}, β_{e2}) of the exducer outlet. The angles of slip ($\beta_2 - \beta_{e1}$) are shown in Figures 5.18, 5.19, and 5.20. Figures 5.18 and 5.19 show the slip angles of the test turbine No. 1 using the ST-16-2 nozzle and the ST-20-2' nozzle respectively. Figure 5.20 shows the slip angle of the turbine No. 2. These diagrams indicate the existence of considerable slips at the exducer outlet, on which more will be said later.

5.4.1. The Losses

The work of gas in the turbine is shown in i-s diagram in Figure 5.21.

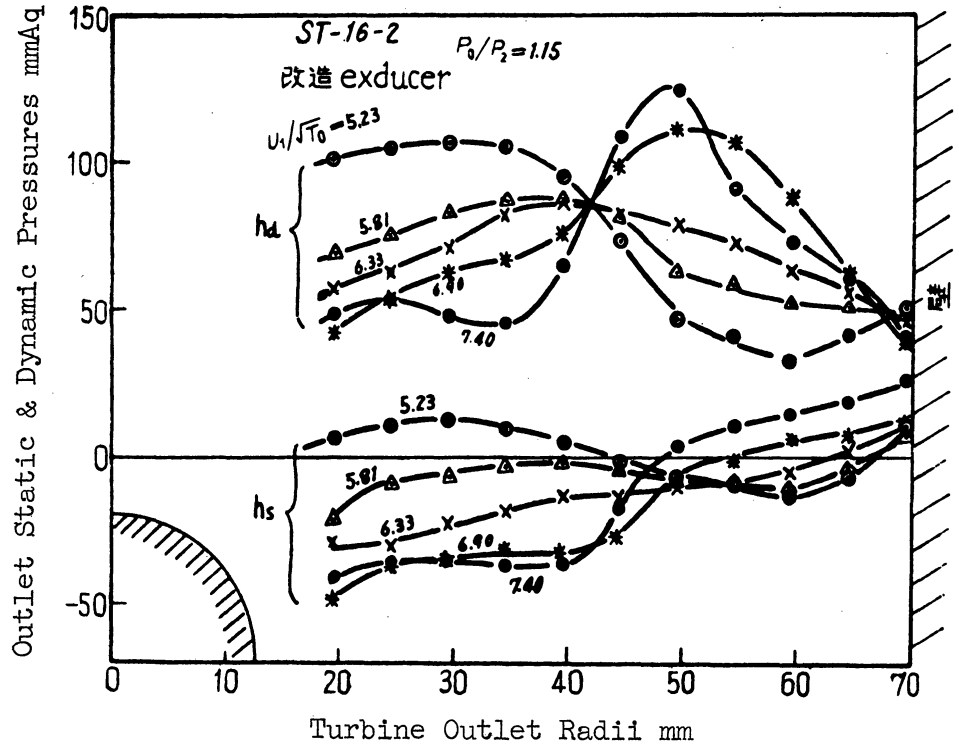

Figure 5.11 Distribution of Outlet Static & Dynamic Pressures
(Test Turbine No. 1)

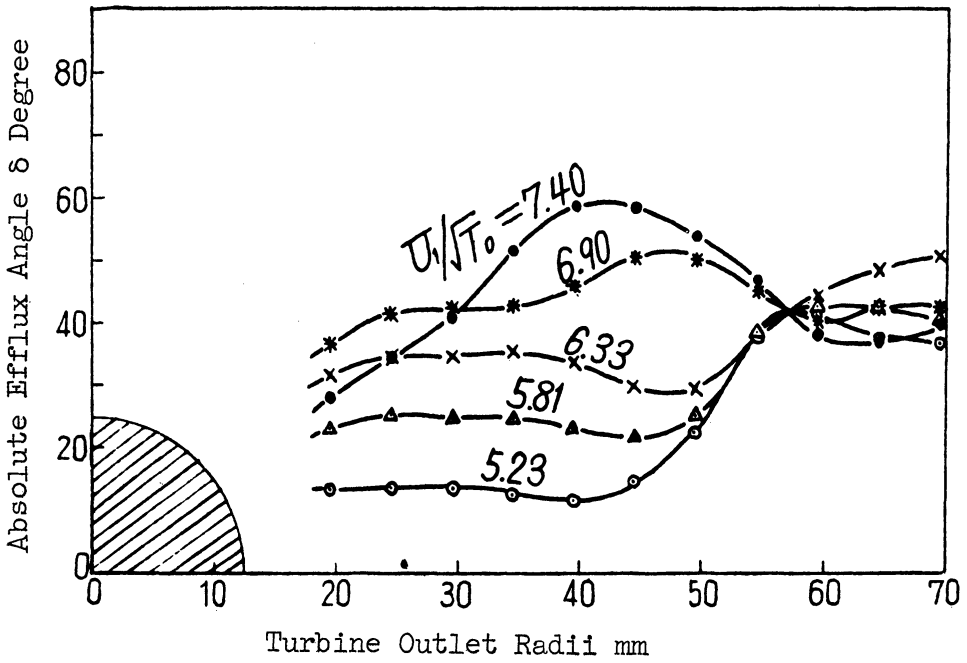

Figure 5.12 Absolute Efflux Angle
(Test Turbine No. 1)

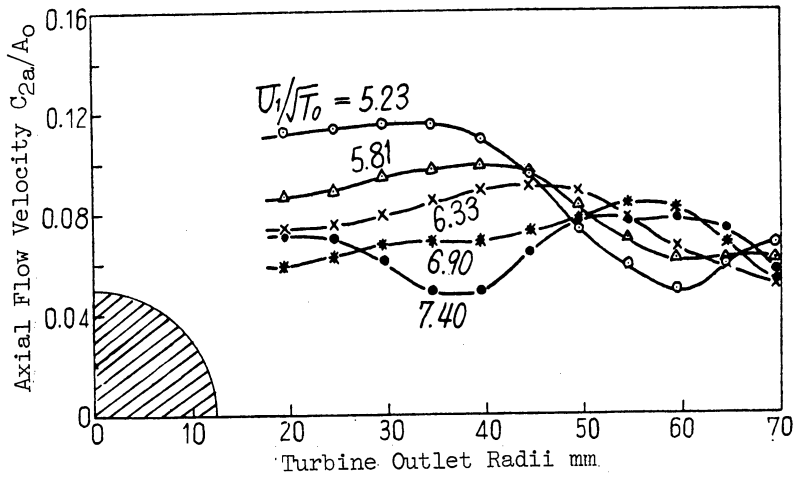

Figure 5.13 Axial Flow Velocity
(Test Turbine No. 1)

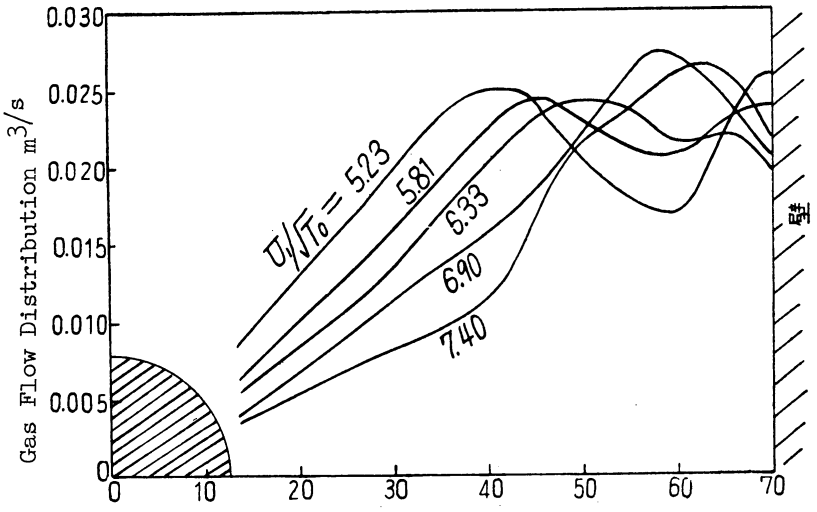

Figure 5.14 Flow Distribution (Test Turbine No. 1)

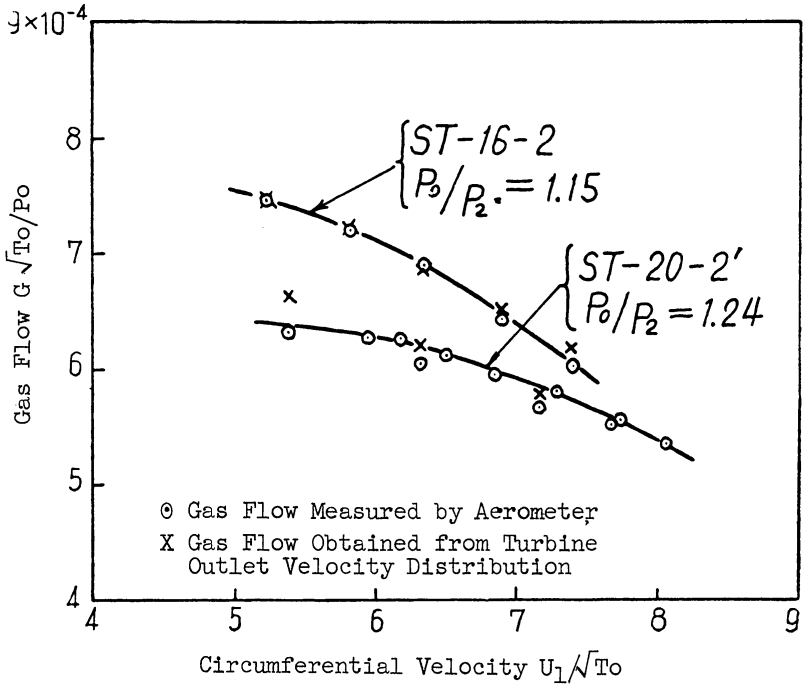

Figure 5.15 Comparison of Gas Flow

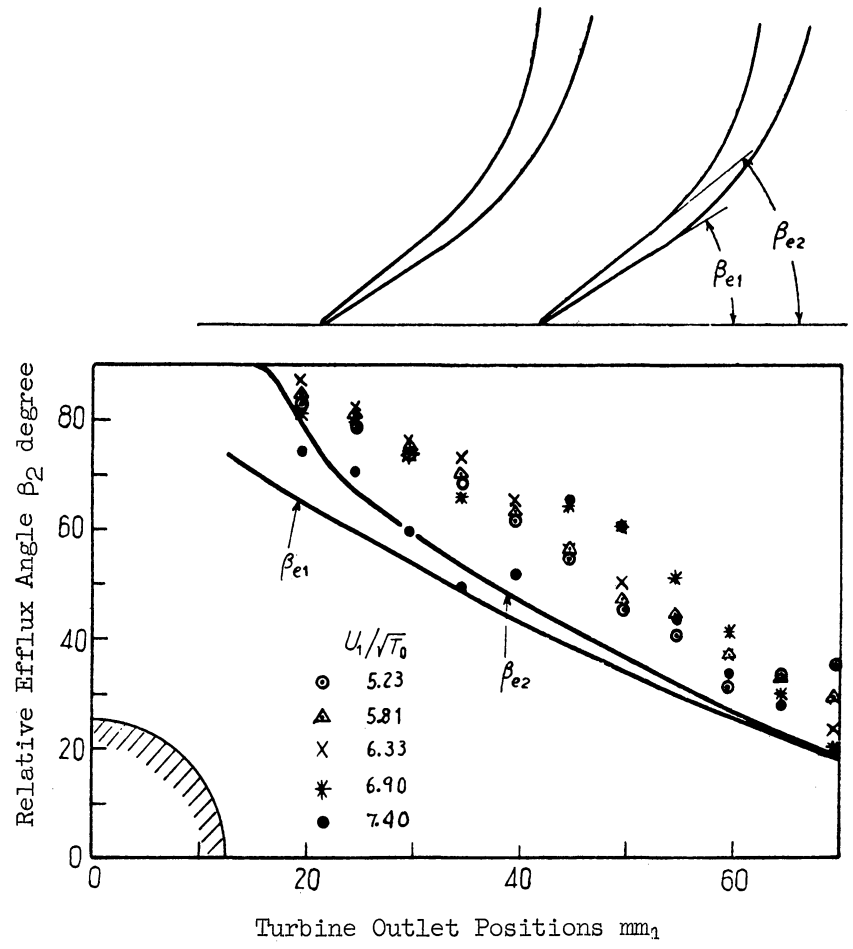

Figure 5.16 Relative Efflux Angle (Test Turbine No. 1)

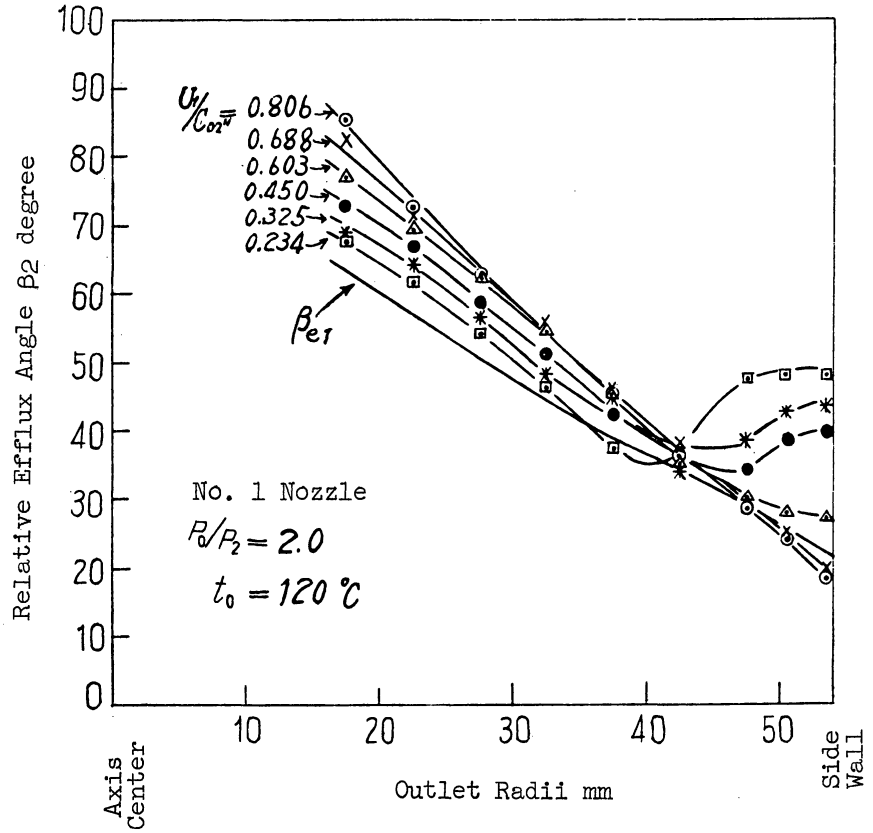

Figure 5.17 Relative Efflux Angle (Test Turbine No. 2)

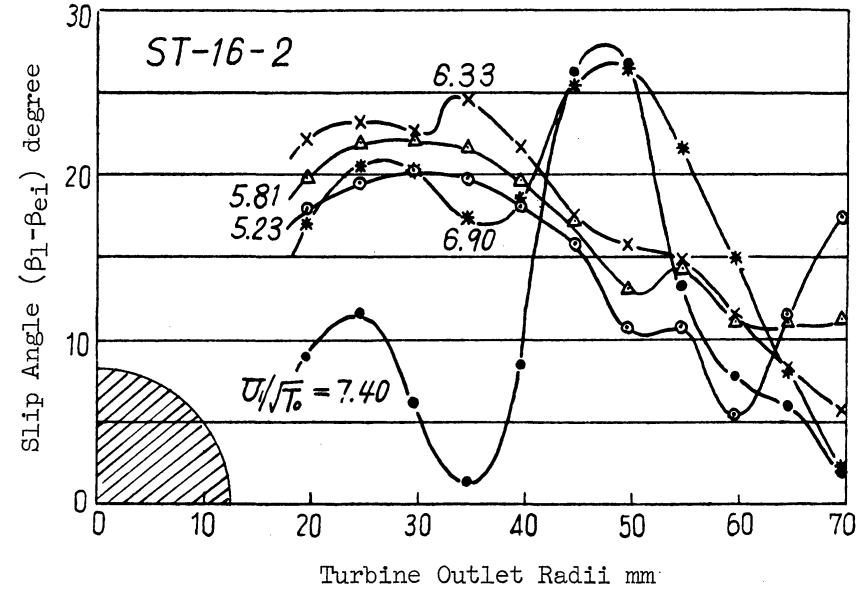

Figure 5.18 Slip Angle (Test Turbine No. 1)

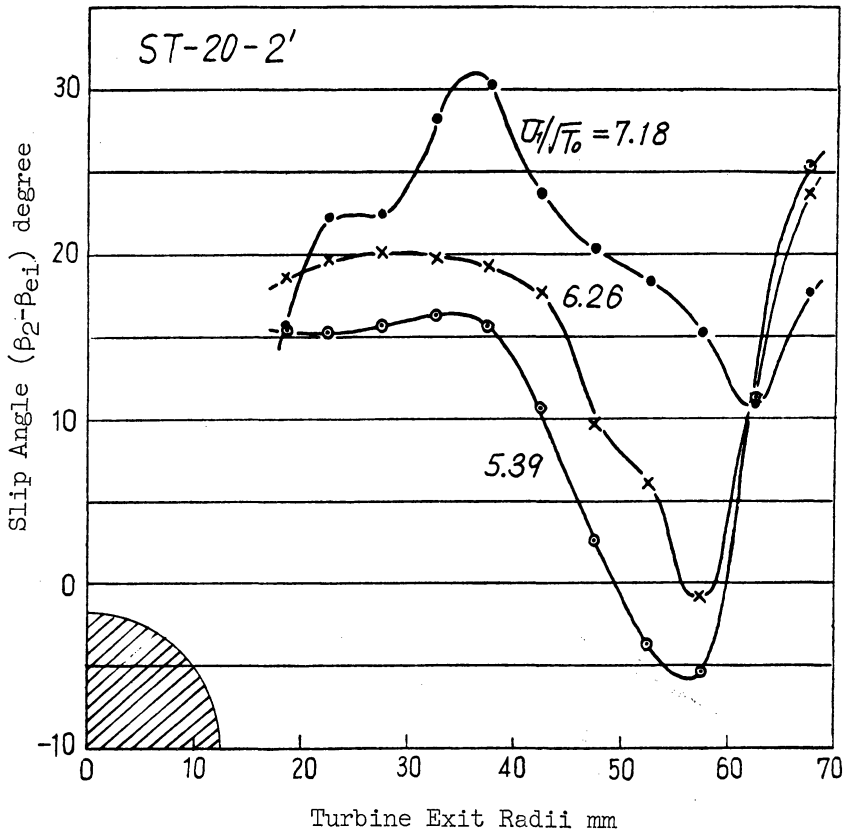

Figure 5.19 Slip Angle (No. 1 Test Turbine)

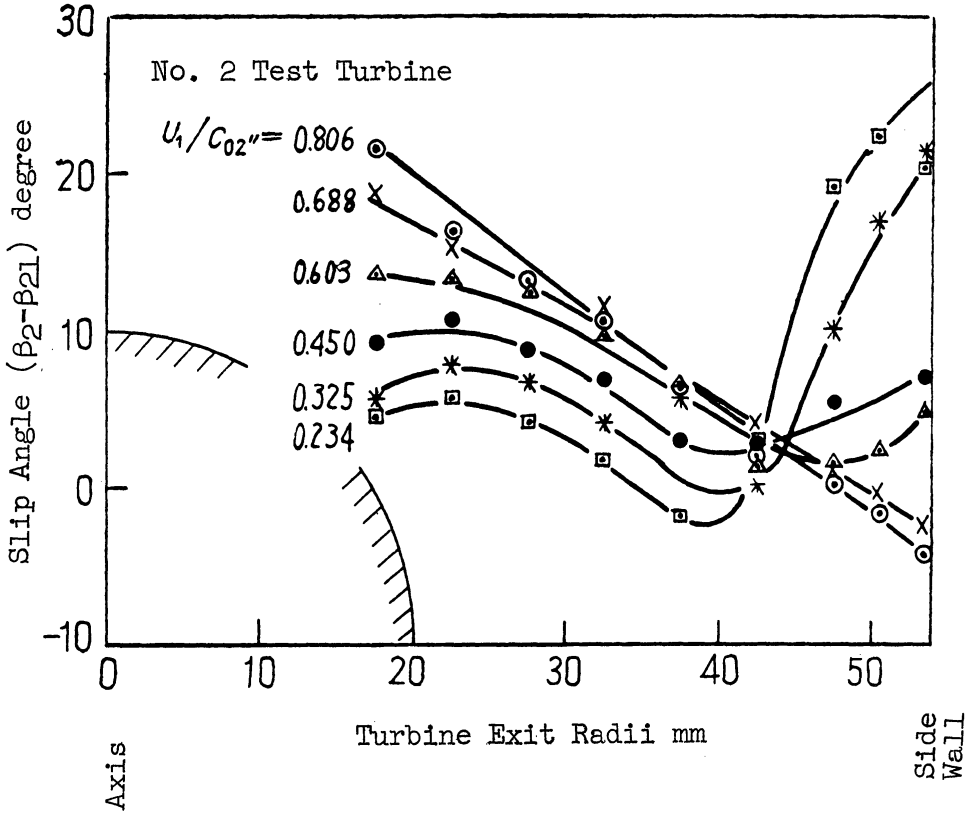

Figure 5.20 Slip Angle (No. 2 Test Turbine)

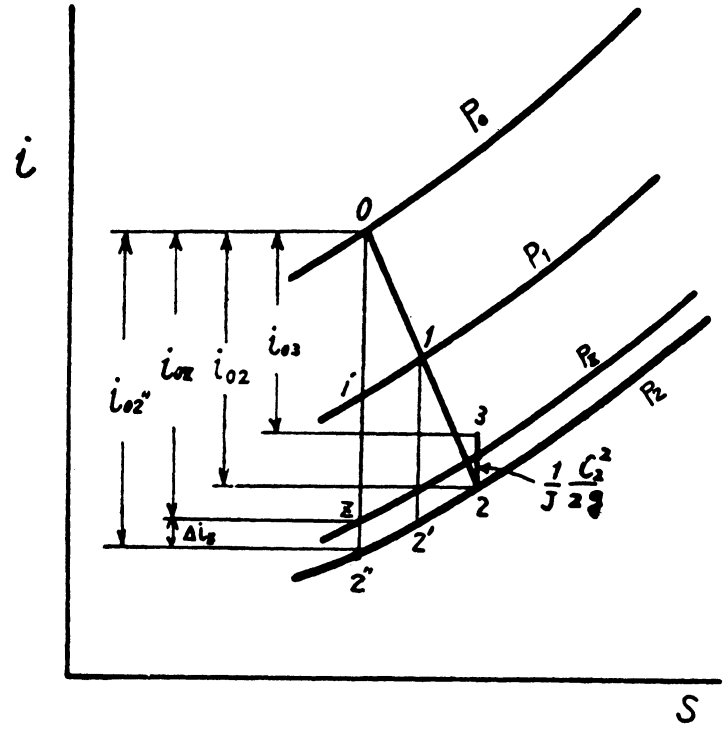

Figure 5.21 i-s diagram

As the turbine inlet conditions (p_0, T_0) and the blade inlet pressure, p_1, are known from the experiment, the velocity, c_1', at the time of the equal entropy expansion from p_0 to p_1 will accordingly be determined. This also enables us to obtain the Reynolds number, R_{e1}, for both c_1' and the nozzle outlet attaching radius, R_{1N}. Using the procedures described in Chapter 3, the velocity coefficient of the nozzle, φ, as well as the average efflux velocity, c_1, of the nozzle are obtained from R_{e1}. The radial component c_{1r} of c_1 is obtained from the measured gas flow, G, and the sectional area of the passage at the blade inlet ($2\pi R_1 \times B_1$). Accordingly the average efflux angle, α, of the nozzle is obtained from c_1 and c_{1r}. The circumferential velocity at the blade inlet, U_1, w_1, as well as the angle of relative elevation, i, are obtained from the number of revolutions. The reaction, r, is obtained from the blade inlet pressure, p_1. The values of α, φ, i, γ, and the non-dimensional quantity of flow $G\sqrt{T_0/p_0}$ thus obtained for the test turbine No. 1 using the ST-16-2 nozzle and $p_0/p_2 = 1.15$ are shown in Figure 5.22. The analysis of the losses observed in the test turbine No. 1 is described below.

(a) The losses in the nozzles.

The loss of energy in the nozzles Δi_N are expressed in the following formula:

$$J\Delta i_N = Ji_{02}'' - \left(\frac{c_1^2}{2g} + Ji_{12}'\right)$$

$$= (1 - \varphi^2)\frac{c_1'^2}{2g} \cdot \frac{s_0}{s} \qquad (5.1)$$

With i_{0z} representing the enthalpy at the time of the equal entropy expansion from the turbine inlet conditions (p_0, T_0) to the atmospheric pressure at the outlet, p_z, the ratio (%) of Δi_N and i_{0z} takes the form as shown in Figure 5.23. i_{0z} is used as the cardinal point simply because the turbine outlet is open to the atmospheric pressure, p_z. In this case, the velocity coefficient of the nozzle is taken in the range of 0.968 ~ 0.973, and the losses in the nozzles are 2-3%. The ratio of the nozzle losses increases as the loss of heat in the nozzles increases and the reaction decreases, even though the velocity coefficient of the nozzles rises with the low number of revolutions.

(b) The losses in the moving blades.

The work done in the turbine blade, L_i, is expressed below.

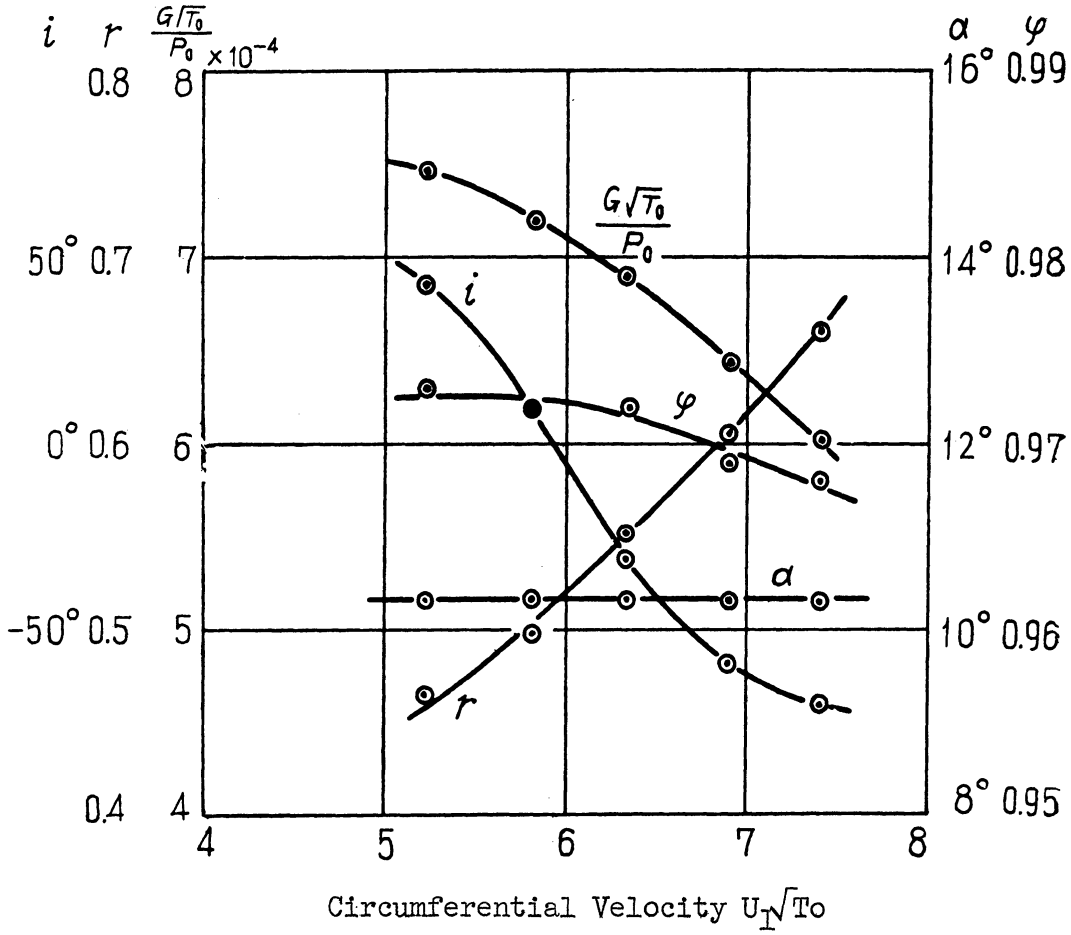

Figure 5.22

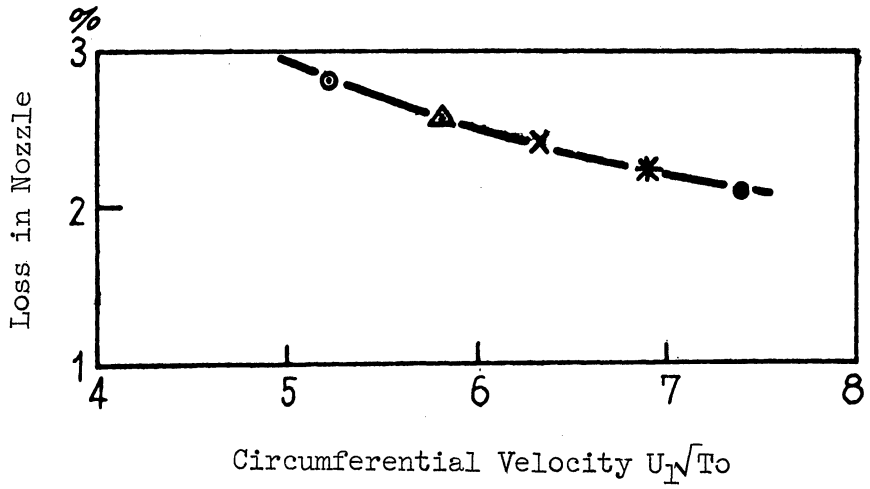

Figure 5.23 Loss in Nozzle (No. 1 Test Turbine)

$$L_i = \frac{1}{2g}(c_1^2 - c_2^2) + \frac{1}{2g}(w_2^2 - w_1^2)$$

$$+ \frac{1}{2g}(U_1^2 - u_2^2) \qquad (5.2)$$

Since L_i is produced with the energy $(c_1^2/2g + Ji_{12'})$ in the blades,

$$\frac{c_1^2}{2g} + Ji_{12'} = L_i + \frac{c_2^2}{2g} + E_s + E_b + E_h \qquad (5.3)$$

$c_2^2/2g$ = the leaving loss

E_s = the shock loss at the blade inlet

E_b = the loss in the blade

E_h = the loss of heat.

The values of the second half (the right-hand side) are obtained entirely from the experiment, which add up to determine the work performed in the turbine blade. The ratio of L_i and the total enthalpy in the turbine makes the internal efficiency η_i.

$$\eta_i = \frac{L_i}{Ji_{0z}} \qquad (5.4)$$

The internal efficiency, η_i, at each radial point of the turbine outlet is shown in Figure 5.24.

As shown in Chapter 2, the work done in turbine blades is by no means equally distributed at the turbine exit radii, the work near the center of exit being higher than that at the outside radii of exit by about 5 ~ 10%. Efficiency can therefore be greatly improved by concentrating the flow upon the center, where a greater work is performed, rather than by giving a uniform axial velocity distribution at the turbine exit. Since an overconcentration of flow upon the center will result in the increase of blade and leaving losses due to the increased velocity, we should determine the exit velocity coefficient most suitable for the maximum efficiency when a certain quantity of flow is discharged into the turbine. This corresponds to the case expressed by the curve (3) of Figure 2.7 of Chapter 2, the condition of which is expressed in (2.48).

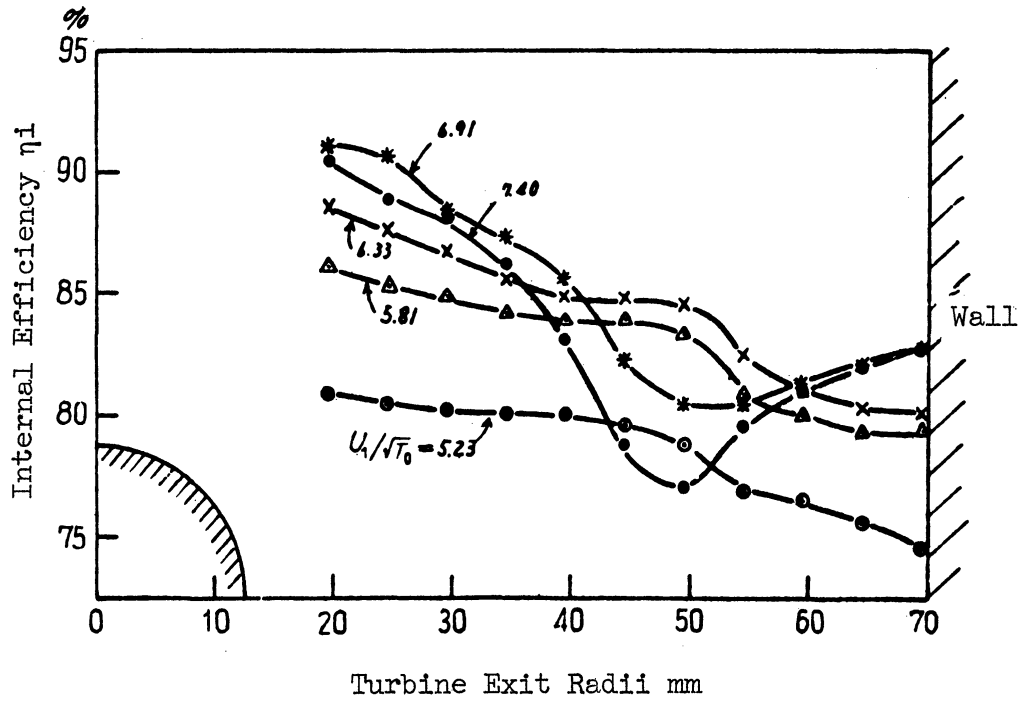

Figure 5.24 Internal Efficiency (No. 1 Test Turbine)

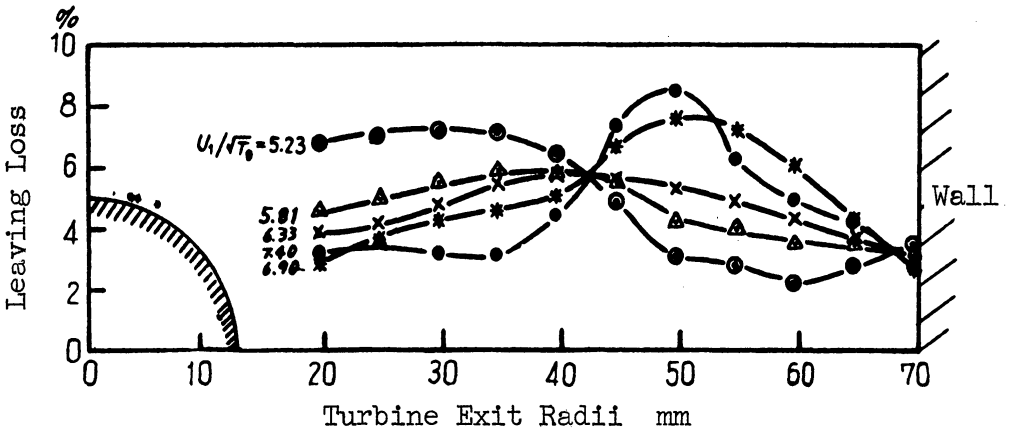

Figure 5.25 Leaving Loss (No. 1 Test Turbine)

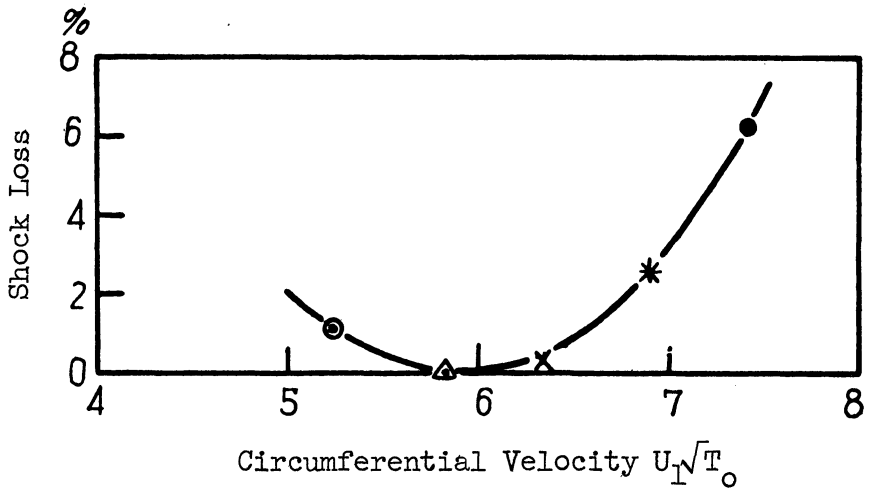

Figure 5.26 Shock Loss (No. 1 Test Turbine)

Figure 5.25 shows the leaving loss at the radii of exit expressed by the ratio of $c_2^2/2g$ and Ji_{0z}.

$$\text{Leaving loss} = \frac{\frac{c_2^2}{2g}}{Ji_{0z}} \tag{5.5}$$

The leaving loss is about $4 \sim 6\%$ near the designing point.

The shock loss, E_s, is caused by the angle of elevation, i, against the blade.

$$E_s = \zeta_s \frac{w_{1u}^2}{2g} \tag{5.6}$$

ζ_s is the coefficient of shock loss, and varies according to the pitch of blades. Figure 5.26 shows the ratio of the shock loss and the total enthalpy $Ji_{0z}(\zeta_s = 0.8)$. Although the angle of elevation is zero near the place where $U_1/\sqrt{T_0} = 5.9$ (in which case there is no shock loss), the angle of elevation varies greatly with a small change in the number of revolutions, due to the small efflux angle of the nozzle α. (See Figure 5.22.) This variance results in an abrupt increase of shock loss.

From (5.1) and (5.3),

$$Ji_{02''} = (1 - \varphi^2) \frac{c_1'^2}{2g} \cdot \frac{s_0}{s} + L_i + \frac{c_2^2}{2g}$$

$$+ E_s + E_b + E_h = Ji_{0z} + J\Delta i_z \tag{5.7}$$

Therefore

$$1 + \frac{\Delta i_z}{i_{0z}} = \underbrace{\frac{(1 - \varphi^2) \frac{c_1'^2}{2g} \cdot \frac{s_0}{s}}{Ji_{0z}}}_{\text{Nozzle Loss}} + \underbrace{\frac{L_i}{Ji_{0z}}}_{\text{Internal Efficiency}} + \underbrace{\frac{\frac{c_2^2}{2g}}{Ji_{0z}}}_{\text{Leaving Loss}}$$

$$+ \underbrace{\frac{E_s}{Ji_{0z}}}_{\text{Shock Loss}} + \underbrace{\frac{E_b}{Ji_{0z}}}_{\text{Blade Loss}} + \underbrace{\frac{E_h}{Ji_{0z}}}_{\text{Heat Loss}} \tag{5.8}$$

The total enthalpy increases when the turbine exit pressure is negative, and decreases when the pressure is positive. The value of Δi_z is approximately expressed in the formula below:

$$\frac{\Delta i_z}{i_{0z}} \fallingdotseq \frac{s_0}{1 - s} \cdot \frac{k - 1}{k} \cdot \frac{h_s}{p_0} \tag{5.9}$$

The negative pressure at the radii of the turbine exit is represented by h_s.

The losses in the nozzles, internal efficiency, leaving, and shock losses are thus obtained by the procedures described above. If we further determine the heat loss, the blade loss can be obtained. The heat loss remains very small when the turbine produces great output power, but rises to a considerable height when the output power is small as in the case of the test turbine No. 1.

Generally speaking, the temperature of the air current measured by a thermometer coincides with the total temperature of the gas. Accordingly, the temperature measured at each radial point of the turbine exit can be regarded as the temperature of the point 3 in Figure 5.21.

The temperature efficiency of the turbine, η_θ, is:

$$\eta_\theta = \frac{i_{03}}{i_{0z}}$$

$$= \frac{i_{02} - \frac{1}{J}\frac{c_2^2}{2g}}{i_{0z}} \tag{5.10}$$

We can also establish the following formula of energy:

$$Ji_{02} = L_i + E_h + \frac{c_2^2}{2g} \tag{5.11}$$

From (5.10) and (5.11),

$$\eta_\theta = \frac{L_i}{Ji_{0z}} + \frac{E_h}{Ji_{0z}} \tag{5.12}$$

The temperature efficiency, η_θ, is obtained directly from the measurement of temperature, as shown in Figure 5.27. A difference of 8 10% will be noted between the inside temperature and the temperature near the side wall. Since it is already determined that $\eta_i = L_i/Ji_{0z}$, the heat loss E_h/Ji_{0z} can be obtained from (5.12). The heat loss thus obtained is shown in Figure 5.28.

When all these losses are made clear, we can determine the blade loss, E_b/Ji_{0z} from (5.8), as shown in Figure 5.29. It will be noted from the figure that while the blade loss is merely about 1 2% near the center of the exit, it rises as high as 10% at the outside radii of the exit, indicating the high internal efficiency near the center, as compared with the low internal efficiency at the outside radii. The distribution of these losses described above is shown in Figure 5.30. The total of all these losses can be obtained by multiplying the gas flow at each point of these losses by the gas flow at each radial point of the exit. The mean number, obtained by dividing the total losses by the total gas flow, is shown in Figure 5.31. The high percentage of the heat loss is due to the small output power of the turbine. If the output power of more than 50 horse powers could be made, the heat loss would be reduced below 1 2%. The leaving loss of about 4%, the blade loss of about 5%, and the loss in the nozzle of about 3% are shown.

(c) Blade loss coefficient.

With E_b standing for the blade loss, w_2 for the relative velocity of the flow, we assume the relative velocity of flow w_2' when no loss is incurred in the blade. In this case, the velocity coefficient in the blade, ψ_2, can be given in the formula below:

$$\psi_2 = \frac{w_2}{w_2'} \tag{5.13}$$

From the formula of energy,

$$\frac{w_2'^2}{2g} = \frac{w_2^2}{2g} + E_b \tag{5.14}$$

From (5.13) and (5.14), the velocity coefficient, ψ_2, is:

$$\psi_2 = \frac{1}{\sqrt{1 + \dfrac{E_b}{\dfrac{w_2^2}{2g}}}} \tag{5.15}$$

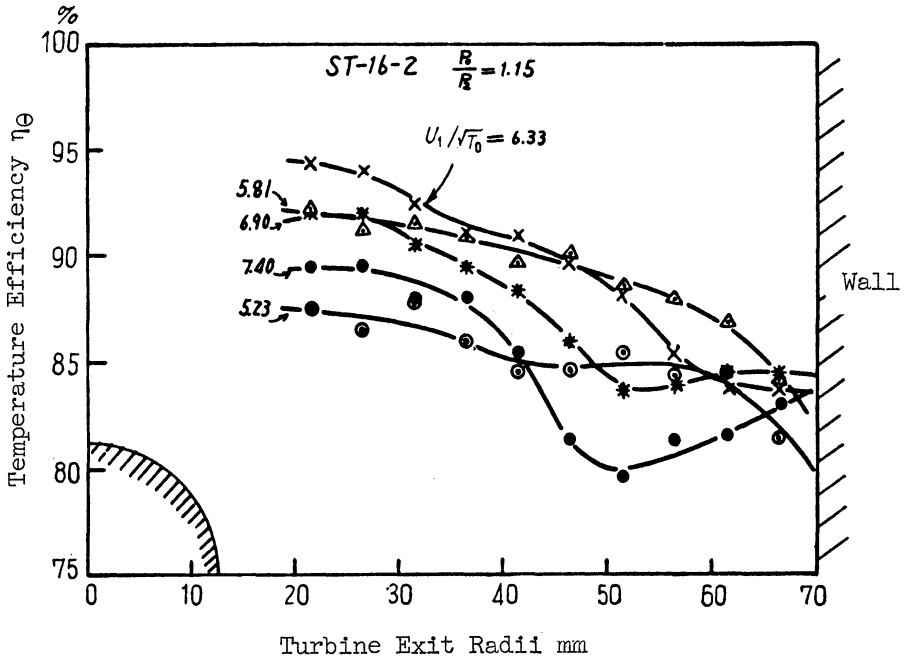

Figure 5.27 Temperature Efficiency (No. 1 Test Turbine)

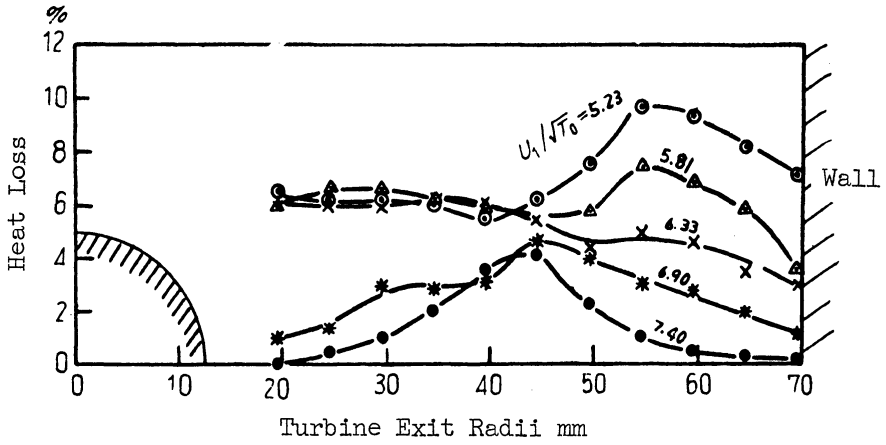

Figure 5.28 Heat Loss (No. 1 Test Turbine)

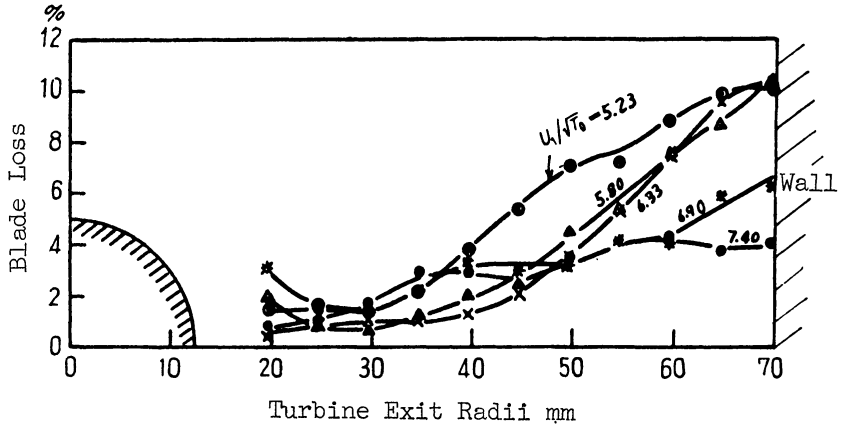

Figure 5.29 Loss in Blade (No. 1 Test Turbine)

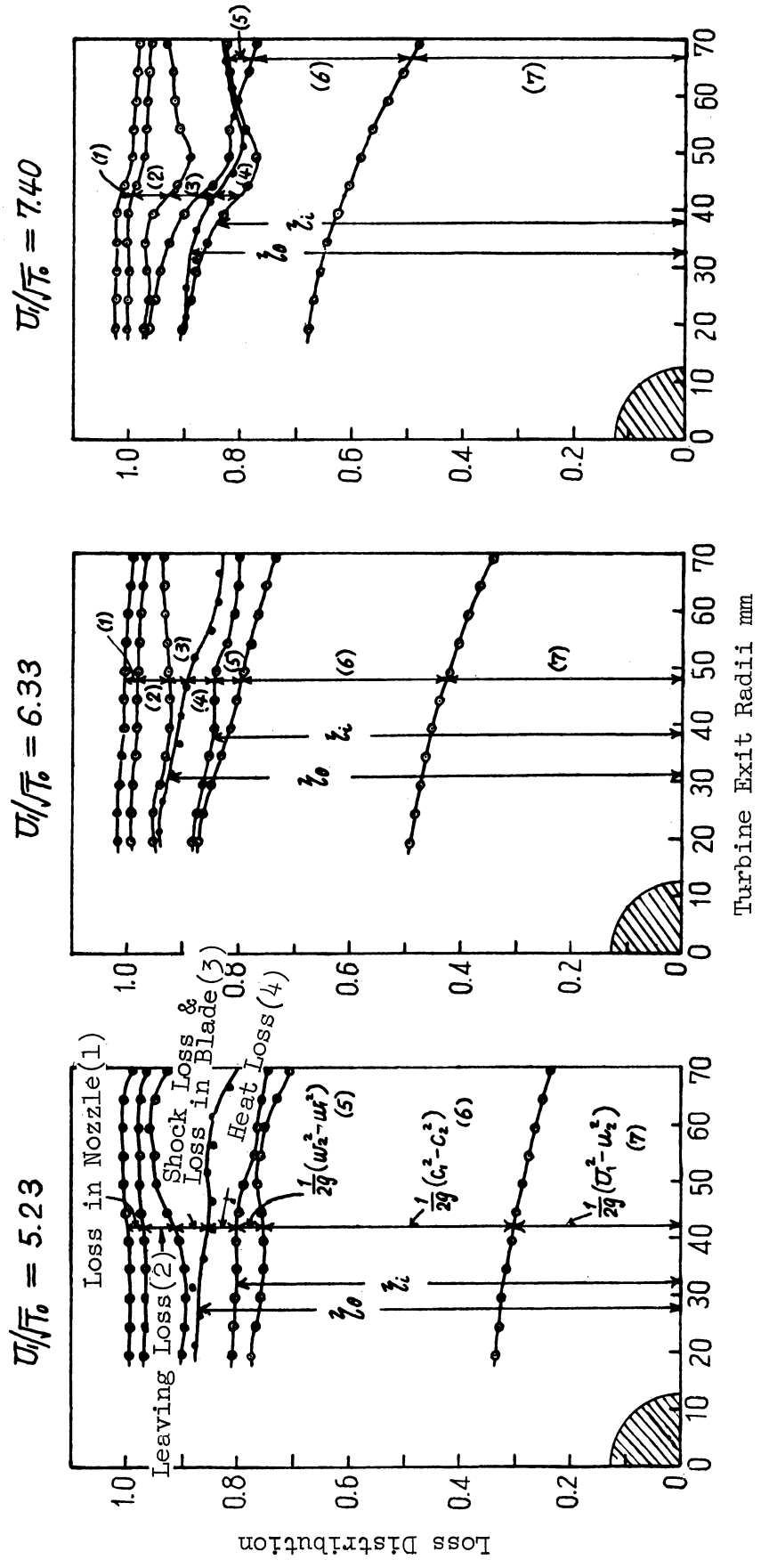

Figure 5.30 Distribution of Losses (No. 1 Test Turbine)

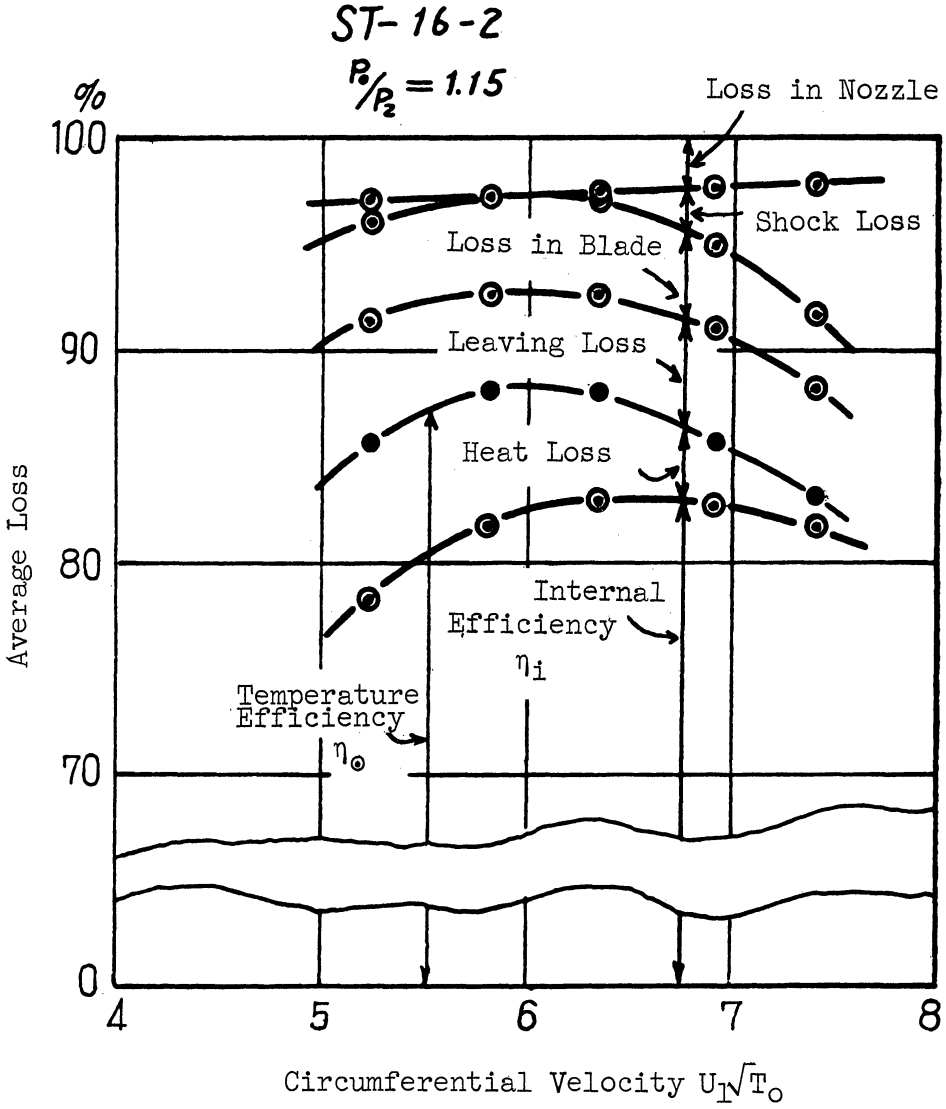

Figure 5.31 Ratio of Mean Loss (No.1 Test Turbine)

Since both E_b and w_2 are already determined in the above formula, ψ_2 can be calculated. The velocity coefficient in the blade is shown in Figure 5.32. Figure 5.33 shows the blade velocity coefficient of the test turbine No. 2 obtained by the same procedure. Little difference between the velocity coefficient near the center of the exit and that near the exit outside will be noticed, in spite of a great difference in the blade loss (that is, the ratio of the blade loss and the total enthalpy). The central part of the exit passage is slightly better than either the center or the outside of the exit. The increase of blade loss near the outside of the exit is therefore due to the increase in the relative velocity, w_2.

Figure 5.34 shows the average velocity coefficient, ψ_{2m}, with regard to the total gas flow, obtained by multiplying the velocity coefficients at the turbine exit radii by the gas flow distribution ratio at the corresponding exit radii. It will be noted from the figure that the blade-velocity coefficient of a radial turbine of this type is about 0.77 0.79, which is rather poor as compared with the axial-turbine, blade-velocity coefficient of 0.90 0.93. The following reason can be pointed out to explain the high efficiency reached by a radial turbine in spite of its poor blade-velocity coefficient. Since $U_1 = u_2$ in an axial turbine, the second possibility (the second row) of the second half (the right-hand side) of (4.14.2) equals zero. On the other hand, a radial turbine has a smaller value of u_2 than that of U_1, and consequently a considerable value is given to the same possibility of (2.14.2). (See Figure 5.30.) When the equal enthalpy is incurred in the blades of both the axial and radial turbines, the value of w_2 in the axial turbine proves accordingly to be greater than that of w_2 in the radial turbine. (Since the loss in the blade, E_b,

$$E_b = \left(\frac{1}{\psi_2^2} - 1 \right) \frac{w_2^2}{2g} \tag{5.16}$$

the radial turbine takes a smaller value of E_b than the axial turbine, mainly due to the smaller value of w_2 in the former, in spite of its poor velocity coefficient in the blade. Though the small loss in the blade is one of the characteristics of a radial turbine, more study and research should be required to improve its poor velocity coefficient which is in part due to its complex geometrical forms.

5.4.2. Slip in a Radial Turbine

It will be noted from Figures 5.18, 5.19 and 5.20 that the relative efflux angle of the blade outlet, β_2, differs considerably from the geometrical efflux angle of the exducer. The difference between the two is called the slip, the cause of which will be discussed below.

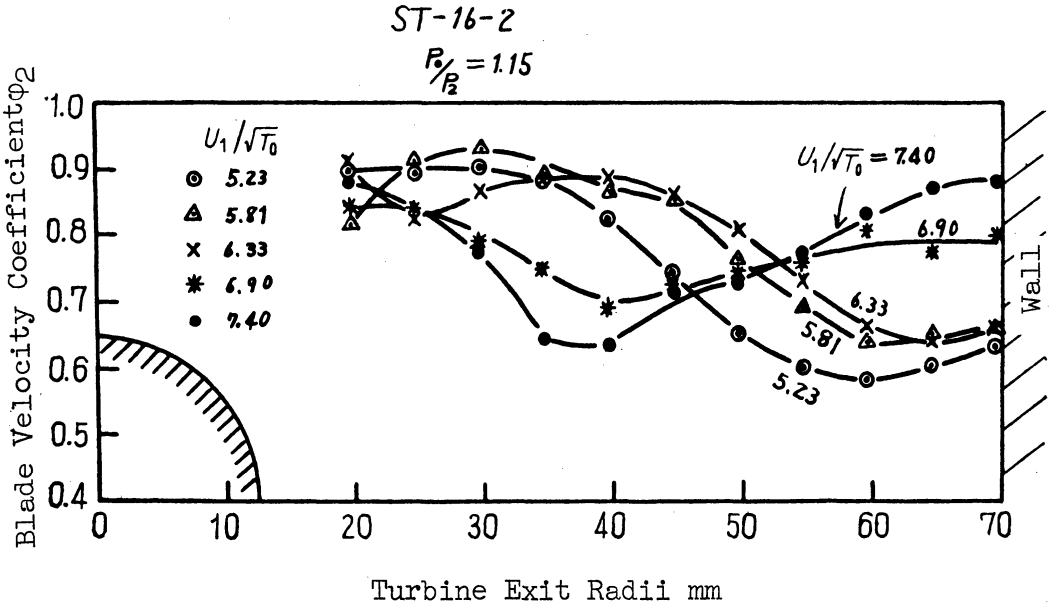

Figure 5.32 Blade Velocity Coefficient (No. 1 Test Turbine)

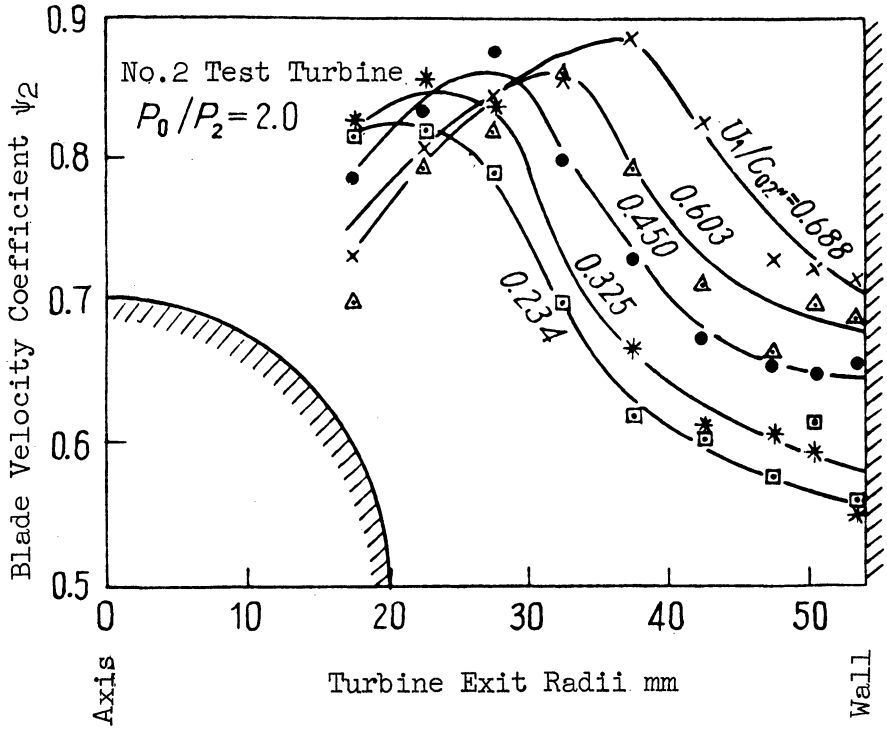

Figure 5.33 Blade Velocity Coefficient (No. 2 Test Turbine)

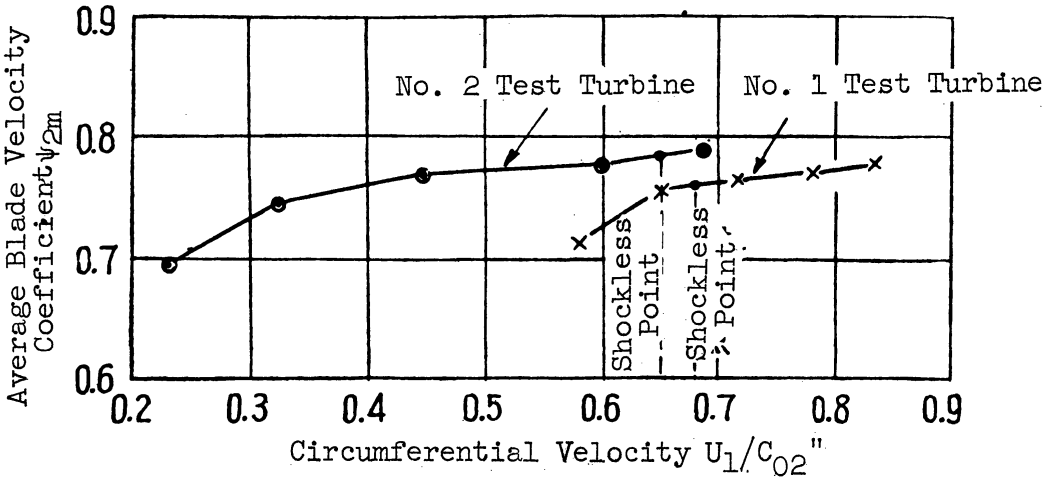

Figure 5.34 Average Blade Velocity Coefficient

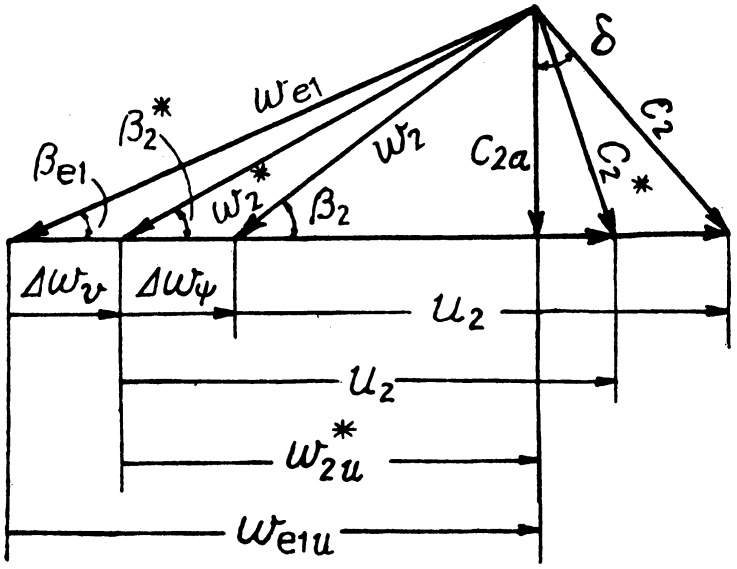

Figure 5.35 Slip Diagram

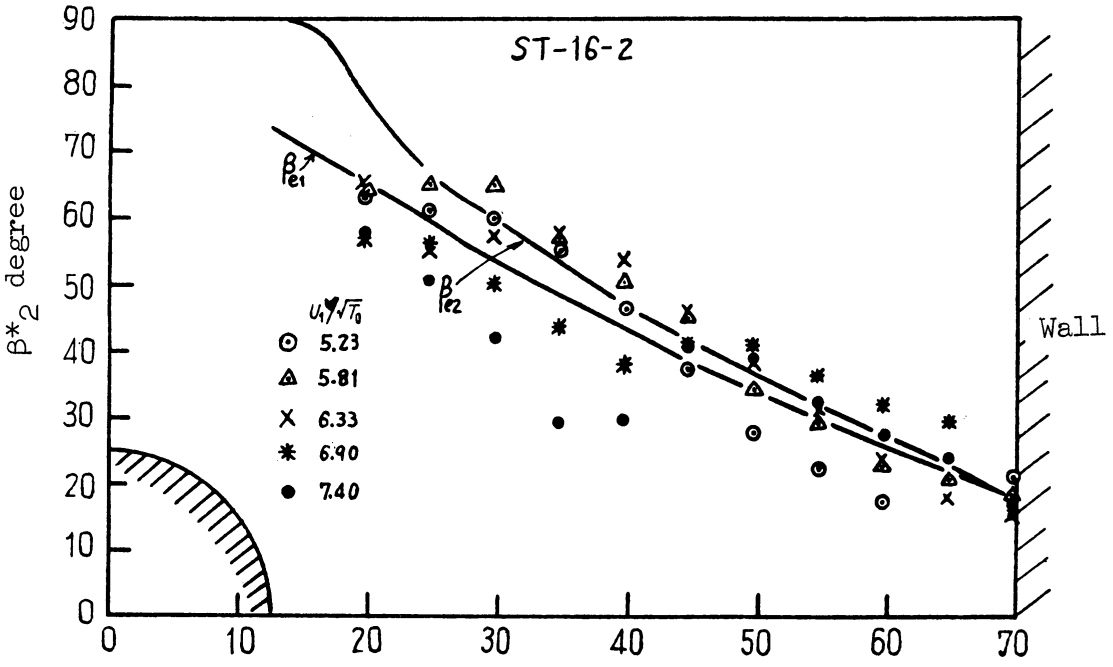

Figure 5.36

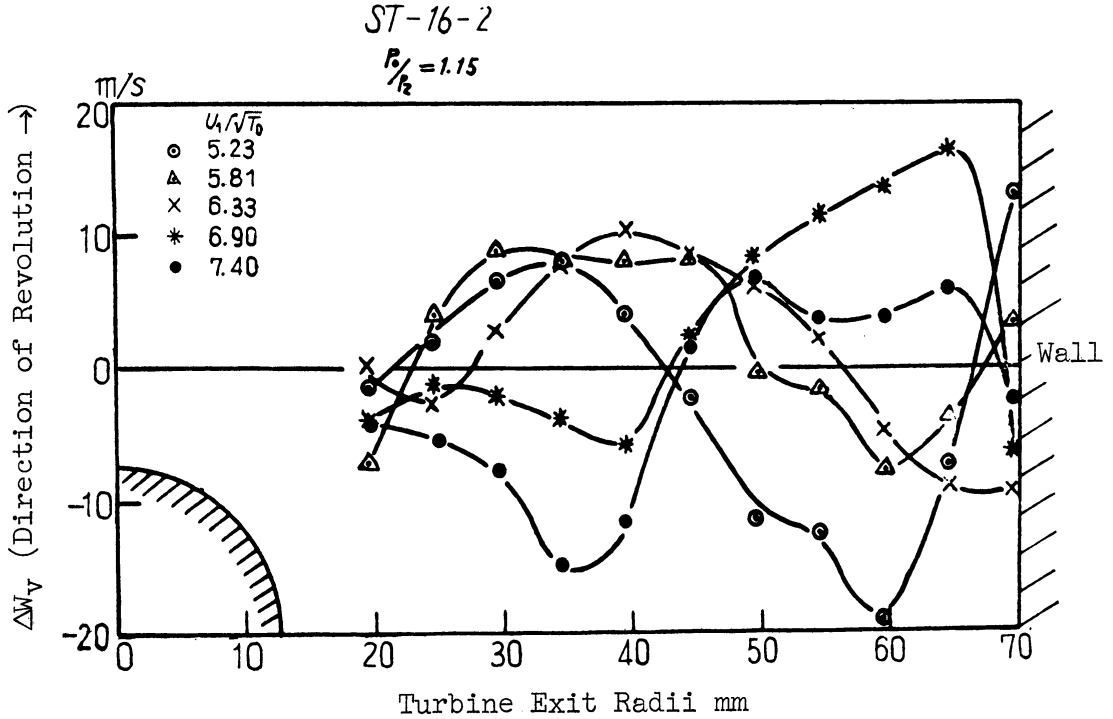

Figure 5.37

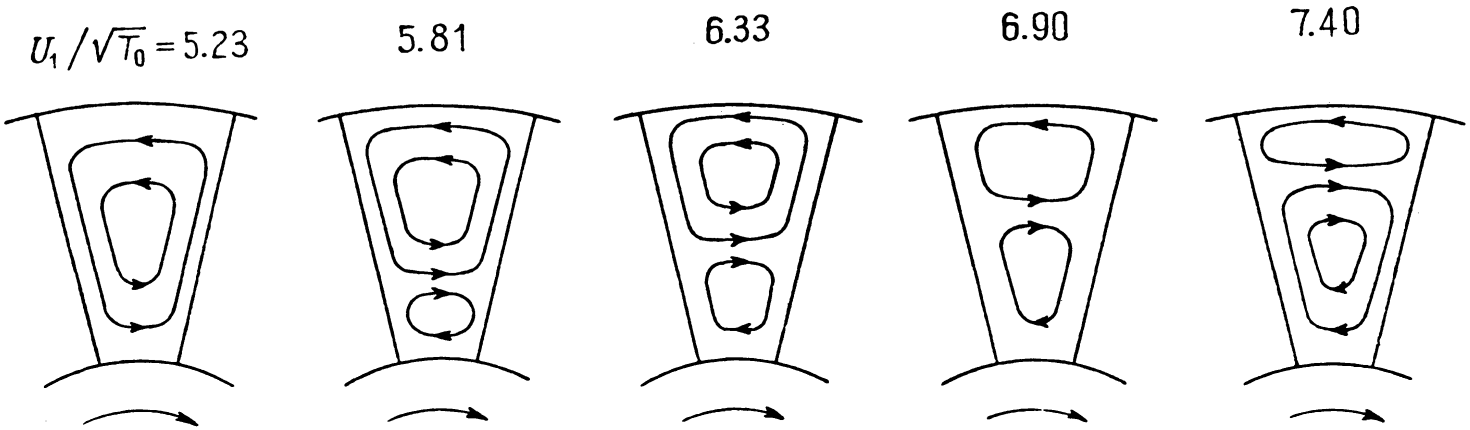

Figure 5.38 Spiral Flows

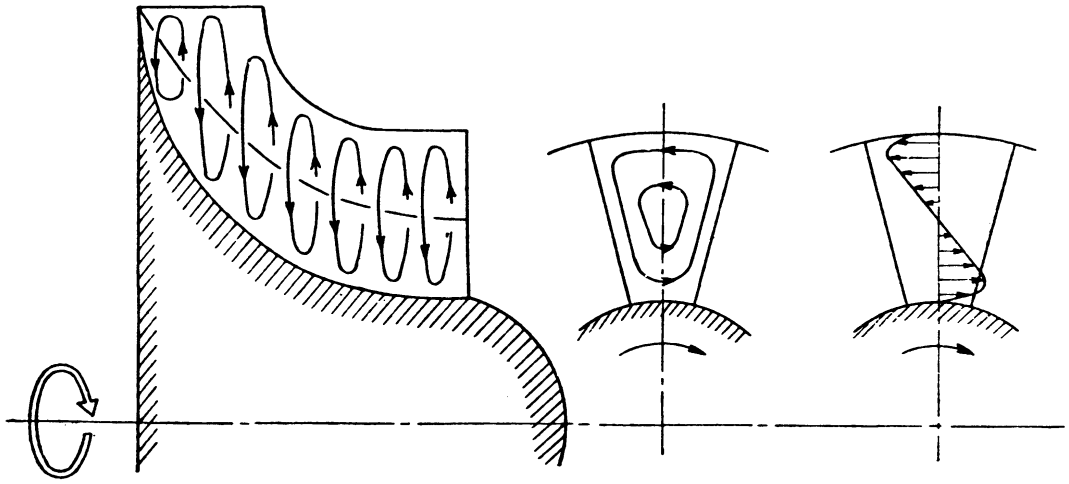

Figure 5.39 Spiral Flow Caused by Blade Rotation

(a) Slip caused by the losses in the blade.

Needless to say the direction of flow coincides with the geometrical direction of the flow in the exducer when the exducer has an indefinite number of pitch, and no loss is incurred and no revolution is made. Since no actual exducer can satisfy such hypothetical conditions, the difference in the efflux angle of exducer must be taken into account.

A comparison between a motionless, two-dimensional pitch turbine with losses, and the same type of turbine without losses will show that the flow becomes more turbulent when the losses are greater. This tendency is attributed to the losses in the blade, E_b. Assuming, in Figure 5.35, that a rotation is incurred in the efflux angle, β_{e1}, by the slip, Δw_v, caused by some reason, as well as by the slip, Δw_ψ, which is due to the loss in the blade, the flow is regarded to be moving at the actual efflux angle of β_2 and at the velocity of w_2. Under such assumptions, the following formula will be established. (β_2^* represents the efflux angle when the slip is caused by reasons other than the losses in the blade.)

$$\left.\begin{aligned} w_2^* &= \frac{w_2}{\psi_2} \\ \sin\beta_2^* &= \psi_2 \sin\beta_2 \end{aligned}\right\} \qquad (5.17)$$

Figure 5.36 shows the value of β_2^* obtained from the above formula in which w_2, β_2, and ψ_2 are already known. It will be noted from the figure that a considerable difference still exists, even though the flow moves generally in the direction of β_{e1}. Since this difference is due to the slip, Δw_v, caused by reasons other than the losses in the blade, Δw_v takes the form as shown in Figure 5.37, the spiral flow of which is shown in Figure 5.38.

(b) Slip caused by the spiral flow of the blade revolution.

As shown in Figure 5.39, the rotatory movement of the blades generates spiral flow in the blade vanes as well as in the exducer passage. The spiral flow moves in a direction opposite to that of the blade revolution, and at the same angular velocity as that of the blade. Consequently, a slip velocity as shown in the extreme right of the figure, can be observed at the exducer outlet. Near the outside exit and the boss, the velocity of spiral flow decreases because of the viscosity friction. In other words, the slope occurs in the direction of revolution near the outside exit. The flow is therefore found to be rotatory (violent) near the boss, and smooth (circular) around the outside exit. The effect

is quite evident when $U_1/\sqrt{T_0} = 5.23, 5.81$, especially when the ST-20-2' nozzle is used. (See Figure 5.19.) The correlation between β_2^* and β_{e1} of the test turbine No. 2 is shown in Figure 5.40, in which case the spiral flow around the boss is almost reduced, while it inclines at about 10° in the opposite direction of the circumferential velocity. The slip velocity, caused by the spiral flow of the blade revolution increases as the geometrical dimensions of the fan-shaped part of the exducer outlet, and the number of revolutions increase.

(c) Slip caused by the curvature of exducer.

The flow moves at the velocity of w_2 and at a curvature of about 90° outside the exducer outlet. As shown in Figure 5.41, a pair of spiral flows will be observed because of this curvature. The spiral flow near the outside moves in the same direction as that caused by the blade revolution, and in the opposite direction to that of the revolution, whereas the spiral flow toward the inside is in the same direction as that of the blade revolution. The spiral flow moving near the inside in the direction of the revolution in Figure 5.38 can also be ascribed to this curvature of the exducer. This inside spiral flow has the effect of reducing the spiral flow caused by the blade revolution, which accounts for the reduction of spiral flow around the boss in the test turbine No. 2. The force of the spiral flow caused by the exducer curvature increases as the angle of the curvature (near the outside exit) and the velocity of flow increases. Therefore, according to the designing procedure presented here, the effect of slip due to the curvature of exducer can be minimized by distributing the wind velocity at the exit in such a way that a greater quantity of flow moves towards the exit center and a smaller quantity of flow towards the outside.

(d) Effect of the number of vanes.

As in the static two-dimensional system, the actual efflux angle becomes sharper with a small number of vanes (that is, with a greater pitch) than the geometrical shape of the vanes. The effect is the same as that of the slip caused by the losses in the blade.

(e) Effect of the blade curvature.

The flow moves in the radial direction into the blade, and in the axial direction at an angle of 90°. Consequently a pair of spiral flow, as shown in Figure 5.42, is seen at the exducer outlet, though this has little effect on the slip. A designing procedure with regard to the curvature of the vanes at the exducer outlet is proposed below: (Figure 5.43.)

(i) The distribution of the axial flow velocity at the radii of exducer outlet will be determined as described in Chapter 2.

(ii) Velocity diagrams will be drawn with reference to this axial flow velocity and the circumferential velocity at each point, in order to determine the actual relative efflux velocity, w_2, and its direction, β_2.

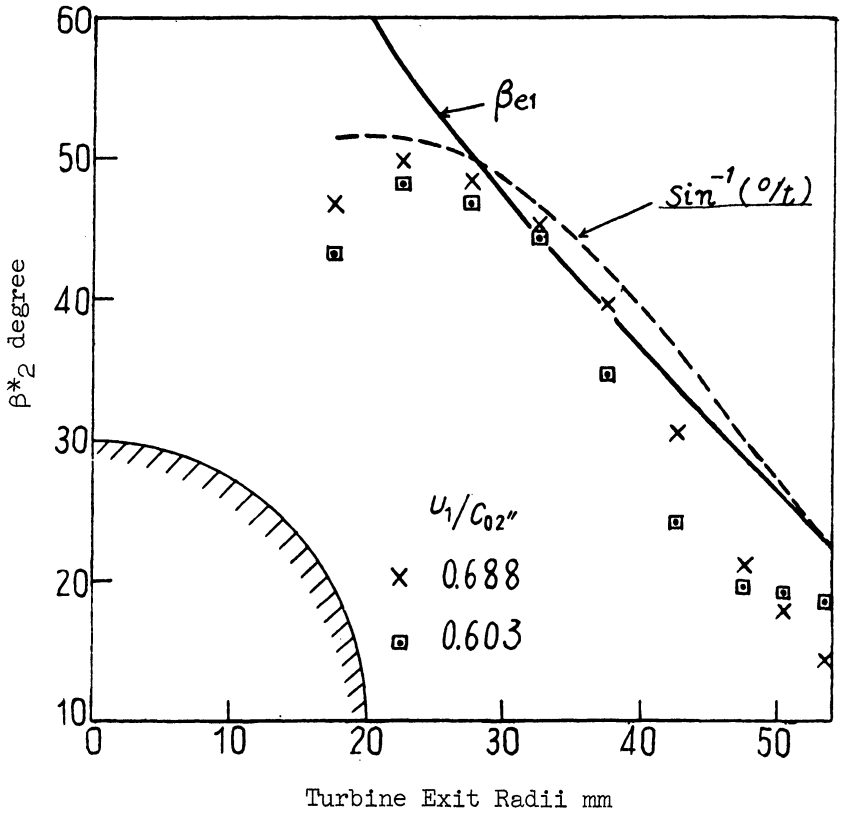

Figure 5.40

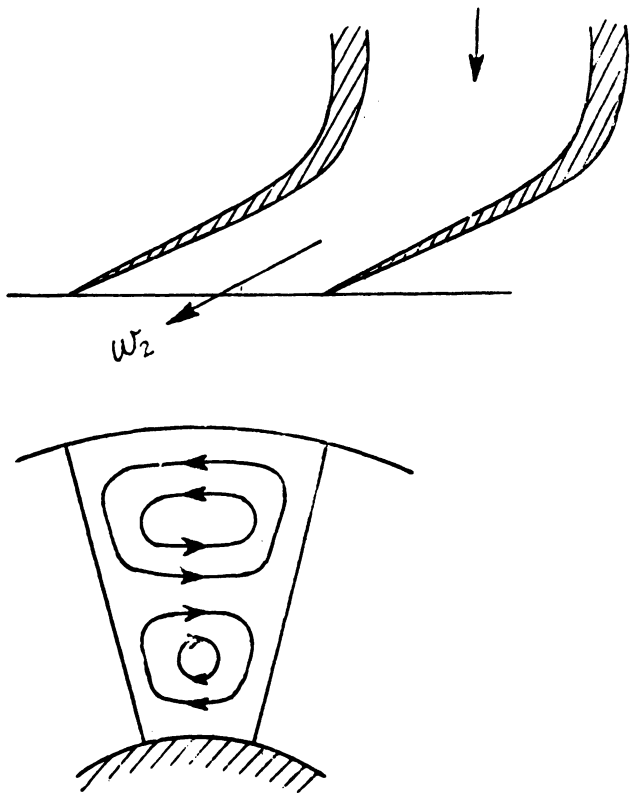

Figure 5.41 Spiral Flow caused by Exducer Curvature

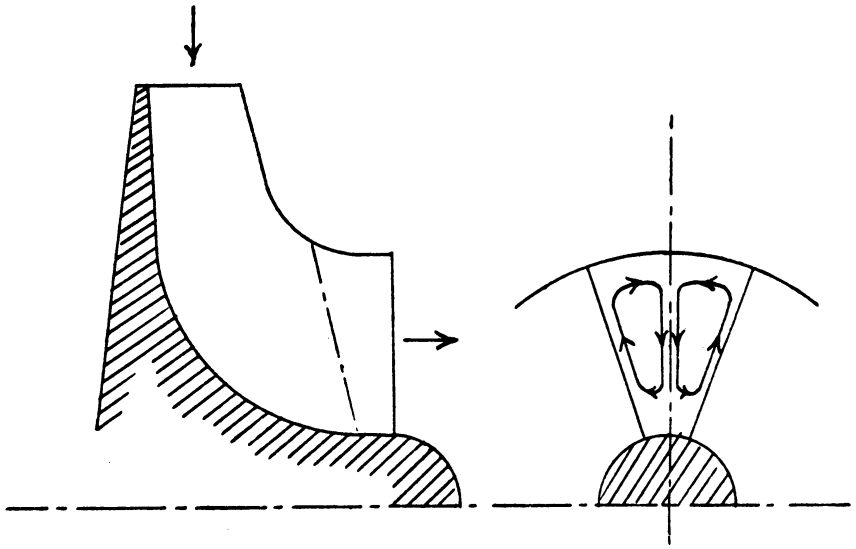

Figure 5.42 Spiral Flow Caused by Blade Curvature

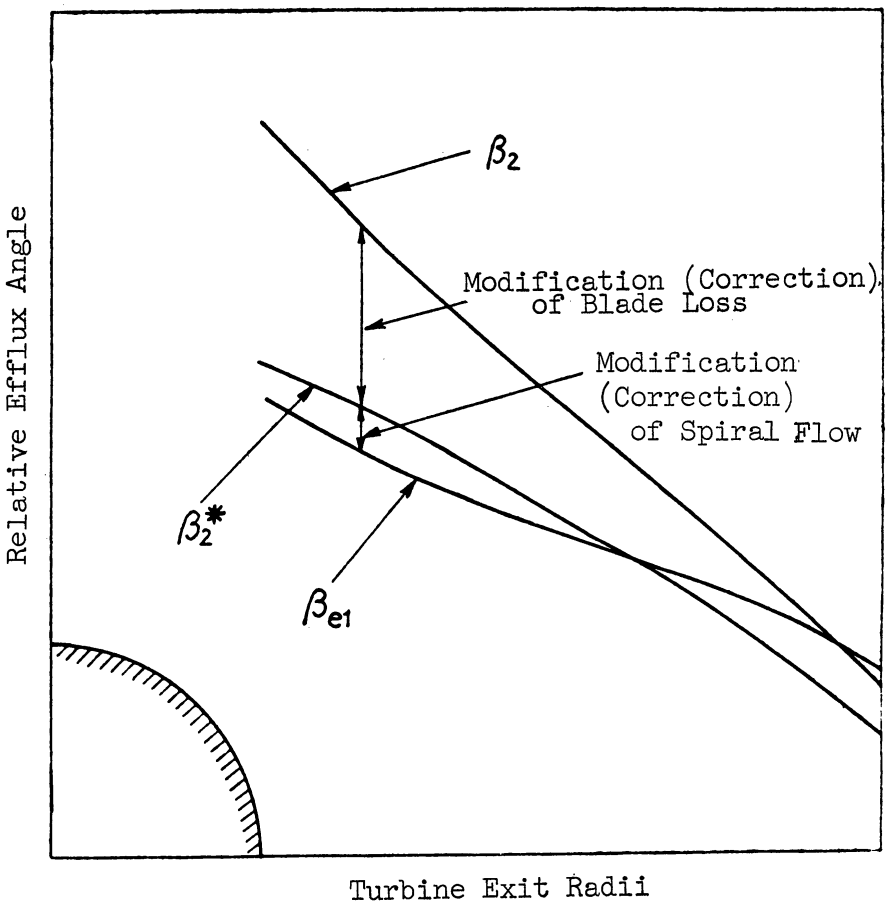

Figure 5.43 Method to Determine Blade Efflux Angle

(iii) β_2^* and w_2^* modifying the slip caused by the losses in blade, will be determined by using the velocity coefficient of the blade, ψ_2.

(iv) The effect of spiral flows caused by the rotatory motion of the blade will be considered with regards to β_2^* thus obtained. Towards the outside, β_{e1} will be made greater than β_2^*, and smaller than β_2^* towards the center. Although in the latter case, the difference between β_{e1} and β_2^* is very slight as the slip caused by the exducer curvature almost eliminates the effect and approximates the value of β_{e1} to that of β_2^*.

5.5. Performance of the Test Turbines

5.5.1. Performance of the Test Turbine No. 1

The No. 1 test turbine is equipped with an exducer designed without consideration for the effects of the slip in the blade. It uses the B-type exducer in which the centrifugal force and the radial pressure gradient are balanced with each other. Two types of nozzles, ST-16-2, and ST-20-2', are also used in the No. 1 test turbine.

The average temperature efficiency, obtained by the procedures described in Section 3 of this chapter, is shown in Figure 5.44 and 5.45, the former using the ST-16-2 nozzle and the latter the ST-20-2' nozzle. The double circles ◎ in Figure 5.44 indicate the average temperature efficiency which is obtained in the loss measurement test from the gas flow and the temperature efficiency distribution at the turbine outlet, and which is slightly lower than the average temperature efficiency that is experimentally measured.

Figures 5.46 and 5.47 show the average internal efficiency obtained by adding the horse power in friction losses of the turbine shaft bearing, of the deceleration gear and of the deceleration equipment shaft bearing to the horse power absorbed by the dynamometer. The double circles ◎ in Figure 5.46 indicate the average internal efficiency which is obtained from the velocity diagrams in the loss measuring test, and which is 2 3% lower than the internal efficiency obtained by adding the horse power in friction losses to the horse power absorbed by the dynamometer. Judging from the results stated above, we can regard the internal efficiency of the No. 1 test turbine as being 84 86%. The gas flow is shown in Figures 5.48 and 5.49.

5.5.2. Performance of the No. 2 Test Turbine

The No. 2 test turbine is equipped with an exducer designed with special consideration for the slip in the blade, made clear by the experiment with the No. 2 test turbine. The designing procedures in the No. 2 test turbine, such as described in Chapter 4, are adopted in an effort to

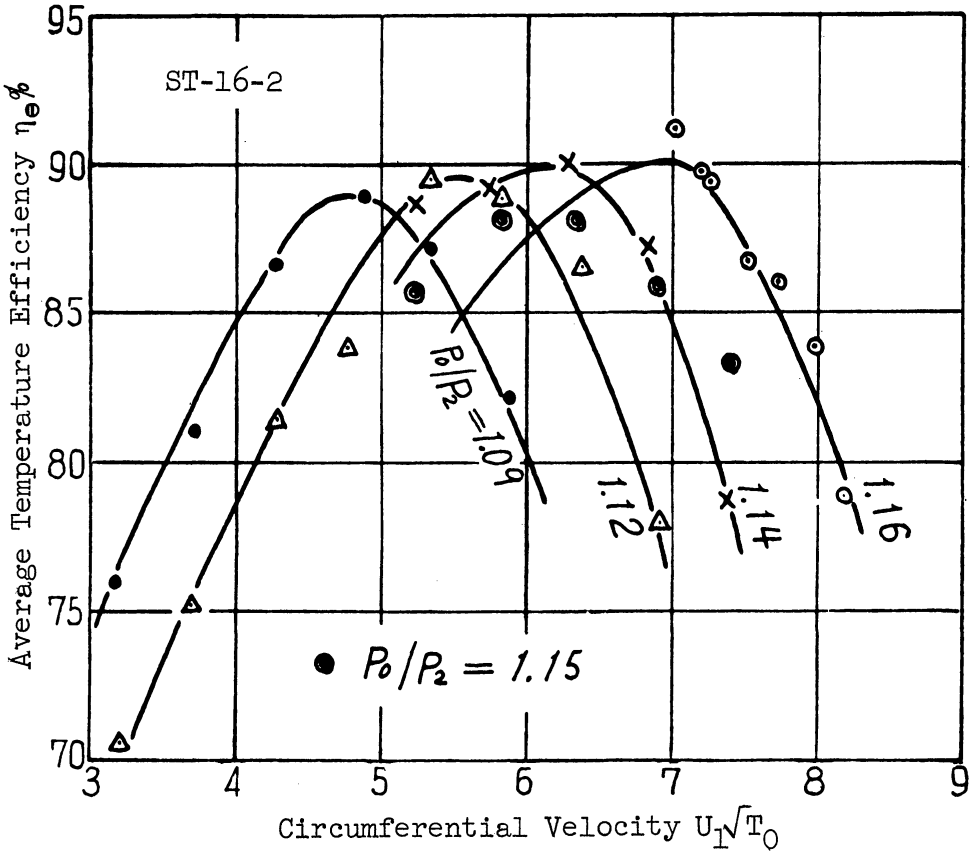

Figure 5.44 Average Temperature Efficiency
(No. 1 Test Turbine)

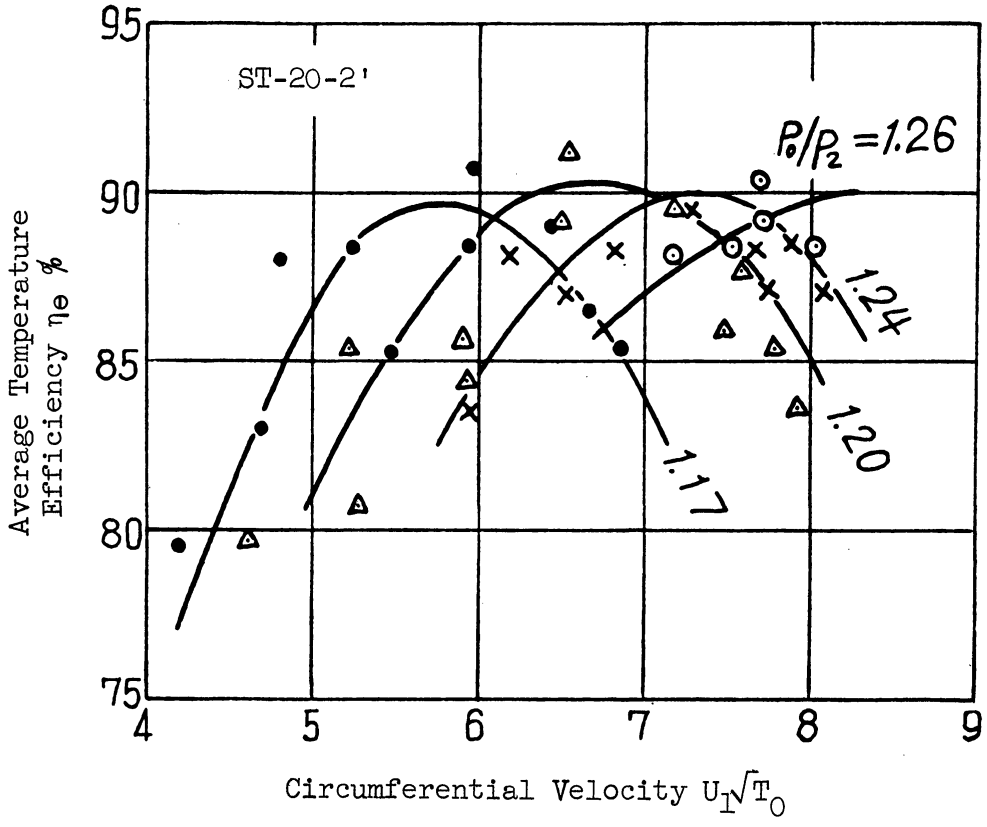

Figure 5.45 Average Temperature Efficiency
(No. 1 Test Turbine)

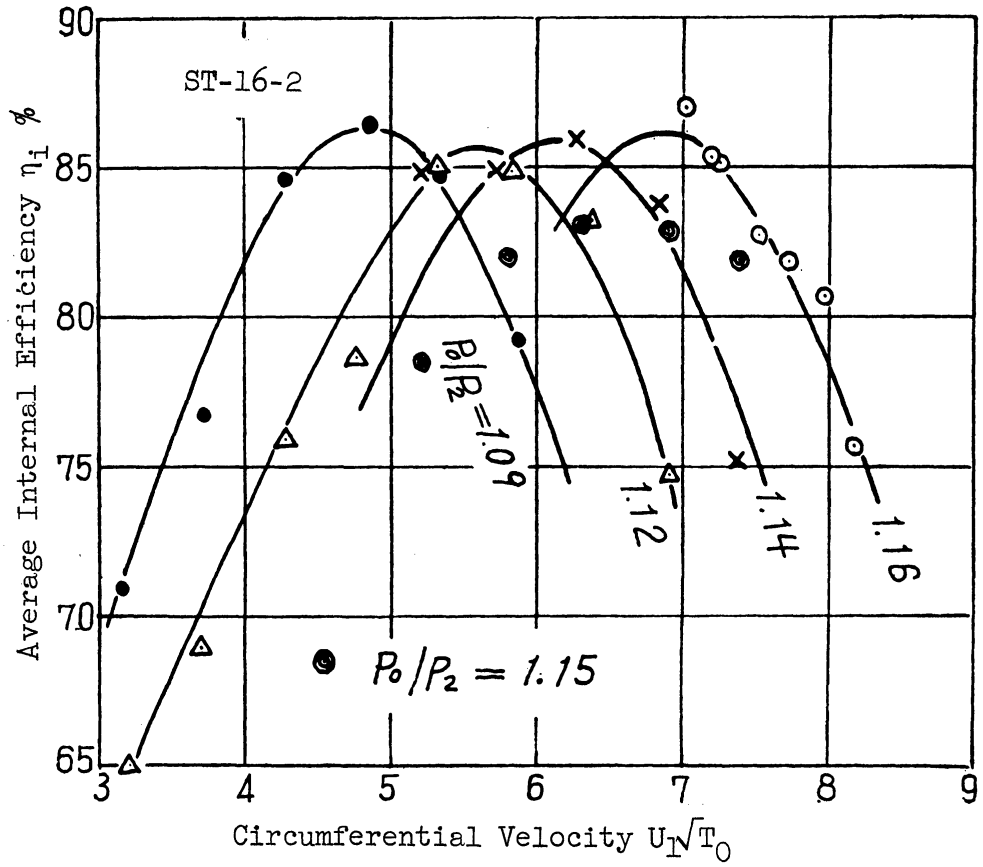

Figure 5.46 Average Internal Efficiency(No. 1 Test Turbine)

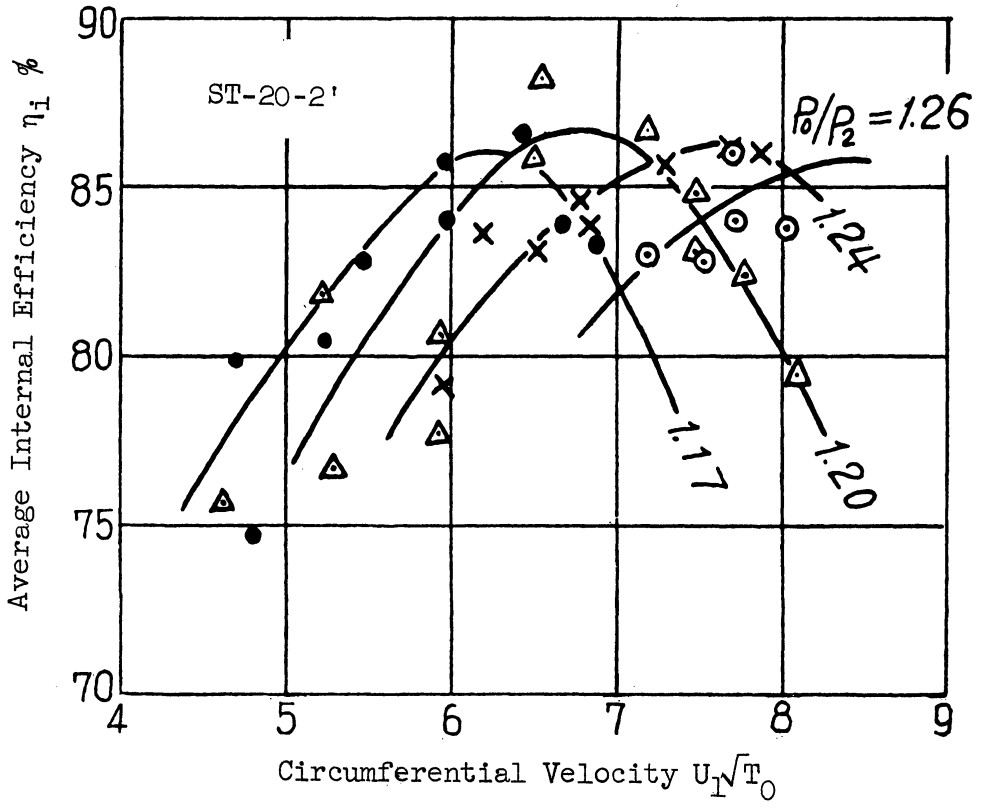

Figure 5.47 Average Internal Efficiency (No. 1 Test Turbine)

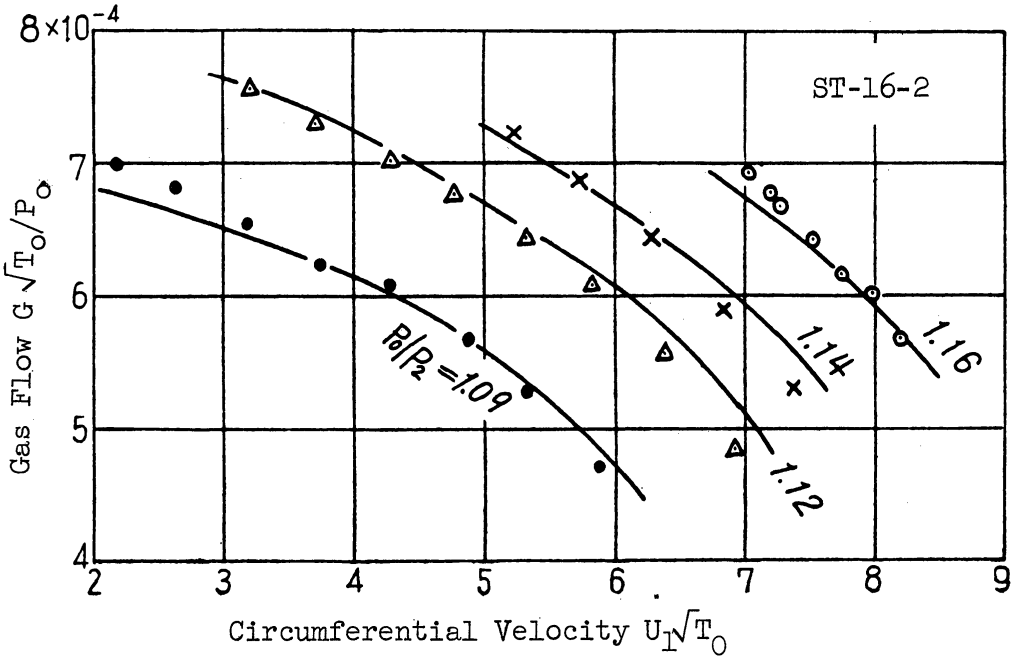

Figure 5.48 Gas Flow (No. 1 Test Turbine)

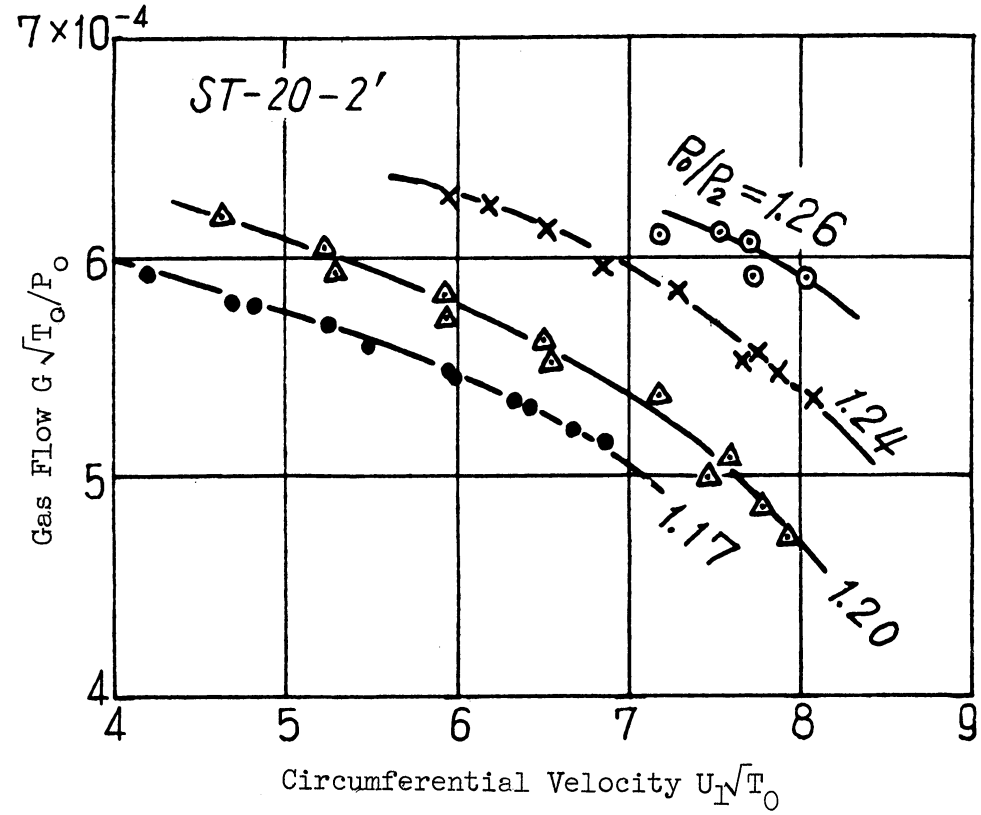

Figure 5.49 Gas Flow (No. 1 Test Turbine)

balance the centrifugal force in the exducer with the radial pressure gradient. It uses both No. 1 and No. 2 nozzles, both of which are of straight type, and have the mean efflux angle of $15^{\circ}40'$ and $9^{\circ}30'$ respectively.

The results of the experiment, described in Section 3 of this chapter, are described below. Figure 5.50 shows the net output power measured by the dynamometer. By adding to the net output power the losses in shaft bearing, disk friction and deceleration equipment, the output power generated in the blade can be obtained. The figure shows the results of both cases in which the expansion ratios of 2.0 and 1.7 and the turbine inlet temperature of t_0 are used. About 110 horse power is produced when adopting the expansion ratio of 2.0, the gas temperature of 610°C, and the revolution number of 35,000 rpm.

Figure 5.51 shows the gas flow in non-dimensional quantities, in which p_0 and T_0 are the units of kg/m^2 and °k respectively. $c_{02}"$ indicates the theoretical velocity of jet at the time of the equal entropy expansion from the turbine inlet conditions to the turbine outlet pressure. When the expansion ratio is fixed it appears on the single curved line regardless of gas temperature at the turbine inlet.

Figure 5.52 shows the mean efflux angle of the nozzle, α, obtained, as in the case of the No. 1 test turbine, from the gas flow and the reaction. Though the mean nozzle efflux angle is generally fixed, regardless of the revolution number and the expansion ratio, it has a slight tendency to increase with the decrease of the revolution number (with the decrease of reaction). This can be explained by the fact that the rise in the nozzle velocity coefficient is caused by the increase in the used Reynolds number when the number of revolutions and the reaction are reduced.

Figure 5.53 shows the reaction which forms a single curved line with regard to $U_1/c_{02}"$ regardless of the expansion ratio and the gas temperature. The No. 1 nozzles indicate the reaction of 53% when $U_1/c_{02}" = 0.65$ and the No. 2 nozzles indicate the reaction of 47% when $U_1/c_{02}" = 0.70$. The gas flow moves, therefore, directly towards the blade without shock or collision.

The velocity distribution at the turbine outlet radii is shown below. Figure 5.55 indicates the angles formed by the axial line and the absolute efflux velocity shown in Figure 5.56. The No. 1 nozzle is used in this case, and no shock or collision is found at the blade inlet when $U_1/c_{02}" = 0.65$. Figure 5.55 also shows the absolute efflux velocity almost in parallel with the axial line, within the range of $+10^{\circ}$ -5°. The velocity distribution in this case coincides fairly well with the distribution designed beforehand (see Figure 5.56) which indicates that the procedures of correcting the slip in the exducer, such as described in the preceding section, are adequate.

Figure 5.57 shows the net adiabatic efficiency, which is the ratio between the horse power measured by the electric dynamometer and the enthalpy[26] at the time of the equal entropy expansion from the turbine

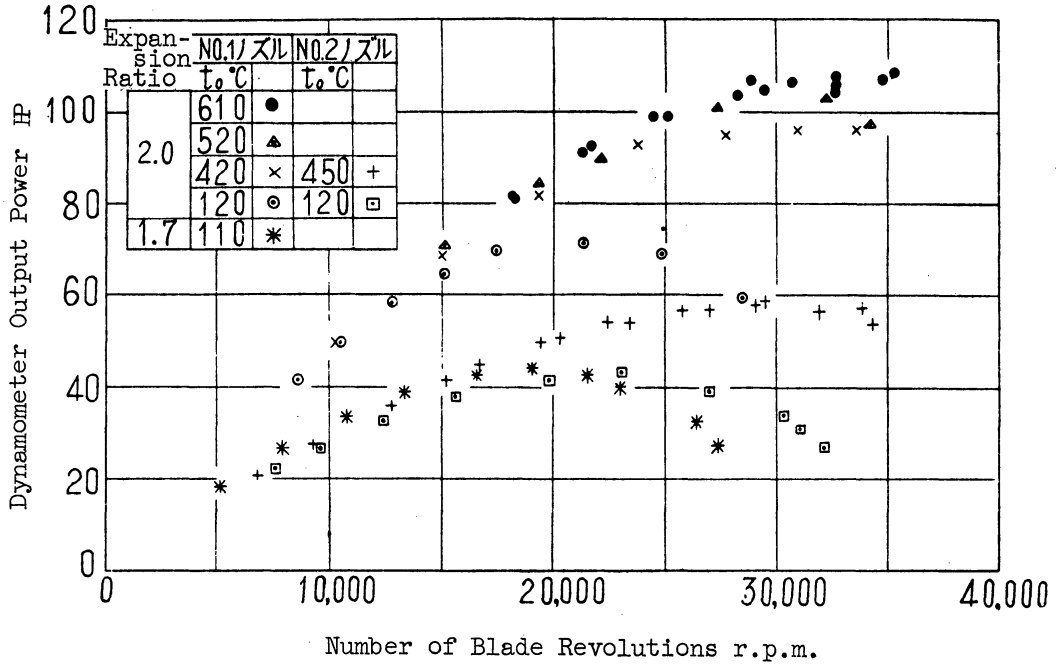

Figure 5.50 Net Output Power (No. 2 Test Turbine)

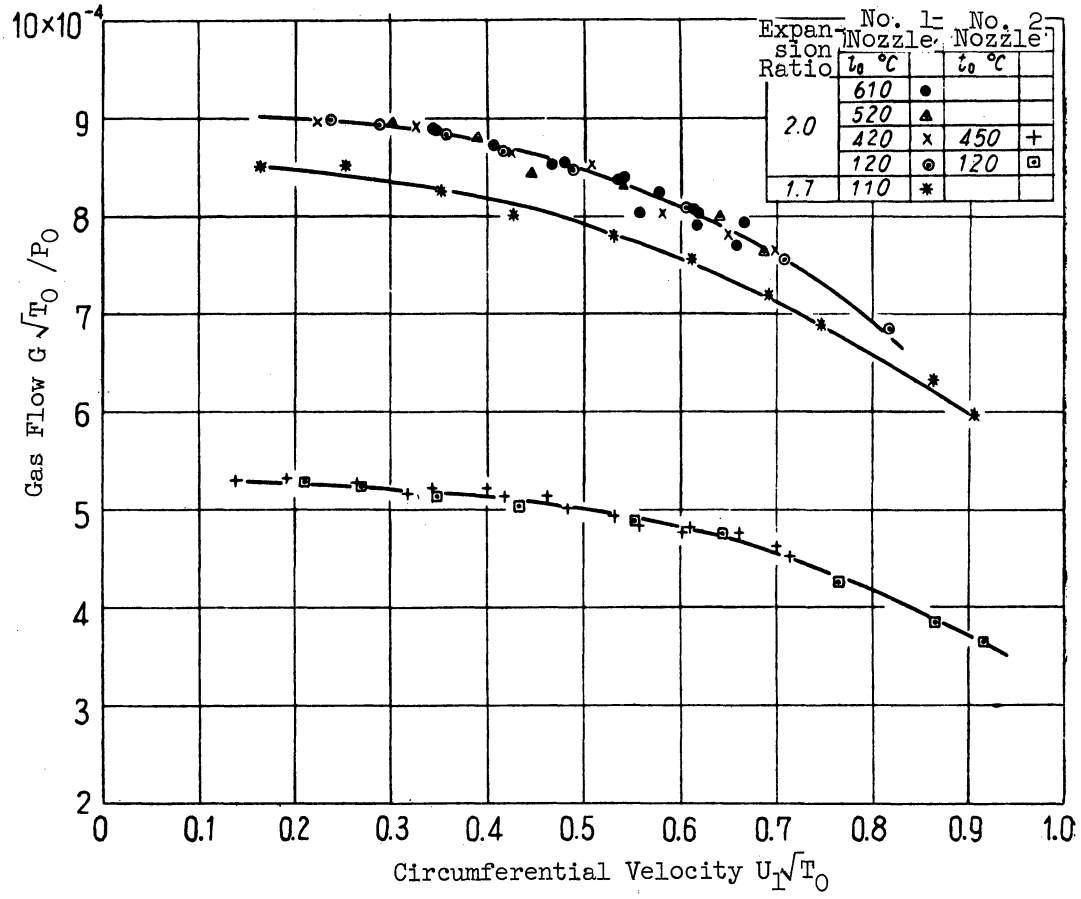

Figure 5.51 Gas Flow (No. 2 Test Turbine)

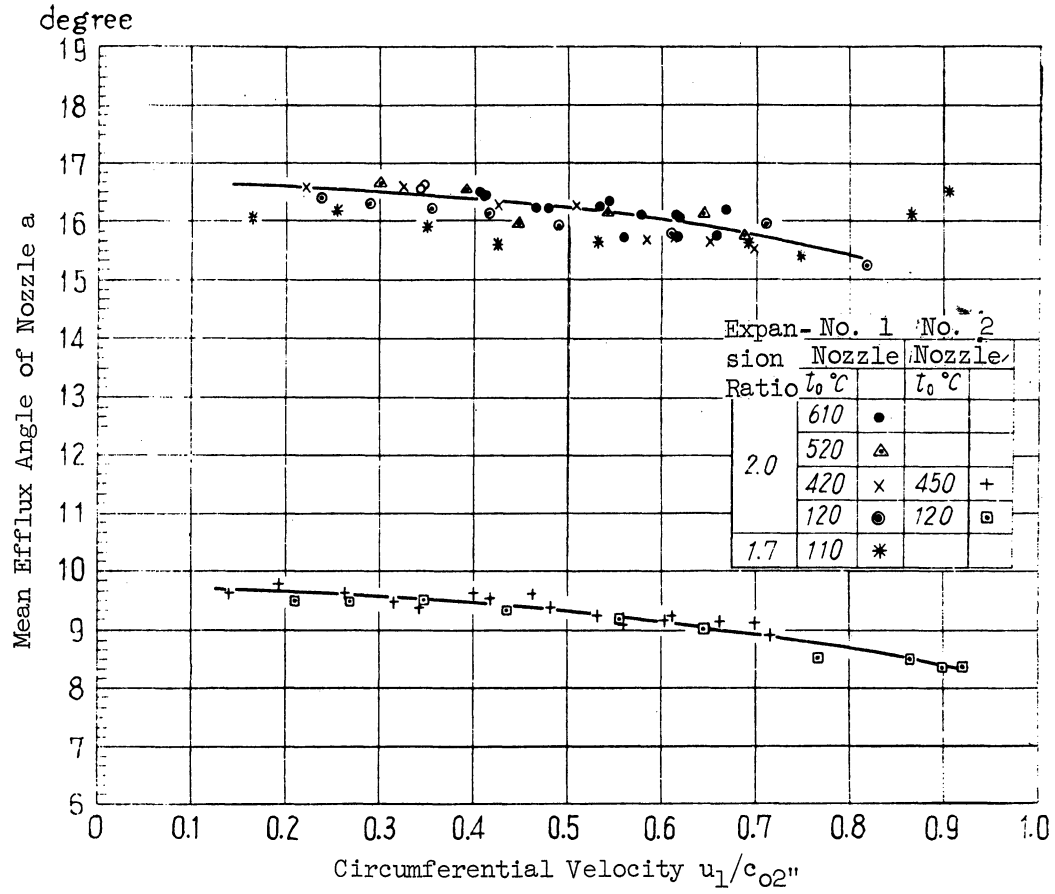

Figure 5.52 Mean Efflux Angle of Nozzle (No. 2 Test Turbine)

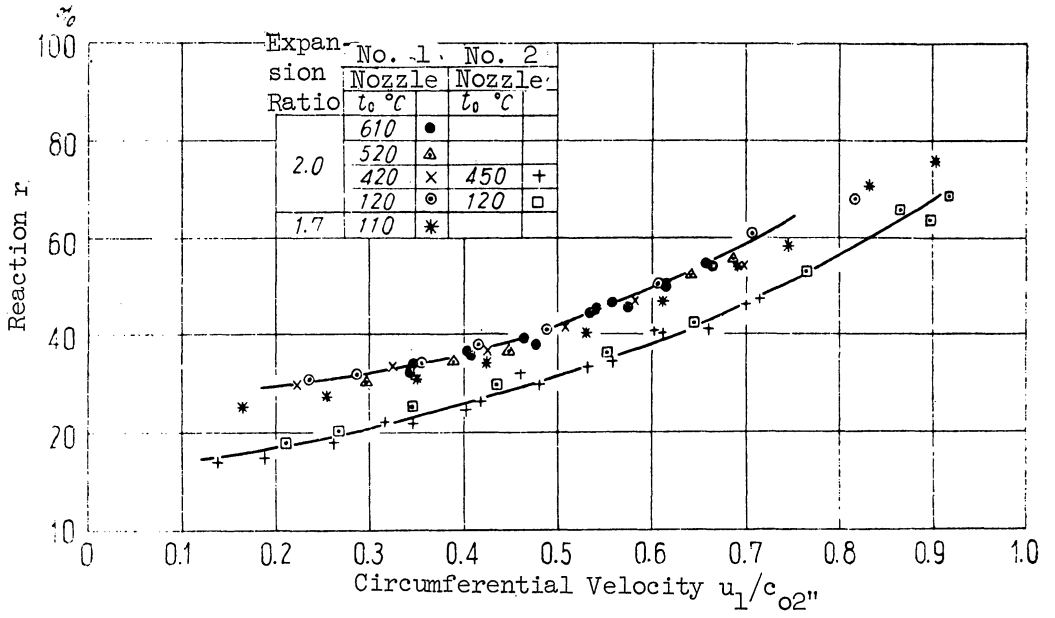

Figure 5.53 Reaction (No. 2 Test Turbine)

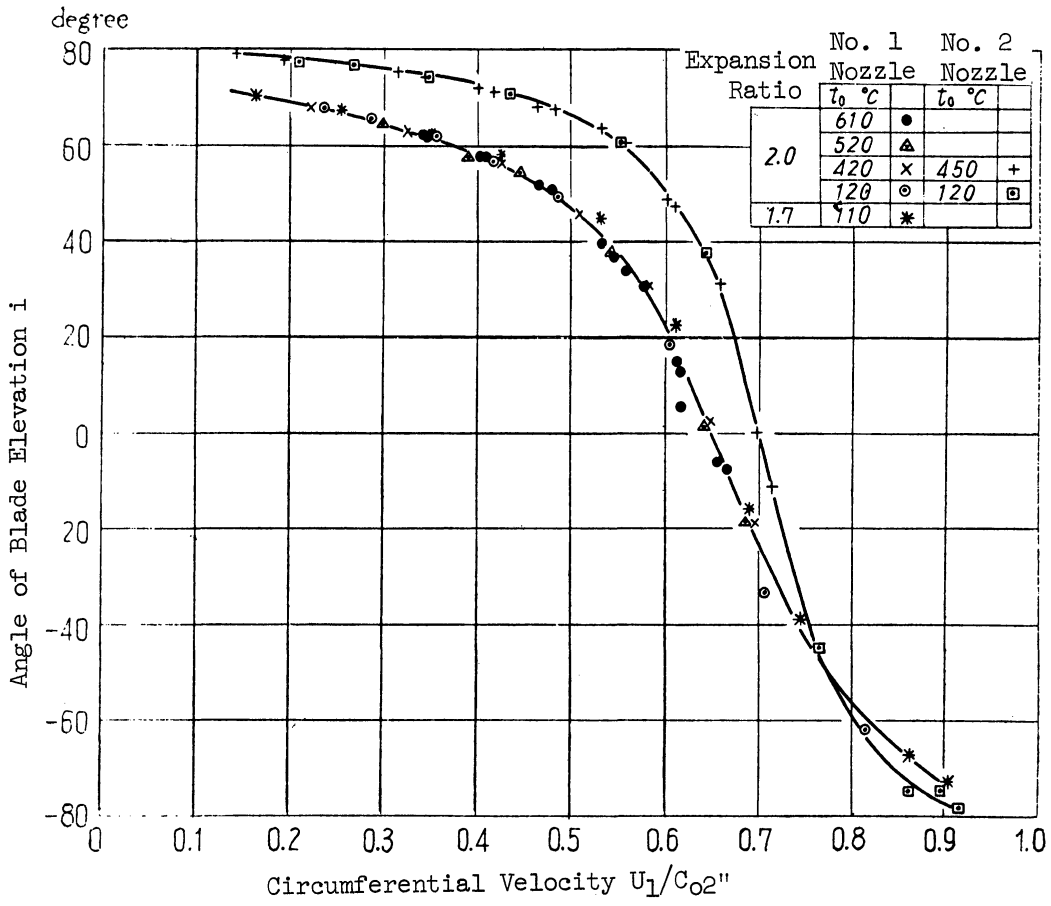

Figure 5.54 Angle of Blade Inlet Elevation (No. 2 Test Turbine)

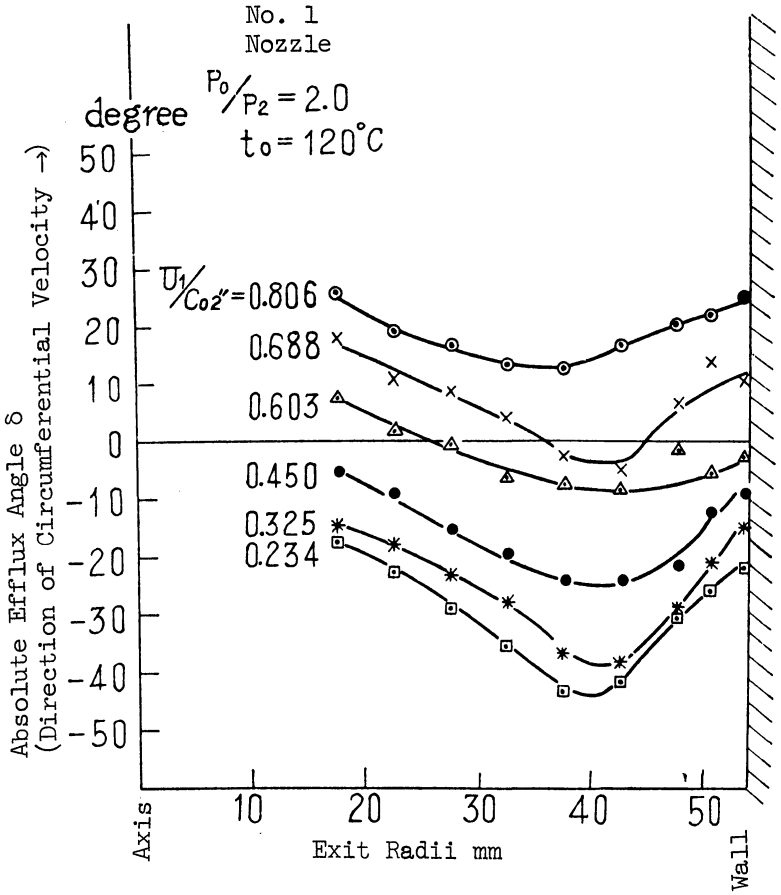

Figure 5.55 Absolute Efflux Angle

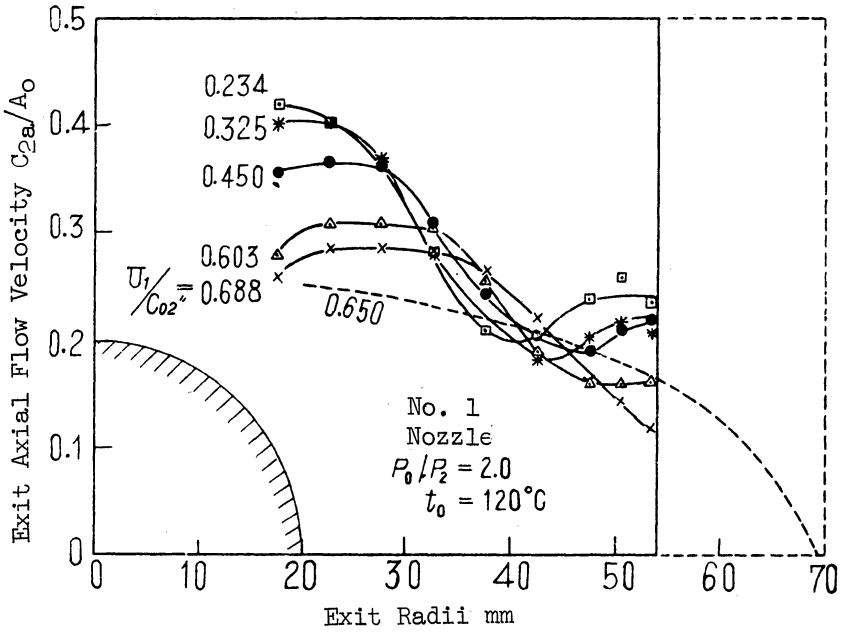

Figure 5.56 Absolute Efflux Velocity

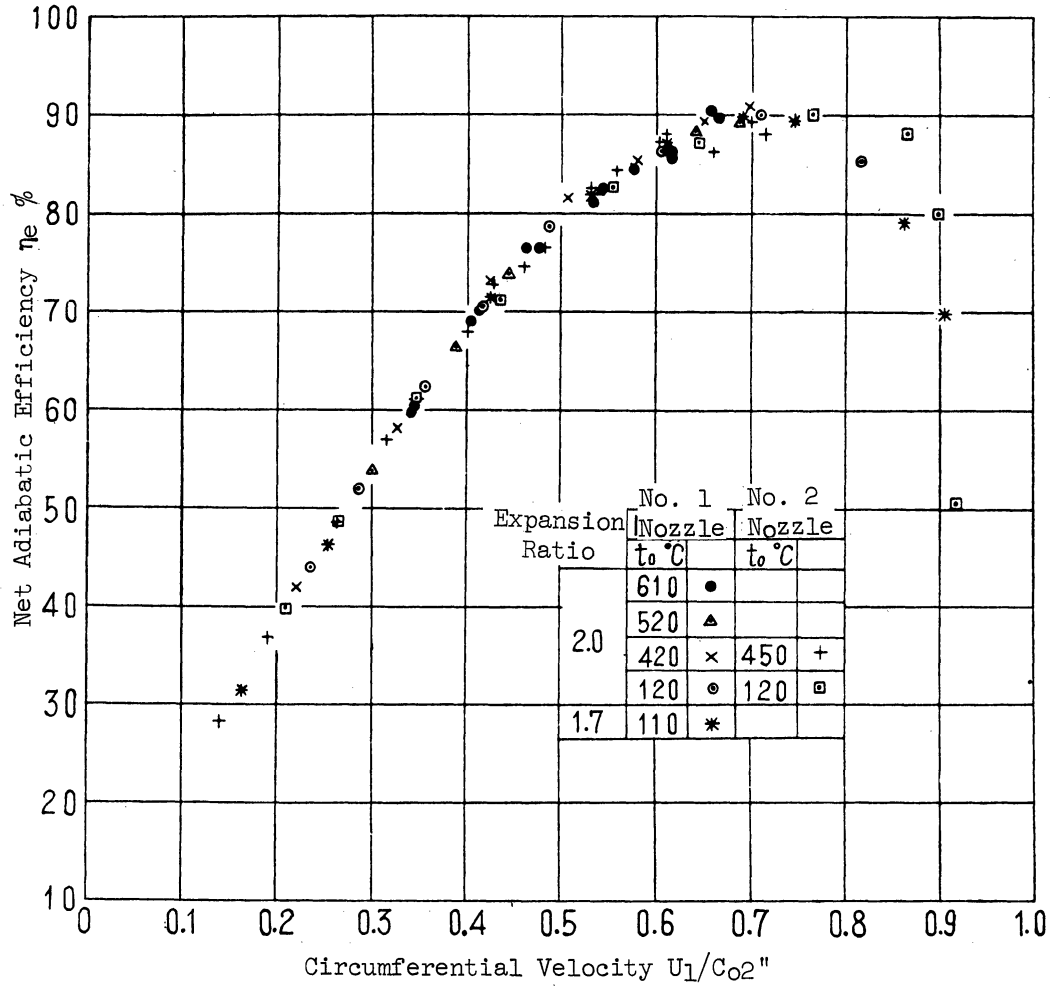

Figure 5.57 Net Adiabatic Efficency (No. 2 Test Turbine)

inlet conditions to the outlet pressure. The maximum efficiency of 90% is obtained both by the No. 1 nozzle with $U_1/c_{02}'' = 0.70$, and by the No. 2 nozzle with $U_1/c_{02}'' = 0.75$, which is far superior to the efficiency (ranging between 78 ~ 86%) of this type of gas turbine used in many countries.

The results of the No. 2 test turbine thus described confirm the appropriateness of the theory of radial turbine designing procedures and its capacity to reach the maximum efficiency of 90%.

5.6. Summary

(1) Various losses in the turbine are explained in this chapter. Namely, the loss in the nozzles is 2 ~ 3%, the loss in the blade 4 ~ 5%, the leaving loss 4 ~ 5%, and the heat loss 4 ~ 5% when very small output power is produced, and none when the output power is great.

(2) The loss in the blade is as little as 1 ~ 2% near the center of exit, and increases as much as 10% at the outside radii of exit. Consequently, the internal efficiency near the center is higher by 8 ~ 10% than that at the outside radii, which proves the theory described in Chapter 2 that the gas flow should be conducted as much as possible towards the center where the loss is small.

(3) As for the blade loss coefficient, both the No. 1 and No. 2 test turbines show the same tendency and take the mean velocity coefficient of 0.78 ~ 0.79 near the designing point. As compared with the axial turbine, the radial turbine shows rather poor blade velocity coefficient, mainly because of its complex geometrical shapes, which should be further investigated and improved.

(4) It is made clear that the phenomena of slope in the blade are caused for the most part by the losses in the blade. Accordingly, designing procedures of exducer are introduced in order to correct the effects of spiral flows accompanying the rotatory motion of the blade.

(5) The results of the No. 2 test turbine show its capacity to develop the maximum efficiency as high as 90%.

CHAPTER 6

CONCLUSION

The basic approach towards the designing of mixed-flow radial turbines is sought after from a new standpoint which results in clarifying the conditions giving the maximum turbine efficiency, as well as in finding the best designing procedures of nozzles. Investigations are also conducted on various losses that occur in the blade and emphasis is given to the study of the flow in the exducer which has particular importance in a mixed-flow radial turbine. The experiments, based on the above investigations, are then worked out with the test turbine that has proved to be capable of developing 90% of the highest adiabatic efficiency.

A gas turbine prime mover that has 90% of the maximum efficiency, is also capable of reaching 22% of heat efficiency at the pressure ratio of six and without using a heat exchanger even when its compressor efficiency is only 80%, and of raising its heat efficiency as high as 32 ~ 40% at the pressure ratio of 3 ~ 4, and the gas temperature of 600 ~ 800°C, when using a heat exchanger of 80% temperature efficiency. Such high heat efficiency that far surpasses the quality of most of the internal combustion engines heretofore in use, indicates the possibility of producing small gas turbines of 50 ~ 300 horse powers capable of excellent performance. The present study thus provides solid and significant grounds to rely upon the utility of small gas-turbine prime movers.

BIBLIOGRAPHY

1. Sugawara, S., and Nakamura, Y. "A Theoretical Study of Steam Turbine Efficiency," Nihon Kikaigaku Ronbunshu, Feb., 1942, Vol. 8, No. 30.

2. Balje, O.E., "A Contribution to the Problem of Designing Radial Turbomachines." Trans. ASME., May, 1952, Vol. 74, No. 4.

3. Mori, Y. "A Theoretical Study of Radial Gas Turbines." Nihon Kikaigaku Ronbunshu, Aug., 1954, Vol. 20, No. 96.

4. von der Nuell, W.T. "Single-State Radial Turbines for Gaseous Substances with High Rotative and Low Specific Speeds." Trans. ASME., May, 1952, Vol. 74, No. 4.

5. Birmann, R. "The Elastic-Fluid Centripetal Turbine for High Specific Outputs." Trans. ASME., Feb., 1954, Vol. 76, No. 2.

6. Wosika, L.R., "Radial-Flow Compressors and Turbines for the Simple Small Gas Turbine." Trans. ASME., Nov., 1952, Vol. 74, No. 8.

7. Martinuzzi, P.F., "Gas Turbine Progress Report--Cycle Component," Trans. ASME., Feb., 1953, Vol. 75, No. 2.

8. Schwartz, F.L., "Gas Turbine Progress Report--Automotive," Trans., ASME., Feb., 1953, Vol. 75, No. 2.

9. Oil Engine and Gas Turbine, 1954, Vol. XXI, No. 250, 1954, Vol. XXII, No. 251, 1955, Vol. XXII, No. 262, 1955, Vol. XXII, No. 264, 1956, Vol. XXIV, No. 278, 1957, Vol. XXIV, No. 283, 1957, Vol. XXV, No. 287, 1957, Vol. XXV, No. 288.

10. Mori, Y, "A Theoretical Study of Radial Gas Turbines (Report No. 2: Mixed-Flow Turbines)", September, 1955, Vol. 21, No. 109.

11. Mizumachi, N. "A Study of Radial Gas Turbines (Report No. 1: Theoretical Study)." Nihon Kikaigakkai Sapporo Rinji Taikai Conference, September, 1955.

12. Flugel, G. "Die Dampfturbinen".

13. Stodola, A. "Dampf-und Gas-Turbinen".

14. Emmert, H.D. "Current Design Practices for Gas Turbine Power Elements," Trans. ASME., Feb., 1950, Vol. 72, No. 2.

15. Ainley, D.G., "Performances of Axial Flow Turbines (Internal Combustion Turbine)". Proc. IME. No. 159, 1948.

16. Pfleiderer, C. "Die Kreiselpumpen fur Flussigkeiten und Gase."

17. Mizumachi, N. "A Study of Radial Gas Turbines (Report No. 5: Partial Load Characteristics).", Nihon Kikaigakkai Sixtieth Anniversary Conference in Tōkyō, Oct., 1957.

18. Mizumachi, N. "A Study of Radial Gas Turbines (Report No. 3: Nozzles)." Nihon Kikaigakkai Tsūjō Sōkai Conference, April, 1957.

19. Wislicenus, G.F. "Fluid Mechanics of Turbo-machinery."

20. Vincent, E.T. "The Theory and Design of Gas Turbines and Jet Engines."

21. Morley, A.W. "Aircraft Propulsion--Theory and Performance."

22. Ainley, D.G., and Mathieson, G.C.R. "An Examination of the Flow and Pressure Losses in Blade Rows of Axial-Flow Turbines," R & M No. 2891, 1955.

23. Mizumachi, N. "A Study of Radial Gas Turbines (Report No. 2: Performance Test Turbines).", Nihon Kikaigakkai Okayama Rinji Taikai Conference, Nov., 1956.

24. Mizumachi, N. "A Study of Radial Gas Turbines (Report No. 4: Losses and Slips in the Blade).", Nihon Kikaigakkai, 636th Combined Conference, June, 1957.

25. Mizumachi, N. "A Study of Radial Gas Turbines (Report No. 6: Performance Test Turbines)." Nihon Kikaigakkai Combined Conference, May, 1958.

26. Keenan and Kaye, "Gas Tables."